

# **FLUID MANAGEMENT TECHNOLOGY: LIQUID SLOSH DYNAMICS AND CONTROL**

by

Franklin T. Dodge  
Steven T. Green  
Daniel D. Kaña

**INTERIM REPORT**  
for  
Period October 1, 1988–July 1, 1991

Contract NAS3-25365  
SwRI Project 04-2453

Prepared for

National Aeronautics and Space Administration  
Lewis Research Center  
Cleveland, Ohio 44135

November 1, 1991

(NASA-CR-189107) FLUID MANAGEMENT  
TECHNOLOGY: LIQUID SLOSH DYNAMICS AND  
CONTROL Interim Report, 1 Oct. 1988 – 1 Jul.  
1991 (Southwest Research Inst.) 185 p

N92-14320

Unclass

CSC 200 63/34 0058078



**SOUTHWEST RESEARCH INSTITUTE**  
SAN ANTONIO  
DETROIT  
HOUSTON  
WASHINGTON, DC



# **FLUID MANAGEMENT TECHNOLOGY: LIQUID SLOSH DYNAMICS AND CONTROL**

by

Franklin T. Dodge  
Steven T. Green  
Daniel D. Kaña

INTERIM REPORT

for

Period October 1, 1988 - July 1, 1991

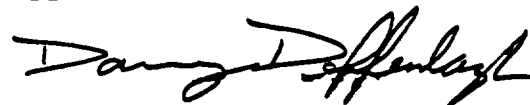
Contract NAS3-25358  
SwRI Project 04-2453

Prepared for

National Aeronautics and Space Administration  
Lewis Research Center  
Cleveland, Ohio 44135

November 1, 1991

Approved:



---

Danny M. Deffenbaugh, Director  
Department of Fluid Systems



REPORT DOCUMENTATION PAGE			Form Approved OMB No. 0704-0188	
Public reporting burden for this collection of information is estimated to average 1 hour per response, including the time for reviewing instructions, searching existing data sources, gathering and maintaining the data needed, and completing and reviewing the collection of information. Send comments regarding this burden estimate or any other aspect of this collection of information, including suggestions for reducing this burden, to Washington Headquarters Services, Directorate for Information Operations and Reports, 1215 Jefferson Davis Highway, Suite 1204, Arlington, VA 22202-4302, and to the Office of Management and Budget, Paperwork Reduction Project (0704-0188), Washington, DC 20503.				
1. AGENCY USE ONLY (Leave blank)	2. REPORT DATE November 1, 1991	3. REPORT TYPE AND DATES COVERED Interim Rpt Oct 1, 1988 - July 1, 1991		
4. TITLE AND SUBTITLE Fluid Management Technology: Liquid Slosh Dynamics and Control		5. FUNDING NUMBERS Contract NAS3-25365		
6. AUTHOR(S) Franklin T. Dodge, Steven T. Green, and Daniel D. Kana				
7. PERFORMING ORGANIZATION NAME(S) AND ADDRESS(ES) Southwest Research Institute Division of Mechanical and Fluids Engineering 6220 Culebra Road San Antonio, Texas 78228		8. PERFORMING ORGANIZATION REPORT NUMBER Interim Report, Project 04-2453		
9. SPONSORING/MONITORING AGENCY NAMES(S) AND ADDRESS(ES) National Aeronautics and Space Administration Lewis Research Center Cleveland, Ohio 44135		10. SPONSORING/MONITORING AGENCY REPORT NUMBER NASA CR-189107		
11. SUPPLEMENTARY NOTES				
12a. DISTRIBUTION/AVAILABILITY STATEMENT		12b. DISTRIBUTION CODE		
13. ABSTRACT (Maximum 200 words) <p>Flight experiments were defined for the COLD-SAT test bed satellite and the Shuttle middeck to help establish the influence of the gravitational environment on liquid slosh dynamics and control. Several analytical and experimental studies were also conducted to support the experiments and to help understand the anticipated results.</p> <p>Both FLOW-3D and NASA-VOF3D computer codes were utilized to simulate low Bond number, small amplitude sloshing, for which the motions are dominated by surface forces; it was found that neither code provided a satisfactory simulation. Thus, a new analysis of low Bond number sloshing was formulated, using an integral minimization technique that will allow the assumptions made about surface physics phenomena to be modified easily when better knowledge becomes available from flight experiments. Several examples were computed by the innovative use of a finite-element structural code. An existing spherical-pendulum analogy of nonlinear, rotary sloshing was also modified for easier use and extended to low-gravity conditions.</p> <p>Laboratory experiments were conducted to determine the requirements for liquid-vapor interface sensors as a method of resolving liquid surface motions in flight experiments. The feasibility of measuring the small slosh forces anticipated in flight experiments was also investigated.</p>				
14. SUBJECT TERMS Low Gravity, Sloshing, Rotary Slosh, Liquid-Vapor Sensors, Load Cells, Low Gravity Experiments, COLD-SAT			15. NUMBER OF PAGES 198	
			16. PRICE CODE	
17. SECURITY CLASSIFICATION OF REPORT Unclassified	18. SECURITY CLASSIFICATION OF THIS PAGE Unclassified	19. SECURITY CLASSIFICATION OF ABSTRACT Unclassified	20. LIMITATION OF ABSTRACT	

NSN 7540-01-280-5500

PRECEDING PAGE BLANK NOT FILMED

Standard Form 298 (Rev. 2-89)  
Prescribed by ANSI Std. Z39-18  
298-102



## ACKNOWLEDGEMENTS

The authors gratefully acknowledge the invaluable help of the NASA technical monitor, Mr. John C. Aydelott. At SwRI, the following personnel contributed significantly to the project:

Mr. M. Cruse	—	computer code execution
Mr. F. R. Pitman	—	conduct of laboratory experiments
Mr. D. C. Scheidt	—	design and conduct of laboratory experiments
Mr. J. F. Unruh	—	advice and assistance on finite element modeling
Mr. S. K. Wilson	—	conduct of laboratory experiments



## ABSTRACT

Flight experiments were defined for the COLD-SAT test bed satellite and the Shuttle middeck to help establish the influence of the gravitational environment on liquid slosh dynamics and control. Several analytical and experimental studies were also conducted to support the experiments and to help understand the anticipated results.

Both FLOW-3D and NASA-VOF3D computer codes were utilized to simulate low Bond number, small amplitude sloshing, for which the motions are dominated by surface forces; it was found that neither code provided a satisfactory simulation. Thus, a new analysis of low Bond number sloshing was formulated, using an integral minimization technique that will allow the assumptions made about surface physics phenomena to be modified easily when better knowledge becomes available from flight experiments. Several examples were computed by the innovative use of a finite-element structural code. An existing spherical-pendulum analogy of nonlinear, rotary sloshing was also modified for easier use and extended to low-gravity conditions.

Laboratory experiments were conducted to determine the requirements for liquid-vapor interface sensors as a method of resolving liquid surface motions in flight experiments. The feasibility of measuring the small slosh forces anticipated in flight experiments was also investigated.



## TABLE OF CONTENTS

<u>Section</u>	<u>Page</u>
ACKNOWLEDGEMENTS.....	iii
ABSTRACT.....	v
LIST OF FIGURES.....	ix
LIST OF TABLES.....	xi
SYMBOLS.....	xiii
1.0 INTRODUCTION.....	1
1.1 Background.....	1
1.2 Objective.....	2
1.3 Scope of Work.....	2
1.3.1 Task I — Technology Requirements.....	2
1.3.2 Task II — Definition of Flight Experiments.....	2
1.3.3 Task III — Analytical Model Development.....	3
1.3.4 Task IV — Ground Experimentation.....	3
2.0 TECHNOLOGY REQUIREMENTS.....	5
2.1 Data Sources.....	5
2.2 Representative Tank Shapes, Volumes, and Gravity Levels.....	5
2.3 Summary of Parameters.....	6
2.4 Conclusions.....	6
3.0 DEFINITION OF FLIGHT EXPERIMENTS.....	9
3.1 General.....	9
3.1.1 Objectives.....	9
3.1.2 Key Parameters.....	9
3.1.3 Measurements.....	9
3.1.4 Data Analysis.....	11
3.2 Summary of COLD-SAT Experiment Definition.....	11
3.2.1 General Description.....	11
3.2.2 Measurements and Instrumentation.....	12
3.2.3 Hardware Requirements.....	12
3.2.4 Test Matrix.....	12
3.3 Shuttle Flight Experiment.....	12
3.3.1 General Description.....	12
3.3.2 Measurements and Instrumentation.....	15
3.3.3 Hardware Requirements.....	16
3.3.4 Test Matrix.....	16
4.0 ANALYTICAL MODELS.....	21
4.1 General.....	21
4.2 FLOW-3D Simulations.....	21
4.3 NASA-VOF3D Simulations.....	22
4.4 Linearized Low Gravity Sloshing Model.....	22
4.4.1 Background.....	22
4.4.2 Equations of Motion.....	23
4.4.3 Equilibrium Surface.....	25
4.4.4 Slosh Force.....	25

**NO INFORMATION**

4.4.5	Non-Dimensional Equations.....	26
4.4.6	Equivalent Mechanical Model.....	27
4.4.7	Integral Formulation .....	28
4.4.8	Structural Finite-Element Simulation.....	29
4.4.9	Mass Distribution, M(S).....	31
4.4.10	Numerical Examples.....	32
4.5	Spherical Pendulum Rotary Slosh Model.....	34
4.5.1	Background.....	34
4.5.2	Revised Approximate Model.....	37
4.5.3	Numerical Model.....	38
4.5.4	Effects of Low Gravity.....	45
5.0	GROUND-BASED SUPPORTING EXPERIMENTATION.....	49
5.1	Introduction.....	49
5.2	Ground Tests of Liquid-Vapor Sensors.....	49
5.2.1	Background.....	49
5.2.2	Liquid-Vapor Sensors.....	49
5.2.3	Ground Tests of Liquid-Vapor Sensor Arrays.....	50
5.3	Load Cell Requirements.....	54
6.0	CONCLUSIONS.....	57
6.1	Flight Experiments.....	57
6.2	Analytical Studies.....	57
6.2.1	Small Amplitude Linear Sloshing.....	57
6.2.2	Rotary Slosh Model.....	58
6.3	Ground-Based Experimentation.....	59
6.3.1	Liquid-Vapor Interface Sensors.....	59
6.3.2	Slosh Force Transducers.....	59
7.0	REFERENCES.....	61
APPENDIX A		
COLD-SAT Experimental Requirements Document on Liquid Slosh Dynamics and Control (Dated July 25, 1990)		
APPENDIX B		
B.1	Solution for Equilibrium Surface Shape	
B.2	Computation of Low-G Slosh Parameters from the Finite-Element Trial Functions	

## LIST OF FIGURES

<u>Figure</u>	<u>Page</u>
3.1-1 Typical Liquid-Vapor Sensor Array.....	67
3.3-1 Conceptual Design of Shuttle Flight Experiment Package.....	68
3.3-2 Slosh Characteristics of a Half-Full Spherical Tank.....	69
3.3-3 Block Diagram of Shuttle Flight Experiment Instrumentation and Hardware.....	70
4.3-1 NASA-VOF3D Simulation of $Bo = 10$ Sloshing in a Spherical Tank. Time Increases Right to Left, Top to Bottom.....	71
4.4-1 Schematic for Low-G Slosh Analysis.....	72
4.4-2 Details of Low-G Slosh Analysis.....	73
4.4-3 Equilibrium Free Surface Shape.....	74
4.4-4 Finite Element Model.....	75
4.4-5 Trial Potentials for 50% Full, $Bo = 1$ .....	76
4.4-6 Slosh Wave Shape for 50% Full, $Bo = 1$ .....	77
4.5-1 Compound Pendulum Model for Propellant Slosh.....	78
4.5-2 Circumferential and Radial Damping Factors.....	79
4.5-3 Steady Deflection Angle.....	80
4.5-4 Position Lag Angle.....	81
4.5-5 Spherical Pendulum Mass Fraction.....	82
4.5-6 Relationship Between Physical Space Plane and Time-Phase Plane.....	83
4.5-7 Polar $l/\sin\theta$ - Inches, $\phi$ - Radians.....	84
4.5-8 Deflection Angle, $\theta$ - Radians.....	84
4.5-9 Circumferential Angle, $\phi$ - Radians.....	85
4.5-10 Position Angle, $\phi_{01}$ - Radians.....	85
4.5-11 Cross-Axis Weight, $W_c$ - lb.....	86
4.5-12 In-Line Weight, $W_e$ - lb.....	86
4.5-13 Polar Plot ( $\alpha = 1.000$ ).....	87
4.5-14 Polar Plot ( $\alpha = 1.107$ ).....	87
4.5-15 Influence of Radial Damping on Character of Response.....	88
4.5-16 Linear Pendulum Model Parameters for Rotary Liquid Slosh.....	89
4.5-17 Spherical Pendulum Deflection Corresponding to Rotary Slosh Amplitude.....	90
4.5-18 Dependence of Spherical Pendulum Response on Frequency and Damping.....	91
5.2-1 Schematic of Fiber Optic Liquid-Vapor Sensor.....	92
5.2-2 Slosh Test Apparatus for Liquid-Vapor Interface Sensors.....	92

5.2-3	Reproduction of Strip Chart Recording of Sensor Output.....	93
5.2-4	Probe Arrays for Liquid-Vapor Interface Sensors.....	94
5.2-5	Interpolated Test Data and Predicted Wave Shape for Four-Sensor Probe Array.....	95
5.2-6	Interpolated Test Data and Predicted Wave Shape for Six-Sensor Probe Array.....	97
5.3-1	Strain-Gauge SLOSH Force Dynamometer.....	99

## LIST OF TABLES

<u>Table</u>		<u>Page</u>
3.2-1	Measurement Requirements for COLD-SAT Liquid Dynamics Experiment....	13
3.2-2	COLD-SAT Test Matrix.....	14
3.3-1	Subsystem Power Requirements, Sizes, and Weights for Shuttle Flight Experiment.....	17
3.3-2	Preliminary Shuttle Flight Experiment Matrix.....	18
4.4-1	Summary of Low-G Slosh Parameters for a Spherical Tank.....	33
5.3-1	Dynamometer Requirements.....	55



## SYMBOLS

An attempt was made to ensure that each symbol used in the report had a unique definition. Since that was not entirely possible because of the large number of symbols used, the principal symbols used in each major section of the report are listed separately.

### Symbols For Section 1.0

$Bo$	Bond number
$f_n$	slosh natural frequency
$R_o$	tank radius
$\nu$	liquid kinematic viscosity
$\beta$	ratio of liquid surface tension to density
$\zeta$	slosh damping ratio

### Symbols for Section 2.0

$g_o$	earth's gravitational acceleration
-------	------------------------------------

### Symbols for Section 3.0

$A_i$	impulsive acceleration
$A_p$	periodic acceleration
$g_o$	earth's gravitational acceleration
$\tau_i$	duration of impulsive acceleration
$\tau_p$	period of periodic acceleration
$\tau_s$	period of slosh wave
$\mu g$	$10^{-6}g_o$

### Principal Symbols for Section 4.4

$a_i$	coefficients in reactive force expression, Eq. (4.4-32)
$b_i$	coefficients in series expansion of $\phi$ , Eq. (4.4-34)
$Bo$	Bond number, $\rho g R_o^2 / \sigma$
$f(s)$	equilibrium free surface
$F(S)$	equilibrium free surface (non-dimensional)
$F_\sigma, F_p$	net lateral forces due to surface tension and pressure
$g$	effective gravitational acceleration
$H$	wave height (non-dimensional)

$K_s$	torsional spring
$l_s$	pendulum length
$m_s$	slosh mass
$M(S)$	fictitious mass distribution at free surface nodes (non-dimensional)
$\vec{n}$	outward-pointing normal at a surface
$p$	liquid pressure
$p_g$	gas pressure
$r, \theta, z$	cylindrical coordinate system fixed at center of free surface
$r_c$	r-coordinate of equilibrium contact line
$R_c$	r-coordinate of equilibrium contact line (non-dimensional)
$r_1, r_2$	radii of curvature of equilibrium free surface
$R_1, R_2$	radii of curvature of equilibrium free surface (non-dimensional)
$R_o$	radius of tank
$R, \theta, Z$	cylindrical coordinate system (non-dimensional)
$s$	arc length along equilibrium free surface
$S$	arc length along equilibrium free surface (non-dimensional)
$t$	time
$U_i$	trial potential functions
$\gamma_c$	equilibrium contact angle at the liquid surface-tank wall contact line, measured in the liquid
$\xi$	arc length along tank wall
$\Xi$	arc length along tank wall (non-dimensional)
$\eta$	slosh wave height normal to free surface
$\eta_c$	slosh wave height at contact line, tangential to wall
$\kappa$	mean curvature of equilibrium free surface (dimensional)
$\rho$	liquid density
$\sigma$	liquid surface tension
$\phi$	velocity potential
$\Phi$	velocity potential (non-dimensional)
$\chi$	angle the tank wall makes with horizontal at the contact line
$\psi$	angle the free surface makes with horizontal at the contact line
$\omega$	slosh frequency
$\Omega$	slosh frequency (non-dimensional)

### Symbols for Section 4.5

$C_\theta, C_\phi$	Radial and circumferential damping coefficients
$F_L(\alpha)$	Amplification factor for linear pendulum response, $\theta_2$
$F_S(\alpha)$	Amplification factor for spherical pendulum response, $\theta_1$
$g$	Gravity acceleration
$l$	Length for both linear and spherical pendulums
$m$	Mass of spherical pendulum corresponding to $\beta_1 W_1$ weight
$t$	Time
$W_1$	Total weight of liquid
$W_R, W_I$	Real and imaginary components of system in-line weight response
$W_{CC}, W_{CQ}$	CO and QUAD phase components of cross-axis weight
$W_{eR}, W_{eI}$	Real and imaginary components of spherical pendulum in-line weight response
$x$	Excitation displacement
$x_0$	Amplitude of oscillatory excitation displacement
$\alpha$	Frequency ratio
$\beta_1$	Fraction of liquid weight, $W_1$ , represented by weight of spherical pendulum
$\beta_2$	Fraction of liquid weight, $W_1$ , represented by weight of linear pendulum
$\gamma_0$	Time phase lag of oscillatory component $\theta_1$ relative to excitation displacement
$\gamma_{0r}$	Space phase lag of rotating pendulum with oscillatory component $\theta_1$
$\psi_0$	Time phase lag of oscillatory component $\theta_2$ relative to excitation displacement
$\xi_{0c}$	Time phase lag of spherical pendulum cross-axis weight relative to excitation displacement
$\xi_{0e}$	Time phase lag of spherical pendulum in-line weight relative to excitation displacement
$\psi$	Angle relative to excitation plane of pendulum rotating with lag $\gamma_{0r}$
$\lambda_0$	Combined phase angle of cross-axis weight component
$\epsilon_0$	Phase distortion for oscillatory component $\theta_1$
$\epsilon_{02}$	Coupling difference angle for linear pendulum
$\phi, \theta$	Circumferential and radial coordinates for spherical pendulum
$\phi_0, \phi_{0r}$	Position lag angle of spherical pendulum relative to excitation plane
$\theta_0$	Steady amplitude of spherical pendulum
$\theta_1$	Oscillatory amplitude of spherical pendulum
$\theta_2$	Oscillatory amplitude of linear pendulum

$\omega$	Circular frequency
$\omega_n$	Linear natural circular frequency of both pendulums
$\zeta_\theta, \zeta_\phi$	Radial and circumferential damping ratios
$\zeta_{\theta 1}$	Radial damping ratio of spherical pendulum oscillatory component at frequency $2\omega$
$\zeta_{\theta 2}$	Radial damping ratio of linear pendulum oscillatory component at frequency $\omega$

### **Symbols for Section 5.0**

$A_o$	average height of equilibrium free surface above sensor
$A_I$	amplitude of slosh wave
$F$	peak slosh force
$Q$	resonance magnification factor
$R_o$	tank radius
$t$	time
$x_o$	amplitude of tank oscillatory motion
$\tau_s$	slosh wave period
$\mu_o$	phase difference
$\omega_n$	slosh natural frequency

## 1.0 INTRODUCTION

### 1.1 Background

Many of the future spacecraft planned by NASA and DOD will contain large quantities of liquids for propellants, life support, and other uses. As two examples, space vehicles for the ambitious Space Exploration Initiative will transport and store hundreds of thousands of kilograms of cryogenic propellants, and Space Station Freedom will contain tens of thousands of both cryogenic and storable liquids that must be re-supplied in orbit. Future deep space probes and space-based optical systems will also have a large fraction of their mass in the form of liquids. Controlling, pointing, or docking of such spacecraft is critically dependent upon understanding and managing the motion (sloshing) of the large masses of liquids in their tanks.

When liquid body forces are large, the "high gravity" motions of a liquid contained in a tank are well understood, and analytical, numerical, and scale-model test methods have been well established to treat them [1, 2, 3]. But, when liquid body forces are small, the "low gravity" motions of liquid free surfaces are not nearly so well understood because they are dominated by surface forces that are completely masked on earth by the much larger body forces. Note that the true indicator of "low" gravity is the Bond number  $Bo$ , defined as  $Bo = g_{eff} R_o^2 / \beta$  where  $g_{eff}$  is the effective gravity or settling acceleration,  $R_o$  is a representative dimension of the tank such as diameter, and  $\beta$  is the specific surface tension of the liquid; Bond numbers of ten or less are generally considered to represent "reduced" gravity and  $Bo \ll 1$  to represent "micro" gravity. Spacecraft in near-earth orbit usually have  $Bo \approx 0.1$  while deep space probes have  $Bo \ll 1$ .

The rudimentary flight tests that have been conducted to date [e.g., 4] have provided little quantitative data about low gravity sloshing. Some information is available from drop tower and ground test simulations for  $Bo \approx 10$  [e.g., 5, 6, 7] but these kinds of studies are hampered by the small size of the tanks that must be used, the short test time, and (at least up to the present) the need to use non-cryogenic liquids. As an example of the available information, it appears that viscous slosh damping  $\zeta$  is larger in low gravity and, for a cylindrical tank, can be correlated by [5, 7]:

$$\zeta = A(v/f_n R_o^2)^{1/2} [1 + C(Bo)^{-b}] \quad (1.1-1)$$

where  $v$  is the kinematic viscosity,  $f_n$  is the slosh natural frequency, and  $A$ ,  $b$ , and  $C$  are empirically-determined constants. Although  $\zeta$  should increase in low gravity because of the larger wetted area of the liquid on the tank walls, the increase predicted by Eq. (1.1-1) for small  $Bo$  is much larger than can be accounted for merely by the larger wetted area. Since the low gravity response of a liquid to tank motions depends strongly on the physics of the contact line of the liquid at the tank wall [8, 9], the anomalously high damping may be the result of poorly understood effects at the contact line. Furthermore, the natural frequency measured in ground simulations of low gravity sloshing varies by more than a factor of two between the extreme limits of a "free" contact

line and a "stuck" contact line [7]. For cryogenics, the contact line motion may also be affected by evaporation and condensation effects. Contact line effects are totally negligible when liquid body forces are large. Nonlinear sloshing also appears to be more prominent in low gravity [10, 11]. Finally, because of the lack of low gravity slosh test data to provide insight, all methods to date for predicting liquid free surface motions in low gravity have employed potentially unrealistic assumptions about the contact line motion; none of the assumptions has as yet been adequately validated by comparison to test data.

In order to gain the required physical understanding about liquid motions in low gravity, experiments are needed in an actual low gravity environment, using tanks of at least moderate size and long test durations. The study documented in this report defines such a set of space-based experiments and summarizes the supporting analytical models and ground-based testing. The study initially concentrated on experiments using liquid hydrogen that were to be conducted with NASA-LeRC's COLD-SAT test-bed satellite, but it was later extended to include the definition of experiments using non-cryogenic liquids that can be conducted in the Space Shuttle.

## **1.2 Objective**

The objective of the program was to conduct research to establish the influence of the gravitational environment on liquid slosh dynamics and control, including analytical and experimental studies.

## **1.3 Scope of Work**

The project work was conducted in four technical tasks described below and one administrative task. Succeeding sections of this Final Report discuss the accomplishments of each technical task in detail.

### **1.3.1 Task I — Technology Requirements**

For this task, future and planned NASA and DOD missions were reviewed to determine typical ranges of parameters that are important for liquid dynamics and control. The parameters included: tank shape, size, and fill level; internal tank structure and anti-slosh devices; spacecraft maneuvers; and liquid thermophysical properties.

### **1.3.2 Task II — Definition of Flight Experiments**

The efforts of this task were devoted to defining the specifications, instrumentation, and data requirements for space experimentation on liquid free surface dynamics. It was composed of three subtasks:

1. Review the preliminary COLD-SAT slosh dynamics experimental requirements document and prepare an updated version, based on the conclusions from Task I.
2. Define an alternative flight experiment for the Space Shuttle, using a non-cryogenic liquid.

3. Provide technical oversight to NASA as requested on the detailed development of all COLD-SAT experiments.

### **1.3.3 Task III — Analytical Model Development**

The efforts of this task were devoted to developing analytical methods and models that would allow liquid free surface experimental results to be analyzed and extended. It was composed of four subtasks:

1. Investigate methods of improving the representation of surface physics effects in FLOW-3D (conducted by Flow Science, Inc.).
2. Investigate NASA-VOF3D as a method of simulating liquid slosh in a low gravity environment.
3. Develop a linearized slosh model of low gravity sloshing and implement it using available finite-element computational technology.
4. Extend an existing spherical pendulum model of nonlinear rotary sloshing to low gravity conditions.

Subtasks 3 and 4 constituted the bulk of the effort for Task III.

### **1.3.4 Task IV — Ground Experimentation**

The efforts of this task were devoted to ground tests in support of instrumentation development for the space experiments. It was composed of two subtasks:

1. Investigate liquid-vapor interface sensors as a method of tracking moving free surfaces in a low gravity environment.
2. Determine the specifications for load cells and accelerometers that could be used to measure low gravity slosh forces and moments.



## 2.0 TECHNOLOGY REQUIREMENTS

The definitions of low-gravity liquid-motion flight experiments were based on the ranges of parameters that are anticipated for future NASA and DOD missions. The parameters selected for this study were: (1) tank shape, size, and filling level; (2) internal tank structure and anti-slosh devices; (3) low gravity environment; (4) vehicle motions; and (5) liquid properties.

### 2.1 Data Sources

Over twenty-five technical reports discussing proposed NASA and DOD missions were reviewed to obtain numerical estimates of the selected parameters; references [12 - 17] are representative examples of the reviewed reports. In addition, cognizant personnel at NASA centers and at the Air Force Astronautics Laboratory were interviewed by project personnel.

### 2.2 Representative Tank Shapes, Volumes, and Gravity Levels

As specific examples, some details of the tanks for six planned or designed space vehicles are summarized below.

**Orbital Transfer Vehicle** — The propellants are  $\text{LH}_2$  and  $\text{LO}_2$ . The baseline design  $\text{LH}_2$  tank is cylindrical with ellipsoidal ends and has a volume of approximately  $5000 \text{ ft}^3$  ( $140 \text{ m}^3$ ) and a diameter of 14 ft (4.4 m). The  $\text{LO}_2$  tank is a sphere with a volume of approximately  $1500 \text{ ft}^3$  ( $42 \text{ m}^3$ ) and a diameter of approximately 14 ft (4.4 m). The gravity environment ranges from about  $1g_0$  to about  $10^{-5}g_0$ . The tanks for the proposed European Space Tug are of similar sizes.

**CRAF/Cassini Space Probe** — The propellants for the main engine are monomethyl hydrazine and  $\text{N}_2\text{O}_4$ ; the propellant for the RCS engines is hydrazine. The main engine tanks are spheres with a diameter of 5.1 ft (1.56 m). The RCS tanks are cylinders with rounded ends, with a total length of 2.6 ft (0.8 m) and a diameter of 1.8 ft (0.56 m). The gravity environment ranges from about  $0.01g_0$  during a main engine firing to practically zero gravity during a deep space coast.

**Liquid Droplet Radiator System** — The planned tanks are of various shapes and sizes, depending on the design, but are typically spheres about 3 ft (1 m) in diameter. The tanks contain liquid metal or a very low vapor pressure oil. The gravity environment is  $10^{-4}g_0$  to  $10^{-6}g_0$ .

**Strategic Defense Initiative Optical Systems** — Specific tank designs are classified. Typical tank shapes are spheres and cylinders with rounded ends. The liquids are cryogenic propellants as well as storables. One unclassified design study tank is a 21 ft (6.4 m) sphere containing up to 21000 lbs (9500 kg) of  $\text{LH}_2$ . The gravity environment can be as low as  $10^{-7}g_0$ .

**Compact Cryogenic Feed System** — The  $\text{LO}_2$  tank of this system is a torus with a major diameter of 9.6 ft (2.9 m) and a minor diameter of 4.6 ft (1.4 m). The gravity environment ranges from high-gravity to  $10^{-6}g_0$ .

**Space Station** — Some designs of the Space Station include tanks that are large enough to refill two Orbital Transfer Vehicle  $\text{LH}_2$  tanks. Typical "large" tanks are spheres with volumes of  $5000 \text{ ft}^3$  ( $140 \text{ m}^3$ ). The gravity environment is about  $10^{-5}g_0$  -  $10^{-6}g_0$ .

### 2.3 Summary of Parameters

Based on the data sources and interviews, it was concluded that the most common tank shapes for future missions are spheres and cylinders with ellipsoidal ends. Tank volumes range from  $5 \text{ ft}^3$  ( $0.14 \text{ m}^3$ ) to over  $5000 \text{ ft}^3$  ( $140 \text{ m}^3$ ). During most missions, the tank filling level will vary from nearly full to nearly empty. Most tanks will contain liquid acquisition devices, typically screened channels running the length of the tank. None of the tanks surveyed contained any specific anti-slosh devices since the designs were not yet sufficiently mature to consider sloshing; however, liquid acquisition devices such as channels and central cruciform vanes are known to damp high-gravity sloshing effectively.

The gravity environment covers the range from  $1g_0$  to  $10^{-6}g_0$  (and even smaller for deep space probes). The non-dimensional Bond number of course depends on tank size and liquid surface tension as well as gravity level. As examples, at the lower range of gravity levels ( $\approx 10^{-6}g_0$ ) the Bond number for  $\text{LH}_2$  is 0.09 for a 1 m diameter tank and 9.1 for a 5 m diameter tank; for  $\text{LO}_2$ , the corresponding Bond numbers are 0.21 and 21. The contact angle for most cryogenics and propellants is close to  $0^\circ$  against tank materials of aerospace interest; that is, the liquid "wets" the tank wall material. The ratio  $\beta$  of surface tension to density for most cryogenics and propellants ranges from  $0.0007 \text{ ft}^3/\text{sec}^2$  ( $20 \text{ cm}^3/\text{sec}^2$ ) to  $0.001 \text{ ft}^3/\text{sec}^2$  ( $30 \text{ cm}^3/\text{sec}^2$ ).

Space vehicle motions are of three general kinds: (1) g-jitter; (2) attitude control maneuvers; and (3) thrusting and other large impulses such as docking. The magnitude and frequency content of g-jitter depends on the space vehicle in question; for the Space Shuttle, as an example, the rms magnitude is of the order of  $10^{-4}g_0$  and almost all the frequency content is above 1 Hz. Attitude control maneuvers are likewise dependent upon the mission; typical maneuvers include slewing around one of the vehicle axes at  $2^\circ/\text{sec}$  and low-frequency, small-amplitude oscillations around all three axes. Thrusting and docking can impose impulsive accelerations typically of the magnitude of  $0.1g_0$ . The variety of tank motions implies that both large and small amplitude liquid motions will be excited.

### 2.4 Conclusions

Based upon the current state of knowledge and the survey described above, the desired technology requirements for a flight experiment can be summarized as:

- Spherical and cylindrical tanks with ellipsoidal ends should be tested; "bare" tanks and tanks with internal liquid acquisition devices are both important.
- Cryogenic liquids are desirable as the test liquid; in any case, the test liquid should wet the tank wall material.
- Bond numbers for the tests should cover a range from  $\approx 10$  to near zero.
- Tank motions should include large and small amplitude impulsive accelerations and sustained small-amplitude oscillatory accelerations.
- Liquid motions investigated in the tests should include small amplitude, linear sloshing; moderate amplitude nonlinear planar and rotary sloshing; and large amplitude, reorientation-like motions that eventually settle down to long-lived small-amplitude sloshing.

Data acquired from the tests should be sufficient in quality and quantity to validate analytical models and guide the development of improved models. Previous ground-based slosh tests have indicated that the most useful forms of data are (in descending order of usefulness): detailed maps of free surface shapes and motions (motion pictures, video recordings, etc.); slosh natural frequencies; time history or frequency sweeps of the forces and torques exerted on the tank; and slosh damping.



### **3.0 DEFINITION OF FLIGHT EXPERIMENTS**

#### **3.1 General**

A flight experiment was defined for both the COLD-SAT satellite and the Space Shuttle middeck. The complete Experiment Requirements Document for the COLD-SAT slosh dynamics experiment is included as Appendix A of this Final Report; it is summarized in Section 3.2. The definition of the Space Shuttle experiment is given in Section 3.3. The characteristics common to both definitions are described below.

##### **3.1.1 Objectives**

The specific objective of both flight experiments is to quantify the liquid motion resulting from typical maneuvers of space vehicles in a low gravity environment. Physical processes to be investigated include:

**Static liquid configurations** — The shape and location of the liquid in the test tanks will be monitored under ambient orbital conditions.

**Liquid response to various discrete accelerations** — Impulsive and periodic accelerations of selected amplitude, frequency, and duration will be applied and the free surface response monitored.

**Slosh damping** — Viscous damping will be determined for all tested conditions; if possible, the damping provided by a ring baffle should also be measured as a demonstration of an anti-slosh device for low gravity sloshing.

##### **3.1.2 Key Parameters**

The key parameters that are expected to influence sloshing in low gravity are: (1) liquid surface tension, density, and viscosity; (2) contact angle of the liquid at the tank wall; (3) tank shape and internal hardware; (4) liquid fill level; (5) steady settling acceleration; and (6) disturbance acceleration. Because most liquids of aerospace technological importance have static contact angles of  $\approx 0^\circ$  against common metals, the static contact angle parameter will not be varied in the flight tests. The steady settling acceleration can be varied in the COLD-SAT experiment alternative but not in the Shuttle experiment. All other parameters will be varied in the relevant non-dimensional form.

##### **3.1.3 Measurements**

The free surface configuration, slosh force, and tank acceleration environment constitute the bulk of the test measurements.

**Free surface configuration** — Mapping the static and dynamic configuration of the free surface is one of the most important methods of understanding and correlating experimental results. For example, the wave shape near the wall indicates whether the contact angle remains constant during sloshing ("free" contact line) or changes. Likewise, rotary slosh is most easily detected by observing the free surface motion. Ideally, the

mapping should employ both visual records such as motion pictures and an array of digital liquid-vapor sensors to track the position of the free surface quantitatively at a number of discrete locations. For the COLD-SAT experiment, visual observations are not possible, so liquid-vapor sensors must be used exclusively.

Liquid-vapor sensors should be positioned in at least two perpendicular arrays, as illustrated in Figure 3.1-1. Ground testing (see Section 5.0) indicated that the *overall* free surface shape and motion can be resolved satisfactorily by a radial spacing of the sensors as large as 40% of the free surface radius and a vertical spacing as large as 10% of the free surface radius. The level of resolution provided by this spacing is satisfactory to determine the predictive accuracy of existing models. More fundamental information may be required to determine weak assumptions and potential sources of improvement in the models. For example, the relation between the dynamic contact angle and the contact line velocity can have a significant effect on the slosh frequency and force [7], even though existing models assume that the dynamic contact angle remains equal to the static contact angle. To acquire detailed data about the wave shape near the wall from which the behavior of the dynamic contact angle can be inferred, a denser array of sensors is required in the vicinity of the wall, for at least one liquid level. Sensors in these denser arrays would have to be spaced symmetrically at about  $0.02R_0$  above and below the selected free surface level over a total vertical distance of about  $0.1R_0$ , and at least two such vertically-spaced arrays would have to be positioned radially at intervals of  $0.02R_0$  from the wall. Because of the "bent over" geometry of the tank-liquid intersection for spherical tanks (see Section 4.0 and Figure 4.4-3), the dense arrays are most readily made applicable to cylindrical (straight wall) tanks, although a dense array of sensors positioned along a radial line could be used for spherical tanks. In addition, the array installation must not significantly interfere with the slosh wave motion. It is understood that the use of dense arrays of liquid-vapor sensors will require substantial data acquisition rates and may interfere with other experiments; thus, their use may be restricted to the Shuttle-based experiment.

**Load cells** — The slosh force and torque exerted on the tank by the liquid in motion will be measured by load cells. The support structure of the tanks must be designed to accommodate these cells.

**Acceleration environment** — Both the effective settling acceleration and the time history of the disturbance accelerations will be measured by accelerometers and gyros.

**Temperature and pressure** — Liquid temperature will be measured at the start and end of each test to determine the liquid properties. For the COLD-SAT experiment in which cryogenics are used, liquid pressure will also be measured.

### **3.1.4 Data Analysis**

The initial configuration of the liquid and the static contact angle will be determined by liquid volume and liquid-sensor measurements (and visual records for the Shuttle experiment) before the perturbation acceleration is applied. Accelerometer and gyro data will be used to determine the motion imposed on the tanks.

For the impulsive perturbation tests, liquid-vapor sensor measurements (and video or cinema recordings for the Shuttle experiment) will be analyzed to determine: (1) slosh wave shape and amplitude as a function of time; (2) slosh natural frequency; and (3) slosh damping from the decay of the slosh wave amplitude. If a dense array of sensors is used near the wall as suggested above, contact angle and contact line velocity will also be computed as a function of time; if not, these quantities will still be estimated but the resolution is not expected to be sufficient to identify the relation between dynamic contact angle and contact line velocity. Load cell force histories will be analyzed to confirm the slosh natural frequency and damping data and to compute the slosh force. For periodic perturbations, the data analysis will be similar to the impulsive acceleration tests. In addition, load cell data, in conjunction with damping data from the impulsive tests for the same Bond number and liquid level, will be analyzed to determine the effective mass of liquid participating in the sloshing. When nonlinear effects are prominent, the line of action and the phasing of the slosh force relative to the excitation will also be determined from the load cell data.

Physical properties of the liquids will be computed from the temperature and pressure measurements, using tabulated data.

## **3.2 Summary of COLD-SAT Experiment Definition**

### **3.2.1 General Description**

Baseline designs of the COLD-SAT satellite envision three LH<sub>2</sub> tanks; a large "supply" tank [volume  $\approx 125 - 175 \text{ ft}^3$  ( $3.5 - 5 \text{ m}^3$ )] and two "receiver" tanks, one that is almost spherical [diameter  $\approx 3.0 \text{ ft}$  ( $0.9 \text{ m}$ )] and one that is cylindrical with ellipsoidal ends [diameter  $\approx 3.0 \text{ ft}$  ( $0.9 \text{ m}$ ), length  $\approx 5.5 \text{ ft}$  ( $1.7 \text{ m}$ )]. Slosh tests are defined for both receiver tanks to investigate the influence of tank shape. The cylindrical receiver tank contains a liquid acquisition device (screened channels), and various spray systems to study tank filling, cooldown, and cryogenic mixing. The spherical receiver tank is nominally "bare" but does contain spray systems. For the slosh tests, it is proposed that the cylindrical tank be fitted with a single ring baffle near its midpoint, to permit the investigation of a typical anti-slosh device. The COLD-SAT propulsion system will be used to provide the steady settling accelerations and the disturbance accelerations for the slosh tests. The slosh experiments can be performed as opportunities permit when the liquid filling levels of interest are available during other tests.

### 3.2.2 Measurements and Instrumentation

The measurement and instrumentation requirements are summarized in Table 3.2-1.

### 3.2.3 Hardware Requirements

The special hardware items required for the experiment are: (1) annular ring mounted in the cylindrical receiver tank; (2) load cells and accelerometers mounted on the support structures of both receiver tanks; and (3) liquid-vapor sensor arrays in both receiver tanks.

### 3.2.4 Test Matrix

Two general kinds of tests will be conducted: (1) oscillatory disturbance acceleration, and (2) impulsive disturbance acceleration. The tests are further arranged as being of *first* and *second* priority. Table 3.2-2 summarizes the test matrix. The steady settling accelerations listed in the table conform to the nominal levels that can be obtained by firing a single COLD-SAT engine or a combination of engines. The nominal perturbation accelerations correspond to levels that can be obtained by firing the appropriate attitude control thrusters or, depending on the COLD-SAT design, a gimbaled engine; impulsive accelerations are obtained by firing the engine for a short time and periodic accelerations by on-off firings for scheduled periods. The predicted natural period of the slosh waves for the various tests is indicated by the symbol  $\tau_s$  under the heading "Comments" in the table.

## 3.3 Shuttle Flight Experiment

### 3.3.1 General Description

The Shuttle flight experiment is designed to fit into two middeck lockers using a double mounting plate. Figure 3.3-1 shows a conceptual design of the flight experiment package. Three spherical tanks will be used in the first flight; cylindrical tanks will be used for a second flight unless the tanks can be changed out during the first flight. Two alternatives are considered: all tanks have different diameters [13 in., 7 in., and 3.5 in (33 cm, 18 cm, 9 cm)] to permit a thorough investigation of tank size effects, or the two smaller tanks have the same size [7 in (18 cm)] to permit liquids of different viscosity to be tested in tanks of the same size and shape. Further trade studies are required to determine the relative advantages of each alternative. The test liquid is either water (containing a surfactant, defoamer, and bactericide) or silicone oil, the choice depending primarily on safety trade studies.

Figures 3.3-2a and 3.3-2b show the Bond number and predicted slosh frequency for a spherical tank as a function of settling acceleration and tank diameter, for a liquid having  $\sigma/\rho = 0.0009 \text{ ft}^3/\text{sec}^2$  ( $25 \text{ cm}^3/\text{sec}^2$ ) typical of silicone oils. (The Bond numbers and frequencies would be slightly larger for water.) For all the tank sizes suggested for the flight experiment, the Bond number is considerably less than one for the steady settling accelerations that are anticipated

**TABLE 3.2-1 MEASUREMENT REQUIREMENTS FOR COLD-SAT LIQUID DYNAMICS EXPERIMENT**

<b>Parameter</b>	<b>Range</b>	<b>Accuracy</b>	<b>Instrument</b>
Liquid temperature	20 - 50°R	± 1°R	COLD-SAT temp. sensors
Tank pressure	5 - 50 psia	± 5 psia	COLD-SAT pressure sensors
Liquid interface position			
Cylindrical tank	0 - 4 ft axial; 0 - 1.3 ft radial	± 5% axial ± 10% radial	Liquid-vapor sensors with 10 - 15 second response
Spherical tank	0 - 1.3 ft		
Slosh force	0 - 0.0001 lb	± 2%	Load cells on tank support structures
Slosh frequency	0.001 - 0.01 hz	± 1%	Load cells and liquid/vapor sensors
Steady linear acceleration	8μg - 100μg	± 1%	COLD-SAT accelerometers or compute from thruster firing histories
Perturbation acceleration	Impulse: $A_i = 8\mu\text{g}$ Periodic: $A_p = 8\mu\text{g}$ $\tau_p = 75 - 125 \text{ sec}$	± 1%	COLD-SAT gyros and accelerometers, or compute from thruster firing histories

**TABLE 3.2-2 COLD-SAT TEST MATRIX**

First Priority Tests					
Tank	Fill	Axial g	Bond No.	Perturbation	Test Time
Cylinder	60%	8 $\mu$ g	0.5	Impulse: $A_f=8\mu$ g $\tau_f=20$ sec	720 sec $\tau_s \approx 180$ sec liquid above baffle
Cylinder	60%	32 $\mu$ g	1.8	Impulse: $A_f=8\mu$ g $\tau_f=20$ sec	600 sec $\tau_s \approx 160$ sec liquid above baffle
Cylinder	60%	100 $\mu$ g	5.8	Impulse: $A_f=8\mu$ g $\tau_f=20$ sec	400 sec $\tau_s \approx 100$ sec liquid above baffle
Cylinder	60%	100 $\mu$ g	5.8	Periodic: $\tau_p=100$ sec $A_f=8\mu$ g	1000 sec $\tau_s \approx 100$ sec liquid above baffle
Cylinder	40%	32 $\mu$ g	1.8	Impulse: $A_f=8\mu$ g $\tau_f=20$ sec	600 sec $\tau_s \approx 160$ sec liquid at baffle
Sphere	50%	8 $\mu$ g	0.5	Impulse: $A_f=8\mu$ g $\tau_f=20$ sec	3400 sec $\tau_s \approx 860$ sec
Sphere	50%	32 $\mu$ g	1.8	Impulse: $A_f=8\mu$ g $\tau_f=20$ sec	800 sec $\tau_s \approx 200$ sec
Sphere	50%	100 $\mu$ g	5.8	Impulse: $A_f=8\mu$ g $\tau_f=20$ sec	430 sec $\tau_s \approx 107$ sec
Sphere	50%	32 $\mu$ g	1.8	Periodic: $\tau_p=107$ sec $A_f=8\mu$ g	2000 sec $\tau_s \approx 200$ sec
Sphere	50%	100 $\mu$ g	5.8	Periodic: $\tau_p=200$ sec $A_f=8\mu$ g	1100 sec $\tau_s \approx 107$ sec
Second Priority Tests					
Tank	Fill	Axial g	Bond No.	Perturbation	Test Time
Sphere	33%	100 $\mu$ g	5.8	Impulse: $A_f=8\mu$ g $\tau_f=20$ sec	500 sec $\tau_p \approx 125$ sec
Sphere	33%	100 $\mu$ g	5.8	Periodic: $\tau_p \approx 125$ sec $A_f=8\mu$ g	1250 sec $\tau_p \approx 125$ sec
Sphere	75%	100 $\mu$ g	5.8	Impulse: $A_f=8\mu$ g $\tau_f=20$ sec	350 sec $\tau_p \approx 125$ sec
Sphere	75%	100 $\mu$ g	5.8	Periodic: $\tau_p \approx 75$ sec $A_f=8\mu$ g	750 sec $\tau_p \approx 125$ sec

for the Shuttle. The flight experiment does not contemplate thrusting to increase the settling acceleration to give larger Bond numbers. The use of very small Bond numbers has the advantage that the slosh characteristics for a given tank size and shape are nearly independent of the magnitude of the settling acceleration; hence, accurate measurements of the Shuttle ambient acceleration are not required. All the tests will be conducted with half-full tanks that have been pre-loaded and sealed on the ground.

The desired perturbation accelerations will be provided by a controllable electrodynamic shaker attached between the locker mounting plate and tank support plate, as shown in Figure 3.3-1. When the test tanks are cylindrical, the axis of the tanks must be aligned with the steady g-vector at the locker location to within  $\pm 2^\circ$  to preserve the symmetry of the liquid free surface configuration. To accomplish this while allowing some flexibility in the experiment integration and mission planning, the orientation of the shaker and tank support plate combination can be manually adjusted over a range of about  $\pm 15^\circ$  before the experiment is installed in the locker. Orientation of the spherical test tanks with respect to the g-vector is not critical, but the axis of the electrodynamic shaker should still be roughly perpendicular to the g-vector in order to excite lateral sloshing.

For the proposed tank sizes, the liquid motions of the types to be studied in the experiment are insensitive to vernier RCS firings because the magnitude and duration of the resulting tank accelerations are less than that required to destabilize the free surface. They should also be insensitive to g-jitter because of the large mismatch between the g-jitter frequencies and the slosh natural frequencies. Accelerations from a main RCS firing will, however, cause the liquid surface to break up or grossly reorient, so the longer duration tests must be conducted during quiet times.

The weights, power, and size requirements are within middeck allowables, assuming that a Shuttle video camcorder can be supplied by NASA without penalty to the experiment. Trade studies during further analysis (i.e., Phase B of a normal flight experiment program) may indicate that motion pictures offer significant advantages over video recordings; if so, the experiment can be expanded to three middeck lockers to permit additional battery power for the motion picture cameras and lighting. The c.g. location of the flight experiment package is about 10 in. (25 cm) from the face of the double adapter plate. Lockout mechanisms will be installed between the tanks and the support plate and between the support plate and the locker side braces to eliminate potential damage during launch and re-entry.

### **3.3.2 Measurements and Instrumentation**

The static orientation and the dynamic motions of the liquid free surface will be measured by liquid-vapor sensors and recorded by a camcorder or motion picture camera focused on the test tank. Slosh force and torques will be measured by load cells. The tank table accelerations will be measured by accelerometers mounted on the table. The table displacement and frequency will be

measured by a linear variable differential transformer (LVDT). All the measurements are within the capabilities of instrumentation used in previous ground studies. Figure 3.3-3 shows a block diagram of the instrumentation.

A controller for the shaker actuator is included in the design to produce the desired excitation waveforms. Frequencies of 0.003 to 0.1 Hz are required. An onboard data logger - controller - mass storage computer will be used to acquire up to 60 channels of analog data which will be converted to 10-bit digital form for storage. All the instrumentation and data acquisition equipment will operate on the 28 volt d.c. power available at the middeck lockers.

### **3.3.3 Hardware Requirements**

Table 3.3-1 lists the weights, sizes, and power requirements of the primary subsystems of the flight experiment. The listed weights, power consumptions, etc., are based on commercially available equipment.

### **3.3.4 Test Matrix**

The test matrix is shown in Table 3.3-2. Five types of tests are defined:

**Ambient configuration** — The liquid interface shape will be measured before each test (i.e., without excitation). The measurements will be used to validate analytical models and to confirm the desired initial conditions.

**Small amplitude impulsive translation** — An impulsive displacement will be applied by the shaker. The free decay of the wave motion (force and wave amplitude) will be recorded for up to eight slosh cycles. The tests will establish the fundamental slosh frequency, the frequency of any excited higher modes, and the viscous damping of the fundamental mode, all of which can be used to validate analytical models. Additionally, the results will allow the controller software to be updated to make subsequent harmonic excitation tests less time consuming.

**Small amplitude harmonic translation** — The table frequency will be swept from 25% below the fundamental slosh frequency to 25% above it. Force amplitude and phase angle and surface wave amplitude will be measured continuously. These tests can be used to improve and validate analytical models and to establish equivalent mechanical models of low gravity sloshing.

**Large amplitude harmonic translation** — The table frequency will be held constant for 8 to 10 cycles at a few specific frequencies near the slosh natural frequency. The amplitude of the shaker actuator will be considerably larger than for the previously described tests in order to excite nonlinear, rotary sloshing. Slosh force (in-line and cross-axis) and phase angle and free surface orientation will be measured. The results will be used to assess the importance of nonlinear effects in low gravity and to validate and improve analytical models.

**TABLE 3.3-1. SUBSYSTEM POWER REQUIREMENTS, SIZES, AND WEIGHTS  
FOR SHUTTLE FLIGHT EXPERIMENT**

<b>Component</b>	<b>Size (in)</b>	<b>Weight (lb)</b>	<b>Power (watts)</b>
Spherical Tank #1	13 (dia)	5.5	---
Spherical Tank #2	7 (diam)	1.1	---
Spherical Tank #3	7 (diam)	1.1	---
Fluid in Tank #1	----	27.7	----
Fluid in Tank #2	----	2.4	----
Fluid in Tank #3	----	0.6	----
Double Adapter Plate	18.1 x 21.9 x 0.9	14.4	----
Experiment Enclosure	18.0 x 22.0 x 20.0	12.5	----
Tank Support Stand	17.0 x 21.0 x 7.0	10.0	----
Table Alignment/Support	8.0 diam x 5.0	20.0	----
Actuator Controller	3.3 x 2.3 x 1.0	0.8	25.0
Strain Gages (12 ea)	----	2.4	----
Strain Gage Elect. (12 ea)	3.0 x 3.0 x 5.4	2.6	36.0
Liquid-Vapor Sensors (27 ea)	----	2.0	----
Liquid Detect. Electronics	3.0 x 3.0 x 5.4	2.0	36.0
Controller/Logger	1.5 x 2.3 x 5.4	1.1	0.3
Misc.			
- Nuts & Bolts		3	
- Wire			
- P,T Sensors	----		
<b>TOTAL</b>		<b>109.2</b>	<b>97.3</b>

**TABLE 3.3-2 PRELIMINARY SHUTTLE FLIGHT EXPERIMENT MATRIX**

<b>Tank</b>	<b>Fill</b>	<b>Bond No.</b>	<b>Perturbation</b>	<b>Test Time</b>	<b>Comments</b>
13 in Sphere	50%	0.025	Impulse: $A_i = 0.5\mu g$ $\tau_i = 20$ sec	1440 sec	$\tau_s \approx 180$ sec 8 slosh cycles
7 in Sphere (2)	50%	0.005	Impulse: $A_i = 0.5\mu g$ $\tau_i = 10$ sec	560 sec	$\tau_s \approx 70$ sec 8 slosh cycles
13 in Sphere	50%	0.025	Periodic: $A_i = 0.2\mu g$ $135 \text{ sec} < \tau_p \leq 225 \text{ sec}$	5400 sec (3 tests total)	$\tau_s \approx 180$ sec frequency sweep
7 in Sphere (2)	50%	0.005	Periodic: $A_i = 0.2\mu g$ $50 \text{ sec} < \tau_p \leq 90 \text{ sec}$	2100 sec (3 tests total)	$\tau_s \approx 70$ sec frequency sweep
13 in Sphere	50%	0.025	Periodic: $A_i = 0.5\mu g$ $\tau_p \approx 180$ sec	2700	$\tau_s \approx 160$ sec study rotary slosh
13 in Sphere 7 in Sphere (2)	50%	0.025 0.005	Impulse: $A_i = 8\mu g$ $\tau_i = 20$ sec	2100 sec	study reorientation- like responses

---

Note: Ambient acceleration assumed =  $2\mu g$

**Large amplitude impulsive translation** — A large translational impulse will be applied to all the tanks simultaneously. After the initial large liquid motion is over, the settling time will be determined by measuring free surface orientations. The results can be used to improve and validate computational fluid dynamics codes of liquid reorientation and settling.

The total test time, not necessarily continuous, is about four hours. Individual tests, which must be continuous, last from about 7 minutes to 35 minutes.



## 4.0 ANALYTICAL MODELS

### 4.1 General

Several different studies were pursued for prediction of liquid motions in low gravity. First, two computational fluid dynamics codes that can model free surface motions — FLOW-3D and NASA-VOF3D — were investigated to determine their ability to simulate sloshing at small Bond numbers. Both codes are widely used to simulate liquid motions in low gravity when *inertia forces* control the motions, as, for example, occurs when a large acceleration is induced by thrusting. The present investigation indicated, however, that neither code yields a satisfactory simulation of liquid motions when *surface forces* are dominant, such as might occur during spacecraft station-keeping or guidance maneuvers or after large amplitude motions have decayed to small amplitude sloshing. For that reason, an analysis of small-amplitude low gravity sloshing in axisymmetric tanks was developed here and implemented computationally using available finite-element technology. This model, which is described in Section 4.4, is meant to supplement FLOW-3D or NASA-VOF3D. In addition, an existing spherical pendulum mechanical analogy of nonlinear, rotary sloshing was modified to allow greater ease of numerical predictions and extended to low gravity conditions. This development is described in Section 4.5.

### 4.2 FLOW-3D Simulations

FLOW-3D (1988 version) was used to simulate sloshing in a one-meter spherical tank for Bond numbers of 0.1, 1.0, and 10.0. The contact angle for the simulations was 5° and it was held constant during motion by activating the "wall adhesion" option. The equilibrium shape and position of the free surface were computed separately and input to FLOW-3D as an initial condition. A small lateral velocity was imparted to the tank to initiate the sloshing.

The simulation was poor for all Bond numbers. In fact, the gas bubble above the free surface did not remain at its equilibrium position even when no motion was imparted to the tank, but instead migrated to the center of the tank. This behavior prevented the computation of realistic sloshing motions. After discussing the results with Flow Science, Inc. (the developers of FLOW-3D), it was concluded that the way surface tension and wall adhesion are modeled in FLOW-3D is not adequate to represent conditions in which surface tension forces are large compared to body forces.

Consequently, Flow Science, Inc., through a subcontract with SwRI, reviewed the modeling of surface effects in FLOW-3D and suggested several possible improvements that would in principle allow the code to be extended to small Bond number conditions; the suggested improvements are documented in [18]. As a result of this review, a significant improvement in the wall adhesion model was incorporated in the 1990 version of FLOW-3D, which removes the tendency of the gas bubble to migrate away from the walls toward the center of the tank. A more exact representation

of surface tension forces is also being evaluated but not yet incorporated in FLOW-3D. Until these improvements are incorporated, FLOW-3D is not capable of realistic simulations of sloshing when surface tension forces are predominant.

#### **4.3 NASA-VOF3D Simulations**

NASA-VOF3D and FLOW-3D both share the same structure and basic VOF (volume of fluid) algorithms. In particular, the representation of surface tension forces is similar for both codes, although NASA-VOF3D does not specifically contain a "wall adhesion" option to maintain a constant contact angle. Los Alamos National Laboratory (LANL) has modified the original VOF series of codes, under NASA sponsorship, to make them more applicable to fluid motions in low gravity. Since NASA-VOF3D is a vectorized code that executed quite slowly on SwRI's VAX 8700, SwRI requested LANL personnel to run the same three simulations attempted with FLOW-3D on LANL's CRAY computer. The sequence of visualizations shown in Figure 4.3-1 gives some typical results from the LANL simulations. The bulk of the liquid surface does move in a sloshing-like wave motion but the contact line appears to be stuck to the wall. Furthermore, numerical convergence problems (which LANL has since eliminated) caused a fictitious wave to appear on the surface at  $r = 0$  which then propagated away from the center. It was concluded that the surface force representation in NASA-VOF3D must be improved before realistic simulations of small Bond number sloshing are possible.

Both FLOW-3D and NASA-VOF3D solve unsteady flow problems by time-stepping from a known initial condition to a final condition that is compatible with a specified motion of the tank. They are thus inherently clumsy to use as a method of predicting, for example, the natural frequency of an oscillatory liquid motion. Consequently, as a tool for control system simulations or as a means of establishing equivalent mechanical models, neither code is as useful as the "eigenvalue" type of codes routinely used for high gravity sloshing.

#### **4.4 Linearized Low Gravity Sloshing Model**

##### **4.4.1 Background**

Since the surface phenomena which can dominate low gravity motions are not yet well understood, previous analyses of low gravity liquid sloshing [7, 19-23, including FLOW-3D and NASA-VOF3D] have assumed simplified and perhaps unrealistic surface conditions; a typical assumption is that the contact angle remains constant during liquid motions, independent of the contact line velocity (i.e., the contact line is "free"). In the analysis described here, the equations of linear low-gravity sloshing are formulated and reduced to an integral-minimization technique that, while at present employing the same simplified surface physics assumptions as previous analyses, does permit a better representation of surface physics phenomena to be incorporated readily when the needed understanding becomes available. Errors in previous analyses of the low-g slosh force are also corrected in the present treatment. The equations are solved by a numerical

method based on a finite element *structural* code; the solution method can thus be easily adopted by other investigators. Several numerical examples are presented, and the parameters of an equivalent mechanical model are also computed.

#### 4.4.2 Equations of Motion

Most tanks used in space applications are axisymmetric, and most liquids used in space applications are incompressible and nearly inviscid. Thus, the following idealizations are employed in the analysis:

- the tank and static liquid configuration are axisymmetric;
- the liquid motion is irrotational and derivable from a velocity potential  $\phi$ ;
- the motions are small enough to permit the equations to be linearized; and
- only those slosh modes are considered that vary as the cosine of angular coordinate  $\theta$ , since such modes are the only ones that produce a net force or moment on the tank.

When needed, viscous damping can be incorporated as a small correction by the methods described by Abramson, et Al. [1].

The geometry is shown in Figure 4.4-1. Because the contact angle  $\gamma_c$  is small, the equilibrium free surface is highly curved. (Both the bottom and top of the tank can be dry for some combinations of low filling levels, tank shape, and  $\gamma_c$  [24], but such cases are not considered here.) A surface-normal coordinate system  $s, \theta, n$  is used to analyze the boundary conditions at the free surface in order to avoid the possibility of double valued expressions.

The velocity potential must satisfy the condition of liquid incompressibility:

$$\nabla^2 \phi = \frac{1}{r} \frac{\partial}{\partial r} \left( r \frac{\partial \phi}{\partial r} \right) + \frac{1}{r^2} \frac{\partial^2 \phi}{\partial \theta^2} + \frac{\partial^2 \phi}{\partial z^2} = 0 \quad \text{in the fluid volume, } V \quad (4.4-1)$$

Since the liquid cannot penetrate the tank walls,  $\phi$  must satisfy the "no flow" condition at the walls:

$$\nabla \phi \cdot \vec{n} \equiv \frac{\partial \phi}{\partial n} = 0 \quad \text{on the walls, } w \quad (4.4-2)$$

where  $\vec{n}$  is the outward-pointing normal. At the free surface, the wave velocity must be compatible with the liquid velocity:

$$\frac{\partial \eta}{\partial t} = \frac{\partial \phi}{\partial n} \quad \text{on the free surface, } f \quad (4.4-3)$$

where  $\eta$  is the wave height measured *normal* to the free surface, as shown in Figure 4.4-1.

The wave height and liquid velocity must be interrelated so as to satisfy the requirement of constant pressure  $p$  at the free surface. This relationship can be expressed as:

$$p + \rho g \left( z + \eta \frac{dr}{ds} \right) + \rho \frac{\partial \phi}{\partial t} = q(t) \quad \text{on the free surface, } f \quad (4.4-4)$$

where  $q(t)$  is a function of at most time, and  $r(s)$  is evaluated on  $f$ . Since the liquid pressure at the surface is less than the gas pressure immediately above the liquid because of surface tension,  $p$  must also satisfy the relation that:

$$p = p_g - 2\sigma\kappa \quad \text{on the free surface, } f \quad (4.4-5)$$

where  $2\kappa$  is the mean curvature of the surface. From differential geometry, the mean curvature is related to the equation of the moving free surface, say  $\mathcal{F}(s, \theta, t) = n - \eta(s, \theta, t) = 0$ , by  $2\kappa = -\nabla \cdot (\nabla \xi / |\nabla \xi|)$ . Linearizing this expression for  $2\kappa$  with respect to the slosh wave height gives:

$$2\kappa = \frac{1}{r} \frac{\partial}{\partial s} \left( r \frac{\partial \eta}{\partial s} \right) + \frac{1}{r^2} \frac{\partial^2 \eta}{\partial \theta^2} + \left( \frac{1}{r_1^2} + \frac{1}{r_2^2} \right) \eta + \left( \frac{1}{r_1} + \frac{1}{r_2} \right) \quad (4.4-6)$$

Here  $r_1, r_2$  are the principal radii of curvature of the *equilibrium* free surface:

$$\frac{1}{r_1} = \left( \frac{d^2 z}{ds^2} \right) \frac{dr}{ds} - \frac{dz}{ds} \left( \frac{d^2 r}{ds^2} \right); \quad \frac{1}{r_2} = \frac{1}{r} \left( \frac{dz}{ds} \right) \quad (4.4-7)$$

where  $r$  and  $z$  are evaluated on  $f$ . By combining Eqs. (4.4-4)-(4.4-7), subtracting out the time-independent terms (which are the equations of the equilibrium free surface described later), and absorbing  $q(t)$  into the gas pressure, the "dynamic" boundary condition of constant pressure at the free surface is obtained:

$$\left[ \left( \frac{\rho g}{\sigma} \right) \left( \frac{dr}{ds} \right) - \frac{1}{r} \frac{\partial}{\partial s} \left( r \frac{\partial}{\partial s} \right) - \frac{1}{r^2} \left( \frac{\partial^2}{\partial \theta^2} \right) - \left( \frac{1}{r_1^2} + \frac{1}{r_2^2} \right) \right] \eta = - \left( \frac{\rho}{\sigma} \right) \frac{\partial \phi}{\partial t} \quad \text{on } f \quad (4.4-8a)$$

Equations (4.4-3) and (4.4-8a) can be combined to eliminate the wave height  $\eta$ :

$$\left[ \left( \frac{\rho g}{\sigma} \right) \left( \frac{dr}{ds} \right) - \frac{1}{r} \frac{\partial}{\partial s} \left( r \frac{\partial}{\partial s} \right) - \frac{1}{r^2} \left( \frac{\partial^2}{\partial \theta^2} \right) - \left( \frac{1}{r_1^2} + \frac{1}{r_2^2} \right) \right] \left( \frac{\partial \phi}{\partial n} \right) = - \left( \frac{\rho}{\sigma} \right) \frac{\partial^2 \phi}{\partial t^2} \quad \text{on } f \quad (4.4-8b)$$

A free contact line (i.e., constant contact angle) is sometimes a reasonable approximation for some liquids and tank wall materials [7]. Hence, pending the acquisition of better knowledge from space experimentation, that condition is assumed here. With reference to the sketch shown in Figure 4.4-2a, this assumption reduces to:

$$\cos \gamma_c = \vec{n}_w(t) \cdot \vec{n}_\eta(t) = (\vec{n}_w + \Delta \vec{n}_w) \cdot (\vec{n}_\eta + \Delta \vec{n}_\eta) \approx \vec{n}_w \cdot \vec{n}_\eta + \vec{n}_w \cdot \Delta \vec{n}_\eta + \vec{n}_\eta \cdot \Delta \vec{n}_w \quad (4.4-9)$$

For the equilibrium surface, the unit vectors in Eq. (4.4-9) can be expressed as:

$$\vec{n}_w = \cos \gamma_c \vec{e}_n - \sin \gamma_c \vec{e}_s; \quad \vec{n}_\eta = \vec{e}_n \quad (4.4-10a)$$

and to the first order in the arc lengths  $\Delta s$  and  $\Delta \xi$ , the changes in the unit vectors as the surface moves away from its equilibrium position are:

$$\Delta \vec{n}_\eta = -\Delta s \left( \frac{d\psi}{ds} \right) \vec{e}_s - \left( \frac{\partial \eta}{\partial s} \right) \vec{e}_s - \frac{1}{r} \left( \frac{\partial \eta}{\partial \theta} \right) \vec{e}_\theta \quad (4.4-10b)$$

$$\Delta \vec{n}_w = -\Delta \zeta \left( \frac{d\chi}{d\xi} \right) (\cos \gamma_c \vec{e}_s + \sin \gamma_c \vec{e}_n) \quad (4.4-10c)$$

Since  $\Delta s \equiv \eta \cot \gamma_c$  and  $\Delta \zeta \equiv \eta / \sin \gamma_c$ , the assumed condition at the contact line thus reduces to:

$$\sin \gamma_c \frac{\partial \eta}{\partial s} + \left( \frac{d\psi}{ds} \cos \gamma_c - \frac{d\chi}{d\xi} \right) \eta = 0 \quad \text{at the contact line, } s = s_c \quad (4.4-11)$$

Note that Eq. (4.4-11) is satisfied identically when  $\gamma_c = 0^\circ$ . Methods of incorporating contact line conditions other than the free condition will be discussed later.

#### 4.4.3 Equilibrium Surface

Dropping the time-dependent terms from the combination of Eqs. (4.4-4) and (4.4-5) gives the equation of the equilibrium free surface  $z = f(s)$ :

$$\rho g f - \sigma \left( \frac{1}{r_1} + \frac{1}{r_2} \right) = p_o - p_s = \lambda_o \quad (4.4-12)$$

with boundary conditions:

$$f = \frac{df}{ds} = 0 \quad \text{at } s = 0 \ (r = 0, z = -z_o); \quad \chi - \psi = \gamma_c \quad \text{at } s = s_c \ (r = r_c, z = z_c) \quad (4.4-13)$$

The second part of Eq. (4.4-13) merely states that the slope angle of the free surface and the slope angle of the wall differ by the contact angle at the contact point. The pressure-reduction parameter  $\lambda_o$  and the coordinates  $z_o$ ,  $s_c$ ,  $r_c$ , and  $z_c$  must be determined as part of the solution such that the volume of liquid under the free surface is equal to the specified liquid volume.

#### 4.4.4 Slosh Force

In normal gravity, the slosh force is due entirely to the time-dependent liquid pressure exerted on the wetted walls. In low gravity, however, the "pull" of surface tension on the tank walls becomes unbalanced, which creates an additional force, and the pressure force itself includes a component that is negligible in normal gravity.

The part of the lateral slosh force that is caused by the pressure on the tank walls is:

$$F_p = \int_0^{2\pi} \int_{-d}^{f_c + \eta_i \sin \chi} [p_o - \rho g z - \rho(\partial \phi / \partial t)] \Big|_{r=r_w} r_w \cos \theta dz d\theta \quad (4.4-14)$$

In this equation,  $\eta_i$  is the wave height at the contact line measured *tangential* to the wall (i.e.,  $\eta_i$  corresponds to the wetted wall), and  $\eta_i \sin \chi$  is the *vertical* displacement of the wave at the contact line (see Figure 4.4-2a). Note that  $\eta_i = \eta_c \cot \gamma_c$ , where  $\eta_c = \eta(s = s_c, \theta, t)$  is the wave height measured

normal to the free surface at the contact line. Since the slosh modes of interest vary with  $\cos \theta$ , the potential can be expressed as  $\phi = \bar{\phi}(r, z, t) \cos \theta$  and the wave height as  $\eta = \bar{\eta}(s, t) \cos \theta$ . Thus, Eq. (4.4-14) can be integrated with respect to  $\theta$  and then linearized with respect to  $\bar{\phi}$  and  $\bar{\eta}$  to give:

$$F_p = [(p_o - \rho g f_c) \pi r_c \cot \gamma_c \sin \chi] \bar{\eta}_c - \pi \rho \int_{-d}^{f_c} (\partial \bar{\phi} / \partial t) |_{r=r_c} r_w dz \quad (4.4-15)$$

The term  $p_o - \rho g f_c$ , which is equal to  $-2\sigma \kappa_c$ , represents the pressure discontinuity from the gas to the liquid at the contact line that is caused by capillarity. Some previous analyses [e.g., 21] have linearized Eq. (4.4-14) before performing the integration and thus have incorrectly neglected this term.

For the equilibrium surface, surface tension pulls on the tank walls equally around the circumference of the contact line, and there is clearly no net lateral force. But during sloshing, the contact line is displaced along the walls, and the surface tension pull becomes unbalanced. With reference to Figure 4.4-2b, a surface tension force  $\sigma da$  is exerted on a differential element  $da$  of the displaced contact line. The component of this force in the plane of the wall is  $\sigma da \cos \gamma_c$ . The force is inclined to the horizontal at the small angle  $\tan^{-1}(-\partial \eta_l / r_w \partial \theta) \approx -\partial \eta_l / r_w \partial \theta$ . Since  $da \approx r_w d\theta$  to first order, the net lateral force  $F_\sigma$  exerted on the tank by surface tension at the contact line is therefore:

$$F_\sigma = -\sigma \cos \gamma_c \cot \gamma_c \int_0^{2\pi} (\partial \eta / \partial \theta) |_{r=r_c} \sin \theta d\theta = (\pi \sigma \cos \gamma_c \cot \gamma_c) \bar{\eta}_c \quad (4.4-16)$$

With the exception of [7], previous analyses of the low-g slosh force have not considered  $F_\sigma$ .

The total lateral slosh force  $F_p + F_\sigma$  is:

$$F = -\pi \rho \int_{-d}^{f_c} (\partial \bar{\phi} / \partial t) r_w dz - [\pi \sigma \cot \gamma_c (2 \kappa_c r_c \sin \chi - \cos \gamma_c)] \bar{\eta}_c \quad (4.4-17)$$

When the first part of Eq. (4.4-15) is neglected [21], the calculated slosh force will be too large. When  $F_\sigma$  is neglected [19, 20], the slosh force will be too small and can even be of the wrong sign.

The slosh moment can be developed similarly but, for brevity, is not presented here. It is included, however, in the computer programs used to make numerical predictions.

#### 4.4.5 Non-Dimensional Equations

For numerical work, it is best to solve the equations in non-dimensional form. Furthermore, since free vibrations are of interest, the equations are reduced to an eigenvalue problem by assuming that  $\phi$  varies harmonically in time as  $\exp(i\omega t)$ , where  $\omega$  is the slosh natural frequency to be determined. Upper case letters are used for non-dimensional coordinates (for example,  $S = s/R_o$ ).

The non-dimensional potential  $\Phi$  is defined as  $\phi/\sqrt{(1+Bo)\sigma R_o/\rho}$ , the non-dimensional frequency  $\Omega$  as  $\omega/\sqrt{(1+Bo)\sigma/\rho R_o^3}$ , and the non-dimensional wave height  $H$  as  $i\eta/R_o$ . After cancelling the common factor  $\exp(i\omega t)$  from all the equations, the non-dimensional form of the equations are:

$$\nabla^2 \Phi = 0 \quad \text{in } V \quad (4.4-18)$$

$$\frac{\partial \Phi}{\partial N} = 0 \quad \text{on } W \quad (4.4-19)$$

$$\Omega H = \frac{\partial \Phi}{\partial N} \quad \text{on } F \quad (4.4-20)$$

$$\left[ Bo \left( \frac{dR}{dS} \right) - \frac{1}{R} \frac{\partial}{\partial S} \left( R \frac{\partial}{\partial S} \right) - \frac{1}{R^2} \frac{\partial^2}{\partial \theta^2} - \left( \frac{1}{R_1^2} + \frac{1}{R_2^2} \right) \right] \left( \frac{\partial \Phi}{\partial N} \right) = (1+Bo)\Omega^2 \Phi \quad \text{on } F \quad (4.4-21)$$

$$\sin \gamma_c \frac{\partial H}{\partial S} + \left( \frac{d\psi}{dS} \cos \gamma_c - \frac{d\chi}{d\Xi} \right) H = 0 \quad \text{at } S = S_c \quad (4.4-22)$$

The non-dimensional slosh force amplitude is:

$$\frac{F}{\sigma R_o} = \pi \Omega (1+Bo) \left\{ \int_{-D}^{F_c} \bar{\Phi}|_{R=R_w} R_w dZ - \left[ \frac{(2K_c R_c \sin \chi - \cos \gamma_c) \cot \gamma_c}{(1+Bo)\Omega} \right] \bar{H}_c \right\} \quad (4.4-23)$$

where as before a bar over a quantity means that the  $\theta$  dependency has already been removed. Equation (4.4-23) clearly shows that the force components caused by surface tension (i.e., proportional to the wave height  $\bar{H}_c$ ) can be significant when the Bond number is small.

#### 4.4.6 Equivalent Mechanical Model

The dynamics of linear sloshing can also be represented exactly by an equivalent mechanical model [1]. An appropriate model is a pendulum of length  $l_s$  that has a mass  $m_s$  which represents the liquid fraction that participates in the fundamental mode of the sloshing, and a rigidly-attached mass which represents the rest of the liquid. (The mass participating in the higher frequency sloshing modes is usually negligible.) However, in contrast to normal sloshing, the pendulum of the low-gravity model must be attached to the tank through a torsional spring  $k_s$  which represents the stiffening effect of surface tension. From the non-dimensional process described in the previous section, the slosh natural frequency is expressed as:

$$\omega^2 = \Omega^2 [(1+Bo)\sigma/\rho R_o^3] \quad (4.4-24)$$

whereas the pendulum frequency is:

$$\omega_{pend}^2 = k_s/(m_s l_s^2) + g/l_s \quad (4.4-25)$$

Since these two frequencies must be the same for dynamic similarity, the parameters of the pendulum can be seen to be:

$$l_s = R_o \Omega^2 \quad (4.4-26a)$$

$$k_s = \Omega^2 \sigma m_s l_s^2 / \rho R_o^3 = \sigma R_o^2 m_s / \rho R_o^3 \Omega^2 \quad (4.4-26b)$$

Note that the ratio of the spring moment to the gravity moment,  $k_s / m_s l_s g$ , exerted on the pendulum pivot is equal to  $1/Bo$ , and thus becomes negligible when  $Bo$  is large; that is, the mechanical model reduces to the usual high gravity form when  $Bo$  is large.

The slosh mass  $m_s$  can be computed from the amplitudes of the slosh force and liquid kinetic energy, as can be seen by considering the equivalent development for the mechanical model. For the model, the amplitude of the force when the pendulum is undergoing free oscillations is  $F_{model} = m_s \omega^2 x_o$ , where  $x_o$  is the amplitude of the oscillation, and twice the kinetic energy is  $2KE_{model} = m_s \omega^2 x_o^2$ . The slosh mass is therefore equal to the ratio of the force squared to twice the kinetic energy, a result that is independent of the arbitrary amplitude  $x_o$ . The slosh mass can thus be computed by forming this ratio for the liquid. Twice the kinetic energy of the liquid is:

$$2KE = \rho \int \int \phi (\partial \phi / \partial n) dA \quad (4.4-27)$$

where the integral is evaluated on the free surface. The combination of Eq. (4.4-23) and the non-dimensional form of Eq. (4.4-27) then gives an expression for the slosh mass of the mechanical model:

$$\frac{m_s}{\pi \rho R_o^3} = \left\{ \int_{-D}^{F_c} \bar{\Phi} |_{R=R_w} R_w dZ - \frac{[(2K_c R_c \sin \chi - \cos \gamma_c) \cot \gamma_c] H_c}{[(1 + Bo) \Omega]} \right\}^2 / \int_0^{S_c} \bar{\Phi} \left( \frac{\partial \bar{\Phi}}{\partial N} \right) R dS \quad (4.4-28)$$

Although not developed here, an expression for the location of the pendulum pivot can be determined similarly from the slosh moment exerted on the tank. It is included, however, in the computer programs used to make numerical predictions.

#### 4.4.7 Integral Formulation

Equations (4.4-18)-(4.4-22) completely describe linear sloshing for the stated assumptions. They are, however, not solvable in closed form except when  $\gamma_c = 90^\circ$  and then only for tank shapes that are coordinate surfaces. Hence, an approximate analytical method or a numerical method is needed. Most such methods apply only to the particular set of equations for which they have been developed and cannot be generalized. The solution method can be made much more amenable to changes in the surface physics assumptions by transforming the basic equations to an integral function form. The functions that minimize the integral are the desired solution. The appropriate integral can be derived by considering the kinetic, gravitational, and surface energies of the sloshing [25], or by partial integration and combination of Eqs. (4.4-18)-(4.4-22). The integral is:

$$\begin{aligned}
I(\Phi, H) = & \frac{1}{2}(1 + Bo)\Omega \int \int \int \nabla \Phi \cdot \nabla \Phi dV - (1 + Bo)\Omega^2 \int \int (\Phi H) dA_F \\
& + \frac{1}{2}\Omega \int \int \left[ \left( \frac{\partial H}{\partial S} \right)^2 + \left( \frac{1}{R} \frac{\partial H}{\partial \theta} \right)^2 + \left( \frac{1}{R_1^2} + \frac{1}{R_2^2} \right) H^2 - Bo \left( \frac{dR}{dS} \right) H^2 \right] dA_F \quad (4.4-29) \\
& - \frac{1}{2}\Omega \int \left[ \frac{R}{\sin \gamma_c} \left( \frac{d\psi}{dS} \cos \gamma_c - \frac{d\chi}{d\zeta} \right) H^2 \right]_{s=s_c} d\theta
\end{aligned}$$

This formulation has the additional advantage that, if trial solutions for  $H$  and  $\Phi$  can be derived from any convenient method, the actual sloshing potential can be determined by using the trial functions to minimize  $I(\Phi, H)$ . The trial functions do not necessarily have to satisfy all the boundary conditions. The biggest advantage is, however, that an improved contact line condition can be treated by modifying the line integral in Eq. (4.4-29), without changing the solution method.

#### 4.4.8 Structural Finite-Element Simulation

A finite element *structural* code was selected as the general method of finding *trial* solutions of Eqs. (4.4-18)-(4.4-22), for two reasons: (1) such codes can easily model the irregular and three-dimensional shapes that are typical of low- $g$  liquid geometries, and (2) expertise in the use of such codes is widespread.

By suppressing all the displacements of an elastic body but the  $x$ -component  $U$ , a structural finite element code can be forced to solve the following field equation [26]:

$$\left( \frac{\lambda + 2G}{G} \right) \frac{\partial^2 U}{\partial x^2} + \frac{\partial^2 U}{\partial y^2} + \frac{\partial^2 U}{\partial z^2} + \frac{\lambda + G}{G} \left( \frac{\partial^2 U}{\partial x \partial y} + \frac{\partial^2 U}{\partial x \partial z} \right) + \frac{1}{G} \mathcal{F}_x = \frac{\rho_s}{G} \frac{\partial^2 U}{\partial t^2} \quad (4.4-30)$$

where  $\lambda$  and  $G$  are elastic constants,  $\mathcal{F}_x$  is the body force, and  $\rho_s$  is the material density. By arbitrarily choosing  $\lambda = -G$  and  $\mathcal{F}_x = \rho_s = 0$ , Eq. (4.4-30) can be further reduced to:

$$\frac{\partial^2 U}{\partial x^2} + \frac{\partial^2 U}{\partial y^2} + \frac{\partial^2 U}{\partial z^2} \equiv \nabla^2 U = 0 \quad (4.4-31)$$

which is the desired governing equation for potential flow, Eq. (4.4-1) or Eq. (4.4-18).

A reactive traction force can be applied at any surface node (i.e., the nodes at the free surface or at the tank walls). The general form of this force is:

$$\frac{F_x}{GA_{j_s}} \equiv \frac{\partial U}{\partial n} = - \left[ a_1 U + a_2 \frac{\partial U}{\partial t} + a_3 \frac{\partial^2 U}{\partial t^2} + a_4 \right] \quad (4.4-32)$$

where  $A_{j_s}$  is the surface area of the finite element in question. Equation (4.4-32) will be used to simulate the slosh boundary conditions. For nodes on the tank walls, the no-flow boundary condition can be treated exactly by choosing  $a_1 = a_2 = a_3 = a_4 = 0$  since this makes  $\partial U / \partial n = 0$  at the nodes. However, the boundary condition of constant pressure at the free surface cannot be treated so easily.

The best feasible approximation to the free surface condition is to set  $a_1 = a_2 = a_4 = 0$  and to choose  $a_3$  (which is a mass-like parameter) as a representative value of all the terms within the square brackets in Eq. (4.4-8b); this choice makes  $\partial U / \partial n$  proportional to  $-\partial^2 U / \partial t^2$ , which is at least of the same form as Eq. (4.4-8b). [Since the  $a_i$  must be calculated in advance, they cannot depend on  $U$ , but this is what would be required to make Eq. (4.4-32) exactly the same as Eq. (4.4-8b).] The boundary condition that is actually applied to the nodes on the free surface is therefore:

$$\frac{\partial U}{\partial N} = -(1 + Bo)M(S)\frac{\partial^2 U}{\partial t^2} \quad (4.4-33a)$$

or, after eliminating the  $\exp(i\Omega\tau)$  factor:

$$\frac{\partial U}{\partial N} = (1 + Bo)\Omega^2 M(S)U \quad (4.4-33b)$$

where  $a_3 = (1 + Bo) M(S)$  is the specified distribution of fictitious masses at the surface nodes and the factor  $1 + Bo$  is included for analytical convenience.

Using the values for the  $a_i$  determined in this way, the structural code will yield a set of trial potential functions, say  $U_i$  for  $i = 1, 2, 3, \dots, K$ , and corresponding trial eigenvalues  $\Omega_i^2$ . The velocity potential for low-g sloshing is then expressed as:

$$\Phi = \sum_{i=1}^K b_i U_i \quad (4.4-34)$$

where the  $b_i$  are arbitrary parameters that must be chosen to minimize the integral, Eq. (4.4-29). Because the  $U_i$  trial functions identically satisfy Eqs. (4.4-18)-(4.4-20), the minimization process is simplified considerably. In addition,  $M(S)$ , as discussed below, will be chosen to satisfy the contact line condition, Eq. (4.4-11), which further simplifies the minimization process. The result is that Eq. (4.4-29) reduces to the simpler form:

$$\int_0^{S_c} \sum_j b_j \left\{ \left[ BoR \left( \frac{dR}{dS} \right) - \frac{\partial}{\partial S} \left( R \frac{\partial}{\partial S} \right) + \frac{1}{R} - R \left( \frac{1}{R_1^2} + \frac{1}{R_2^2} \right) \right] \frac{\partial \bar{U}_j}{\partial N} - \Omega_j^2 (1 + Bo) \bar{U}_j \right\} \frac{\partial \bar{U}_i}{\partial N} dS = 0 \quad (4.4-35)$$

for  $i = 1, 2, 3, \dots, K$ , evaluated on the free surface.. Integration with respect to  $\theta$  has already been performed. From Eq. (4.4-33), the  $\partial \bar{U}_j / \partial N$  terms in Eq. (4.4-35) can be replaced by the corresponding  $(1 + Bo)M\Omega_j^2 \bar{U}_j$  terms. The integration can therefore be performed readily using only the nodal values  $\bar{U}_i$  along the line  $\theta = 0^\circ$  (i.e., without any need for numerical differentiation of  $U_i$ ). Equation (4.4-35) is a matrix eigenvalue problem which yields the non-dimensional slosh frequency  $\Omega^2$  and eigenvectors  $b_i$ . For cases when the trial functions cannot be made to satisfy the contact line condition, the contribution from the appropriate form of the line integral in Eq. (4.4-29) must also be included in Eq. (4.4-35).

#### 4.4.9 Mass Distribution, $M(S)$

In common with most integral-approximation solution techniques, it is relatively easy to insure that the numerical method predicts natural frequencies, or eigenvalues, with good accuracy. It is more difficult to insure that mode shapes, or eigenvectors, are predicted accurately. Nonetheless, it is important to predict the mode shapes accurately, because, as shown by Eq. (4.4-23), the slosh force, and therefore the slosh mass, is a function of the *point* value of the wave amplitude at the wall rather than on an *integral average*. Equation (4.4-20) shows that the wave shape is proportional to the value of the normal derivative of  $\partial U/\partial N$  of the trial mode  $U$  evaluated at the free surface, and Eq. (4.4-33), shows that the choice of the mass-distribution function  $M(S)$  has a strong influence on  $\partial U/\partial N$ . Hence, the selection of  $M(S)$  is a critical part of the numerical method.

There are several conditions that  $M(S)$  should satisfy to make the trial functions  $U$  a good approximation to the true potential  $\Phi$ . Since the wall is impermeable,  $\partial U/\partial N$  is identically zero on the *tank wall*; thus, if  $\gamma_c$  were also zero, continuity would require that  $\partial U/\partial N$  on the *free surface* at the contact line should also be zero.. For numerical work,  $\gamma_c$  cannot be chosen to be exactly zero but it can be chosen to be small. Consequently,  $\partial U/\partial N$  on the free surface at the contact line should be "small," and the first requirement on  $M(S)$  is that it have a small numerical value at  $S = S_c$ . By symmetry, both  $U$  and the wave amplitude are zero at the centerline of the tank  $S = 0$ . Hence, the wave amplitude must have a maximum between the centerline and the wall of the tank. Thus, the second requirement on  $M(S)$  is that it must cause the wave to have its maximum amplitude somewhere between  $S = 0$  and  $S = S_c$ . A mass distribution that satisfies both requirements is:

$$M(S) = 1 + e - (S/S_c)^m \quad (4.4-36)$$

The small parameter  $e$  determines how closely  $\partial U/\partial N$  approaches zero at the contact point, and the exponent  $m$  helps fix the overall shape of the wave.

The parameters  $e$  and  $m$  must be interrelated in order to satisfy the contact line condition, Eq. (4.4-22). To derive this condition it is assumed that  $U$  is proportional to  $S$  for the *fundamental* mode (which is known to be approximately true for high-g sloshing and, as shown by the following numerical examples, is also true for low-g sloshing). With this assumption, Eq. (4.4-22) can be manipulated to give:

$$e = \left\{ \frac{\sin \gamma_c}{S_c [(d\psi/dS) \cos \gamma_c - (d\chi/d\Xi)] + \sin \gamma_c} \right\}^m \quad (4.4-37)$$

The term in curly brackets can be computed directly from the shape of the free surface. Equation (4.4-37) is not correct for the higher order trial modes, since they are not even approximately linearly proportional to  $S$ . Fortunately, the contact line is always satisfied reasonably well when  $\gamma_c$  is small, so the discrepancy between  $e$  and  $m$  for the higher modes is not a serious limitation.

#### 4.4.10 Numerical Examples

Several numerical examples were computed for a spherical tank to demonstrate the use of the analytical and numerical methods described above. To begin the calculations, a FORTRAN computer code was written to predict the equilibrium free surface shape  $F(S)$  by numerically integrating Eqs. (4.4-12) and (4.4-13), as a function of  $Bo$ , contact angle, and fill percentage. This computer code is described in Appendix B. Predictions were made for Bond numbers of 1 and 2, fill levels of 25%, 50%, and 78%, and a contact angle of  $5^\circ$ . Figure 4.4-3 shows the predicted equilibrium surfaces. ( $\gamma_c > 0$  was chosen because a contact angle of exactly  $0^\circ$  cannot be treated in the finite element structural code. The reason for not choosing  $Bo = 0$  as an example case will be discussed later. The 78% fill level was chosen, rather than the obvious choice of 75%, because for  $Bo = 2$  the lowest part of the surface coincides with the center of the tank,  $r = 0$ ,  $z = 0$ .)

A pre-processor (GIFTS) was used to compute the nodal coordinates for the finite elements of the structural simulation, using as input the tank shape and the free surface shape  $F(S)$  predicted by the FORTRAN code. ADINA, a commercially available structural code, was used for the example simulations, but other codes, such as NASTRAN, would have been equally suitable. The finite element model is shown in Figure 4.4-4. Because of the  $\cos \theta$  dependency of the desired trial modes, only one-quarter of the tank had to be simulated, with the lateral surface aligned with  $\theta = 0^\circ$  being a no-flow boundary  $\partial U / \partial N = 0$ , and the lateral surface aligned with  $\theta = 90^\circ$  being an anti-symmetrical boundary  $U = 0$ . It was found from preliminary numerical examples that 20 - 25 nodal points along the  $\theta = 0$  line were more than sufficient to ensure convergence.

All the wave shapes of the predicted trial modes were visualized with the aid of a graphical post-processor in order to select the desired subset of  $\cos \theta$  modes from the complete set of  $\cos(2N + 1)\theta$  modes which satisfy the imposed conditions for the one-quarter tank model. Generally, three such modes were selected. A QUICK BASIC computer code was written to perform the numerical integration of Eq. (4.4-35) and to compute the actual sloshing modes and the parameters of an equivalent mechanical model; this code is also described in Appendix B.

Numerical experimentation was required to find suitable values for the parameter  $m$ . Wave shapes predicted by previous finite difference analyses [20] allowed a reasonable starting value to be chosen for some cases, such as  $m = 2.5$  (and  $e = 0.1$ ) for a 50% full tank with  $Bo = 1$ . An iterative process was used to refine the starting values; the first set of trial functions was used to determine an estimate of the true wave shape, from which a second estimate of  $m$  and  $e$  was obtained, and so on. In practice, only one or two iterations were required. Perhaps an even better procedure would have been to use the first estimate of the wave shape to determine a new, *discrete* distribution of  $M(S)$  for the second and later iterations, rather than continue to use Eq. (4.4-36); however, this procedure was not used for these example numerical calculations.

Figure 4.4-5 shows typical results for the trial mode predictions, in this case for  $Bo = 1$  and 50% filling level. The corresponding trial eigenvalues  $\Omega_i^2$  were 0.4565, 1.5375, and 2.8853. The fundamental low-g slosh eigenvalue for this case was computed to be  $\Omega^2 = 0.7064$  and the corresponding eigenvectors were  $b_2/b_1 = 0.0158$  and  $b_3/b_1 = -0.0028$ . The eigenvalue of the second slosh mode was computed similarly to be  $\Omega^2 = 14.306$  and the eigenvectors were  $b_1/b_2 = 0.2611$  and  $b_3/b_2 = -0.0147$ . Figure 4.4-6 shows the computed slosh wave heights  $\bar{H}_1$  and  $\bar{H}_2$  for this case, along with the wave heights  $(\partial U_1/\partial N)/\Omega_1$  and  $(\partial U_2/\partial N)/\Omega_2$  of the first two trial functions, all normalized to have a peak amplitude of one.

**TABLE 4.4-1. SUMMARY OF LOW-G SLOSH PARAMETERS  
FOR A SPHERICAL TANK**

	Fill %	$\omega^2/(1 + Bo)\sigma/\rho R_o^3$	$\omega^2/(g/R_o)$	$m_s/m_{liquid}$	$l_s/2R_o$	$k_s/\sigma R_o^2$
$Bo = 1$	25	0.667	1.335	0.210	0.749	0.330
	50	0.706	1.413	0.200	0.708	0.593
	78	1.013	2.026	0.130	0.494	0.419
$Bo = 2$	25	0.738	1.106	0.308	0.678	0.437
	50	0.816	1.228	0.250	0.613	0.642
	78	1.221	1.832	0.168	0.410	0.450
$Bo = \infty$	25	1.299	1.299	0.745	0.385	0.601
	50	1.573	1.573	0.580	0.318	0.772
	78	2.193	2.193	0.350	0.228	0.521

Note:  $m_{liquid} = \frac{4}{3}\pi\rho R_o^3 \times [\text{filling fraction}]$

Table 4.4-1 summarizes the computations of the fundamental slosh frequency and the mechanical model parameters, together with previous results [1] for high-g sloshing (i.e., for  $Bo = \infty$ ). For comparison purposes, the predicted low-g frequencies are also presented in the conventional high-g non-dimensional form  $\omega^2/(g/R_o)$ . As can be seen, the non-dimensional eigenvalue  $\Omega^2 = \omega^2/(1 + Bo)\sigma/\rho R_o^3$  for a given fill level decreases as  $Bo$  decreases. From physical reasoning, it is expected that the eigenvalue would be exactly zero for  $Bo = 0$  when  $\gamma_c = 0$ ; for these examples, the contact angle was  $5^\circ$ , so  $\Omega^2$  is probably not quite zero for  $Bo = 0$ , but the excessive amount of finite element computations required for  $Bo = 0$ , for which the static free surface is nearly a total spherical bubble, prevented this conclusion from being verified numerically. It should be noted

that  $\omega^2/(g/R_o)$  does not decrease monotonically as  $Bo$  decreases but first decreases and then shows a slight increase for  $Bo = 1$ , as a result of the changing interaction of the stiffening effect of surface tension and the softening effect of the increased wave length, compared to a high-g slosh wave.

The predicted low-g slosh masses shown in the table are much smaller than the corresponding high-g masses and decrease as  $Bo$  decreases as a result of the increasing influence of the term proportional to  $H_c$  in Eq. (4.4-28). The pendulum length increases significantly as  $Bo$  decreases. Since the pendulum attachment point is the center of the tank (for the physical reason that liquid cannot be set in motion in a spherical tank by changing only its angular orientation), the line of action of the pendulum mass can be outside the tank when  $Bo$  is small; that is,  $l_p > R_o$ .

Experimental results for low-g sloshing in spherical tanks [6, 27] are limited to the range  $Bo > 10$  and  $\gamma_c \approx 0$ , so a direct comparison cannot be made with these predictions. The trend of the data indicates that  $\omega^2/(g/R_o)$  decreases as  $Bo$  decreases, which is thus in agreement with the trend shown in Table 4.4-1 for  $Bo > 1$ . The trend of the experimental slosh masses is also in agreement with the predictions. Furthermore, the frequencies given in Table 4.4-1 agree fairly well with those predicted by a previous finite-difference numerical analysis [20], although the results in [20] are consistently slightly smaller; for example, for  $Bo = 1$ , the predicted  $\Omega^2$  given in [20] is 0.619, compared to 0.794 by the present method. The slosh masses given in [20] are negative for  $Bo$  less than about five, because of an error in the slosh force analysis, and thus cannot be compared to the present results.

## **4.5 Spherical Pendulum Rotary Slosh Model**

### **4.5.1 Background**

It has long been recognized that for liquids in symmetrical tanks, there is a strong tendency for rotational motion to occur throughout the steady acceleration range, even though the excitation to the tank may be planar. Although confirmation of this tendency under controlled experiments for low gravity in orbit remains yet to be accomplished, Peterson [28] has indicated its presence even in suborbital experiments conducted in parabolic flight trajectories. Thus, analytical modeling of the rotary slosh problem and its partial verification through earthbound experiments is an essential prelude to design of orbital experiments whose objective is the final confirmation of this complex fluid behavior.

Development of a prediction for rotary slosh via hydrodynamic theory has not yet been accomplished. However, insight into the problem has been sought through studies of a spherical pendulum, which has been recognized as a potential analog for rotary liquid slosh. Nevertheless, even this approach quickly results in a relatively complex dynamics problem. Significant analytical study of the spherical pendulum has been reported by Miles [29]. Some experiments reported by Tritton [30] show that this classical system can display a variety of motions, including chaotic responses for certain conditions. On the other hand, Kaña [31] has shown that the most significant

amplitude rotary liquid slosh in a scale model Centaur tank is at least periodic in nature, and can be modeled by a compound system which contains both a spherical and a linear pendulum. This report presents an extension of the latter work, and includes improvements to a harmonic balance model, which can be used to develop approximate dynamic parameters for both the spherical and the linear pendulums, and to a numerical approach which can be used to refine these results to more exact values. Finally, the effects of low gravity on this type of response are also explored.

The physical configuration for the compound pendulum rotary slosh model originally reported by Kaña [31], is repeated for convenience herein in Figure 4.5-1. The major developments of this report deal with the spherical pendulum, although the results will affect parameters for the linear pendulum part of the model as well. A summary of pertinent expressions which allow determination of parameters for the spherical pendulum will first be given.

The general dynamic equations for the spherical pendulum were derived as:

$$\ddot{\theta} + \left( \omega_n^2 - \dot{\phi}^2 \cos \theta \right) \sin \theta + 2\omega_n \zeta_\phi \dot{\theta} + \frac{\ddot{x}}{l} \cos \phi \cos \theta = 0 \quad (4.5-1a)$$

and

$$\ddot{\phi} \sin \theta + 2\dot{\phi} \ddot{\theta} \cos \theta + 2\omega_n \zeta_\phi \dot{\phi} \sin \theta - \frac{\ddot{x}}{l} \sin \phi = 0 \quad (4.5-1b)$$

wherein there has been included:

$$\omega_n^2 = \frac{g}{l}, \quad m = \frac{\beta_1 W_1}{g}, \quad \zeta_\theta = \frac{C_\theta}{2m\omega_n}, \quad \zeta_\phi = \frac{C_\phi}{2m\omega_n} \quad (4.5-1c)$$

Expressions for the cross-axis effective weight  $W_c(\omega)$  and the in-line effective weight  $W_e(\omega)$  were derived as:

$$W_c(\omega) \cos \omega t = -\frac{\beta_1 W_1 l}{x_0 \omega^2} \left[ \dot{\phi}^2 \sin \theta \sin \phi - 2\omega \dot{\theta} \cos \theta \cos \psi - \ddot{\theta} \cos \theta \sin \psi \right] \quad (4.5-2a)$$

and

$$W_e(\omega) \cos \omega t = \frac{\beta_1 W_1 l}{x_0 \omega^2} \left[ \dot{\phi}^2 \sin \theta \cos \phi + 2\omega \dot{\theta} \cos \theta \sin \psi - \ddot{\theta} \cos \theta \cos \psi \right] + \beta_1 W_1 \cos \omega t \quad (4.5-2b)$$

A harmonic balance approximate solution to Eqs. (4.5-1a, 4.5-1b, and 4.5-1c) was first developed. Radial force equilibrium resulted in the expression:

$$\tan \theta_0 - \alpha^2 \sin \theta_0 = \frac{\alpha^2}{2} \left( \frac{x_0}{l} \right) \cos \phi_0 \quad (4.5-3a)$$

in which

$$\alpha = \frac{\omega}{\omega_n} \quad (4.5-3b)$$

Circumferential force equilibrium resulted in the expression:

$$\zeta_\phi = \pm \left( \frac{\alpha x_0}{4l} \right) \frac{\sin \phi_0}{\sin \theta_0} \frac{CCW}{CW} \quad (4.5-4)$$

A corresponding harmonic balance expression for the complex cross-axis weight was developed from Eqs. (4.5-2a and 4.5-2b) to result in:

$$\begin{aligned} \vec{W}_s(\omega) = & -\beta_1 W_1 l \frac{\ddot{\phi}}{x} \sin \theta e^{i\phi} + 2\omega \beta_1 W_1 l \frac{\dot{\theta}}{x} \cos \theta e^{i(\psi + \frac{\pi}{2})} \\ & + \beta_1 W_1 l \frac{\ddot{\theta}}{x} \cos \theta e^{i\psi} + \beta_1 W_1 \frac{\ddot{x}}{x} \end{aligned} \quad (4.5-5a)$$

in which there was included:

$$\psi = \omega t - (\gamma_0 + \phi_0) = \phi - \gamma_0 \quad (4.5-5b)$$

and

$$\tan \gamma_0 = \frac{2\zeta_{\theta 1} \alpha}{1 - \alpha^2}, \quad \zeta_{\theta 1} = \frac{\zeta_\theta}{2} \quad (4.5-5c)$$

From this, there was defined along the real cross-axis a co-phase component  $W_{CC}$  as:

$$W_{CC} = \beta_1 W_1 \left[ \frac{l}{x_0} \sin \theta_0 \sin \phi_0 + \cos^2 \theta_0 F_s(\alpha) \sin \lambda_0 \right] = W_c(\omega) \quad (4.5-6a)$$

and along the in-line axis a quadrature-phase component  $W_{CQ}$  as:

$$W_{CQ} = -\beta_1 W_1 \left[ \frac{l}{x_0} \sin \theta_0 \cos \phi_0 + \cos^2 \theta_0 F_s(\alpha) \cos \lambda_0 \right] = \beta_1 W_1 - W_c(\omega) \quad (4.5-6b)$$

where  $W_{CQ}$  is taken as positive to the left. In these expressions, there was also used:

$$\lambda_0 = 2(\gamma_0 + \phi_0) + \epsilon_0 \quad (4.5-7a)$$

and

$$F_s(\alpha) = \frac{\alpha^2}{[(1 - \alpha^2)^2 + 4\zeta_{\theta 1}^2 \alpha^2]^{\frac{1}{2}}} \quad (4.5-7b)$$

The distortion angle  $\epsilon_0$  was included to allow the pendulum weight ratio  $\beta_1$  to remain in the realistic range between zero and one.

In [31], development of model parameters from the above equations was accomplished by the following steps:

- 1) Circumferential damping  $\zeta_\phi$  with corresponding position lag angle  $\phi_0$  and steady deflection  $\theta_0$  were obtained by simultaneous iteration on Eqs. (4.5-3 and 4.5-4). The condition was that  $\phi_0$  match experimentally observed values, where they could be discerned (i.e., for  $\alpha > 1.0$ ). For  $\alpha < 1.0$ , only guesses on  $\phi_0$  could be made, since  $\theta_0$  was too small to isolate.
- 2) These values of  $\zeta_\phi$ ,  $\phi_0$ , and  $\theta_0$  were then used in Eqs. (4.5-5, 4.5-6, and 4.5-7) to calculate cross-axis weight components. For this, an assumed value of radial damping  $\zeta_{\theta 1}$  and error angle  $\epsilon_0$  were varied until the calculated weight components matched those which were measured for a given excitation frequency during the slosh experiments, and the resulting weight ratio  $\beta_1$  was a realistic value.

With the above steps, all parameters for the spherical pendulum were first determined from the approximate solution. Thereafter, the damping values  $\zeta_\phi$ ,  $\zeta_\theta$  and natural frequency  $\omega_n$  were used in Eqs. (4.5-1a, 4.5-1b, and 4.5-1c) for a numerical time-step solution for  $\theta(t)$  and  $\phi(t)$ . These solutions were then subsequently input to Eqs. (4.5-2a and 4.5-2b) to obtain more accurate weight components as functions of time. However, in doing this, the results were compared on a magnitude basis only, with phase being ignored.

The primary objective of the present work is to develop more accurate parameters for the spherical pendulum part of the slosh model by use of similar numerical solutions of the governing equations. However, both magnitude and phase of the cross-axis weight components will be included. As a result, parameters for the linear pendulum part of the compound slosh model will also be shown to be affected. Thus, a more accurate slosh model which matches all dynamic properties of the cross-axis and in-line weights will result.

#### 4.5.2 Revised Approximate Model

As indicated in the previous section, judicious choices of damping parameters must first be made for the spherical pendulum before a direct numerical solution of the governing equations can be attempted. These values must be such that the solutions for  $\theta(t)$  and  $\phi(t)$  will produce cross-axis weights which can be made to match the experimental slosh data when a plausible mass ratio  $\beta_1$  is included. Therefore, to assure that judicious initial values are selected, the harmonic balance approximate solution is still first used to estimate values of damping, deflection, and position lag angles. However, in the present work, the model is revised so that  $\epsilon_0$  is set to zero in Eq. (4.5-7a).

By further search, it was found that plausible solutions for  $\beta_1$  indeed could be obtained by significant revision of the damping values  $\zeta_\phi$  and  $\zeta_{\theta 1}$ . Otherwise, the approximate parameters are all determined using the same detailed approach described previously in Steps 1 and 2.

The results obtained from the revised approximate model with  $\varepsilon_0 = 0$  are shown in Figures 4.5-2 - 4.5-5. Note that numerical solution results are also given, but will be ignored until later. Here the approximate results are presented as continuous solid and dashed lines, although it is understood that values were obtained only at frequencies where experimental data were available. By comparing these results with those presented in [31], it can be seen that for values of  $\alpha < 1.0$ , significantly greater values of damping for both  $\zeta_\phi$  and  $\zeta_{\theta 1}$  are necessary to develop a plausible model. At the same time, the steady deflection angle  $\theta_0$  was not changed very much, but the values of position lag angle  $\phi_0$  and mass fraction  $\beta_1$  change significantly. Even so, they remain in a plausible range (i.e.,  $\beta_1 \leq 1.0$ ). The net result of this development is that a better model of the experimental slosh data can be achieved, as will be described further with the numerical approach.

#### 4.5.3 Numerical Model

As previously indicated, the objective of the numerical model is to seek solutions for  $\theta(t)$  and  $\phi(t)$  so that matching of all dynamic properties of the experimental slosh data can be achieved. Since the spherical pendulum alone produces the cross-axis weights, it is given attention first, and then the linear pendulum is established by means of the in-line weights. However, in developing the approach to the spherical pendulum, it is first appropriate to provide some preliminary discussion about the expected forms of the solutions and to modify the cross-axis weight expressions.

##### Forms of Solutions

Steady state polar solutions for  $\theta(t)$  and  $\phi(t)$  from Eqs. (4.5-1a and 4.5-1b) are of elliptical shape similar to the example shown in Figure 4.5-6a. This polar plot represents counter-clockwise motion, as will all the solutions considered in this report. (Discussion of clockwise solutions will be given in the conclusions). Furthermore, a modified notation (compared to that used in [31]) has been employed in Figures 4.5-6a and 4.5-6b in order to allow more generalization, and to emphasize in which plane a given variable is defined.

Solutions of interest are periodic in  $\omega t$ , and in order to study the details of a single period one can pick an initial reference time:

$$t_0 = 2\pi n / \omega \quad (4.5-8)$$

where  $n$  is an integer. By referring to Figures 4.5-6a and 4.5-6b, we can define:

$$\phi_i(t) = \omega t - \phi_0(t) \quad (4.5-9a)$$

and

$$\phi_s(t) = \phi_i(t) - \phi_{0s} = \omega t - \phi_{01}(t) \quad (4.5-9b)$$

where

$$\phi_{01}(t) = \phi_0(t) + \phi_{0\alpha} \quad (4.5-9c)$$

Furthermore, combining Eqs. (4.5-9b) and (4.5-9c) there results:

$$\phi_s(t) = \omega[t - \phi_0(t)/\omega] - \phi_{0\alpha} \quad (4.5-10)$$

From these equations, we further note that at  $t = t_0$ :

$$\phi_0(t_0) = 0 \quad \text{and} \quad \phi_{01}(t_0) = \phi_{0\alpha} \quad (4.5-11)$$

Note that if the solutions of Eqs. (4.5-1a and 4.5-1b) are such that the polar plot in Figure 4.5-6a becomes circular, then Eq. (4.5-10) takes on the more familiar monotonically-increasing straight line form, in which  $\phi_0(t)$  is zero. However, if the solutions form an elliptical polar plot as shown in Figure 4.5-6a, it will be shown later that  $\phi_0(t)$  is a periodic function superposed on the otherwise straight line  $\phi_s(t) = \omega t - \phi_{0\alpha}$ .

### Modification of Cross-Axis Weight Expressions

It is now appropriate to use Eqs. (4.5-2a and 4.5-2b) to develop effective weights as functions of time so that comparisons with experimental data can be made. However, as given, these expressions include some restrictions which were useful for the approximate model solution, and will be eliminated for the numerical model. In particular, the last two terms in the brackets on the right-hand side of Eqs. (4.5-2a and 4.5-2b) were defined in terms of a rotating pendulum whose plane of oscillation lags at a constant angle  $\gamma_{0\alpha}$  relative to the space-plane angular displacement  $\phi_s(t)$ . As indicated in Figures (4.5-6a and 4.5-6b), it was assumed that:

$$\gamma_{0\alpha} = \phi_s(t_m) = \gamma_0 - \phi_{0\alpha} \quad (4.5-12)$$

where  $\phi_s(t_m)$  is the angle between the apex of the ellipse and the x-axis. To account for coupled radial [i.e.,  $\theta(t)$ ] and rotational [ $\phi(t)$ ] effects, the angle  $\psi_i(t)$  was defined by Eq. (4.5-5b) as:

$$\psi_i(t) = \omega t - [\gamma_0 + \phi_0(t)] \quad (4.5-13)$$

and using Eqs. (4.5-9a, 4.5-9b, and 4.5-9c) there results:

$$\psi_i(t) = \phi_s(t) - \gamma_0 + \phi_{0\alpha} \quad (4.5-14)$$

Use of this approach only partially accounts for coupling effects that are present, and will now be generalized for development of the numerical model.

Equations (4.5-2a and 4.5-2b) are considered directly for a pendulum which is rotating with variable angular velocity  $\dot{\phi}(t)$  and with a plane of oscillation which makes the angle  $\phi_s(t)$  relative to the excitation plane. For this, Eqs. (4.5-2a and 4.5-2b) become:

$$\vec{W}_c(t) \cos \omega t = -\frac{\beta_1 W_1 l}{x_0 \omega^2} \left[ \ddot{\phi}^2 \sin \theta \sin \phi - 2\dot{\phi}\ddot{\theta} \cos \theta \cos \phi - \ddot{\theta} \cos \theta \sin \phi \right] \quad (4.5-15a)$$

and

$$\begin{aligned}\vec{W}_e(t) \cos \omega t = & \frac{\beta_1 W_1 l}{x_0 \omega^2} \left[ \dot{\phi}^2 \sin \theta \cos \phi + 2 \dot{\phi} \ddot{\theta} \cos \theta \sin \phi - \ddot{\theta} \cos \theta \cos \phi \right] \\ & + \beta_1 W_1 \cos \omega t\end{aligned}\quad (4.5-15b)$$

In which it is understood that  $\phi = \phi_s(t)$  and  $\theta = \theta_s(t)$  are each calculated from coupled numerical time-step solutions of Eqs. (4.5-1a and 4.5-1b), and  $\vec{W}_c(t)$  and  $\vec{W}_s(t)$  are vectors which have a time-phase relative to  $\cos \omega t$ .

Thus, we have:

$$\vec{W}_c(t) \cos \omega t = |\vec{W}_c(t)| e^{-j\xi_{0c}} \cos \omega t \quad (4.5-16a)$$

and

$$\vec{W}_s(t) \cos \omega t = |\vec{W}_s(t)| e^{-j\xi_{0s}} \cos \omega t \quad (4.5-16b)$$

where  $\xi_{0c}$  and  $\xi_{0s}$  are lag angles for the respective weight components. These lag angles are found by:

$$\xi_{0c} = \omega(t_c - t_0) \quad (4.5-17a)$$

$$\xi_{0s} = \omega(t_s - t_0) = \xi_{0c} + \pi/2 \quad (4.5-17b)$$

where  $t_0$  is given by Eq. (4.5-8) and  $t_c$  and  $t_s$  are the times for a maximum occurrence of the respective weight just succeeding the reference time  $t_0$ . (Note that if a preceding maximum occurrence is used, then  $\xi_{0c}$  becomes a lead angle rather than a lag angle).

When the cross-axis weight solutions are developed according to Eqs. (4.5-15a and 4.5-15b), it is found that a time lag error exists relative to the experimental weight measurements. This error is found to be dependent on the variation of  $\phi_0(t)$  with time. In view of Eq. (4.5-10) we note that:

$$W_c[\phi_s(t)] = W_c\{\phi_s[t - \phi_0(t)/\omega]\}$$

Guided by this, we set:

$$t'_0 = t_0 - \phi_0(t_c)/\omega \quad (4.5-18a)$$

This results in a lag angle:

$$\xi'_{0c} = \omega(t_c - t'_0) = \xi_{0c} + \phi_0(t_c) \quad (4.5-18b)$$

Therefore, since the cross-axis weight is expressed as:

$$\vec{W}_c(t) = W_{CC} - jW_{CQ}$$

there results:

$$W_{CC} = |\vec{W}_c(t)| \cos \xi'_{0c} \quad \text{and} \quad W_{CQ} = |\vec{W}_c(t)| \cos(\xi'_{0c} - \pi/2) \quad (4.5-19)$$

Similarly for the in-line weight:

$$\overline{W}_e(t) = W_{eR} - jW_{eI}$$

there results:

$$W_{eR} = |\overline{W}_e(t)| \cos \xi'_{0e} \quad \text{and} \quad W_{eI} = |\overline{W}_e(t)| \cos(\xi'_{0e} - \pi/2) \quad (4.5-20a)$$

where

$$\xi'_{0e} = \omega(t_e - t'_0) = \xi_{0e} + \phi_0(t_e) = \xi'_{0c} + \pi/2 \quad (4.5-20b)$$

### Spherical Pendulum Procedure

The procedure for development of model parameters will be described in steps along with results for a specific frequency point. For illustration, the point at  $\alpha = 0.9720$  was selected, which includes the following experimental slosh data (see [31]):

$$W_{CC} = 108.0 \text{ lb}(480.4 \text{ N}) \quad \text{and} \quad W_{CQ} = 59.57 \text{ lb}(265.0 \text{ N})$$

- 1) For this case, Step 1 of the approximate model provides values of damping as

$$\zeta_{\phi} = 0.017 \quad \text{and} \quad \zeta_{\theta 1} = 0.022$$

These values appear as part of the solid and dashed lines, respectively, in Figure 4.5-2. However, after trial in the rest of the steps to follow, it was found that even more damping was necessary to produce sufficient cross-axis force. Therefore, these values were increased to:

$$\zeta_{\phi} = 0.025 \quad \text{and} \quad \zeta_{\theta 1} = 0.045$$

so that  $\zeta_{\theta} = 0.090$

- 2) The above values of damping were used along with the DYSIM (Dynamic Simulation) computer program to compute  $\theta(t)$  and  $\phi(t)$  from Eqs. (4.5-1a and 4.5-1b). This program is based on a fourth-order Runge-Kutta numerical integration scheme. The results are plotted for reference in Figures 4.5-7, 4.5-8, and 4.5-9 for the time period 45 to 50 seconds. This time was sufficient to establish steady-state after using the following initial conditions:

$$\theta(0) = 0.0038 \text{ radian} \quad \phi(0) = -1.534 \text{ radian}$$

$$\dot{\theta}(0) = 0.000 \text{ rad/sec} \quad \dot{\phi}(0) = 2.7300 \text{ rad/sec}$$

In this and all cases developed herein, the time step increment was 0.002 sec.

- 3) For convenience  $\phi_{01}(t)$  was also computed from Eq. (4.5-9b) as:

$$\phi_{01}(t) = \omega t - \phi_s(t)$$

and plotted in Figure 4.5-10. It is clearly seen to be a periodic function for this case.

- 4) From the above results, the following parameters are obtained from Eqs. (4.5-8 and 4.5-11) for  $n = 21$  periods:

$$t_0 = 48.331 \text{ sec} \quad \phi_{0e} = 0.42 \text{ rad}$$

- 5) The above results for  $\theta(t)$  and  $\phi(t)$  are now used to compute  $\overline{W}_c(t) \cos \omega t$  and  $\overline{W}_s(t) \cos \omega t$  from Eqs. (4.5-15a and 4.5-15b). The results for the periodic component filtered at frequency  $\omega$  are plotted in Figures 4.5-11 and 4.5-12, respectively. For this computation, the value of  $\beta_1$  is adjusted so that the magnitude of  $|\overline{W}_c(t)|$  equals that for the experimental data:

$$|\overline{W}_c(t)| = [W_{cc}^2 + W_{c0}^2]^{\frac{1}{2}} = 123.3 \text{ lb (548.4 N)}$$

This results in  $\beta_1 = 0.160$ . Furthermore, from the results in Figure 4.5-11 we obtain  $t_c = 48.162 \text{ sec}$ . With this and the results from Figure 4.5-10 used in Eq. (4.5-9c), we obtain  $\phi_0(t_c) = 0.94 \text{ radian}$ . Therefore, from Eq. (4.5-18a) we obtain  $t'_0 = 47.987 \text{ sec}$ , and from Eq. (4.5-18b) there results  $\xi'_{0e} = 27.4^\circ$ , which agrees with the experimental value.

Thus, a very close matching of both magnitude and phase has been achieved for the cross-axis weight data, and has resulted in a very plausible value for the weight ratio  $\beta_1$ . Generally, this is accomplished only after some additional adjustment of the damping ratios, as was indicated above in Step 1.

- 6) The in-line components for the spherical pendulum are obtained from  $\overline{W}_s(t) \cos \omega t$ , which is plotted in Figure 4.5-12. Note that the scale on this plot has been adjusted according to  $\beta_1 = 0.160$ , as found in Step 5 above, so that Figure 4.5-12 also provides  $|\overline{W}_s(t)| = 107.7 \text{ lb (479.1 N)}$ . The time  $t_s = 48.70$  also is established from this plot. Therefore, from Eq. (4.5-20b) the in-line lag angle is obtained as  $\xi'_{0e} = 111.8^\circ$ . From this and Eq. (4.5-20a), there results  $W_{sR} = -40 \text{ lb (177.9 N)}$  and  $W_{sI} = 99.5 \text{ lb (442.6 N)}$ .

This information is required for determination of the linear pendulum parameters, as will be shown later.

## Spherical Pendulum Results

Spherical pendulum model parameters were similarly calculated for several other frequency points, and the results plotted as discrete points in Figures 4.5-2 - 4.5-5. Generally, it can be seen that the resulting damping ratios  $\zeta_\phi$  and  $\zeta_{\phi_1}$  and mass ratio  $\beta_1$  all are higher than the corresponding values estimated from the approximate model, only for the frequency range  $\alpha < 1.0$ . This could be expected, since for  $\alpha > 1.0$  the polar plots rapidly become circular, and the approximate and numerical solutions become more identical. Even so, the approximate values are useful in all cases to use as initial values for numerical model development. Note also that the steady deflection angle  $\theta_0$  is essentially the same for both cases (for the numerical model  $\theta_0$  is taken as the average value from the  $\theta(t)$  - plot). Finally, from Figure 4.5-4, it can be seen that the values for position angle  $\phi_0$  also deviate somewhat only for  $\alpha < 1.0$ . In this case,  $\phi_0$  is taken as:

$$\phi_0 = \phi_{\alpha_r}$$

i.e., the value for  $\phi_{01}(t)$  at  $t = t_0$ . For  $\alpha > 1.0$  and more circular orbits,  $\phi_{01}(t)$  becomes constant and  $\phi(t)$  in Figure 4.5-9 becomes a straight line.

Some further examples of types of polar plots are shown in Figures 4.5-13 - 4.5-15. Figures 4.5-13 and 4.5-14 show samples of plots from actually developed model data given in Figures 4.5-2 - 4.5-5. From Figures 4.5-7, 4.5-13, and 4.5-14, it can be seen that dramatic changes in the orbits occur (i.e., in magnitudes and shapes), which correspond qualitatively with what is observed experimentally in the liquid behavior. These changes result from variation of damping values as well as frequency. For example, Figure 4.5-15 shows several orbits computed for fixed excitation frequency  $\alpha = 0.972$  and circumferential damping  $\zeta_\phi = 0.017$ , but with varying radial damping  $\zeta_{\phi_1}$ . For large  $\zeta_{\phi_1}$ , the orbit is nearly circular, so that a relatively large cross-axis weight would be produced. For small  $\zeta_{\phi_1}$ , the orbit reduces to the limiting case of a linear pendulum, and zero cross-axis weight results. For this also  $\phi(t_0)$  becomes essentially zero, so that the in-line weight reduces to that for a linear pendulum with amplitude and phase determined by  $\zeta_{\phi_1}$ . Furthermore, the function  $\phi(t)$  approaches a straight line for the more circular orbit, while corresponding results for the linear pendulum form a stair-step function. In the other cases, the results are similar to those of Figures 4.5-7 - 4.5-10.

## Linear Pendulum Discussion

In [31], the parameters for the linear pendulum in the compound model are developed totally from the experimental data. Herein, this approach is changed to recognize that for less circular (i.e., more elliptical) orbits, the corresponding cross-axis and in-line components of the spherical pendulum are not equal, since  $\phi$  is not a constant for such orbits. That is  $W_{CC} \neq W_{eI}$  and  $W_{CQ} \neq W_{eR}$ . This conclusion is evident from the results of the numerical model. Therefore, the combined system weight equations are now formed as follows:

$$W_R = W_{eR} + \beta_2 W_1 + \beta_2 W_1 F_L(\alpha) \cos \psi_0 \quad (4.5-21a)$$

$$W_I = W_{eI} + \beta_2 W_1 F_L(\alpha) \sin \psi_0 \quad (4.5-21b)$$

where the total complex in-line weight is:

$$\vec{W}_I = W_R - iW_I$$

and

$$F_L(\alpha) = \frac{\alpha^2}{[(1 - \alpha^2)^2 + 4\zeta_{\theta 2}^2 \alpha^2]^{\frac{1}{2}}} \quad (4.5-22a)$$

$$\tan \gamma_{\theta 2} = \frac{2\alpha\zeta_{\theta 2}}{1 - \alpha^2} \quad (4.5-22b)$$

Equations (4.5-21a and 4.5-21b) indicate that the total in-line weight is produced by the two pendulums. The contribution from the spherical pendulum results from the numerical solutions for  $W_{eR}$  and  $W_{eI}$  as indicated previously for the spherical pendulum procedure. The contribution of the linear pendulum results from its amplitude given by Eq. (4.5-22a) and phase given by the angle  $\psi_0$ . However, if there is some coupling between the two pendulums required for matching the in-line slosh data, then there will result:

$$\gamma_{\theta 2} \neq \psi_0$$

For this case,  $\psi_0$  is obtained from combining Eqs. (4.5-21a and 4.5-22b) to obtain:

$$\tan \psi_0 = \frac{W_I - W_{eI}}{W_R - W_{eR} - \beta_2 W_1} \quad (4.5-23)$$

Then a coupling difference angle  $\epsilon_{\theta 2}$  will result such that:

$$\epsilon_{\theta 2} = \psi_0 - \gamma_{\theta 2} \quad (4.5-24)$$

### Linear Pendulum Procedure

Parameters for the linear pendulum can now be developed by means of the above results. For illustration, the data for the frequency point  $\alpha = 0.972$  will be continued. For this, the total measured in-line weights (see [31]) are:

$$W_R = 389.6 \text{ lb } (173.9 \text{ N}) \text{ and } W_I = 343.3 \text{ lb } (1527.0 \text{ N})$$

- 1) Given the above total measured in-line weight values  $W_R$  and  $W_I$  and the in-line weight components  $W_{eR}$  and  $W_{eI}$  computed from the numerical model one may then assume a value for  $\zeta_{\theta 2}$ . For this case, this damping value will be taken as constant for all frequencies at:

$$\zeta_{\theta 2} = 0.010$$

With this,  $F_L(\alpha)$  is computed from Eq. (4.5-22a) and  $\gamma_{02}$  is computed from Eq. (4.5-22b). For this example:

$$F_L(\alpha) = 16.14 \quad \text{and} \quad \gamma_{02} = 19.40^\circ$$

- 2) Equations (4.5-21a, 4.5-21b) are now manipulated to where  $\beta_2$  is eliminated from them. This results in:

$$\left[ \frac{(W_R - W_{eR})}{(W_I - W_{eI})} \sin \psi_0 - \cos \psi_0 \right] = \frac{1}{F_L(\alpha)} \quad (4.5-25)$$

With the above data, this equation is solved for  $\psi_0$  by trial and error. For the example case, there results:

$$\psi_0 = 30.7^\circ$$

and from Eq. (4.5-24) this results in:

$$\epsilon_{02} = 11.3^\circ$$

Thus, a non-zero angle indicates that some degree of coupling between the two pendulums is necessary to match the in-line weight data. Furthermore, the linear pendulum mass ratio can then be obtained from Eqs. (4.5-21a) or (4.5-21b) as:

$$\beta_2 = 0.310$$

### Linear Pendulum Results

Further results for the linear pendulum which correspond to the data developed for the numerical spherical pendulum model are shown in Figure 4.5-16. The resulting mass ratio  $\beta_2$  varies more or less similarly to  $\beta_1$  for the spherical pendulum. The coupling angle  $\epsilon_{02}$  varies significantly over the frequency range, which indicates a corresponding large variation of coupling between the two pendulums, as long as  $\zeta_{\theta 2}$  is held constant.

It is appropriate to raise the question of whether this coupling can be reduced to zero providing that  $\zeta_{\theta 2}$  is allowed to vary. It was found that this approach led to impossible values of damping at the lower frequencies. Therefore, for simplicity, the  $\zeta_{\theta 2}$  constant value was selected. This may or may not be the optimum approach for every set of experimental data developed.

#### 4.5.4 Effects of Low Gravity

The preceding developments have concentrated on an approach for developing parameters for a compound slosh model that can match the effective weights measured for liquid motions in a tank which is subject to a given steady acceleration. The experimental data was acquired in an earthbound system, and the equations were derived for a spherical pendulum in an earthbound system. The next logical question deals with whether the model developed can be used to predict

results that might be expected in a low gravity environment in orbit. The methods developed for both the harmonic balance approximate model and the numerical model will be used to shed some light on this question, by showing how low gravity can affect the response of the compound slosh model.

An immediate effect of low gravity on both a spherical and a linear pendulum is that the natural frequency is dramatically reduced. For a liquid, this effect is so pronounced that surface tension forces then dominate, rather than gravity forces, as has been described earlier in this report. For a pendulum in low gravity, this corresponds to adding a weak, torsional spring at its support. Thus, if no other forms of nonlinearity enter the problem and if one can assume that excitation will still occur in the vicinity of the natural frequency, however low it may be (i.e., near  $\alpha = 1.0$ ), then the essential modeling approach developed herein remains applicable. However, a very important effect on the results will additionally occur because of changes in damping, as the previous development shows that dramatic differences in response of a spherical pendulum occur for a given frequency when either  $\zeta_\phi$  or  $\zeta_{\theta 1}$  change by only slight amounts. Although the effects of low gravity on damping in a given tank are not yet completely understood, it is known that damping tends to increase as gravity decreases [i.e., Eq. (1.1-1)]. Therefore, the subsequent discussion concentrates on what can happen to a spherical pendulum excited near  $\alpha = 1.0$ , when the damping  $\zeta_\phi$  and  $\zeta_{\theta 1}$  are allowed to increase.

Equations (4.5-3, 4.5-4) which represent part of the harmonic balance approximate model are first used for this purpose. Equation (4.5-3a) was first solved for a variety of position angles  $\phi_0$  for incremented values of frequency ratio near  $\alpha = 1.0$ , and the corresponding values of steady deflection  $\theta_0$  were noted. This results in the plot shown in Figure 4.5-17. Then, corresponding values of  $\zeta_\phi$  were calculated from Eq. (4.5-4), and the results plotted in Figure 4.5-18. By using the two figures together, one can estimate what type of responses occur at a given frequency for an initial value of damping  $\zeta_\phi$ , and also how the character of the response changes as this value of damping is increased.

As the previous model developments indicate, generally an increase of damping  $\zeta_\phi$  leads to larger values of  $\phi_0$ , and therefore, correspondingly larger values of cross-axis effective weights, all of which is independent of  $\zeta_{\theta 1}$  only for the approximate model. However, this alone is not the whole story. As was previously shown, at a fixed value of  $\zeta_\phi$  the character of the response also changes with  $\zeta_{\theta 1}$  increase. Therefore, use of the numerical model is ultimately necessary for a more exact determination of response changes that occur due to variations in damping that result from low gravity.

Relating these results to changes in gravity may be accomplished by estimating the damping change according to Eq. (1.1-1). However, the computed value is most directly associated with the radial damping  $\zeta_{o1}$  in this model. At present, it must be assumed that some similar relationship exists for the circumferential damping  $\zeta_{\phi}$ . On the other hand, the problem is even more complicated than such an approach may imply. By programming various combinations of damping into Eqs. (4.5-1a and 4.5-1b), for the spherical pendulum, it was quickly found from numerical solutions that steady state response occurs only within certain regions of damping—otherwise drifting or chaotic responses occur, as predicted by Tritton [30]. For the present case, it was found that stable periodic motions could be found for the ranges of frequency, damping and associated phase angles indicated in Figures 4.5-17 and 4.5-18. However, these values were found only by trial and error, and more work is required before a better understanding of the behavior is possible. Furthermore, establishment of more accurate relationships for both  $\zeta_{\phi}$  and  $\zeta_{o1}$  as functions of low-g are required before any predicted results can be meaningful.



## **5.0 GROUND-BASED SUPPORTING EXPERIMENTATION**

### **5.1 Introduction**

Several different studies were conducted to help establish requirements for flight instrumentation. The response characteristics of liquid-vapor interface sensors were investigated by laboratory experiments to determine an appropriate set of spatial and frequency response requirements; these experiments used non-flight hardware and instrumentation. Load cell designs were surveyed to determine if designs exist that can measure the small slosh forces anticipated for a flight experiment. This section summarizes those investigations.

### **5.2 Ground Tests Of Liquid-Vapor Sensors**

#### **5.2.1 Background**

The geometric description of the static and dynamic free surface is among the most useful fundamental information that can be obtained about liquid motions in moving tanks. This is especially true for low-gravity conditions, since the shape of the free surface slosh wave is the only evidence obtainable from tests that is directly related to the contact line condition (i.e., to the dynamic contact angle). In addition, the natural frequency of the motions can also be determined from the time history of the dynamic free surface location, and the damping can be obtained by the time-decay of the free surface wave motion after the tank motion itself ceases. All this information obtained from surface location measurements is needed to validate and improve analytical models and to acquire fundamental understanding about the relevant surface physics. Thus, it is imperative that the static and dynamic free surfaces be "visualized" in some way during flight experiments.

The most common visualization method used in *laboratory* studies of sloshing is a combination of: (1) cinema or video recording of the free surface motion; and (2) probes that measure the time history of the free surface location at one or more points. Cinema or video recording is an appropriate method of obtaining a qualitative overview of the motion and of selecting conditions for further study, while an array of surface probes is an appropriate method of obtaining quantitative data about frequencies, damping, resonant conditions, etc. For the COLD-SAT flight experiment defined in Section 3.2, cinema or video recording from outside the tanks is not possible because the COLD-SAT cryogenic tanks are not transparent; internally-mounted cameras are also not possible because of the substantial insulation required for the camera and the need for a source of lighting. For the Shuttle-based experiment defined in Section 3.3, the use of external cameras is practical and is therefore included in the plan. For both experiments, liquid-vapor interface probes are proposed as a method to obtain quantitative data.

#### **5.2.2 Liquid-Vapor Sensors**

Liquid surface sensors of the type commonly used in laboratory studies of sloshing cannot be used in the "weightlessness" of low gravity because they depend on the weight of any liquid adhering to the sensing elements to remove the liquid rapidly when the probes exit the liquid.

Instead, some other mechanism must be used to remove the adhering liquid so that a time-correlated signal can be generated which indicates when the sensing element is no longer immersed in liquid. At least one space experiment has used a temperature sensing element containing an electrical resistor for this purpose [32]. When the sensor was immersed in liquid, the heat generated by the electrical current in the resistor was conducted away more rapidly than when it was immersed in vapor; consequently, the temperature of the sensor was lower in liquid than in vapor, and the change of temperature thus indirectly indicated when the element entered and exited the liquid. These kinds of devices have been investigated more thoroughly for the COLD-SAT experiments [33, 34]. In addition, fiber optic devices have also been proposed as liquid-vapor surface sensors [34, 35]; Figure 5.2-1 shows the principle upon which these sensors operate.

Although the temperature response time of most resistive sensors is slow (on the order of five to ten seconds), the required response time for the slosh flight experiments is not particularly demanding; Tables 3.2-2 and 3.3-2 indicated that the slosh waves for the two defined space experiments all have periods greater than 70 seconds. Consequently, the response time of resistive sensors should be adequate. In laboratory tests, the response of fiber optic sensors is practically instantaneous; it remains to be shown, however, whether liquid adhering to the probe tip in low gravity can degrade the performance of the probe.

It is concluded that resistive sensors, and possibly fiber optic sensors, can be adapted to the requirements of determining the location of the liquid-vapor interface in low gravity flight experiments. The number and location of such probes required to obtain an accurate resolution of the shape and motion of the surface were therefore the objectives of the present laboratory experiments.

### **5.2.3 Ground Tests of Liquid-Vapor Sensor Arrays**

An existing 1/5-scale model Centaur G-Prime tank was available for the laboratory studies. Water was the test liquid. Near-resonant planar sloshing was excited by oscillating the tank with a horizontal shaker. The test apparatus is sketched in Figure 5.2-2.

Modified "wheatstone" wave height transducers [36] were used in the tests to simulate the resistive or fiber optic sensors of a flight experiment. Each such liquid-vapor sensor was made of a pair of thin insulated conductors, slightly separated, with a short section of each conductor exposed for contact to water, and connected electrically across part of the resistance in one leg of a wheatstone bridge. The short exposed section of the sensor was oriented horizontally (i.e., parallel to the static liquid surface) so that a distinct indication could be obtained of the time when the liquid surface passed the sensor. An individual probe was composed of four sensors mounted on a thin vertical rod and separated vertically by one inch (2.54 cm). Three probes (R1, R2, and R3) were constructed and mounted in the tank on a brace along the tank diameter as shown in Figure 5.2-2. The entire array of probes could be adjusted angularly relative to the tank excitation direction, and vertically

to position the sensors at any desired location relative to the static liquid level. About seventy-five slosh tests (not counting repeats) were conducted for a number of different orientations of the probes and for three different slosh wave amplitudes. No attempt was made to simulate the curvature of the static liquid surfaces that will occur in low gravity.

Figure 5.2-3 shows a reproduction of the strip-chart recording of the output of the probe array from a typical test. When the slosh wave passed upward across a sensor, the sensor went from a "dry" state to a "wet" state, and there was a consequent abrupt increase of the bridge output voltage. When the wave passed downward, the sensor went from a "wet" to a "dry" state, and there was a consequent decrease of the bridge voltage, which was, however, not as abrupt as for the upward passage since some water adhered to the sensor and later dripped off. The magnitude of these voltage jumps is related to the sensor sensitivity and calibration, but not to the height or depth of the wave above or below the sensor.

**Slosh frequency** — The time period between successive dry or successive wet indications for a given sensor, which is, of course, the slosh wave period, was repeatable to high accuracy. As an example, the average period (derived from the known chart travel speed) for the test results shown in Figure 5.2-3 was 1.205 seconds, and the maximum variation from one cycle to another, or between sensors, was 0.005 seconds. The actual slosh period, which was set by the shake table frequency, was 1.205 seconds. It was concluded that digital sensors are easily capable of establishing slosh frequencies.

**Static liquid level and slosh wave shape** — The output of the entire array was available to establish the static liquid level and the shape of the slosh wave. As an example of one method that can be used to interpret the sensor data to obtain this kind of information, the test that yielded the data shown in Figure 5.2-3 will be analyzed. Figure 5.2-4a shows the configuration of the probe array, which was aligned with the tank excitation direction. The static liquid level was halfway between the middle two sensors of each probe. The initial uncertainty in the static liquid level (assuming that there was no visual evidence, such as would be the case for COLD-SAT experiments) was, therefore,  $\pm 0.5$  in (1.27 cm) because the level could have been anywhere between adjacent wet and dry sensors.

Since the sensors at a given vertical level did not all indicate "dry to wet" or "wet to dry" at the same time, a technique was developed to interpolate the discrete data from each of the four sensors of a probe to determine a continuous time history. The slosh motion is periodic, so an appropriate interpolation technique was to fit a least-squared-error sine wave to the data:

$$\eta = A_0 + A_1 \sin(2\pi t/\tau_s + \mu_0) \quad (5.2-1)$$

Here,  $\eta$  is the position of the liquid surface relative to lowest sensor of the selected probe,  $\tau_s$  is the period of the slosh motion (1.205 sec for this example), and  $\mu_o$  is a phase shift relative to probe R1. The parameter  $A_o$  is interpreted as the position of the static liquid level above the lowest sensor of the probe and  $A_l$  as the amplitude of the slosh wave at the radial location of the probe. The data used to derive the least-squared-error sine wave consisted of: (1) the time (after an arbitrary starting point) when each sensor went from dry to wet and from wet to dry, and (2) the vertical position of each sensor relative to the lowest sensor. The time data were obtained from the strip chart recordings of each test by measuring the length intervals between voltage "jumps" which were then converted to seconds. As can be inferred from Figure 5.2-3, there was almost no ambiguity in the dry-to-wet measurements and very little in the wet-to-dry measurements; generally, measurements for three or four slosh periods were averaged to remove what ambiguity existed. The position data for the sensors were determined from direct measurements; as indicated earlier, the corresponding sensors of each probe were at the same vertical position, and each sensor was separated vertically by 1 in (2.54 cm).

For this example, the results of the interpolation for the three probes are summarized as:

Probe R1:	$A_o = 1.701$ in	$A_l = 1.859$ in	$\mu_o = 0^\circ$
Probe R2:	$A_o = 1.511$ in	$A_l = 1.972$ in	$\mu_o = -0.06^\circ$
Probe R3:	$A_o = 1.440$ in	$A_l = 1.974$ in	$\mu_o = -0.75^\circ$

The interpolation method established the location of the static free surface (by averaging the  $A_o$  data) as 1.551 in (3.940 cm) above the lowest line of sensors, and reduced the uncertainty in that position from  $\pm 0.5$  in (1.27 cm) to  $\pm 0.110$  in (0.279 cm). The true position is 1.5 in (2.54 cm) to within the accuracy of the test setting.

The sine waves fitted through the data for each probe are shown in Figures 5.2-5a - 5.2-5c. The predicted shape of the slosh wave, obtained from the amplitudes  $A_o$  and  $A_l$  of each sine wave, is shown in Figure 5.2-5d. Considering the small phase differences  $\mu_o$  between the probes, the phase has been neglected in this composite wave shape. The predicted slosh wave shape is a reasonable approximation of the actual wave shape, and in fact, if the static surface level had been predicted to be flat, the prediction would have been even more realistic. It is apparent that the sloshing was slightly nonlinear, which was also visually observed during the test. The predicted value of  $\approx 2$  in (5 cm) for the slosh wave amplitude at the wall was somewhat smaller than the true upward value of 2.65 in (6.7 cm) and even slightly smaller than the true downward value of  $\approx 2.2$  in (5.588 cm). A Fourier series interpolation scheme could account for the nonlinearity, which would further improve the estimate of the static liquid position and the wave shape.

Figure 5.2-6 shows an example of the improved results that can be obtained by using more sensors per probe. The predictions shown in this figure were actually obtained by combining the data from two identical slosh tests, but in which for one the array was positioned with the *lowest* sensor 0.5 in (1.27 cm) below the static surface (i.e., three sensors were exposed) and for the other the array was positioned with the *highest* sensor 0.5 in (1.24 cm) below the static surface (i.e., three sensors were submerged). This data set thus simulates an array in which there are six sensors along each probe, equally spaced at 1 in (2.54 cm) intervals. (Two of the sensors for each test overlapped, which is the reason that the simulation does not represent eight sensors per probe.) The slosh frequency and wave amplitude were the same as for the test discussed previously. The static liquid level was now predicted to be 2.550 in (6.480 cm) above the line of lowest sensors, compared to 2.5 in (6.35 cm) of the test, with an uncertainty of  $\pm 0.068$  in (0.172 cm), and the slosh amplitude at the wall was predicted to be  $\approx 2.4$  in ( $\approx 6.1$  cm), compared to 2.65 in (6.7 cm) for the test.

Other tests were conducted with the sensor array not aligned with the tank excitation direction; typically, angles of  $15^\circ$ ,  $30^\circ$ ,  $45^\circ$ , and  $60^\circ$  with respect to the excitation were used. The direction of the excitation can be computed from the data from two or more such tests (or from two or more arrays). It is assumed that the maximum wave amplitude at a given radial position varies with the cosine of the angle between the excitation direction and line of the array. For example, using the data from two separate tests in which the array was aligned at  $15^\circ$  and at  $45^\circ$  to the excitation direction, the excitation direction, and thus the line of the peak wave amplitude, was predicted to be  $9.3^\circ$ , compared to the true angle of  $0^\circ$ .

All the tests gave equally good predictions as the examples discussed above. Several conclusions can be drawn from the tests. First, there is no advantage and there is possibly a disadvantage in using an absolutely uniform array of probes. For example, if the sensor positions had been staggered vertically from one probe to another as shown in Figure 5.2-4b, the uncertainty in the position of the flat static position of the surface could have been reduced substantially. This improvement can also be obtained for static liquid surfaces that are curved, such as occur in low gravity. Second, the sensors in an array should be concentrated near the locations of the liquid surfaces used in the tests, rather than distributed uniformly along the entire depth of the tank. Third, the radial spacing of the probes should be no more than about  $0.3R_o - 0.4R_o$  to obtain an adequate resolution of wave shape, and a closer spacing would be desirable near the wall to resolve the contact angle. Fourth, unless the direction of tank excitation can be fixed in advance and the array aligned with that direction, at least two probe arrays are required to resolve the line of peak slosh amplitude; these arrays cannot be at right angles.

### 5.3 Load Cell Requirements

Measurement of liquid slosh forces is an essential requirement for both of the flight experiments. Therefore, a preliminary study was conducted to develop requirements for a force measurement system, and feasibility of a design for it.

The peak slosh force at resonance can be estimated from:

$$F \approx m_s \omega_n^2 x_0 Q \quad (5.3-1)$$

The slosh mass  $m_s$  and natural frequency  $\omega_n$  for a spherical tank can be obtained from the results given in Section 4.0. The amplitude  $x_0$  of the tank oscillatory motion and the resonance magnification factor  $Q$  can be estimated for linear sloshing to be:

$$x_0 = 0.05 R_0 \quad (5.3-2a)$$

$$Q = 25 \quad (5.3-2b)$$

For  $Bo \approx 0$ , the slosh force for the  $LH_2$  spherical tank of the COLD-SAT flight experiment is thus estimated to be about 0.0006 lb (0.00025 N). For the Shuttle flight experiment using water as the test liquid, the slosh force is about 0.0003 lb (0.0014 N) for the 13 in (33 cm) tank and 0.00018 lb (0.0008 N) for the 7 in (15 cm) tank. Compared to ordinary dynamics experiments, these are extremely small forces with extremely long (almost d.c.) time variations (see Tables 3.2-2 and 3.3-2).

A survey of commercially-available force transducers that may be suitable for flight experiments is summarized in [10]. The highest sensitivity listed in this survey is 500 mV/lb; thus, voltage variations of about 0.05 mV must be detected to measure the anticipated slosh forces. Custom-designed transducers using semiconductor strain gauges have therefore been used in previous laboratory studies of miniature slosh tanks [7, 27], and forces as small as 0.0001 lb [0.00044 N] were measured reliably. Figure 5.3-1 shows a schematic of how these kinds of sensitive strain gauges can be used in a dynamometer to measure slosh forces, in this case in the plane of the figure; a similar set of dynamometers at right angles is required to measure slosh forces perpendicular to the plane of the figure. Note that the dynamometer is rigid in bending and actually senses the tensile and compressive strains in the legs. The data acquisition system used in [7, 27] cancelled the inertia force of the empty tank electronically, so the force that was detected was only the oscillating slosh force; this method of measurement increased the force sensitivity of the dynamometers by several orders of magnitude. Further optimization of the design would improve the force sensitivity even more. It is concluded, therefore, that a force measurement system for the flight experiments can be achieved. The specifications for such a system are listed in Table 5.3-1.

Both in-line and cross-axis response must be measured by means of an X-Y coordinate system. This is necessary in order to determine whether rotary slosh occurs. Static longitudinal dead load cancellation must be included in order to concentrate on the accuracy of the dynamic load measurement. Similarly, cancellation of empty tank dynamic load is desirable for the same reason. The requirement for the very low frequency range has already been mentioned, and will be aggravated by drift in the electronic circuits. Finally, static lockout will be required to avoid the effects of dead loads during high-g phases of the flights (both static and dynamic). Although all these requirements are extremely severe in terms of comparative requirements for high-g testing, it was concluded that a design which uses existing state-of-the-art technology is entirely feasible.

**TABLE 5.3-1 DYNAMOMETER REQUIREMENTS**

- |   |
|---|
| <ul style="list-style-type: none"><li>• <math>10^{-4}</math> to <math>10^{-3}</math> lbs. Range</li><li>• In-Line and Cross-Axis Response</li><li>• Static Longitudinal Dead Load Cancellation</li><li>• Empty Tank Dynamic Load Cancellation</li><li>• DC to 1 Hz Frequency Range</li><li>• Static Lockout</li></ul> |
|---|



## **6.0 CONCLUSIONS**

### **6.1. Flight Experiments**

This study of liquid slosh dynamics and control has shown that there is a real need for flight experiments to gain fundamental understanding about the phenomena that dominate liquid motions in low gravity and to improve and validate analytical models. Many planned space missions depend upon the ability to predict and control liquid motions, using information that can only be gained from realistic flight experiments. To that end, two flight experiments were defined: an experiment using liquid hydrogen in the spherical and cylindrical "receiver" tanks of NASA's proposed COLD-SAT test bed satellite; and an experiment designed for the Shuttle middeck using water or other nonhazardous liquids. The types of liquid motions to be investigated include small-amplitude sloshing, nonlinear or rotary sloshing, and the decay of large-amplitude motions to long-lived, small-amplitude sloshing. To produce these motions, the test tanks will be subjected both to transient impulsive accelerations and to oscillatory accelerations sustained for up to eight to ten cycles. Both experiments will investigate the range of Bond numbers near zero. For the COLD-SAT experiment, the Bond number for each tank can be varied over about a factor of four by employing the satellite thrusters, while for the mid-deck experiment, the Bond number is constant. The specifications and data requirements for the flight experiments are within the capabilities of each respective carrier.

Analytical efforts and ground-based experiments were conducted in support of the flight definitions. The conclusions from these efforts are summarized separately below.

### **6.2 Analytical Studies**

#### **6.2.1 Small Amplitude Linear Sloshing**

The computational fluid dynamics codes FLOW-3D and NASA-VOF3D were used to simulate low gravity sloshing in spherical tanks. Neither code was able, however, to make a realistic simulation, primarily because of their difficulty in modeling the "free" contact line condition (i.e., constant contact angle) and in accurately representing surface tension forces. Therefore, a new analysis of linear sloshing in low gravity was developed in an integral-minimization form; this formulation permits the relatively simple surface physics assumptions used in the analysis to be modified readily when better knowledge becomes available from flight experiments, which is thought to be a distinct advantage. Several errors in previous analyses of the slosh force were also corrected. "Trial" solution functions were computed by an innovative use of a finite-element structural code, which were then used in the integral-minimization technique to compute the sloshing frequencies, forces, and mechanical model. Since the method is based on a finite element structural code, it can be adapted readily by other investigators.

Examples were computed for a spherical tank to demonstrate the use of the methods. The examples employed fill levels of 25%, 50%, and 78%, for Bond numbers of 1 and 2. Methods were developed to "start" the finite element structural simulation such that rapid convergence of the numerics is ensured. The results of the examples show that the non-dimensional slosh frequency decreases as the Bond number decreases, in agreement with the limited experimental data available, although the frequencies were consistently slightly larger than previous finite difference simulations. The slosh masses of the mechanical model were predicted to be substantially smaller than the corresponding high-g slosh masses.

### **6.2.2 Rotary Slosh Model**

An existing pendulum analogy of rotary sloshing was investigated more thoroughly and extended in a preliminary way to low gravity conditions, in order to estimate the importance of nonlinear effects in low gravity sloshing.

A numerical scheme for integrating the equations of motion of the compound spherical and linear pendulum was developed. The scheme can be used effectively to establish all the pertinent model parameters for rotary slosh and is sufficiently general to be applied to any slosh test in which the cross-axis and in-line slosh forces (i.e., effective weights of the pendulum masses) can be measured. Some initial guessing of damping parameters is required, with help from the harmonic balance approximate model, to start the process. The guessing process also is helped by the fact that, at a given frequency point, an increase of both the circumferential damping and the radial damping tends to increase the cross-axis weight produced. Since damping increases in low gravity, this result indicates an increased tendency for cross-axis forces in low gravity, which thus impacts the design of control systems.

The rotary slosh problem is complex in the sense that the mechanical model parameters vary with frequency throughout the pertinent range. Hence, no one set of parameters can be claimed to represent the compound system. Because of this complexity, the questions remains of what is the best approach to studying the system response to transient inputs. If one set of parameters must be selected, those associated with  $\alpha > 1.0$  are the most appropriate. This is the frequency range in which the maximum rotary motion occurs and the largest rotary forces. The harmonic balance approximation provides good estimates of the system parameters when the response is nearly circular. The next logical step is to make a numerical study of the transient response of the compound pendulum model for low gravity conditions. It is also appropriate to determine whether the addition of other mechanical components to the model might eliminate some of the coupling problems as well as the variation of the system parameters with frequency. Finally, although only counter-clockwise rotational motions were used in the present modeling study, clockwise solutions also exist for each case. The direction of rotation that actually occurs depends on the initial conditions and any lack of true rotational symmetry in the physical system.

## **6.3 Ground-Based Experimentation**

### **6.3.1 Liquid-Vapor Interface Sensors**

Miniature electrical resistor sensors and, possibly, fiber optic sensors can be used to determine the location of a discrete point on a liquid interface. An array of such sensors can therefore be used in flight experiments to track and "visualize" the motions of the liquid surface. The frequency response of these sensors is substantially better than the relatively slow frequencies of the liquid surface motions expected in low gravity. Ground testing, using non-flight sensors, was employed to determine the spatial distribution of such arrays of sensors that are required to resolve low gravity surface configurations and slosh wave shapes. Since the sensors give only a "wet to dry" or "dry to wet" indication, an interpolation scheme was also developed as part of the testing to convert this digital data from the sensors to a continuous time history of the motion of each discrete surface point. The test results proved that the free surface configuration and the slosh wave shape could be resolved satisfactorily by arrays that were spaced radially at distances of no more than 15% to 30% of the tank radius, and spaced vertically at about 10% of the tank radius. Better resolution could be obtained with denser arrays, especially near the tank walls. In any case, the number and spacing of the sensor arrays can be optimized for specific liquid levels. It was concluded that (a) the frequency response of available sensors is more than adequate for flight experiments, and (b) the required number and distribution of the sensors does not appear to be impractical.

### **6.3.2 Slosh Force Transducers**

The slosh forces that must be measured are in the range of 0.0006 lb (0.00025 N) for the COLD-SAT flight experiment and 0.0002 lb (0.0009 N) for the middeck flight experiment. The natural period of the sloshing is about 800 sec for the COLD-SAT experiment and 100 sec for the middeck experiment. Such small forces with such relatively long periods cannot be measured with conventional laboratory transducers. Nonetheless, a survey of commercially-available transducers and of dynamometers used previously in laboratory testing of small Bond number sloshing did reveal that the force measurement requirements can be satisfied. The most promising of the available methods used semiconductor strain gages in a tension-compression arrangement, coupled with electronic cancellation of non-slosh forces, to measure slosh forces as small as 0.0001 lb (0.00044 N). Further optimization of this design, which is inherently rugged and capable of supporting large dead loads, should satisfy the requirements of the flight experiments.



## 7.0 REFERENCES

1. **The Dynamic Behavior of Liquids in Moving Containers**, ed. H. N. Abramson, NASA SP-106, 1966. (Corrected and reprinted, Southwest Research Institute, 1987.)
2. Lomen, D. O., "Digital Analysis of Liquid Propellant Sloshing in Mobile Tanks with Rotational Symmetry," NASA CR-230, 1965.
3. Unruh, J. F., Kaña, D. D., Dodge, F. T., and Fey, T. A., "Digital Data Analysis Techniques for Extraction of Slosh Model Parameters," **J. Spacecraft and Rockets**, **23**, 1986, pp. 171-177.
4. Vreeburg, J. P. B., "Results of the Forced Liquid Motion Experiment 'FLIM'," AIAA Conf. Preprint, AIAA Document A88-27659.
5. Salzman, J. A., and Masica, W. J., "An Experimental Investigation of the Frequency and Damping of Liquids During Weightlessness," NASA TN D-5058, 1969.
6. Coney, T. A., and Salzman, J. A., "Lateral Sloshing in Oblate Spheroidal Tanks Under Reduced- and Normal-Gravity Conditions," NASA TN D-6250, 1971.
7. Dodge, F. T., and Garza, L. R., "Experimental and Theoretical Studies of Liquid Sloshing at Simulated Low Gravity," **Trans. ASME, J. Applied Mechanics**, **34**, 1968, pp. 555-562.
8. Coney, T. A., and Masica, W. J., "Effect of Flow Rate on the Dynamic Contact Angle for Wetting Liquids," NASA TN D-5115, 1969.
9. Dodge, F. T., "The Spreading of Liquid Droplets on Solid Surfaces," **J. Colloid and Interface Science**, **121**, 1988, pp. 154-159.
10. Van Schoor, M. C., Crawley, E. F., and Hansman, J. C., "The Coupled Nonlinear Dynamics of Spacecraft with Fluids in Tanks of Arbitrary Geometry," Report SSL #4-89, Space Systems Laboratory, Massachusetts Institute of Technology, Cambridge, 1989.
11. Crawley, E. F., Miller, D. W., Van Schoor, M., and De Luis, J., "Middeck 0-Gravity Dynamics Experiment (MODE)," Report SS1 9-89, Space Systems Laboratory, Massachusetts Institute of Technology, Cambridge, 1989.
12. Jetley, R. L., and Scarlotti, R. D., "Space Station Experiment Definition: Long-Term Cryogenic Fluid Storage," NASA CR-4072, 1987.
13. Dergance, R. H., Hamlyn, K. M., and Tegart, J. R., "Low Thrust Chemical Orbit to Orbit Propulsion System Propellant Management Study," NASA CR-165293, 1981.
14. Merino, F., Risberg, J. A., and Hill, M., "Orbital Refill of Propulsion Vehicle Tankage," NASA CR-159722, 1980.
15. Anon., "Definition of Technology Development Missions for Early Space Station. Orbital Transfer Vehicle Servicing," Report No. GDC-SP-83-052, General Dynamics Convair Division, 1983.
16. Merino, F., Wakabayashi, I., Pleasant, R. L., and Hill, M., "Low-Thrust Chemical Propellant Expulsion and Thermal Conditioning Study," NASA CR-167841, 1982.
17. Eberhardt, R. N., Cunningham, G. R., and Johns, W. A., "Conceptual Design and Analysis of Orbital Cryogenic Liquid Storage and Supply Systems," NASA CR-165231, 1981.

18. Sicilian, J. M., "FLOW-3D Surface Tension Models: Current Status and Possible Improvements," Report No. FSI-89-30-1, Flow Science Inc., Los Alamos, New Mexico, 1989.
19. Concus, P., Crane, G. E., and Satterlee, H. M., "Small Amplitude Lateral Sloshing in a Cylindrical Tank with a Hemispherical Bottom Under Low Gravitational Conditions," NASA CR-54700, 1967.
20. Concus, P., Crane, G. E., and Satterlee, H. M., "Small Amplitude Lateral Sloshing in Spheroidal Containers Under Low Gravitational Conditions," NASA CR-72500, 1969.
21. Bauer, H. F., and Eidel, W., "Small Amplitude Liquid Oscillations in Rectangular Container Under Zero Gravity," *L'Aéronatique et l'Astronautique*, **139**, 1989, pp. 35-42.
22. Van Schoor, M., Peterson, L. D., and Crawley, E. F., "The Coupled Dynamics of Contained Fluids in Zero Gravity," AIAA Paper 90-0966-CP, 1990.
23. Myshkis, A. D., Babitskii, N. D., Kopachevskii, N. D., Slobozhanin, L. A., and Tyuptsov, A. D., *Low-Gravity Fluid Mechanics*, Springer-Verlag, Berlin, 1987.
24. Concus, P., and Finn, R. "Capillary Surfaces in Microgravity," in *Low Gravity Fluid Dynamics and Transport Phenomena (Progress in Astronautics and Aeronautics, 130)* ed. Koster, J., and Sani, R., AIAA, Washington, D. C., 1990, pp. 183-205.
25. Satterlee, H. M., and Reynolds, W. C., "The Dynamics of the Free Liquid Surface in Cylindrical Containers Under Strong Capillary and Weak Gravity Forces," Technical Report LG-2, Stanford University, 1964.
26. Everstine, G. C., "Structural Analogies for Scalar Field Problems," *Int. J. Numerical Methods in Engineering*, **17**, 1981, pp. 471-476.
27. Dodge, F. T., and Garza, L. R., "Simulated Low-Gravity Sloshing in Spherical, Ellipsoidal, and Cylindrical Tanks," *J. Spacecraft and Rockets*, **7**, 1970, pp. 204-206.
28. Peterson, L. D., "Experimental Observations of Low and Zero Gravity Nonlinear Fluid-Spacecraft Dynamics," Sandia Report SAND88-2473C-VC-13, DOE Contract DE-AC04-76DP00789, Albuquerque, NM, October 198.
29. Miles, J. W., "Resonant Motion of a Spherical Pendulum," *Physica*, Vol. 11D, 1984, pp. 309-323.
30. Tritton, D., "Chaos in the Swing of a Pendulum," *New Scientist*, 24 July 1986, pp. 37-40.
31. Kaña, D. D., "Validated Spherical Pendulum Model for Rotary Liquid Slosh," *Jour. Spacecraft and Rockets*, **26**, May-June 1989, pp. 188-195.
32. Lacovic, R. F., Yeh, F. C., Szabo, S. V., Brun, R. J., Stofan, A. J., and Berns, J. A., "Management of Cryogenic Propellants in a Full Scale Orbiting Space Vehicle," NASA TN D-4571, 1968.
33. Siegwarth, J. D., and Voth, R. O., "Test of Liquid-Vapor Sensors in LN<sub>2</sub>," NIST Progress Report to NASA-LeRC, 1990.
34. Siegwarth, J. D., and Voth, R. O., "A Fiber Optic Device for Liquid-Vapor surface Sensing," NIST Progress Report to NASA-LeRC, 1990.

35. Siegwarth, J. D., Snyder, S. M., and Voth, R. O., "Liquid-Vapor Interface Sensors for Liquid Nitrogen and Hydrogen," **Proc., 1991 Space Cryogenic Workshop**, NASA-LeRC, June 1991.
36. Kaña, D. D., "A Resistive Wheatstone Bridge Liquid Wave Height Transducer," Tech. Rept. 2, Contract NAS8-11045, Southwest Research Institute, 1964.



## **FIGURES**



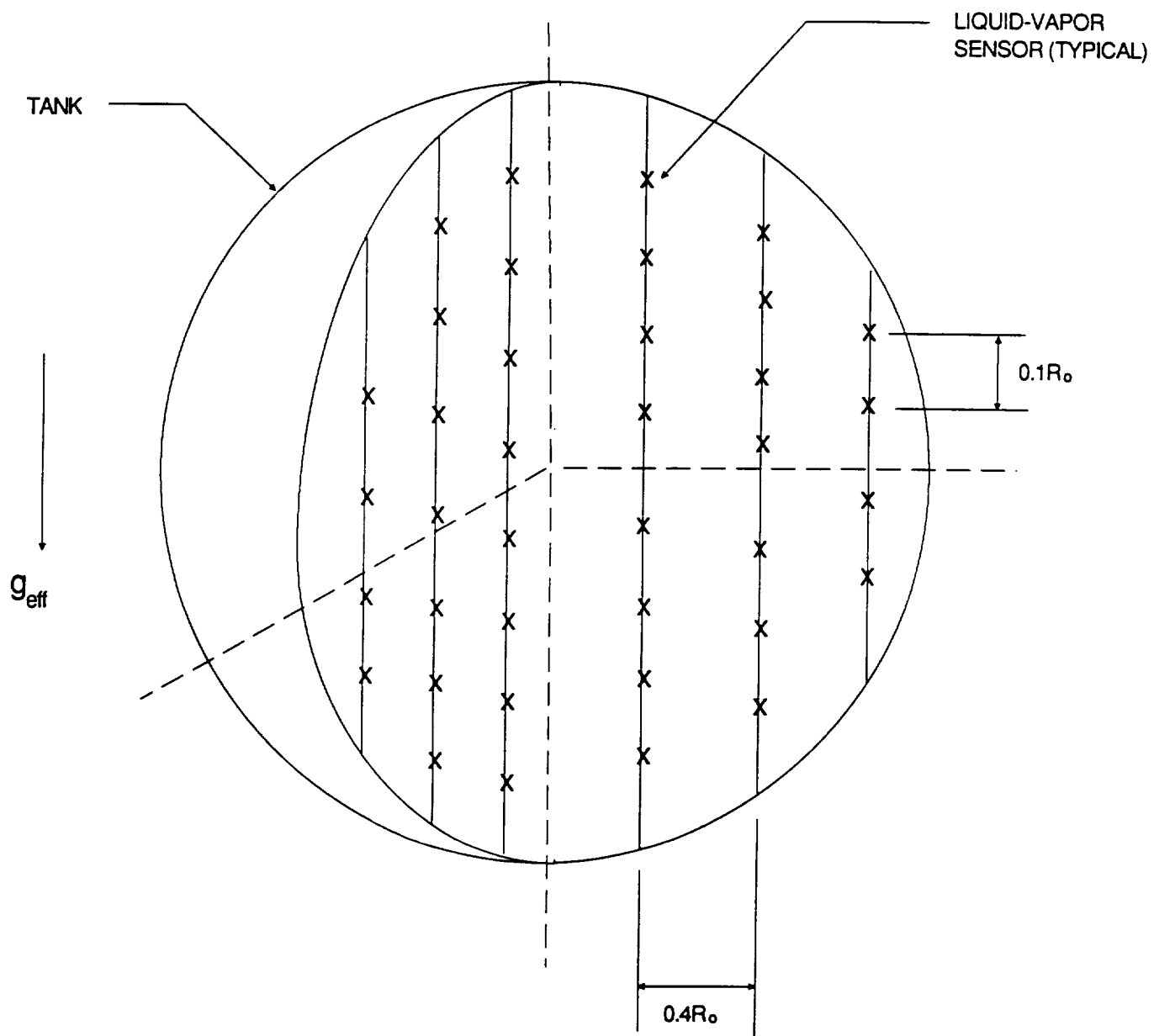


**Figure 3.1-1 Typical Liquid-Vapor Sensor Array**

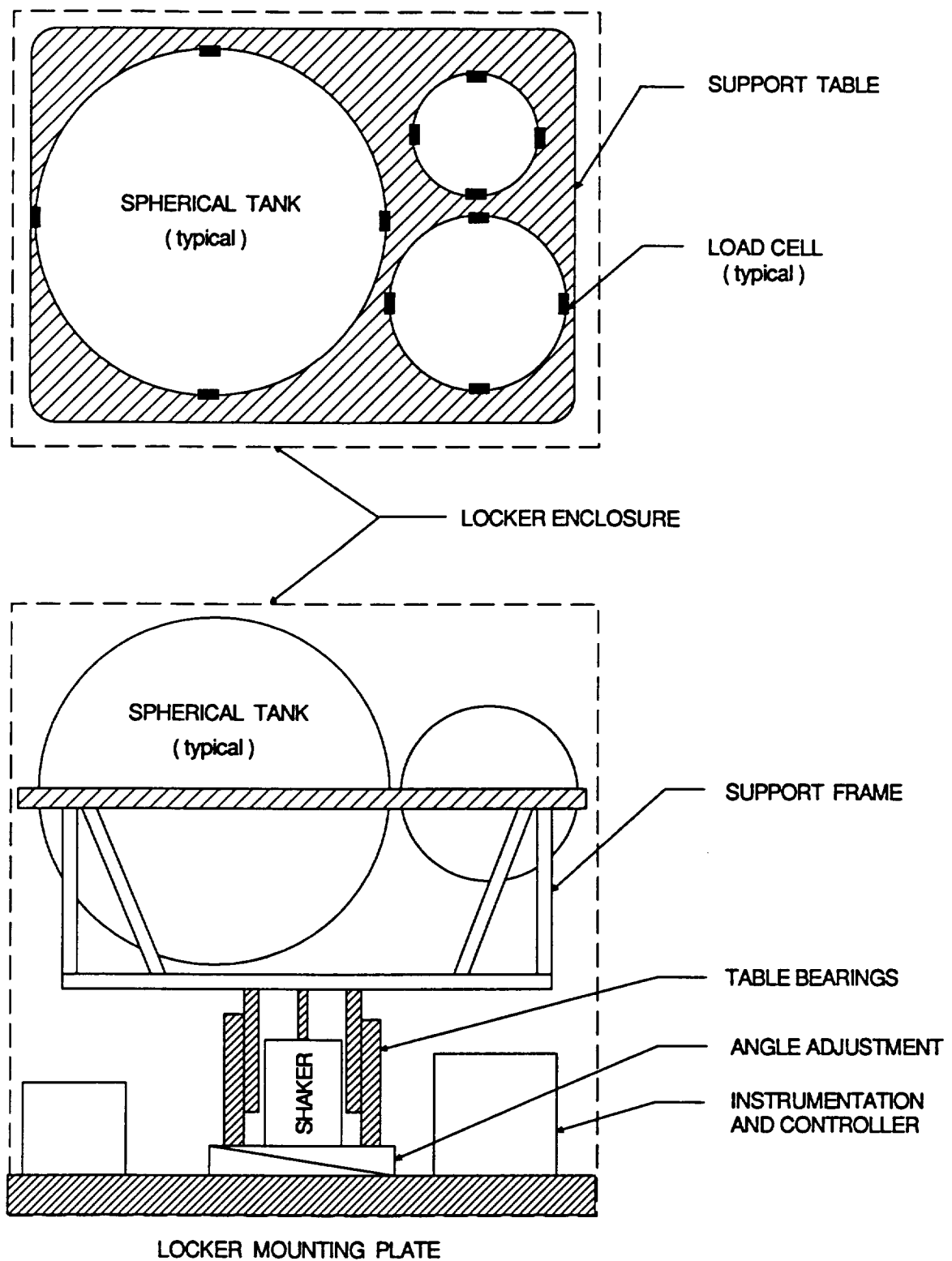


**Figure 3.3-1 Conceptual Design of Shuttle Flight Experiment Package**

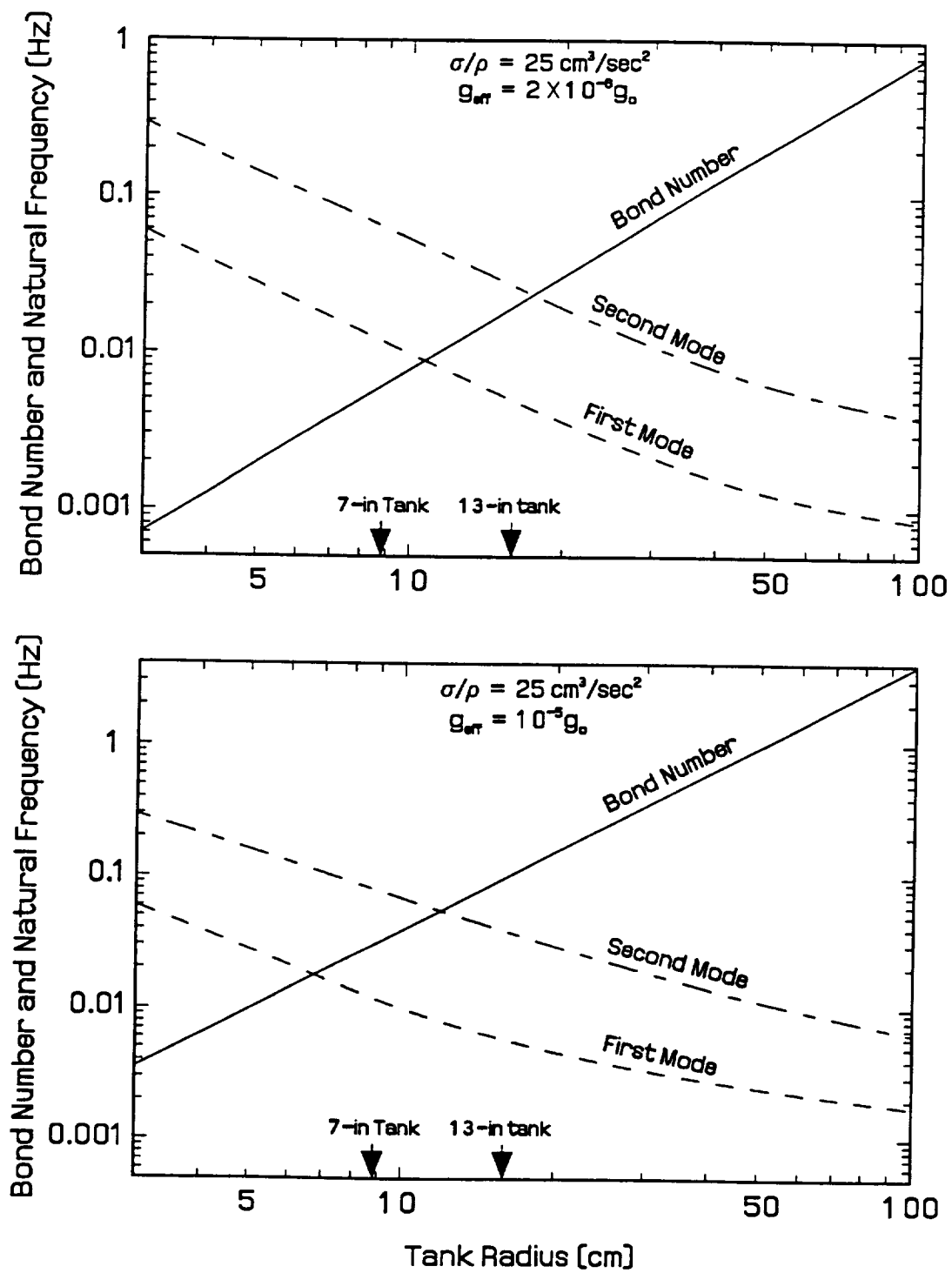


**Figure 3.3-2 SLOSH Characteristics of a Half-Full Spherical Tank**

# CONTROL PROCESSOR

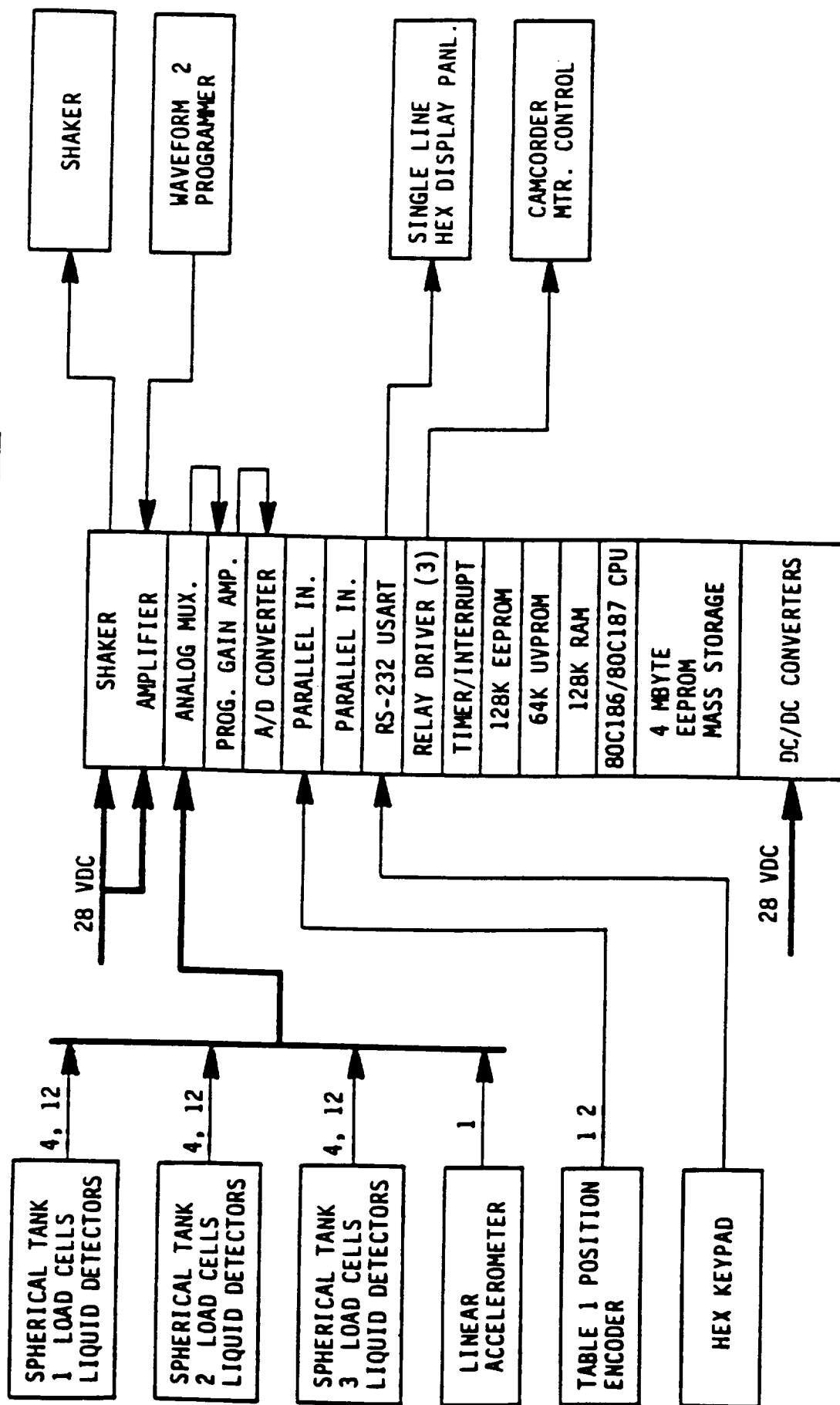
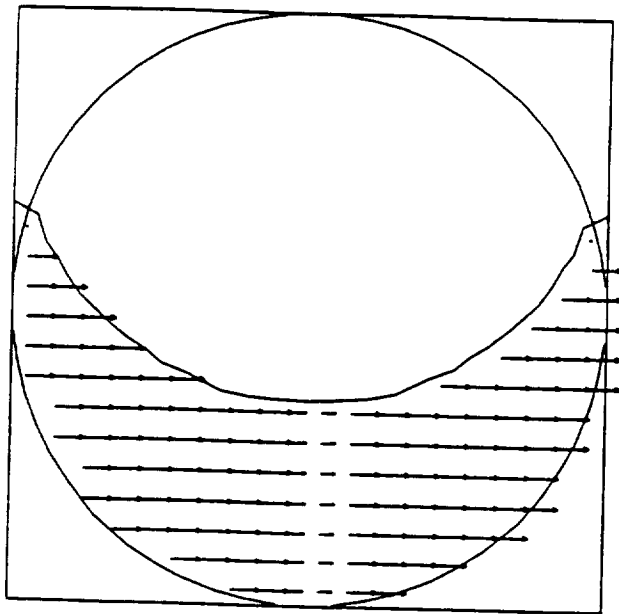
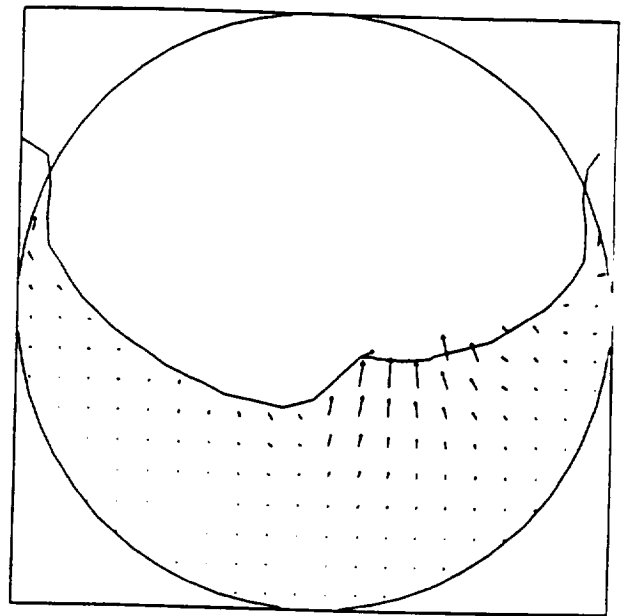


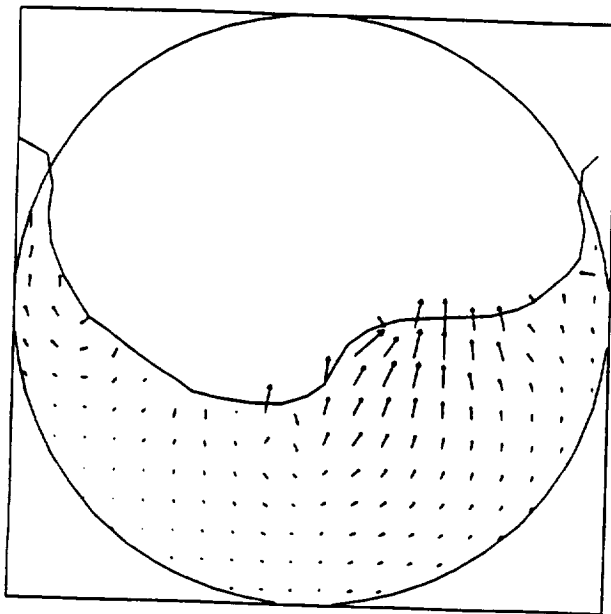
Figure 3.3-3 Block Diagram of Shuttle Flight Experiment Instrumentation and Hardware



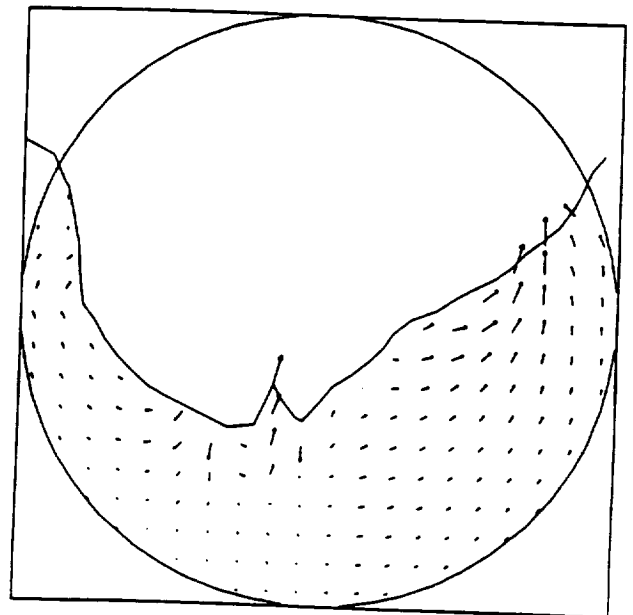
(a)



(b)



(c)



(d)

**Figure 4.3-1 NASA-VOF3D Simulation of  $Bo = 10$  Sloshing in a Spherical tank.  
Time Increases Right to Left, Top to Bottom.**

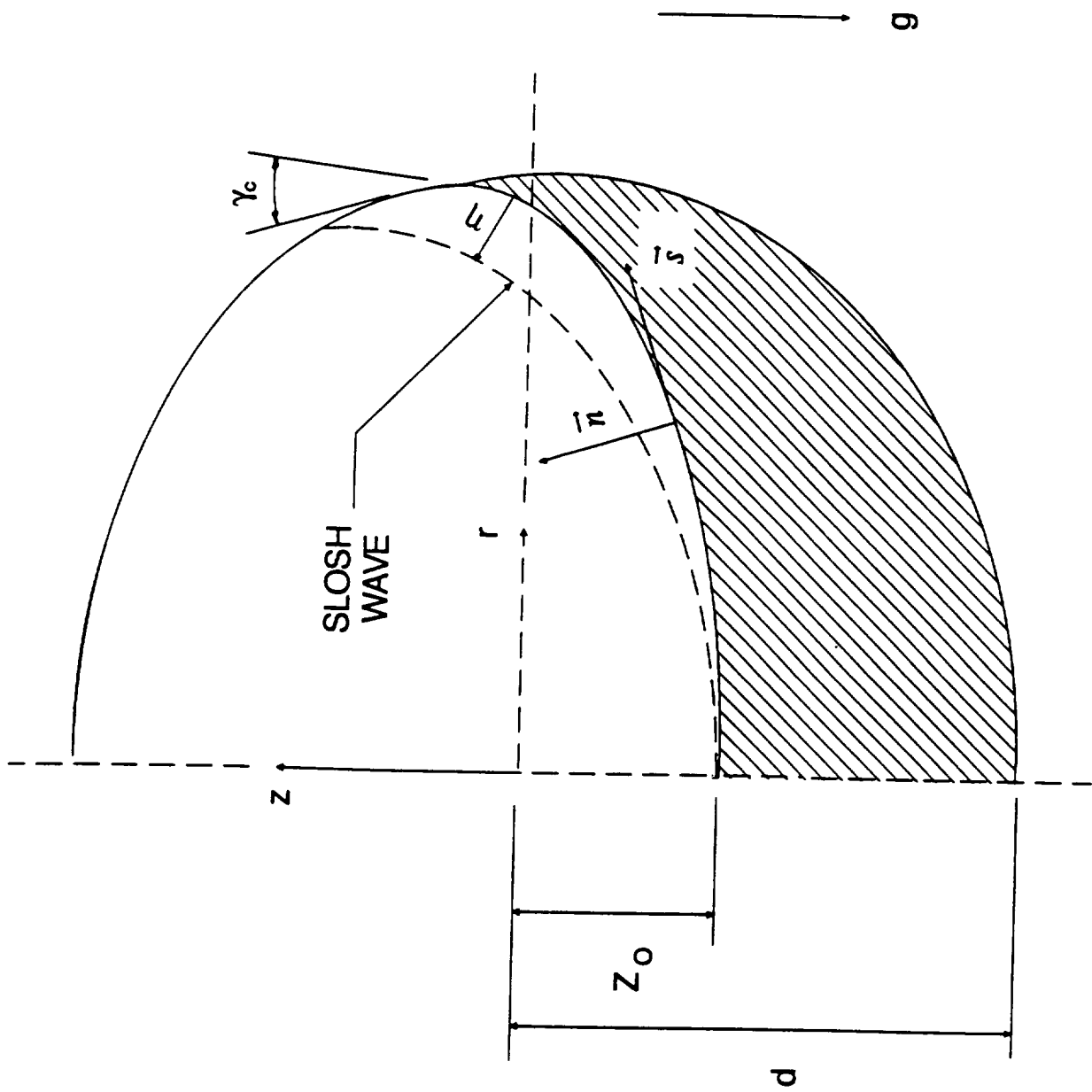
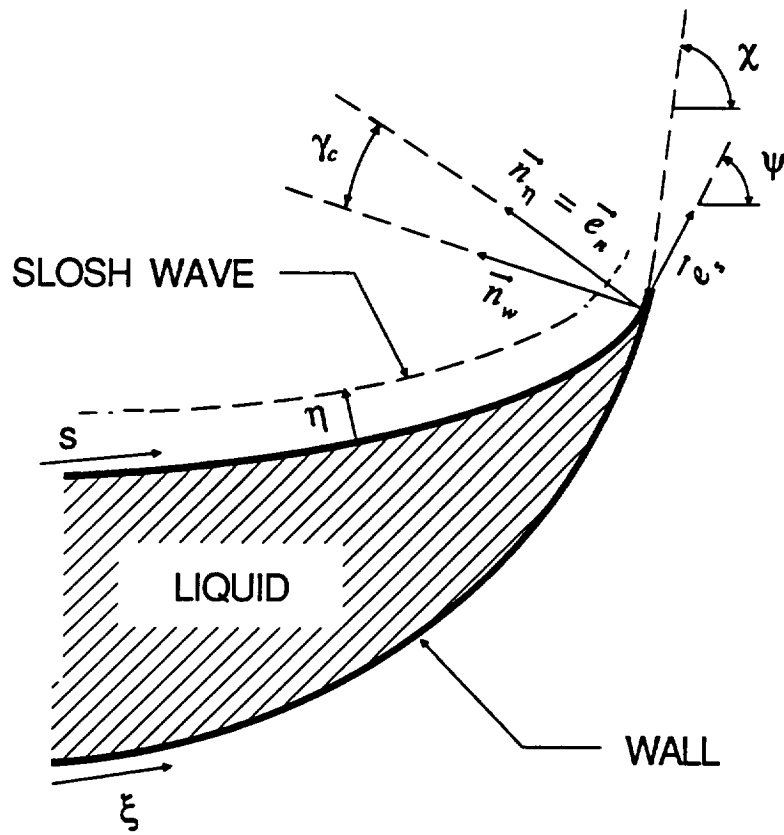
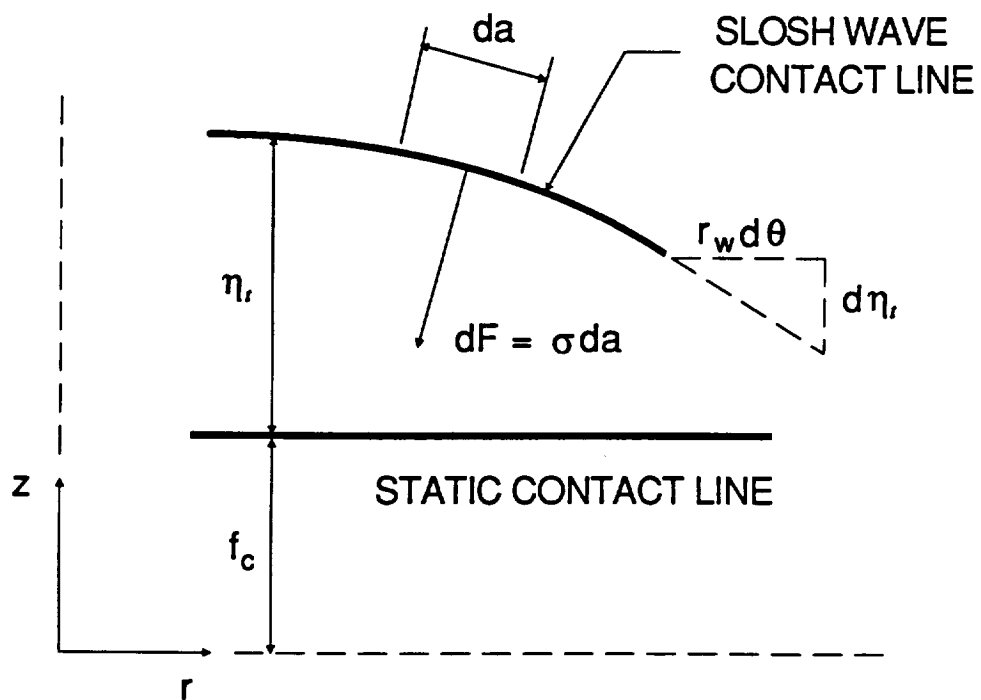


Figure 4.4-1 Schematic for Low-G Slosh Analysis



(a) Contact line



(b) Contact line projections on the tank wall

Figure 4.4-2 Details of Low-G Slosh Analysis

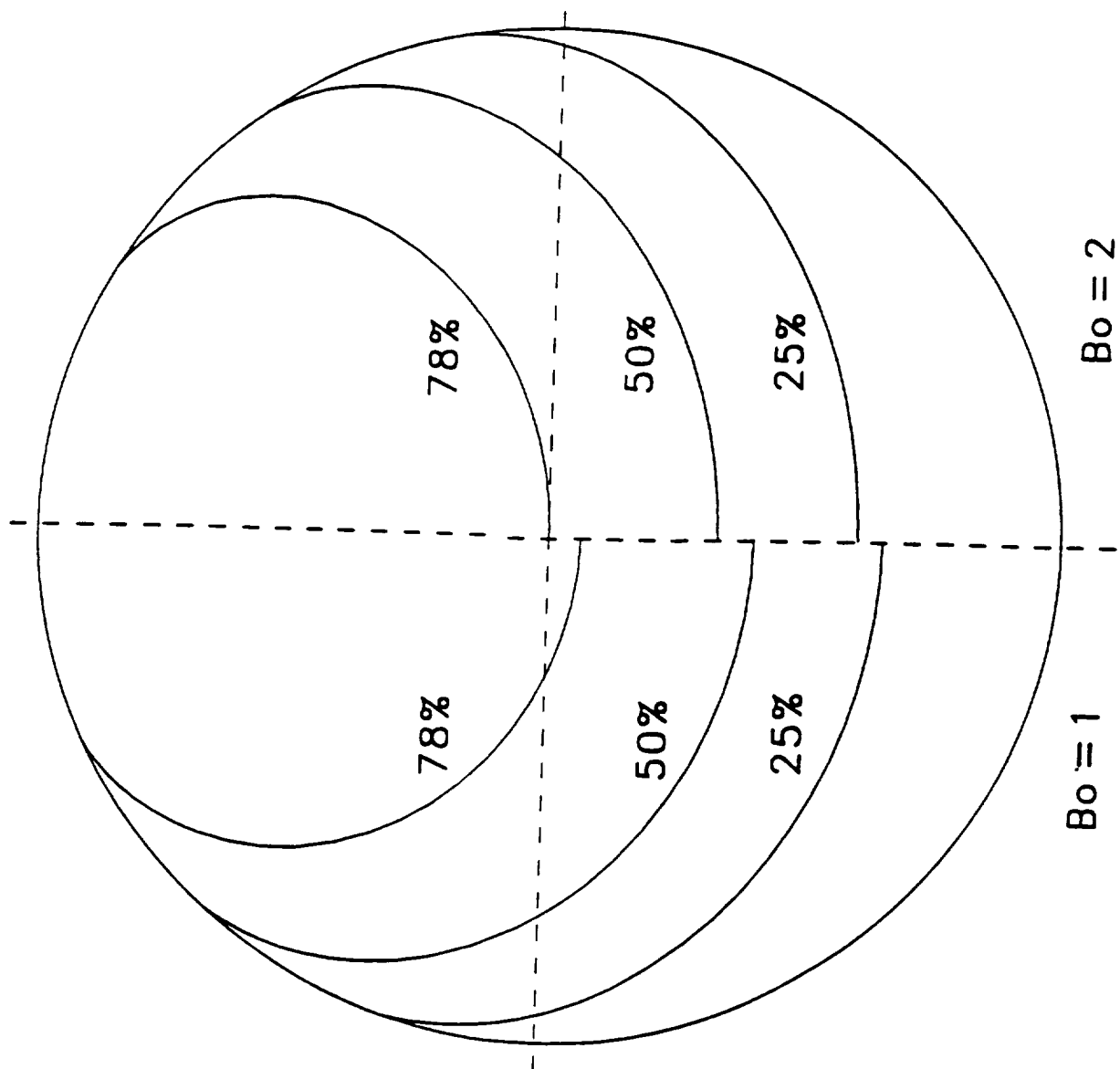


**Figure 4.4-3 Equilibrium Free Surface Shapes**

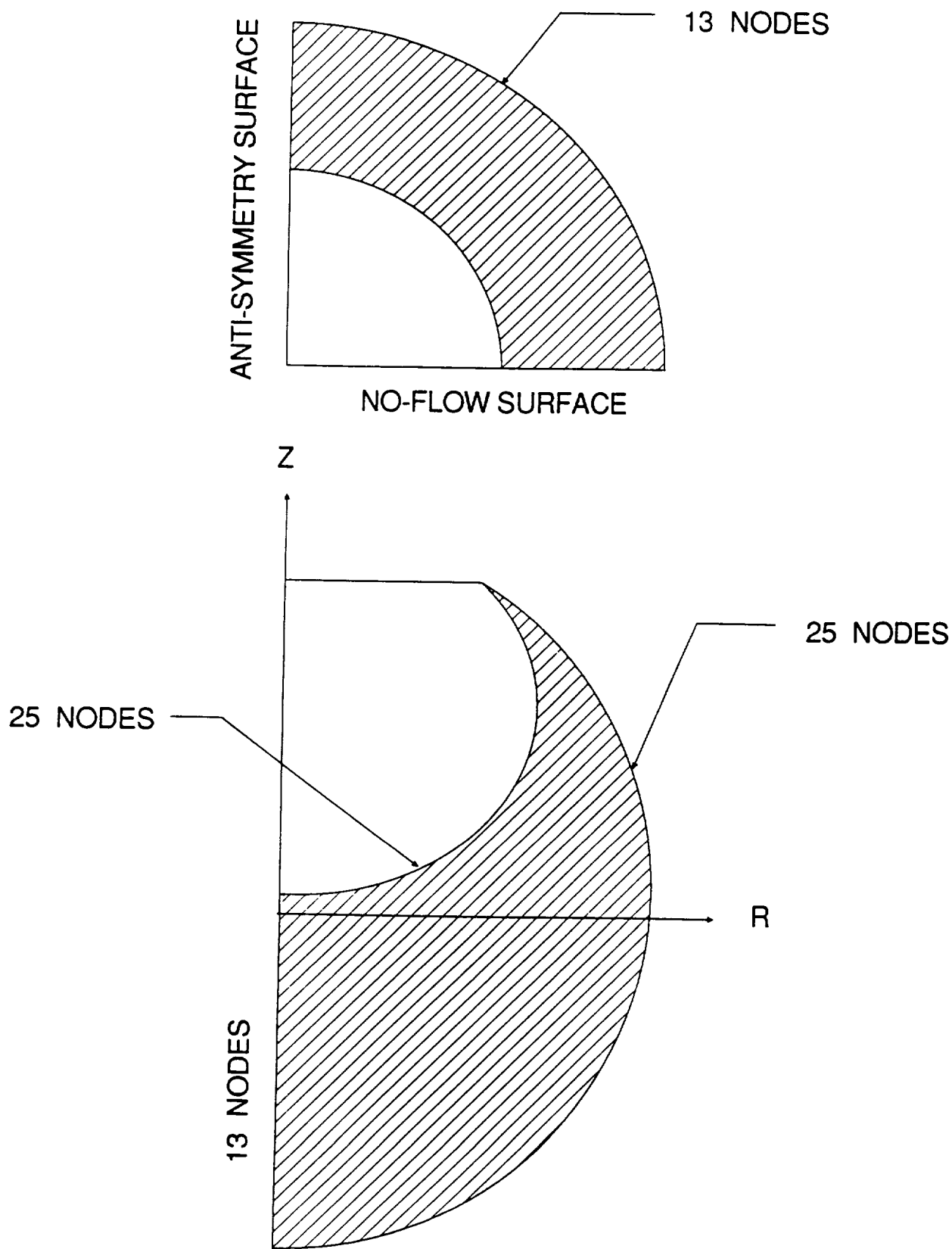


**Figure 4.4-4 Finite Element Model**

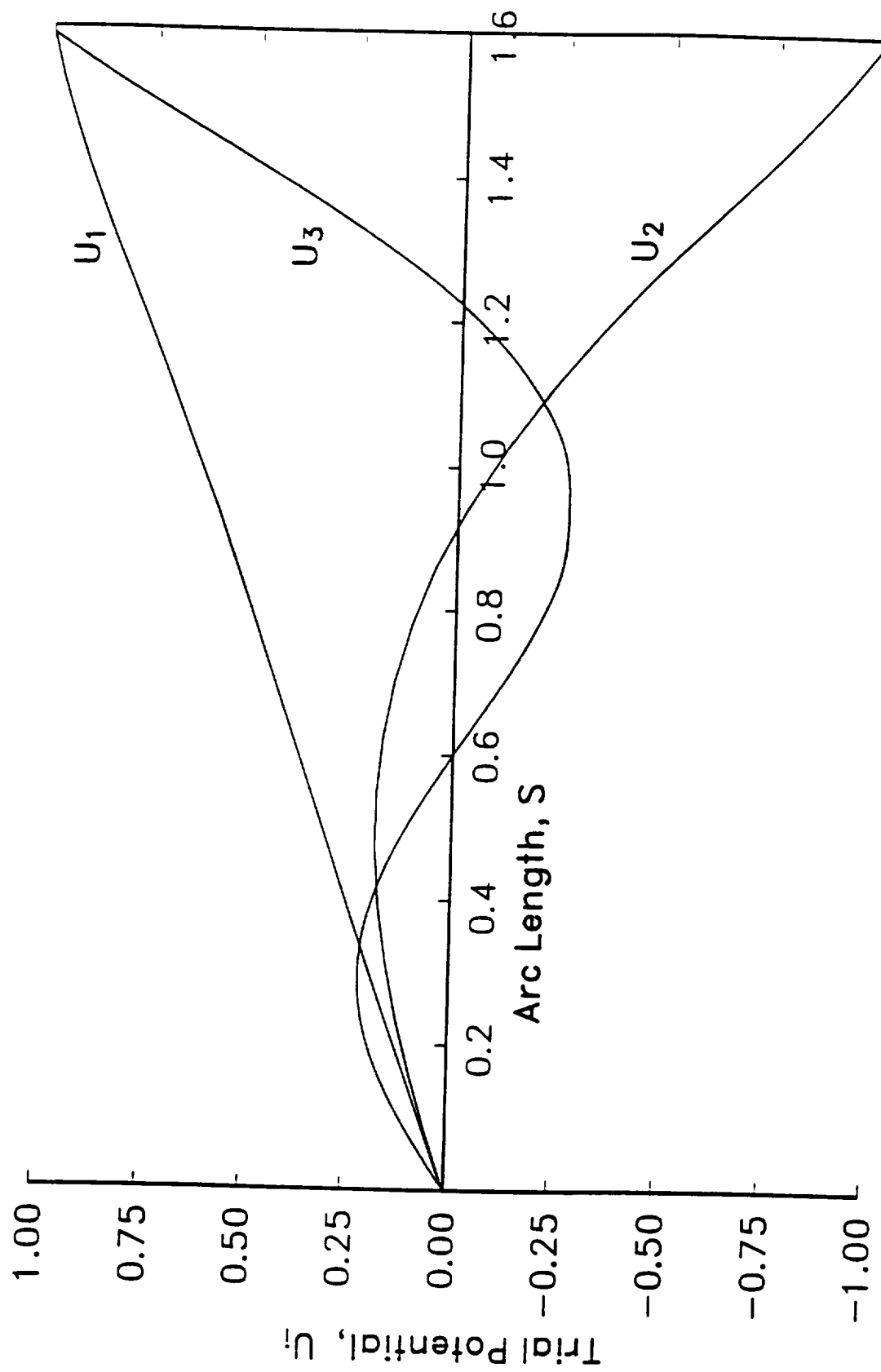


Figure 4.4-5 Trial Potentials for 50% Full,  $Bo = 1$

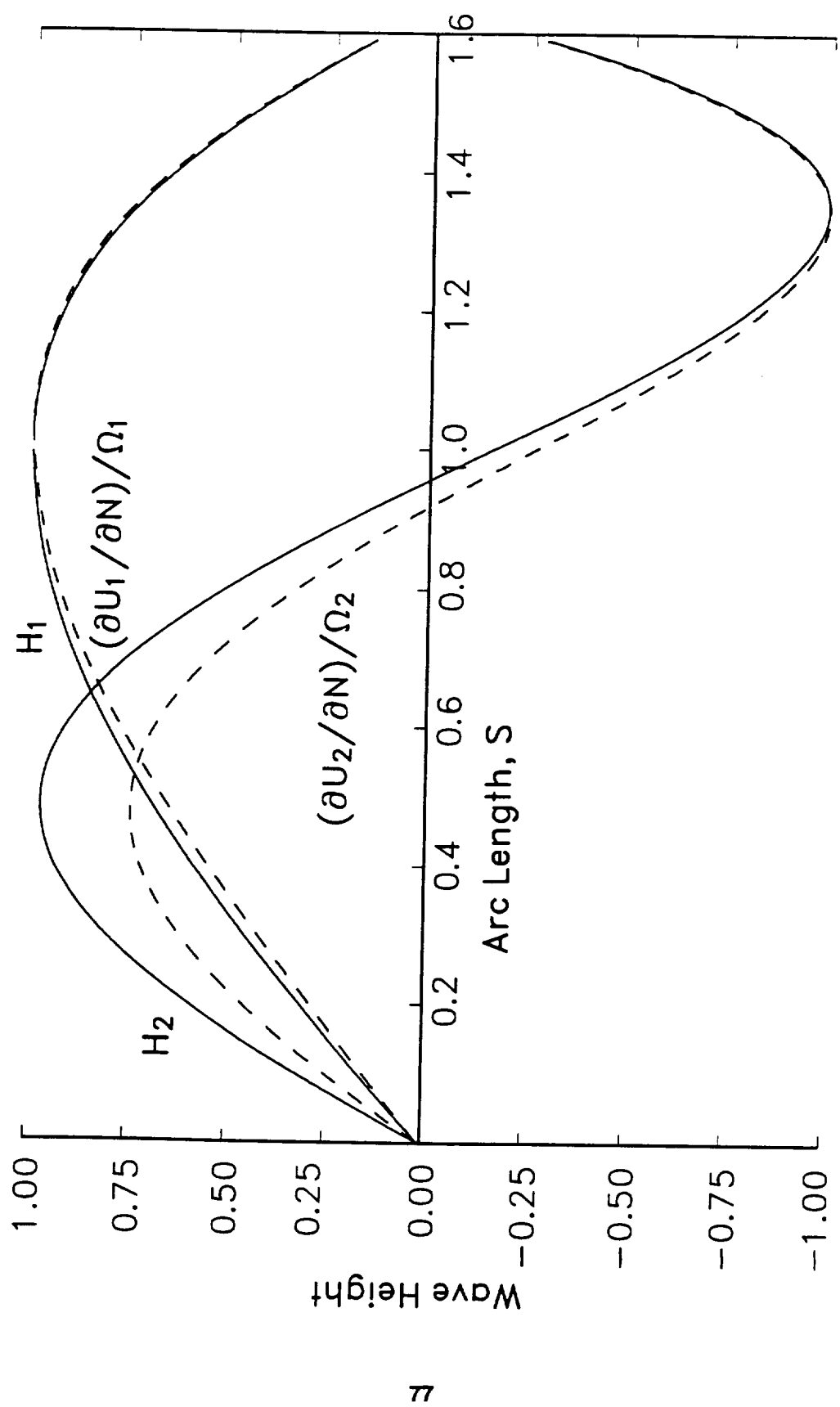
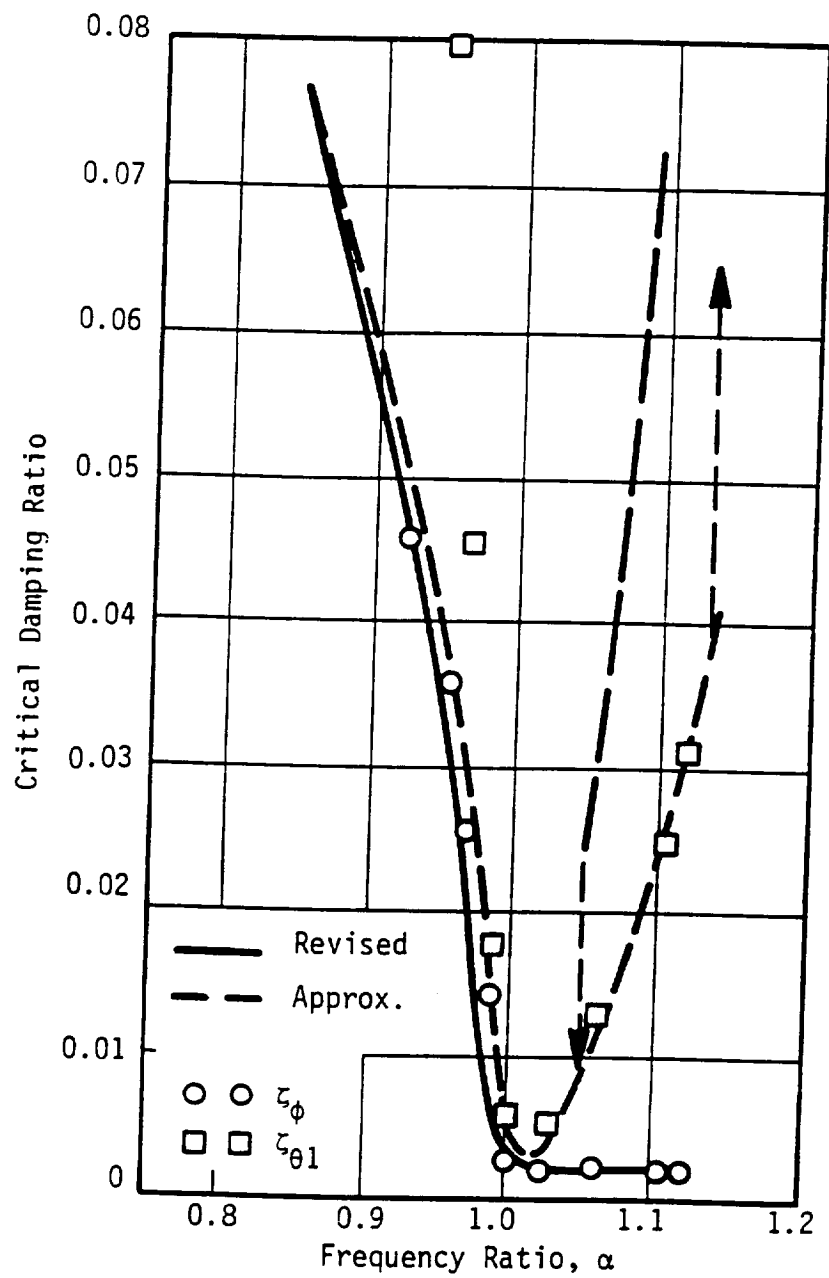
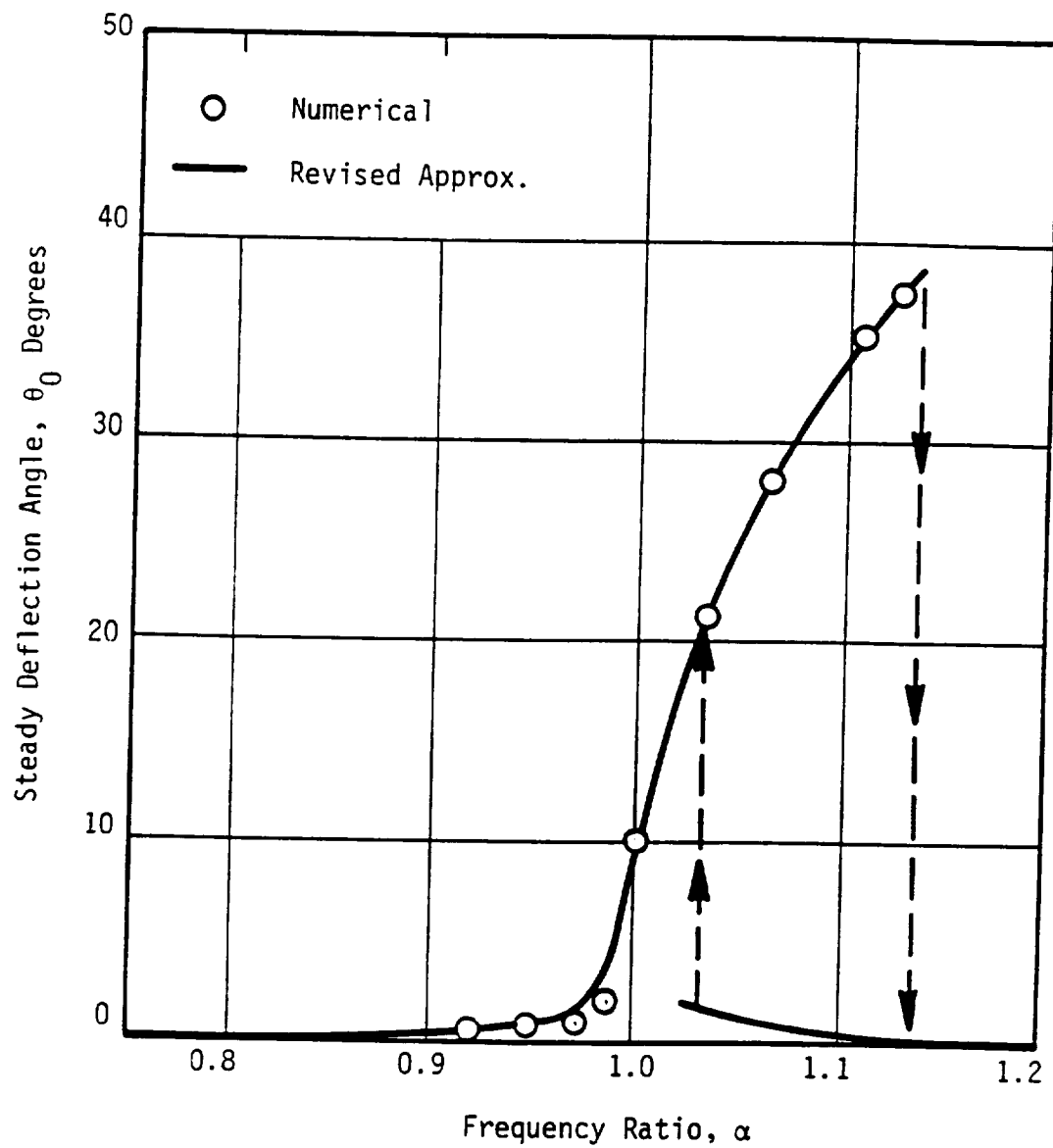


Figure 4.4-6 Slosh Wave Shape for 50% Full,  $Bo = 1$





**Figure 4.5-2 Circumferential and Radial Damping Factors**



**Figure 4.5-3 Steady Deflection Angle**

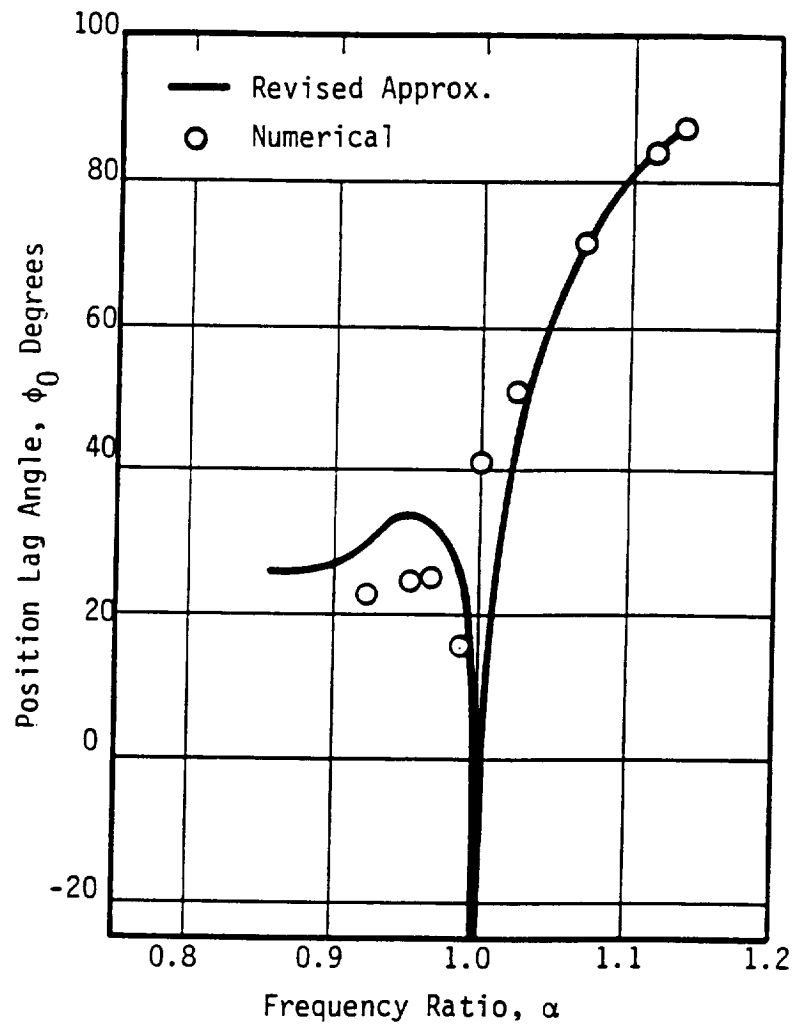


**Figure 4.5-4 Position Lag Angle**

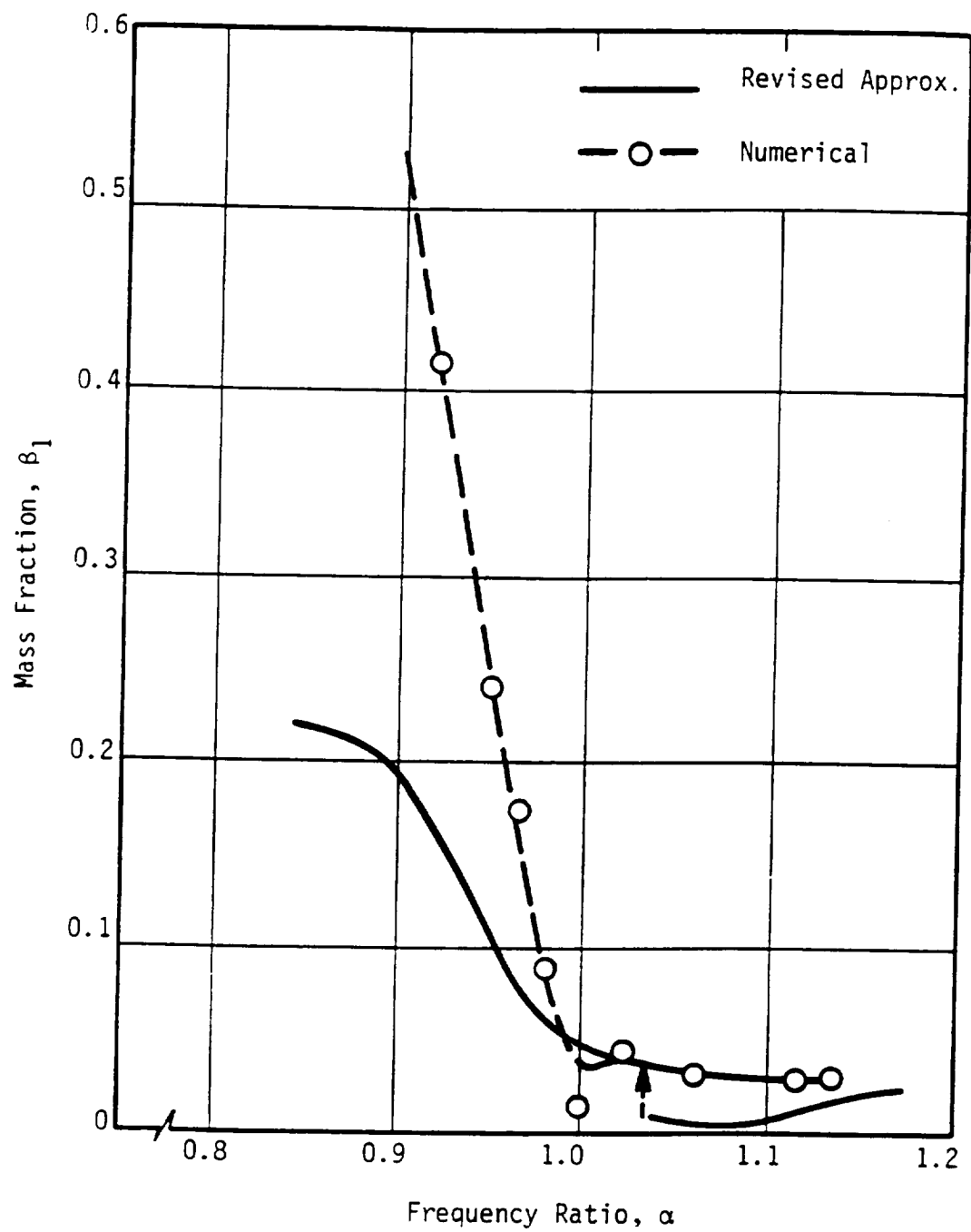
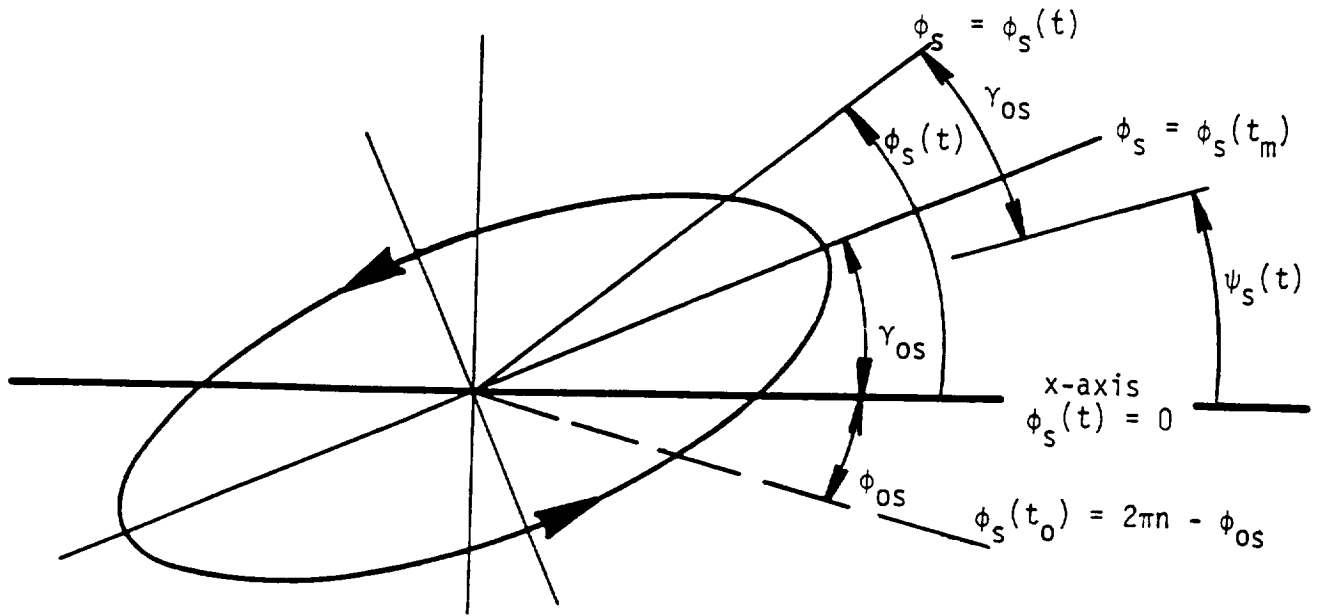
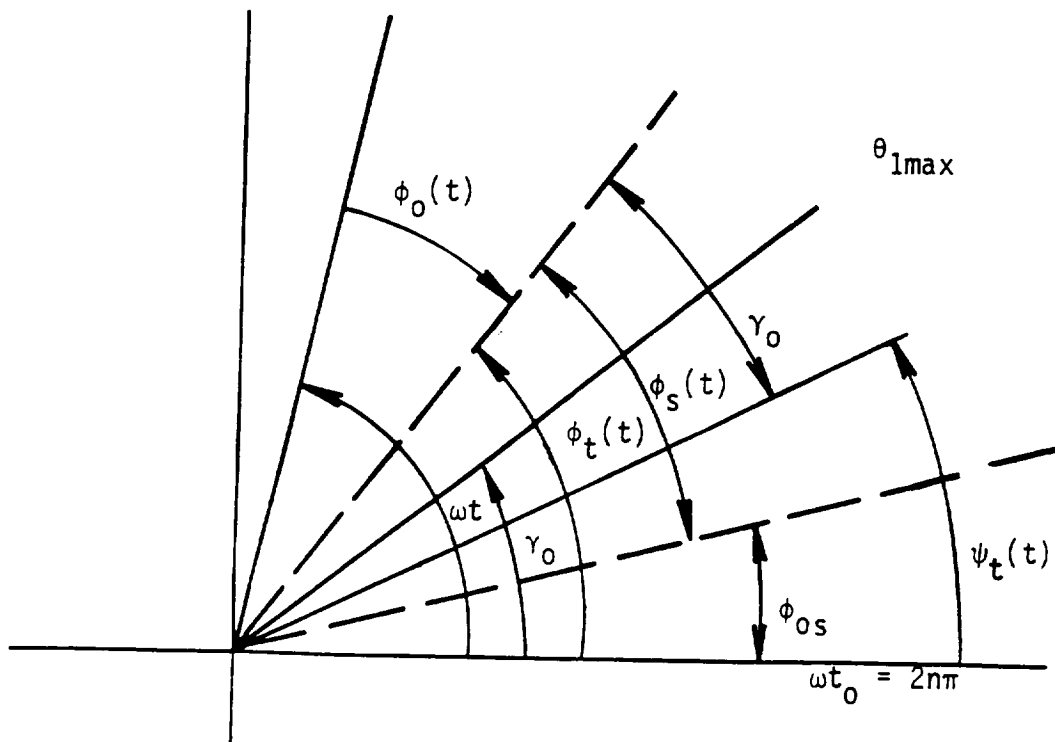


**Figure 4.5-5 Spherical Pendulum Mass Fraction**



a. Space Plane ( $l\theta, \phi$ )



b. Time-Phase Plane

**Figure 4.5-6 Relationship Between Physical Space Plane and Time-Phase Plane**

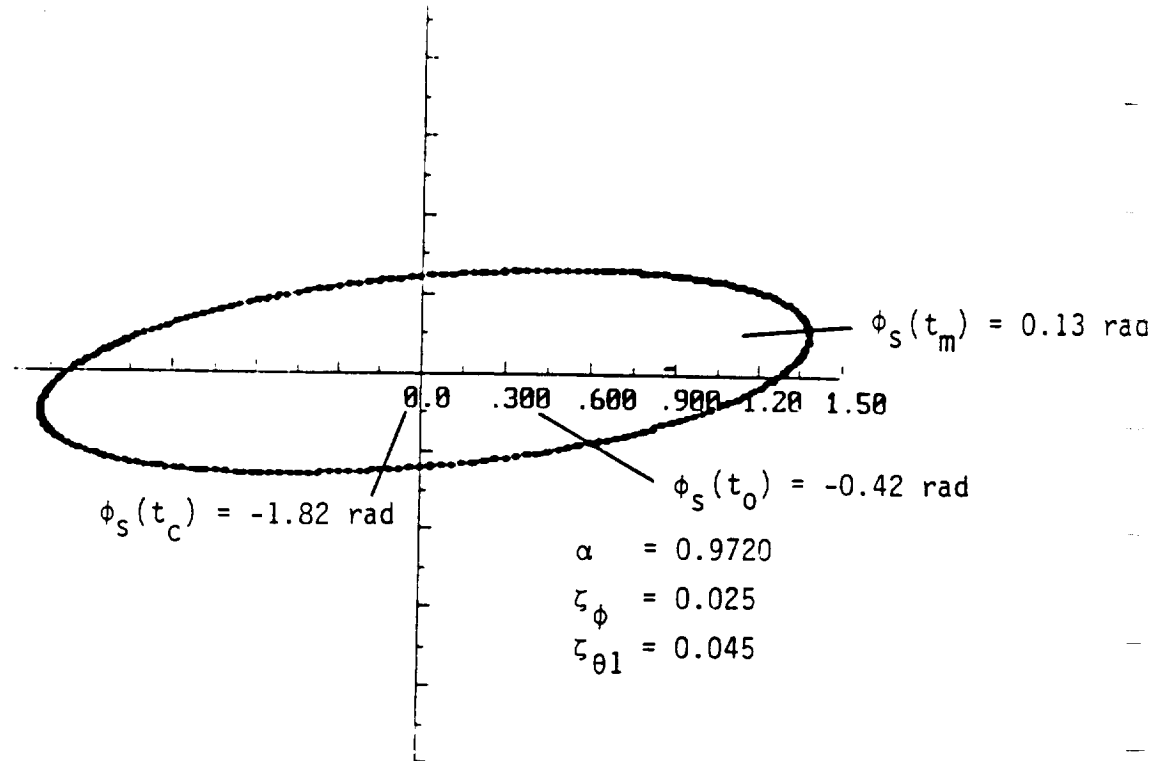


Figure 4.5-7 Polar Plot /  $\sin\theta$  - Inches,  $\phi$  - Radians

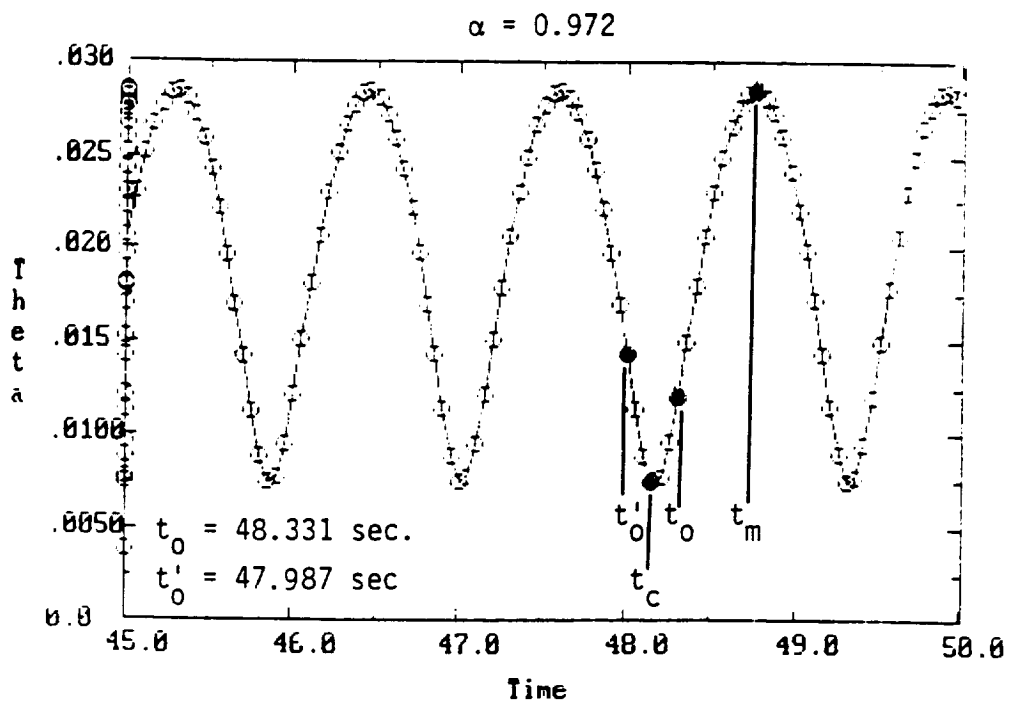
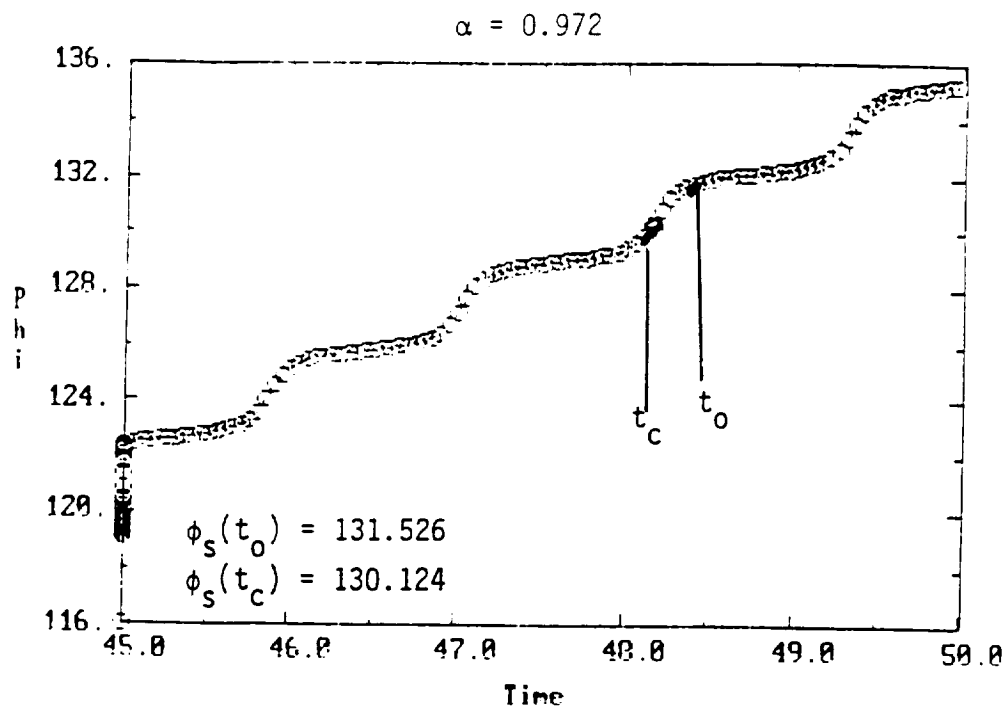
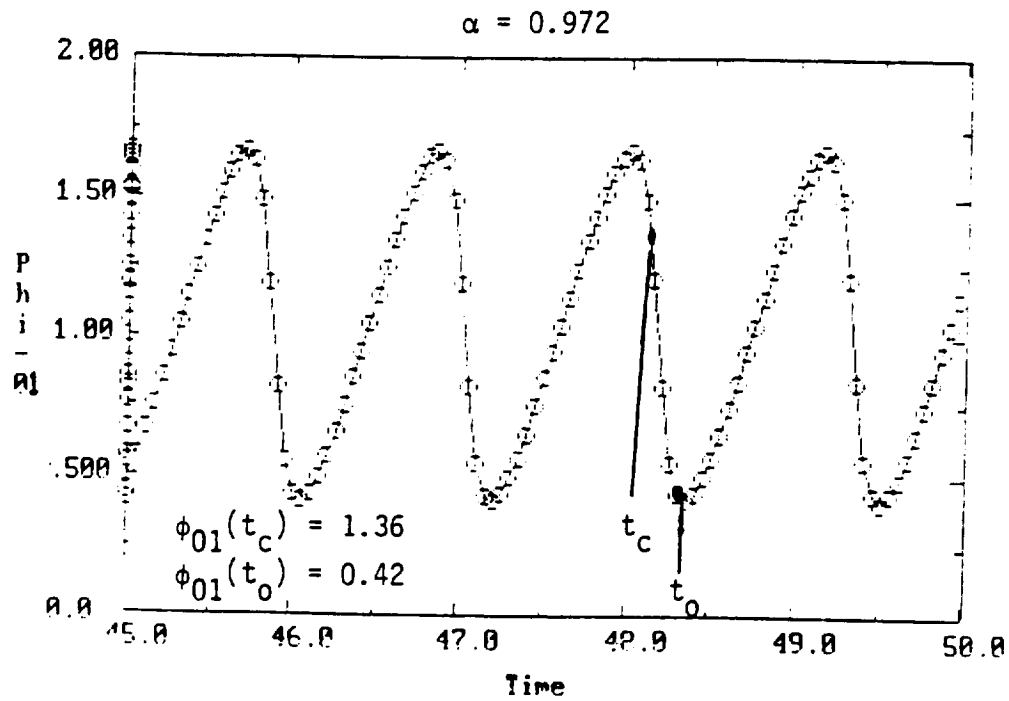


Figure 4.5-8 Deflection Angle,  $\theta$  - Radians



**Figure 4.5-9 Circumferential Angle,  $\phi$  - Radians**



**Figure 4.5-10 Position Angle,  $\phi_{01}$  - Radians**

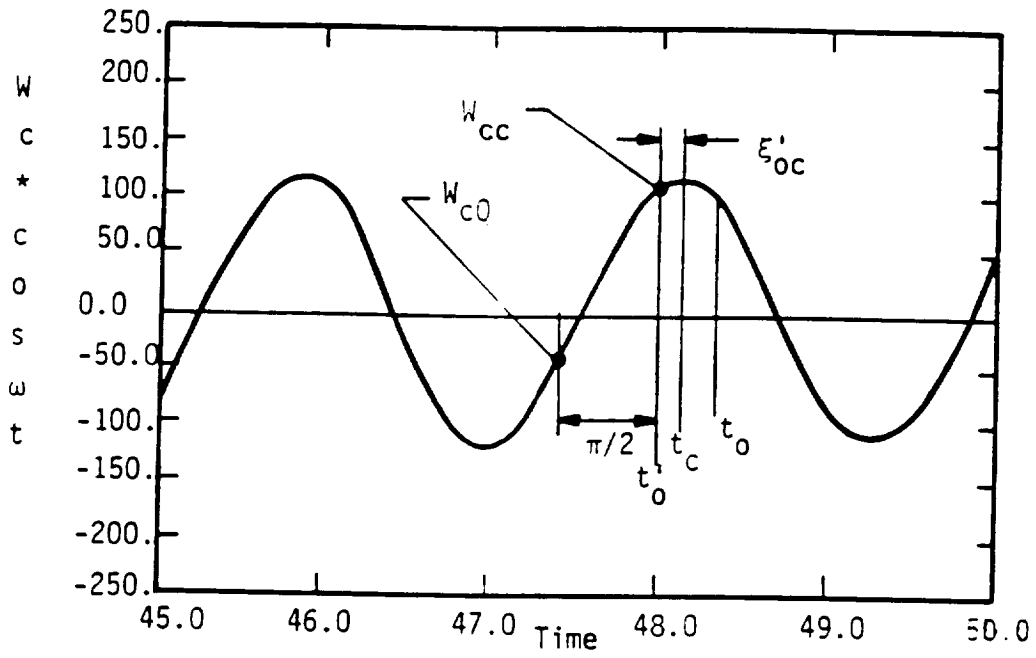


Figure 4.5-11 Cross-Axis Weight,  $W_c$  - lb.

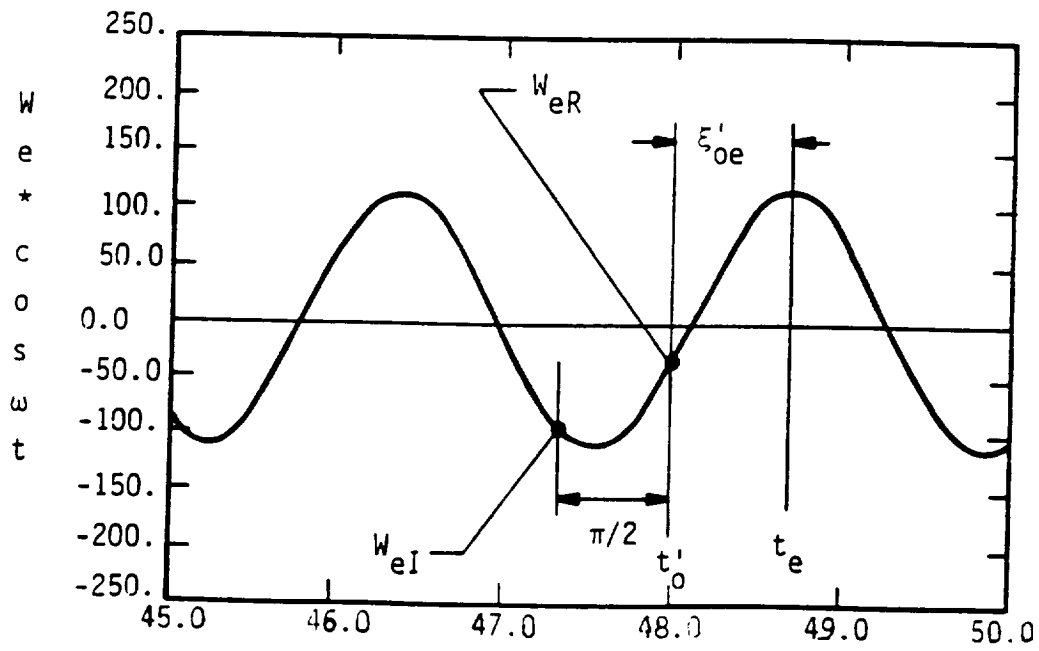


Figure 4.5-12 In-Line Weight,  $W_e$  - lb.

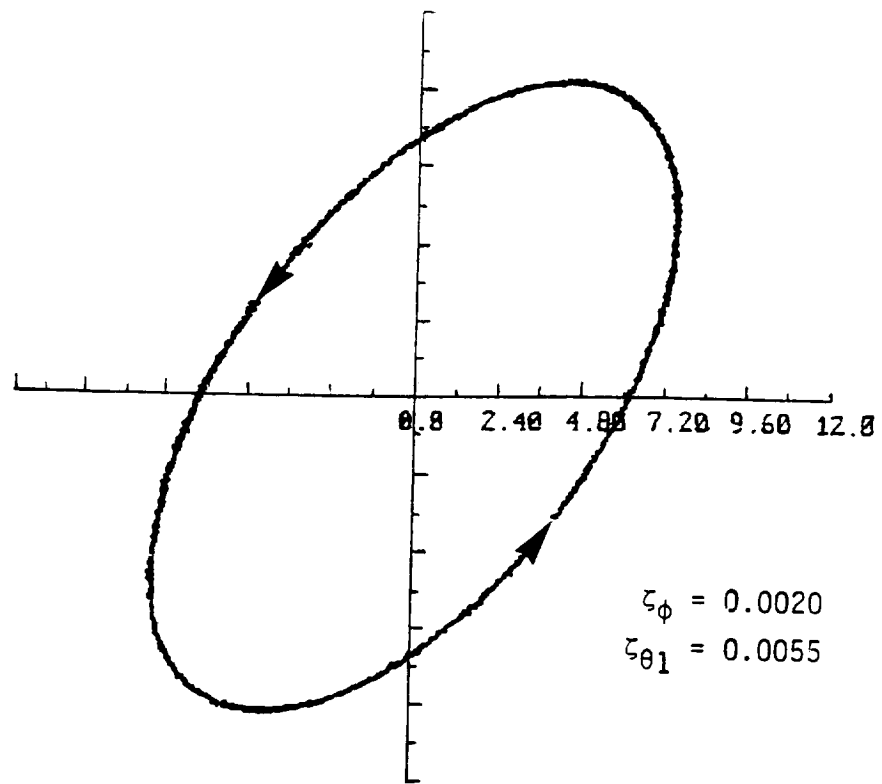


Figure 4.5-13 Polar Plot ( $\alpha = 1.000$ )

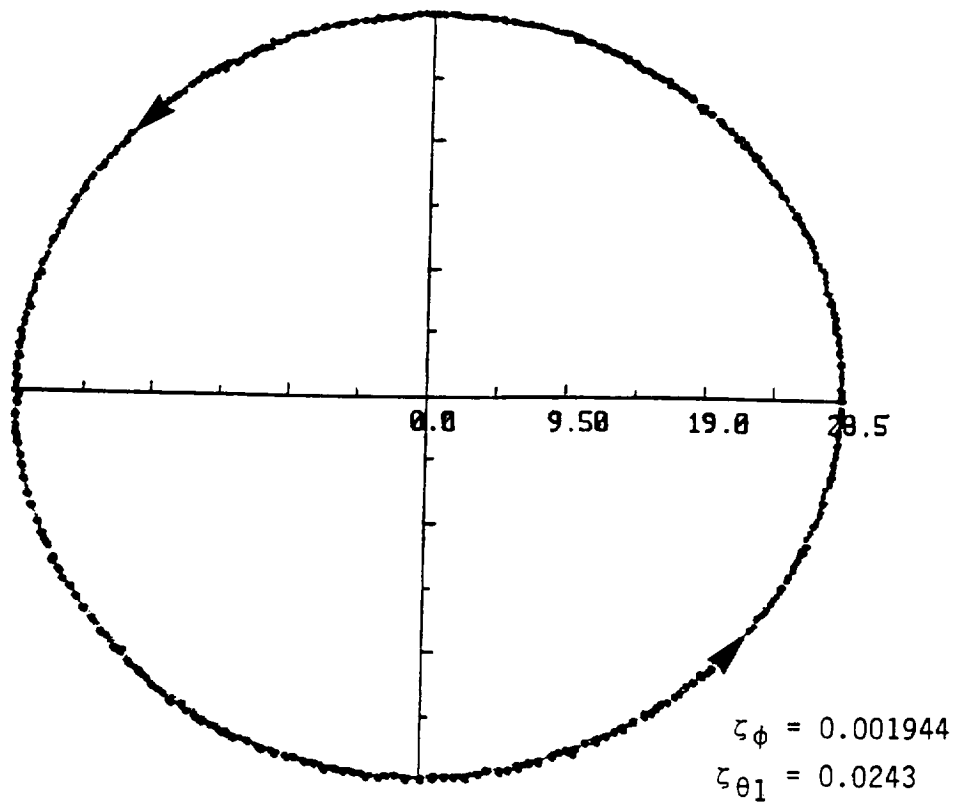


Figure 4.5-14 Polar Plot ( $\alpha = 1.107$ )

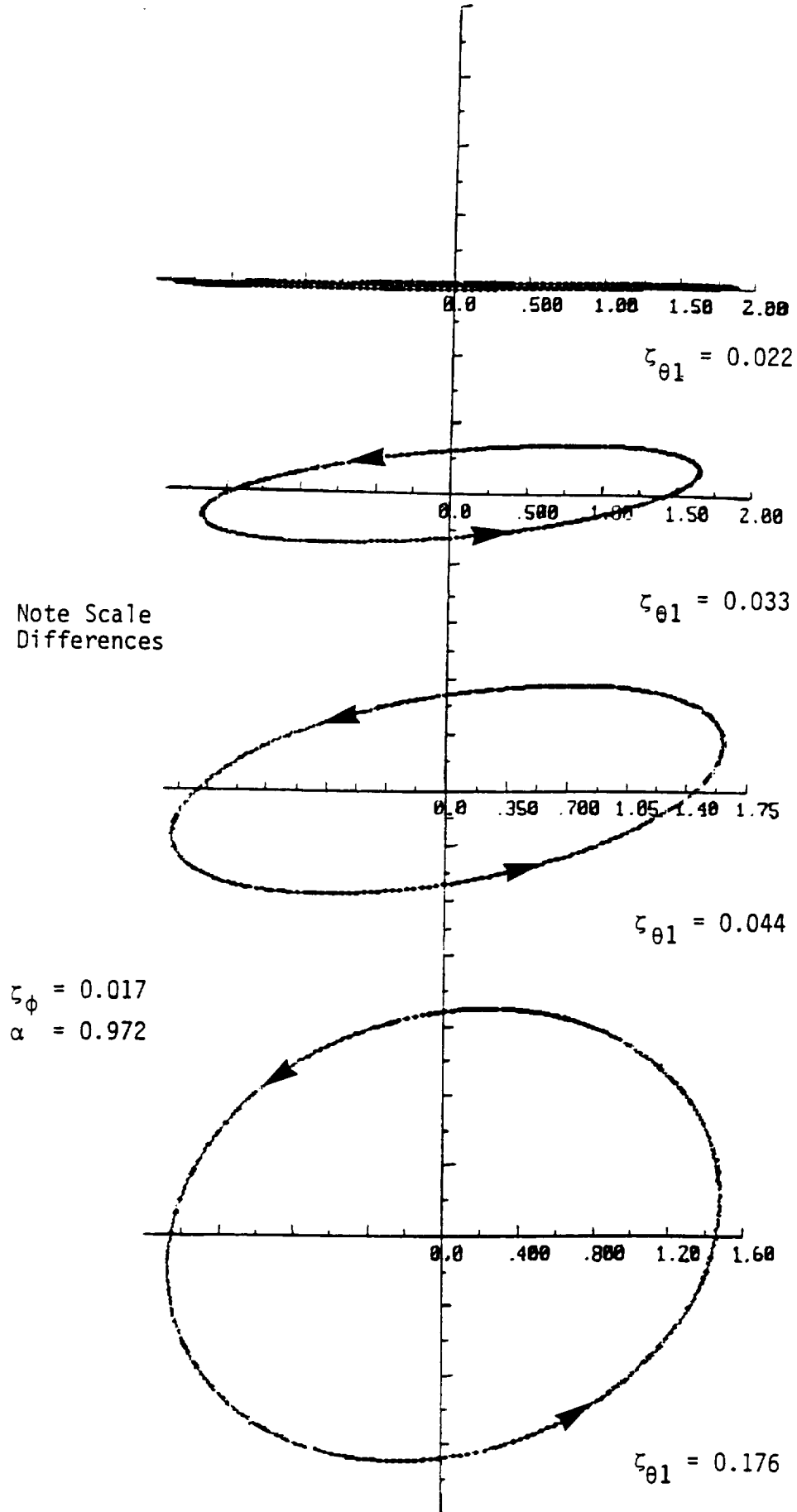
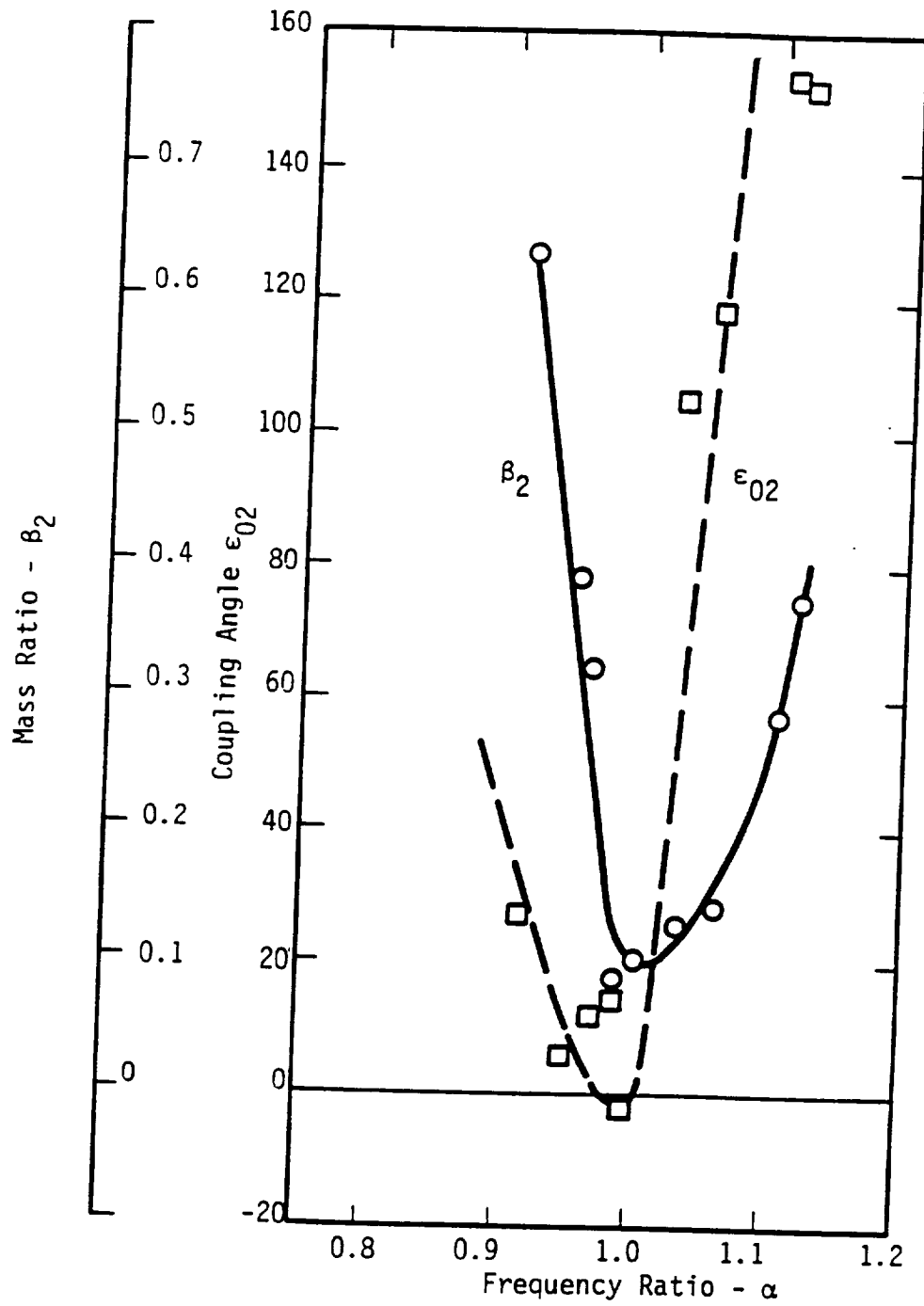


Figure 4.5-15 Influence of Radial Damping on Character of Response



**Figure 4.5-16 Linear Pendulum Model Parameters for Rotary Liquid Slosh**

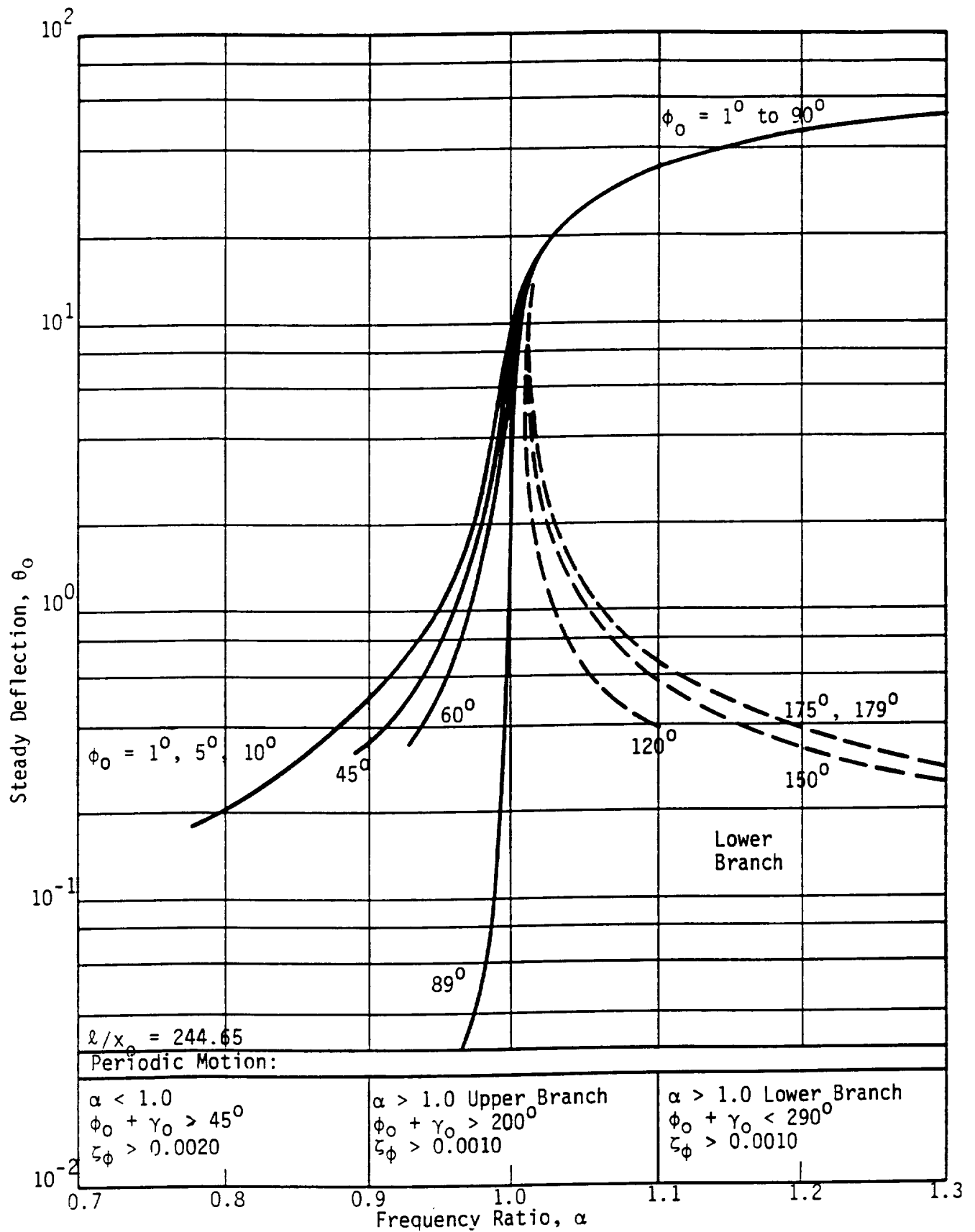


Figure 4.5-17 Spherical Pendulum Deflection Corresponding to Rotary Slosh Amplitude

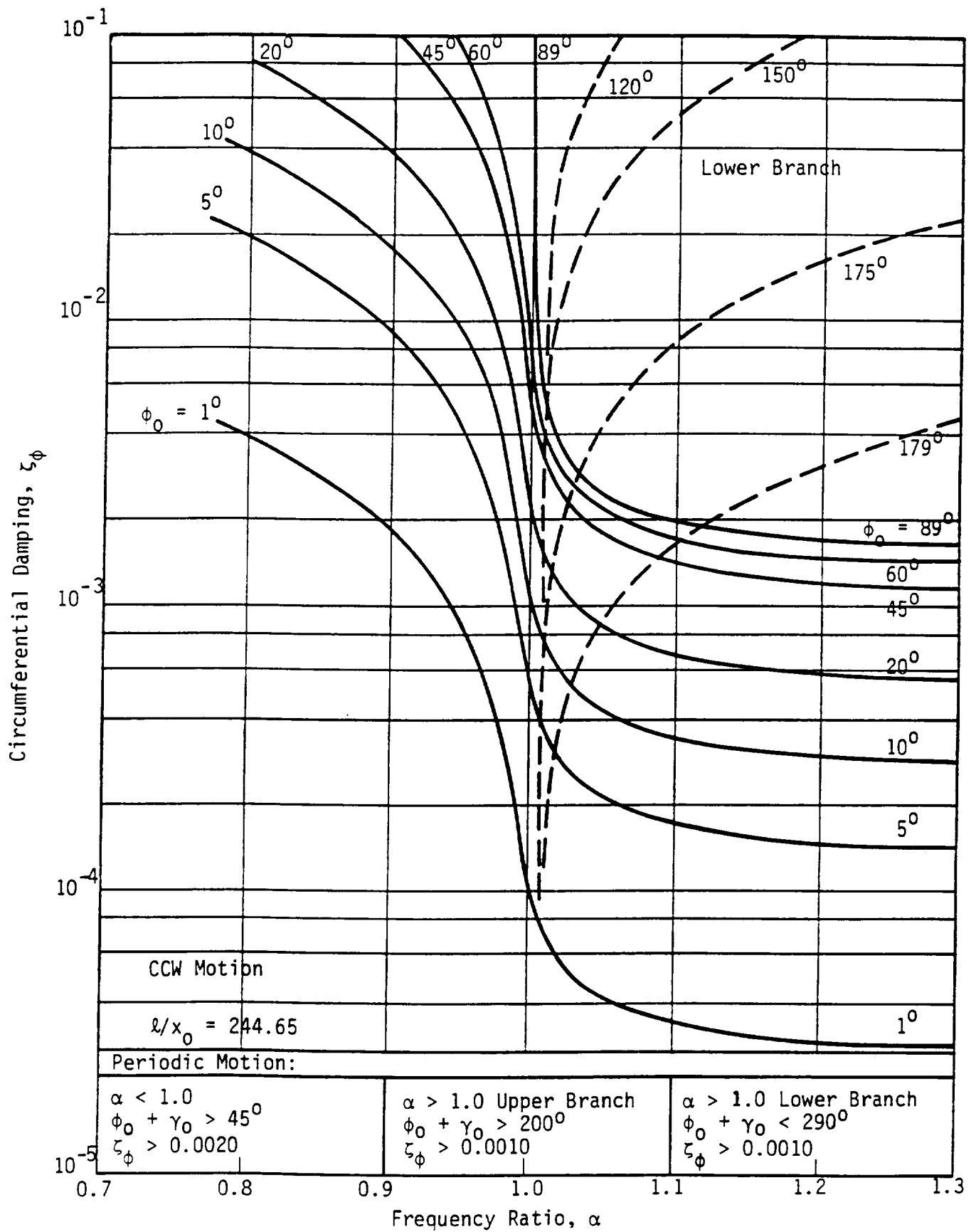
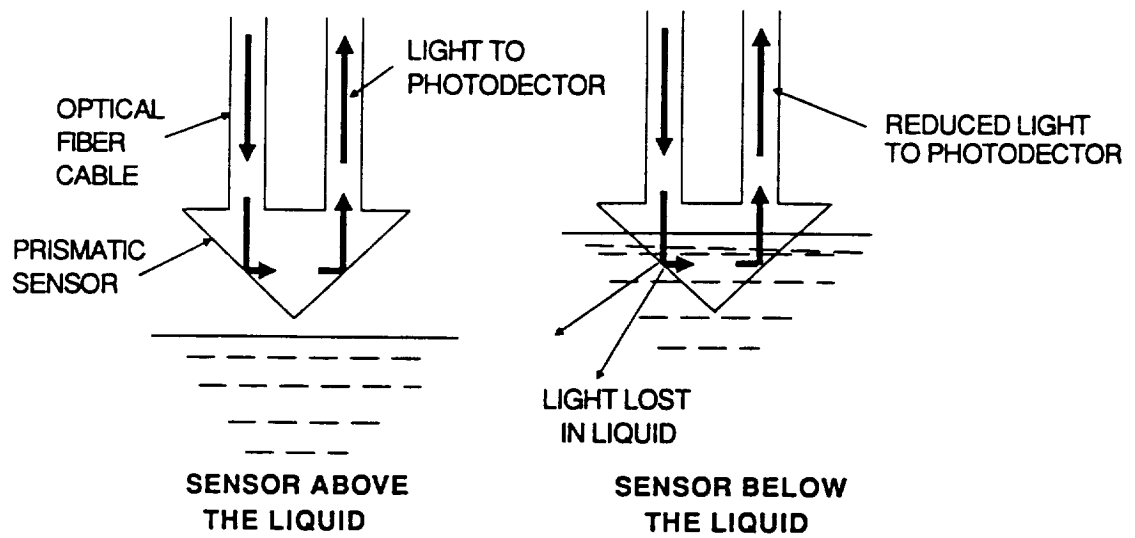
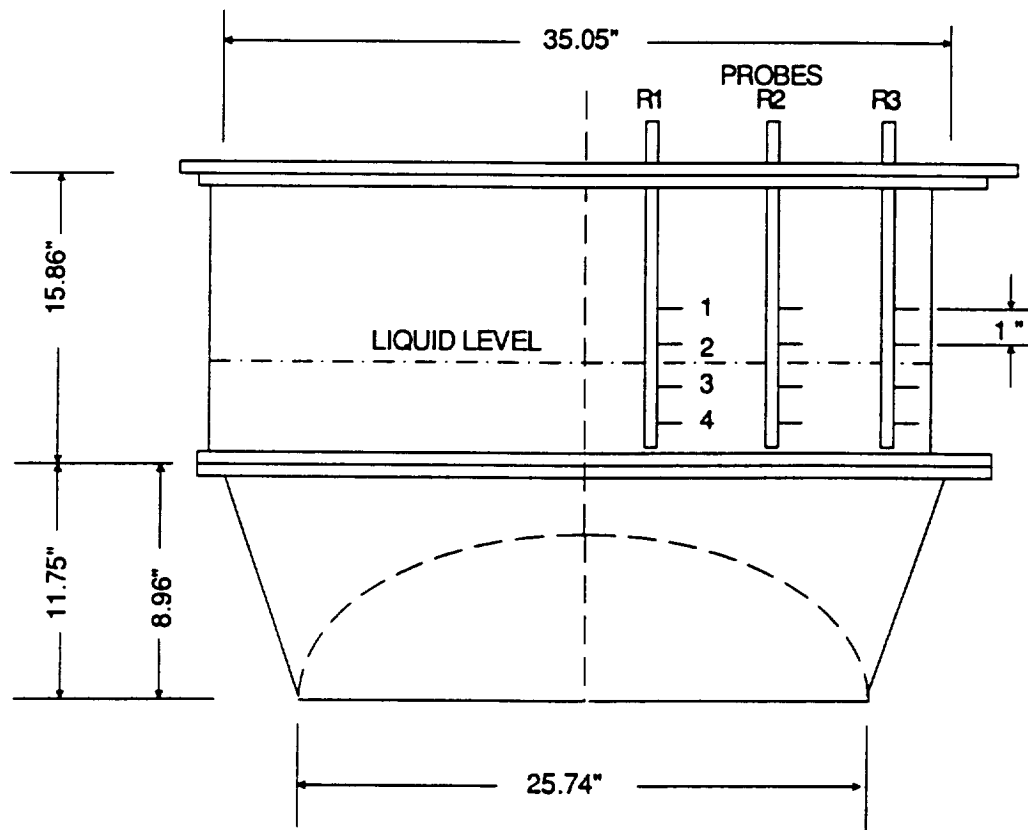


Figure 4.5-18 Dependence of Spherical Pendulum Response on Frequency and Damping



**Figure 5.2-1 Schematic of Fiber Optic Liquid-Vapor Sensor**



**Figure 5.2-2 Slosh Test Apparatus for Liquid-Vapor Interface Sensors**

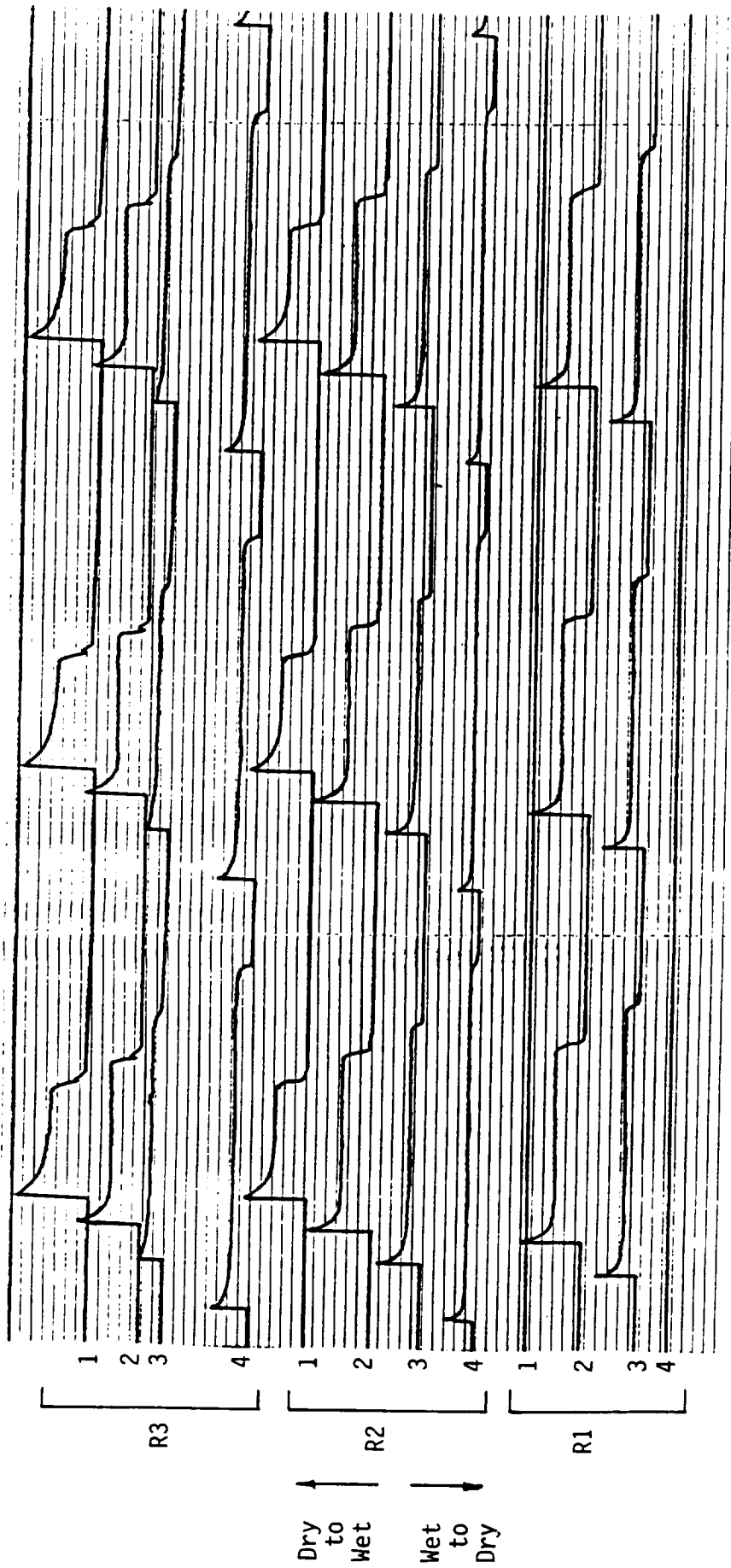
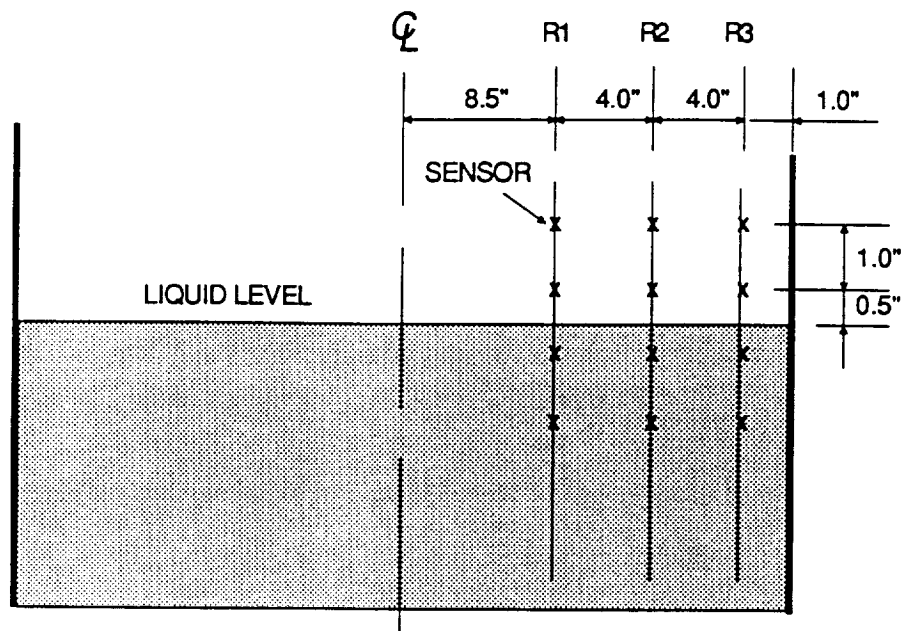
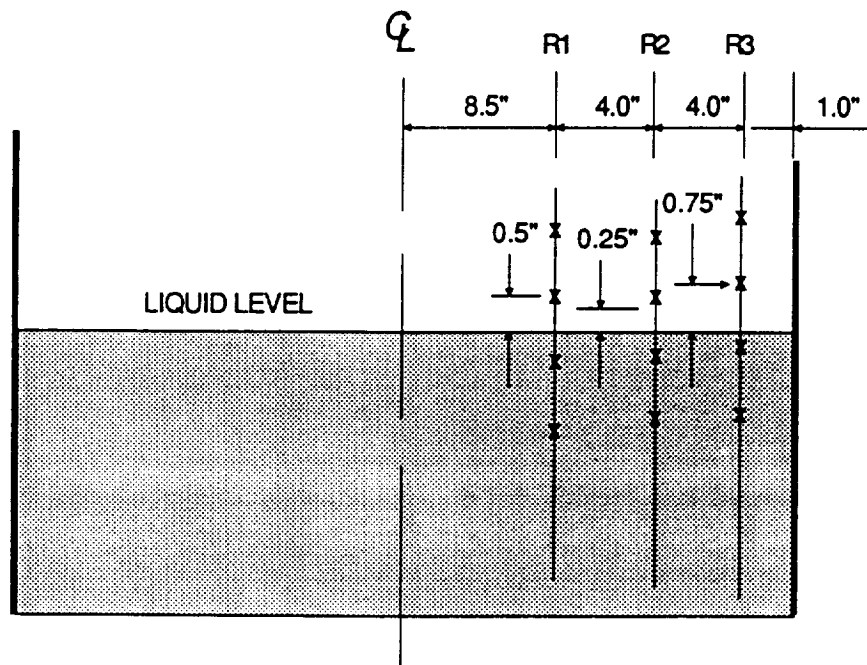


Figure 5.2-3 Reproduction of Strip Chart Recording of Sensor Output

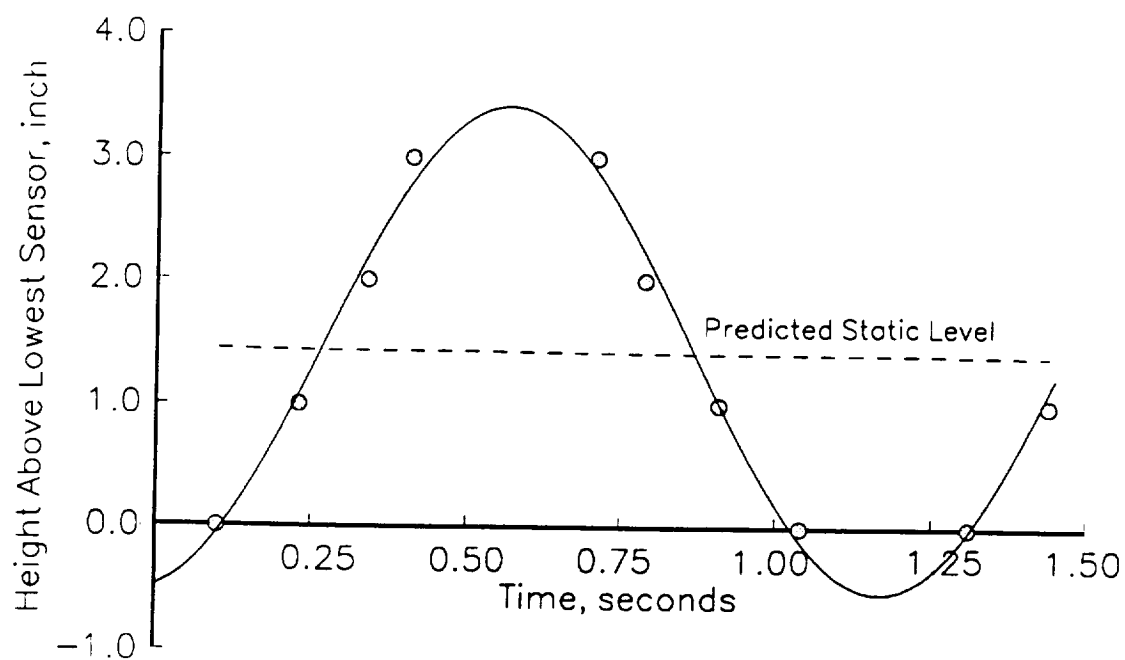


(a) Uniform array used in tests

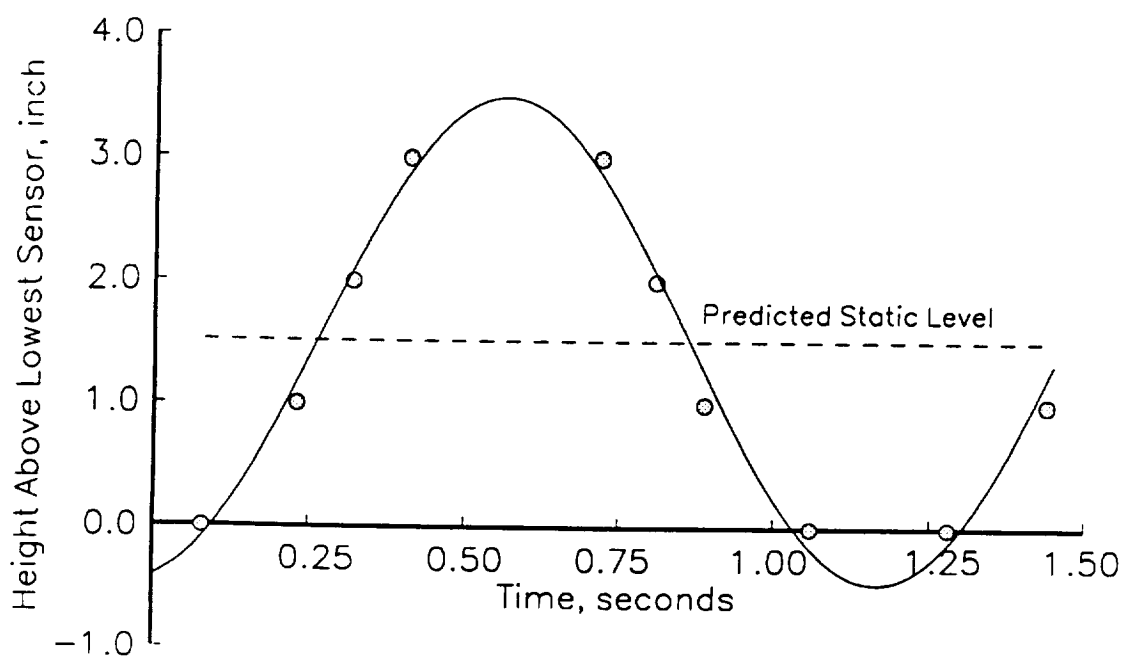


(b) Staggered array

Figure 5.2-4 Probe Arrays for Liquid-Vapor Interface Sensors

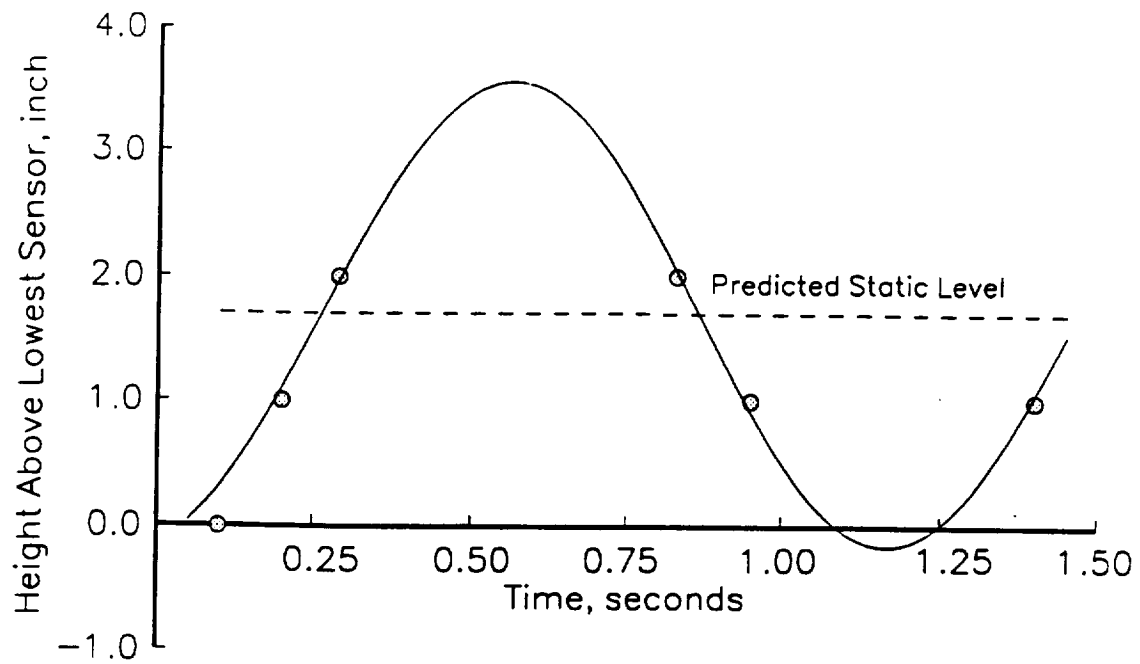


(a) Probe R3

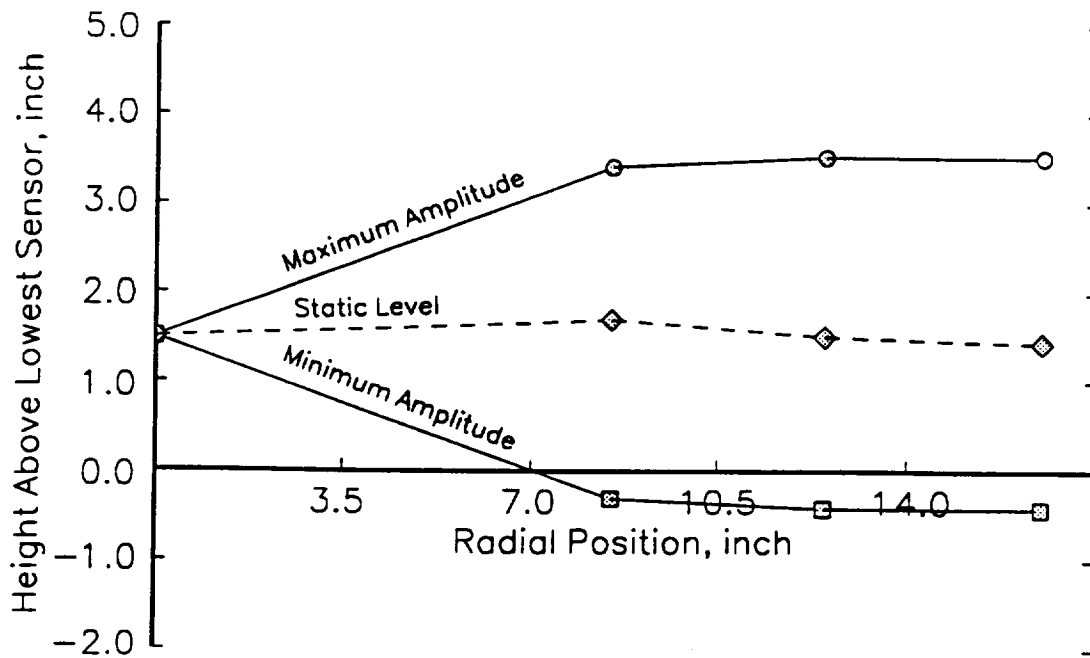


(b) Probe R2

**Figure 5.2-5 Interpolated Test Data and Predicted Wave Shape for Four-Sensor Probe Array**

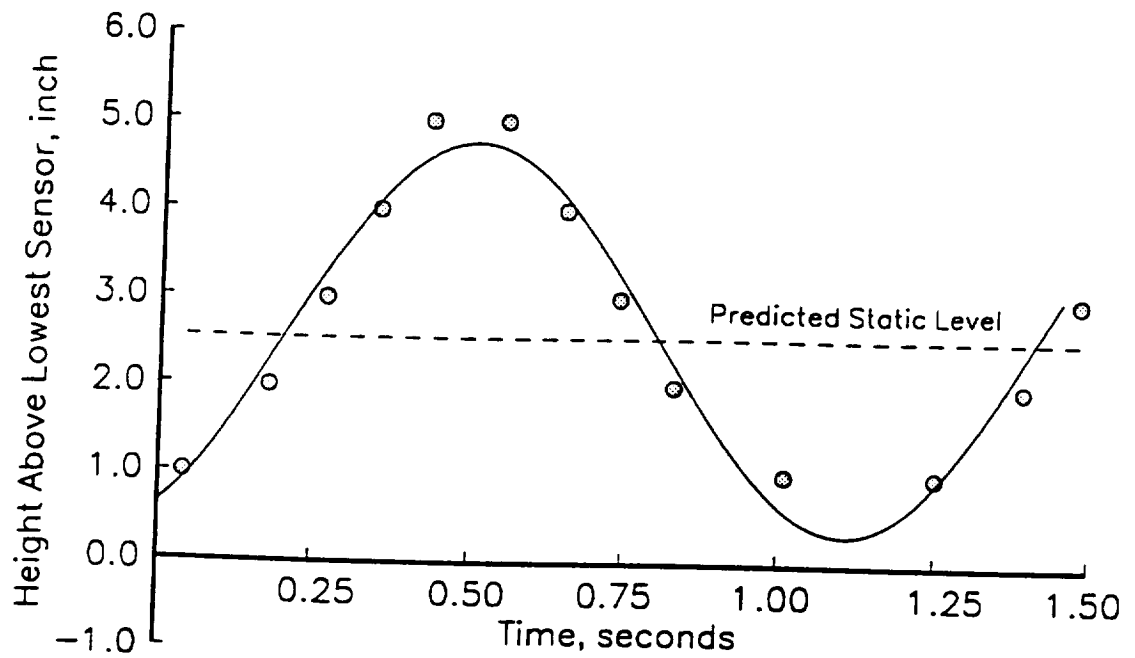


(c) Probe R1

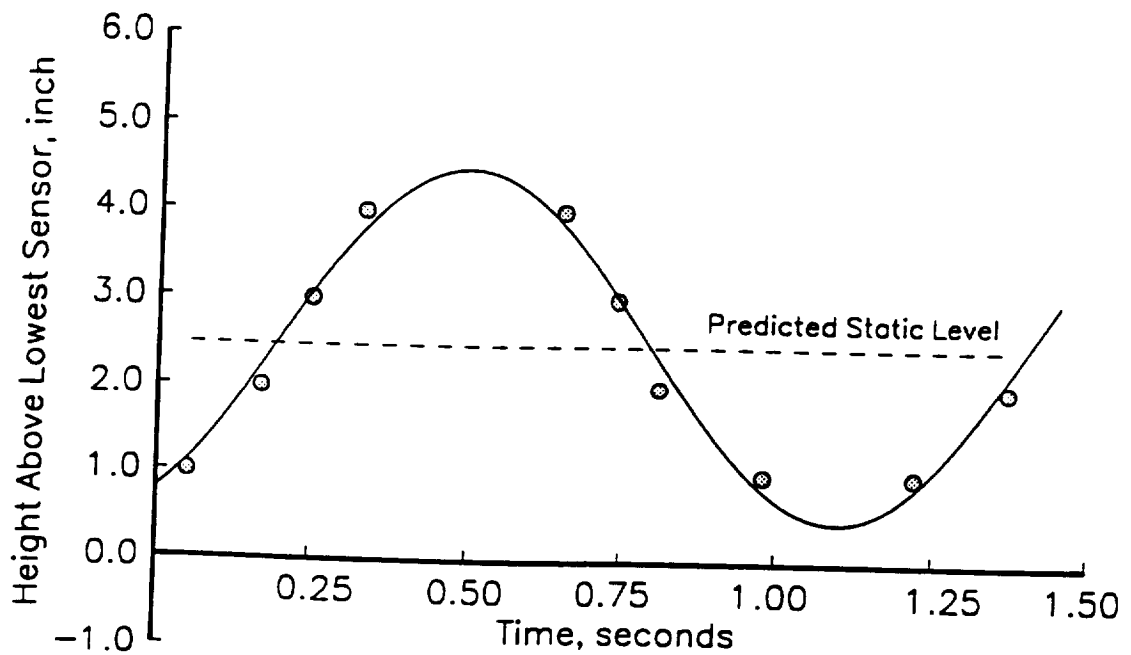


(d) Wave shape

Figure 5.2-5 (Concluded)

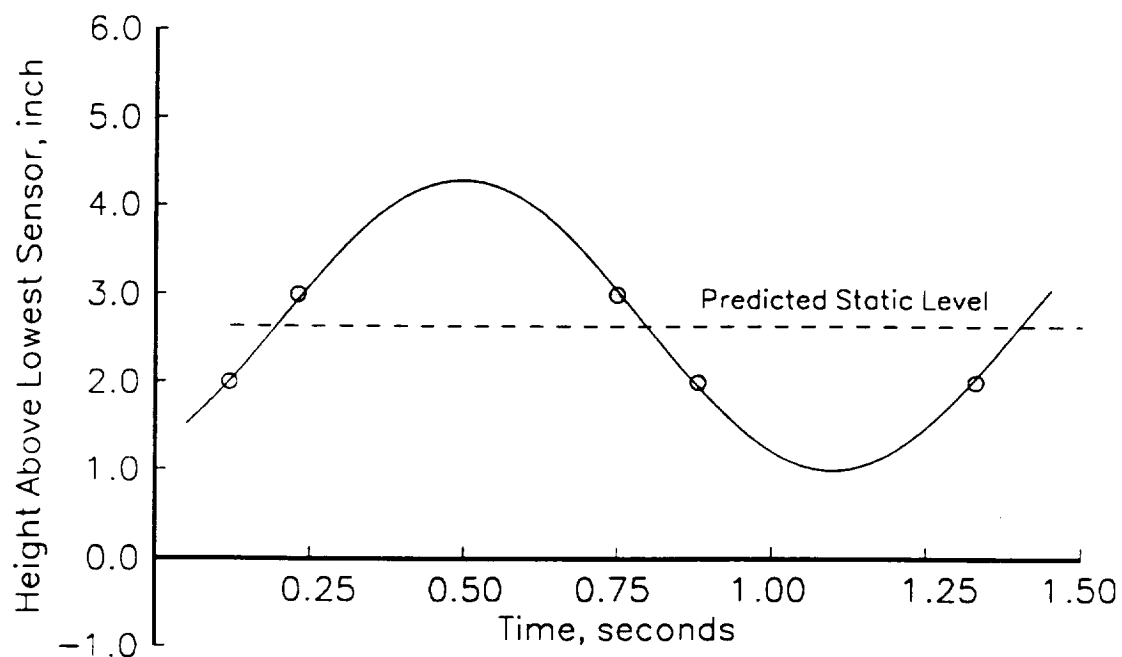


(a) Probe R3

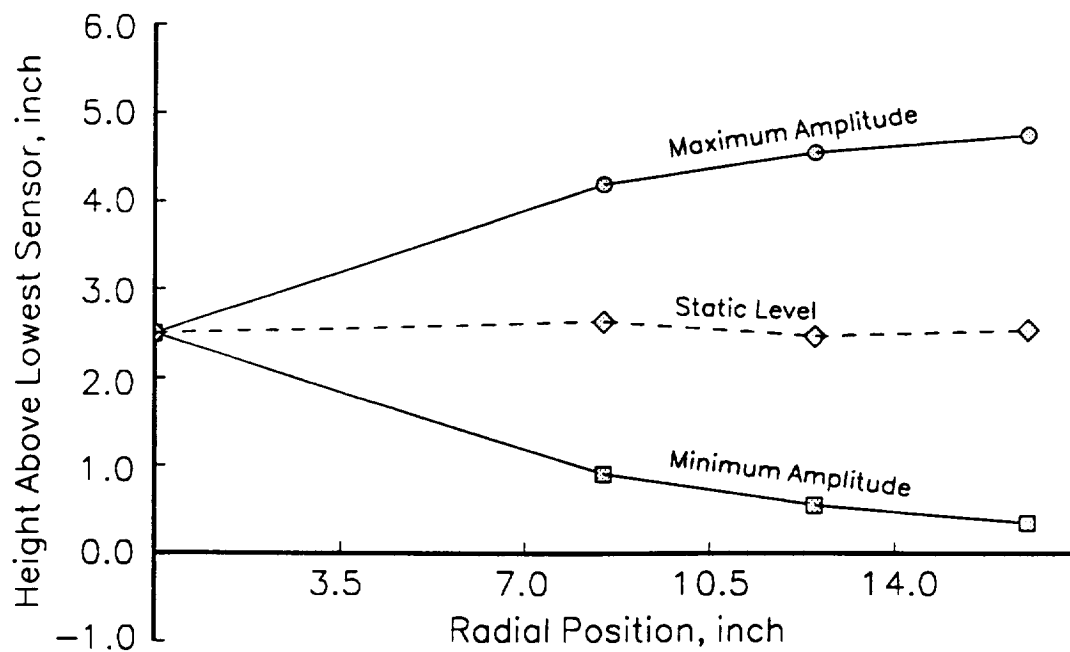


(b) Probe R2

Figure 5.2-6 Interpolated Test Data and Predicted Wave Shape for Six-Sensor Probe Array

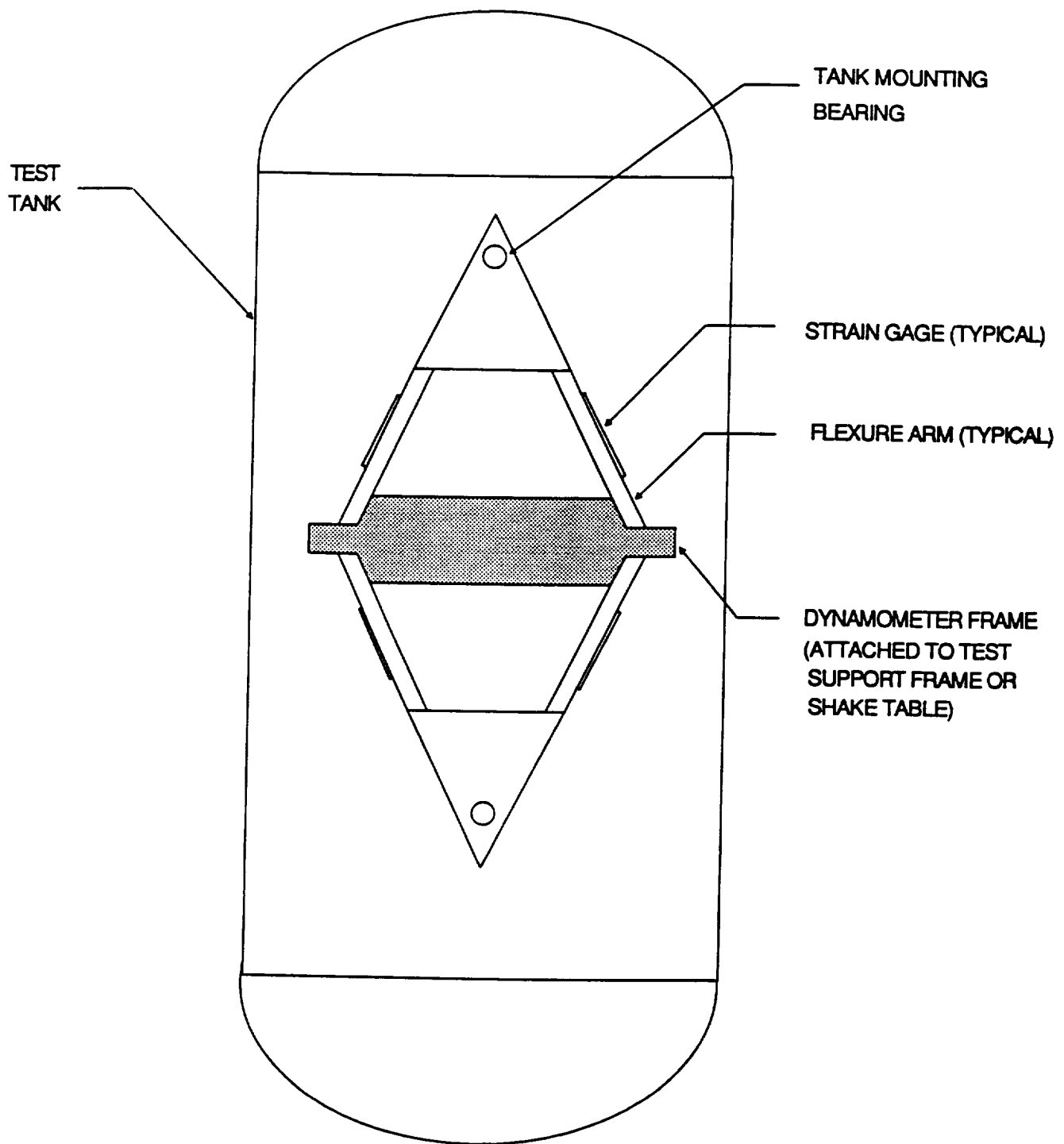


(c) Probe R1



(d) Wave shape

Figure 5.2-6 (Concluded)



NOTE: TWO DYNAMOMETERS PER TANK

**Figure 5.3-1 Strain-Gage Slosh Force Dynamometer**



**APPENDIX A**  
**COLD-SAT**  
**Experimental Requirements Document**  
**on**  
**Liquid Slosh Dynamics and Control**  
**(Dated July 25, 1990)**

**PRECEDING PAGE BLANK NOT FILMED**

## Table of Contents

1.0	INTRODUCTION .....	1
2.0	.....	1
3.0	BACKGROUND .....	1
4.0	TECHNOLOGICAL OBJECTIVES .....	2
5.0	JUSTIFICATION .....	2
6.0	ANALYTICAL MODELS .....	3
7.0	EXPERIMENT REQUIREMENTS .....	4
7.1	Description of Experiment .....	4
7.2	Key Parameters .....	5
7.3	Measurements .....	5
7.4	Hardware Requirements .....	9
7.5	Procedures .....	9
7.6	Data Analysis .....	11

## 1.0 INTRODUCTION

This document describes the requirements for the Liquid Dynamics and Slosh Control Experiment, a Class I experiment, to be performed on COLD-SAT. The purpose of the experiment is, primarily, to gain a physical understanding of the motions of liquids having a free surface in a low gravity environment, including the acquisition of detailed data for several representative cases; this understanding can then be used to develop and verify improved analytical models. A secondary purpose is to characterize the dynamic interaction of the liquid motions with a representative spacecraft (COLD-SAT). Included in the document are some background information on low-g liquid dynamics, a statement of the objectives of the experiment, a description of the physical parameters and processes to be investigated, a description of the experiment, a preliminary test matrix, the experimental procedures, and the data required from the experiment.

Because free-surface motions in a tank depend strongly on container geometry, liquid fill level, liquid physical properties, ambient gravity level, and container motion, it is not practical to determine the dynamics of the motions by low-gravity experimentation for every mission anticipated by NASA and DOD. Instead, analytical and numerical models must be used for most of the missions. But these models must be validated by comparison to a reference set of actual low-gravity data for a few representative cases. The scope of the COLD-SAT experiment has been formulated with this goal in mind.

## 2.0 BACKGROUND

Liquid dynamics in the tanks of space vehicles has long been recognized as being important to stability and structural loading. NASA's plans for an ambitious Space Exploration Initiative to the Moon and Mars involve vehicles that will transport and store enormous quantities of cryogenic propellants in space. Additionally, some kinds of space-based optical systems (e.g., the Strategic Defense Initiative) also involve large mass fractions of liquids. Tank sizes for these and other space vehicles range from a meter or so in diameter to several tens of meters. The control, pointing, and docking of spacecraft containing such large masses of liquid, as well the transfer of liquid between spacecraft, is critically dependent upon understanding and controlling the motions of the liquids.

The dynamics of liquids in tanks in normal gravity is well understood, and analytical, numerical, and scale-model test methods have been established to treat these "high-g" problems [1, 2]. However, low-gravity free-surface liquid motions are not nearly so well understood. The motions are dominated by surface physics effects that cannot be investigated realistically by ground testing in normal gravity. Some information is available from drop tower and zero-g tests [e.g., 3] but all such studies to date have employed small tanks and non-cryogenic liquids. It appears from this limited amount of data that, for reasons that are

not well understood, slosh damping is larger in low-gravity [3, 4] and nonlinear effects such as rotary sloshing are more prominent [5, 6]. As additional evidence of the importance of surface physics, ground-based slosh tests that simulate low-gravity indicate that the response of the liquid depends strongly on the motion of the liquid-tank contact line [e.g., 7]; for example, the natural frequency and damping varies by more than a factor of two between a "free" contact line and a "stuck" contact line condition. Consequently, this COLD-SAT experiment is needed to study surface motion of cryogens in tanks of moderate size, in an actual low-gravity environment for a sufficiently long test duration.

### 3.0 TECHNOLOGICAL OBJECTIVES

The specific objectives of this technology experiment are: (1) determine and understand the liquid motion resulting from typical maneuvers of spacecraft; and (2) characterize the interaction of the motion with spacecraft for a typical spacecraft (COLD-SAT). These objectives will (a) provide physical understanding about the motions of cryogens in low-gravity; (b) supply data from which to establish the adequacy of existing analytical and numerical models of such motions, and indicate where improvement is needed; and (c) yield typical data on the damping of low-gravity motions from which analytical and empirical correlations can be developed.

The physical processes to be investigated include:

Static liquid configuration - The configuration of the liquid in the test tanks will be monitored under ambient on-orbit conditions.

Liquid response to various discrete accelerations - The liquid will be oriented to give a specific initial orientation. Impulsive and periodic accelerations of selected amplitude, frequency, and duration will be applied and the free surface response monitored.

Effectiveness of slosh baffles - The cylindrical receiver tank will contain a single ring baffle to demonstrate the damping of liquid motions in low gravity.

### 4.0 JUSTIFICATION

The motion of contained liquids has a profound influence on the dynamics and control of space vehicles, the transfer of liquids between vehicles, and the docking of one vehicle to another. Future space missions will carry much larger quantities of liquids, primarily cryogens, than is common now, and the mission performance requirements will be much more demanding. As an example of the problems that must be solved, space-based telescopes and strategic defense satellites must be pointed to an angular accuracy of the order of 0.0005° and that accuracy must be maintained even during tracking maneuvers; since the

tracking maneuver will set into motion the contained liquids, one can imagine that the ability to understand, predict, and control the dynamics of the moving liquid will be critical.

Although some spacecraft maneuvers will certainly create large motions of the contained liquid, this experiment will concentrate on liquid motions that are localized about the initial position of the liquid; such motions are usually called "sloshing." There are several reasons for limiting the experiment in this way. First, large motions are dominated by liquid inertia and so can be modeled more easily than motions dominated by little-understood surface physics. Second, large motions eventually decay to smaller amplitude sloshing motions. Third, slosh motions can be excited by a variety of typical control maneuvers of spacecraft and are thus important in their own right.

## 5.0 ANALYTICAL MODELS

Low gravity fluid dynamics in "bare" tanks are currently modeled either by general purpose computational fluid dynamics (CFD) codes, such as NASA-VOF3D or FLOW-3D [8, 9], or by special-purpose linearized analyses [10]. At present, however, only the CFD codes can model slosh baffles and other internal hardware. Both methods employ assumptions about the surface physics that either need to be validated or improved by in-space experimentation with cryogenics.

The parameters needed for the models include tank shape, liquid fill level, and:

Bond number	$Bo = g_{eff} a^2 / \beta$
-------------	----------------------------

Static contact angle	$\theta_s$
----------------------	------------

where  $g_{eff}$  is the effective "gravity" or linear acceleration of the spacecraft,  $a$  is a representative dimension of the tank, and  $\beta = \sigma/\rho$  is the specific surface tension of the liquid. The tank shape and the direction of  $g_{eff}$  with respect to the tank axis must also be specified, and, for investigations of nonlinear effects, the tank motion as well.

Bond numbers  $Bo < 10$  or so represent "low" gravity conditions, while  $Bo \ll 1$  represent "micro" gravity conditions;  $Bo < 1$  is representative of a large tank (> 1-m in diameter) in orbit. Whenever the contact angle of the liquid with the tank is small (as it is for cryogenics and tank materials of interest), the free surface of the liquid is highly curved in low gravity; the extreme case of  $Bo = 0$  and a zero-degree contact angle results in a free surface that is spherical. The stability of the free surface is also a function of  $Bo$  (based on the disturbance acceleration) and contact angle.

The models also require a relationship that specifies how the contact angle changes as a function of the contact line velocity when the liquid surface is in motion. Currently, the only relation that can be employed in the models is that the contact angle remains constant at its equilibrium value, regardless of contact line velocity. Although this assumption appears to agree with most (but not all) of the available small-tank, drop-tower test results, fundamental studies of the spreading of liquids on surfaces indicate that it may be an over-idealization [11]. This COLD-SAT experiment is designed to establish better contact angle - contact line velocity relations for cryogenic liquid and tank materials of importance. If the results of the experiment show that an assumption of constant contact angle is not valid, the models must be modified. Other surface physics phenomena may be important and therefore will need to be included in the models (e.g., surface tension hysteresis) but the nearly complete lack of low-gravity slosh data has so far prevented the establishment of all potentially important parameters.

There are currently no models of the damping provided by slosh baffles in low-gravity. The models that will be evaluated are modifications of high-g results [1]. The models of low gravity viscous, or "bare" tank, damping have not been well validated; for example, some correlations developed from drop-tower and simulation tests show that the viscous damping ratio  $\gamma$  is a function of Bond number as well as viscosity:

$$\gamma = A(v/f_n a^2)^{1/2} [1 + C(Bo)^{-m}]$$

where  $v$  is the kinematic viscosity and  $f_n$  is the slosh natural frequency. These correlations were developed from tests with  $Bo > 1$  and may overestimate the damping significantly when  $Bo < 1$  (because of the negative exponent on the  $Bo$  term). Improved correlations will be developed from the results of this COLD-SAT experiment.

## 6.0 EXPERIMENT REQUIREMENTS

### 6.1 Description of Experiment

To investigate the influence of tank shape, slosh experiments will be conducted in both receiver tanks. The cylindrical receiver tank will be fitted with a single ring-baffle near its midpoint, but the spherical receiver tank will not contain any specific anti-slosh devices. The tank support structures will incorporate load cells to monitor the forces and torques exerted on the tanks by the sloshing liquid. Liquid-vapor sensors in the tanks will be used to monitor the static liquid configuration and the motion of the free surface. The COLD-SAT propulsion system will be used to provide specific linear accelerations ( $g_{eff}$ ) and discrete disturbance accelerations.

These COLD-SAT experiments can be performed as opportunities (which are plentiful) when the liquid fill volumes of interest are available during other tests. Some of the specified disturbance accelerations may also occur during other testing.

## 6.2 Key Parameters

The key parameters expected to influence the low-g slosh experiments are (1) liquid surface tension, density, and viscosity (which are functions primarily of liquid temperature for a given liquid), (2) tank shape and internal hardware, (3) fill level, and (4) acceleration environment. It is not proposed to vary the liquid temperature systematically, so the effect of liquid properties will not be investigated except as the temperature may change for other reasons from test to test. The influence of tank shape will be investigated by tests with both receiver tanks, one of which is basically a cylinder and the other a sphere. The only internal hardware that will be specifically investigated will be a slosh baffle (an annular ring) in the cylindrical tank to investigate the performance of a typical baffle in low gravity when the static liquid surface is near the baffle; other static liquid levels will be chosen to simulate "bare wall" conditions in the same tank. The influence of liquid level will be investigated by conducting tests, to the extent possible, over a variety of fill levels. The influence of effective gravity will be investigated by conducting tests at several thrusting levels, as described later in Section 6.5; the acceleration will be directed along the symmetry axis of the tanks to facilitate comparison with analytical/numerical models. Perturbation accelerations to excite sloshing will include impulsive and periodic motions of the spacecraft. The duration of the periodic acceleration will be varied, depending upon the objective of the test, as described later in Section 6.5.

## 6.3 Measurements

The static and dynamic configuration of the free surface is important in understanding and correlating the experimental results; for example, the slosh wave shape near the wall will indicate whether the contact angle remains constant during sloshing or, alternatively, that the contact line is "free." Liquid-vapor sensors mounted in the receiver tanks will therefore be used to monitor both the static and dynamic configurations and the frequency of the surface motions. To accomplish this, the sensors must be arrayed vertically and radially, as illustrated in Figure 1; ideally, the sensors should be contained in two orthogonal arrays. Ground-based experiments indicate that the free surface shape can be resolved accurately when the radial spacing of the sensors is as large as 20% of the diameter (i.e., spaced at 10%, 30%, 50%, 70%, and 90% of the diameter) and the vertical spacing is as large as 10% of the diameter. More widely spaced intervals can be used without sacrificing accuracy in the frequency estimation

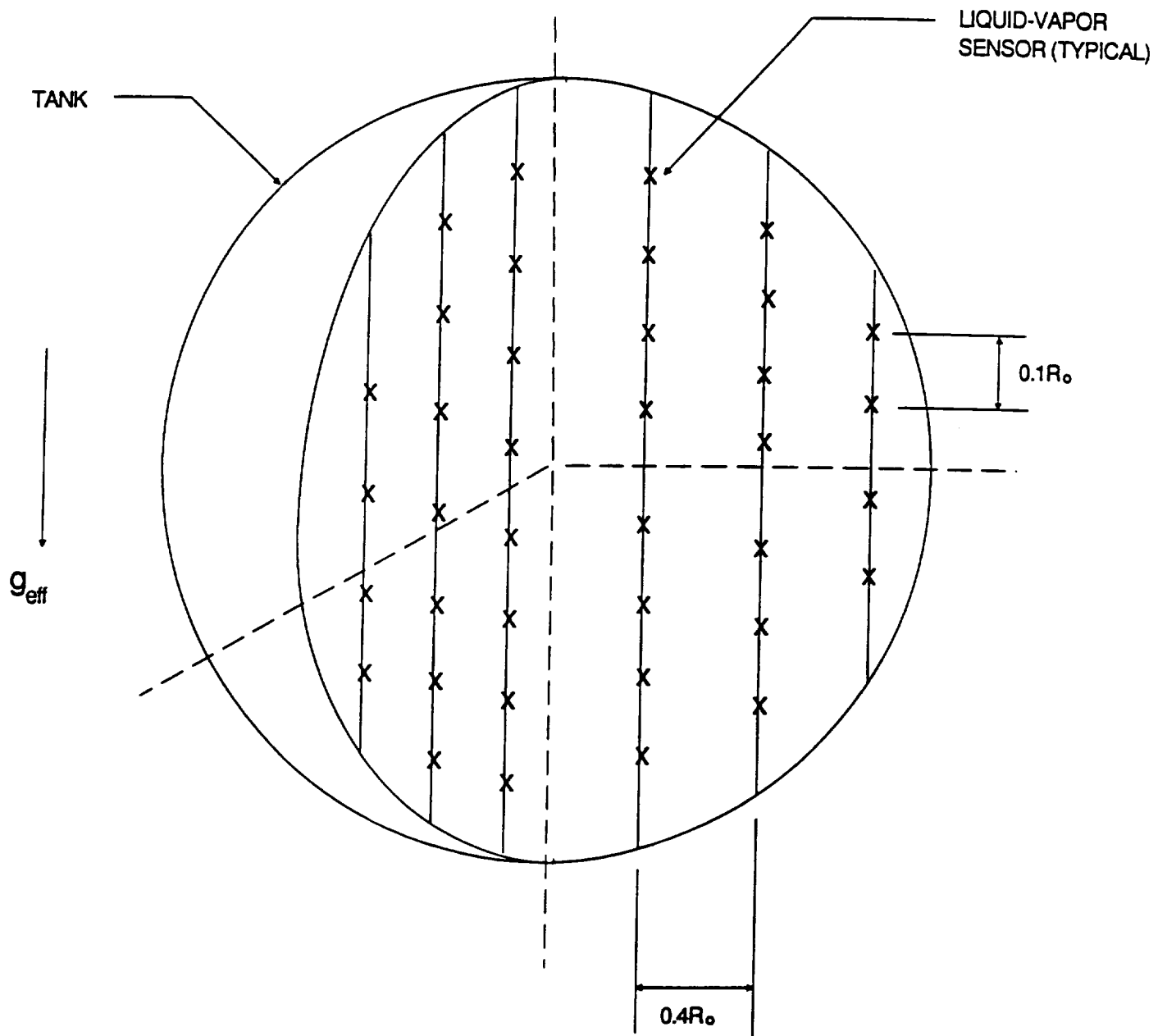


**Figure 1. Liquid-Vapor Sensor Array Recommended for Slosh Wave Shape Measurement**

(which is determined by the data sampling rate) but the surface shape estimation will be degraded. Note that the vertical spacing of the sensors can be concentrated at the static liquid levels employed in the tests, and, if necessary, the radial array locations can be reduced to 10%, 30%, and 50% of the tank diameter. Because of the low frequencies of the anticipated slosh motions, the required frequency response of the liquid-vapor sensors is essentially d.c. Of more importance is the time required for a sensor signal to change from "dry" to "wet" and from "wet" to "dry" as the liquid surface passes the sensor location; ground-based experiments indicate, however, that the signal changes abruptly over a time period that is very small compared to the time between successive passages of the liquid surface; thus, the sensors should function more than adequately.

Knowledge of the overall slosh wave shape and frequency, as acquired by the liquid-vapor sensor array, is sufficient to examine the predictive accuracy of analytical models. More fundamental information may be needed to identify weak assumptions in the models. For example, the relation between the dynamic contact angle at the wall and the contact line velocity can potentially have a significant influence on the slosh frequency and force, even though existing models assume that the dynamic contact angle remains equal to the static contact angle. The liquid-vapor sensor array illustrated in Figure A.1 will not be adequate to acquire detailed data about the wave shape near the wall. To resolve the wave shape near the wall in detail, and thus to infer the behavior of the contact angle as a function of time, will require a denser radial and vertical array of sensors near the wall for at least one selected liquid level. These sensors should be spaced symmetrically at about  $0.02R_0$  above and below the free surface over a total vertical distance of about  $0.1R_0$ , and at least two such arrays should be spaced radially at intervals of  $0.02R_0$  from the wall. Because of the "bent over" geometry of the tank-liquid intersection for spherical tanks, the dense arrays are most readily made applicable to cylindrical (straight wall) tanks, although a dense array of sensors positioned along a radial line could be used for spherical tanks. In addition, the array installation must not significantly interfere with the slosh wave motion. It is understood that the use of such dense arrays will require substantial data acquisition rates and may interfere with other experiments.

The support structure of the receiver tanks must be designed to accommodate load cells with which to measure slosh forces. The slosh force measurements can also be used as a means of independently determining slosh natural frequencies and damping, in the event of difficulties in interpreting the liquid-vapor sensor data for a particular test. The magnitude of the slosh forces that must be measured is a function of  $Bo$  and the amplitude of the imposed disturbance acceleration. For the COLD-SAT receiver tanks and the proposed excitation amplitudes, the expected force amplitudes range from about 0.0001 lbs to about 0.001 lbs. The required frequency response of the load cells also depends on  $Bo$  but is essentially d.c. Such small forces can be measured reliably only by

eliminating (or otherwise compensating) the large non-sloshing dead-load signal from the dynamic slosh force signal. This compensation can be accomplished electronically before the signal is transmitted to the data acquisition system, by methods used previously in ground tests [e.g., 4].

The liquid temperature near the free surface and tank pressure must be measured at the initiation and conclusion of each test, to determine the liquid properties. The accuracy of the required pressure measurement is  $\pm 5$  psia, and the accuracy of the required temperature measurement is  $\pm 1^\circ\text{R}$ . The temperature determination must be made at enough locations to estimate a representative average temperature.

**TABLE 1**  
**MEASUREMENT REQUIREMENTS FOR LIQUID DYNAMICS EXPERIMENT**

Parameter	Range	Accuracy	Instrument
Liquid temperature	20 - 50°R	$\pm 1^\circ\text{R}$	COLD-SAT temp. sensors
Tank pressure	5 - 50 psia	$\pm 5$ psia	COLD-SAT pressure sensors
Liquid interface position	Cylindrical tank: 0 - 4 ft axial; 0 - 1.3 ft. radial Spherical tank: 0 - 1.3 ft	$\pm 5\%$ axial $\pm 10\%$ radial	Liquid/vapor sensors with 2 - 5 second response
Slosh force	0 - 0.0001 lb	$\pm 2\%$	Load cells on tank support structures
Slosh frequency	0.001 - 0.01 hz	$\pm 1\%$	Load cells and liquid/vapor sensors
Steady linear acceleration	$8\mu\text{g}$ - $100\mu\text{g}$	$\pm 1\%$	COLD-SAT accelerometers or compute from thruster firing histories
Perturbation acceleration	Impulse: $A_i = 8\mu\text{g}$ Periodic: $A_p = 8\mu\text{g}$ $\tau_p = 75 - 125$ sec	$\pm 1\%$	COLD-SAT gyros and accelerometers, or compute from thruster firing histories

The effective gravity acceleration and the magnitude and history of the disturbance accelerations will be measured by the satellite accelerometers and gyros. The effective gravity amplitude should be measured to  $\pm 1\%$ . Ideally, the perturbation accelerations should also be measured to within  $\pm 1\%$  in amplitude and continuously in time. If these requirements cannot be met, the steady and perturbation accelerations can be computed from the history of the specified thruster firings.

Table 1 summarizes the measurement requirements.

#### 6.4 Hardware Requirements

The special hardware items required for the experiment are: (1) annular ring baffle mounted in the cylindrical receiver tank; (2) load cells mounted on the support structures of both receiver tanks, and (3) liquid-vapor sensor arrays in both receiver tanks.

The recommended width of the ring baffle is 10% of the tank radius. The baffle should be located at an axial position such that (a) the liquid free surface for 40% filling is slightly above the baffle and (b) no part of the free surface is pierced by the baffle. This location will maximize the damping at the 40% filling level while permitting higher filling levels to be investigated without significant damping from the baffle.

The load cells must be mounted on the tank support structures at locations where the lateral forces can be sensed.

The liquid-vapor sensors must be arrayed in sufficient numbers to determine the liquid interface position with the accuracy indicated in Table 1.

#### 6.5 Procedures

The liquid dynamics experiments will be performed primarily when opportunities arise. Whenever the satellite is maneuvered for other experiments or for operational reasons, the data necessary to define the quantity of liquid in each receiver tank, the disturbance, and the liquid-vapor sensor responses can be acquired. Nonetheless, several tests using periodic excitation probably will not occur as opportunities and must be conducted specifically.

The tests identified in Table 2 will be performed when the desired liquid levels ( $\pm 5\%$ ) are reached over the course of testing. During the tests, the satellite attitude control thrusters will be operated with specific commands to obtain the desired perturbation accelerations. The initial orientation of the liquid will be established by applying a settling acceleration with the thrusters, and this level of steady acceleration must be maintained for the duration of each test. The motion of the liquid surface will be monitored by the liquid-vapor sensors and the slosh forces by the load cells throughout each test.

The steady accelerations listed in Table 2 were selected to conform to the nominal levels that can be obtained by firing a single engine or a combination of engines; the exact acceleration level is not important so long as it is recorded for later data analysis. The perturbation accelerations are nominal also, and correspond to the firing of the appropriate attitude control thrusters or, depending on the COLD-SAT design, a gimballed engine; again, the exact levels of the accelerations are not important with the exception that they should be a small fraction of the steady acceleration. Impulsive perturbations are obtained by firing the engines

TABLE 2 PRELIMINARY TEST MATRIX

First Priority Tests					
Tank	F111	Axial g	Bond No.	Perturbation	Test Time
Cylinder	60%	8 $\mu$ g	0.5	Impulse: $A_t = 8\mu$ $\tau_t = 20$ sec	720 sec $\tau_p = 180$ sec liquid above baffle
Cylinder	60%	32 $\mu$ g	1.8	Impulse: $A_t = 8\mu$ $\tau_t = 20$ sec	600 sec $\tau_p = 160$ sec liquid above baffle
Cylinder	60%	100 $\mu$ g	5.8	Impulse: $A_t = 8\mu$ $\tau_t = 20$ sec	400 sec $\tau_p = 100$ sec liquid above baffle
Cylinder	60%	100 $\mu$ g	5.8	Periodic: $\tau_p = 100$ sec $A_t = 8\mu$	1000 sec $\tau_p = 100$ sec liquid above baffle
Cylinder	40%	32 $\mu$ g	1.8	Impulse: $A_t = 8\mu$ $\tau_t = 20$ sec	600 sec $\tau_p = 160$ sec liquid at baffle
Sphere	50%	8 $\mu$ g	0.5	Impulse: $A_t = 8\mu$ $\tau_t = 20$ sec	3400 sec $\tau_p = 860$ sec
Sphere	50%	32 $\mu$ g	1.8	Impulse: $A_t = 8\mu$ $\tau_t = 20$ sec	800 sec $\tau_p = 200$ sec
Sphere	50%	100 $\mu$ g	5.8	Impulse: $A_t = 8\mu$ $\tau_t = 20$ sec	430 sec $\tau_p = 107$ sec
Sphere	50%	32 $\mu$ g	1.8	Periodic: $\tau_p = 107$ sec $A_t = 8\mu$	2000 sec $\tau_p = 200$ sec
Sphere	50%	100 $\mu$ g	5.8	Periodic: $\tau_p = 200$ sec $A_t = 8\mu$	1100 sec $\tau_p = 107$ sec
Second Priority Tests					
Tank	F111	Axial g	Bond No.	Perturbation	Test Time
Sphere	33%	100 $\mu$ g	5.8	Impulse: $A_t = 8\mu$ $\tau_t = 20$ sec	500 sec $\tau_p = 125$ sec
Sphere	33%	100 $\mu$ g	5.8	Periodic: $\tau_p = 125$ sec $A_t = 8\mu$	1250 sec $\tau_p = 125$ sec
Sphere	75%	100 $\mu$ g	5.8	Impulse: $A_t = 8\mu$ $\tau_t = 20$ sec	350 sec $\tau_p = 125$ sec
Sphere	75%	100 $\mu$ g	5.8	Periodic: $\tau_p = 75$ sec $A_t = 8\mu$	750 sec $\tau_p = 125$ sec

for a short time, and periodic perturbations by on-off firings for scheduled periods. The frequency of the periodic accelerations should be maintained as indicated in the table, since the intent is to excite near-resonance sloshing.

The tests using impulsive excitation are designed primarily to determine the slosh natural frequency and damping. The tests using periodic excitation are designed either to determine slosh forces or to evaluate nonlinear effects, particularly the tendency for rotary slosh.

## 6.6 Data Analysis

Liquid temperature and pressure measurements will be used to determine the liquid surface tension, viscosity, and density from tabulated data. Liquid volume and liquid-sensor measurements before the perturbation acceleration is applied will be used to estimate the initial configuration of the liquid surface and the static contact angle. Accelerometer and gyro data acquired during the test (or computations based on the thruster firing histories) will be used to determine the imposed motion of the test tanks.

For impulsive perturbations, liquid-vapor sensor measurements during the sloshing will be analyzed to compute (1) slosh wave shape and amplitude as a function of time, (2) slosh natural frequency, and (3) slosh damping (from the decay of the slosh wave amplitude). If a dense array of sensors is used near the wall as discussed in Section 6.3, contact angle and contact line velocity will also be computed as a function of time; if not, these quantities will still be estimated but the resolution is not expected to be sufficient for fundamental studies. The load cell force histories will be analyzed to confirm the slosh natural frequency and damping data and to compute the slosh force. For periodic perturbations, the data analysis will be similar to the impulsive acceleration tests, with the exception that neither the liquid-vapor sensor nor the load cell measurements will provide damping data. The load cell data, in conjunction with damping data from the impulsive tests for the same Bond number and liquid level, will be analyzed to determine the effective mass of liquid participating in the sloshing.

Eventually, all the analyzed test data will be used to compare with predictions from the analytical/numerical models for the same Bond number, fill level, contact angle, and excitation.

**Table 3 NOMENCLATURE**

$a$	tank radius, cm
$A_i$	amplitude of impulsive acceleration, g's
$A_p$	amplitude of periodic acceleration, g's
$Bo$	Bond number, $g_{eff}a^2/\beta$
$f_n$	slosh natural frequency, hz
$g_{eff}$	effective gravity or steady linear acceleration, cm/sec <sup>2</sup>
$\beta$	specific surface tension, $\sigma/\rho$ , cm <sup>3</sup> /sec <sup>2</sup>
$\nu$	kinematic viscosity, cm <sup>2</sup> /sec
$\theta_s$	static contact angle, degrees
$\rho$	density, g/cm <sup>3</sup>
$\sigma$	surface tension, dynes/cm
$\tau_i$	length of impulsive acceleration, sec
$\tau_p$	period of periodic excitation, sec
$\tau_s$	slosh period, $1/f_n$ , sec

## REFERENCES

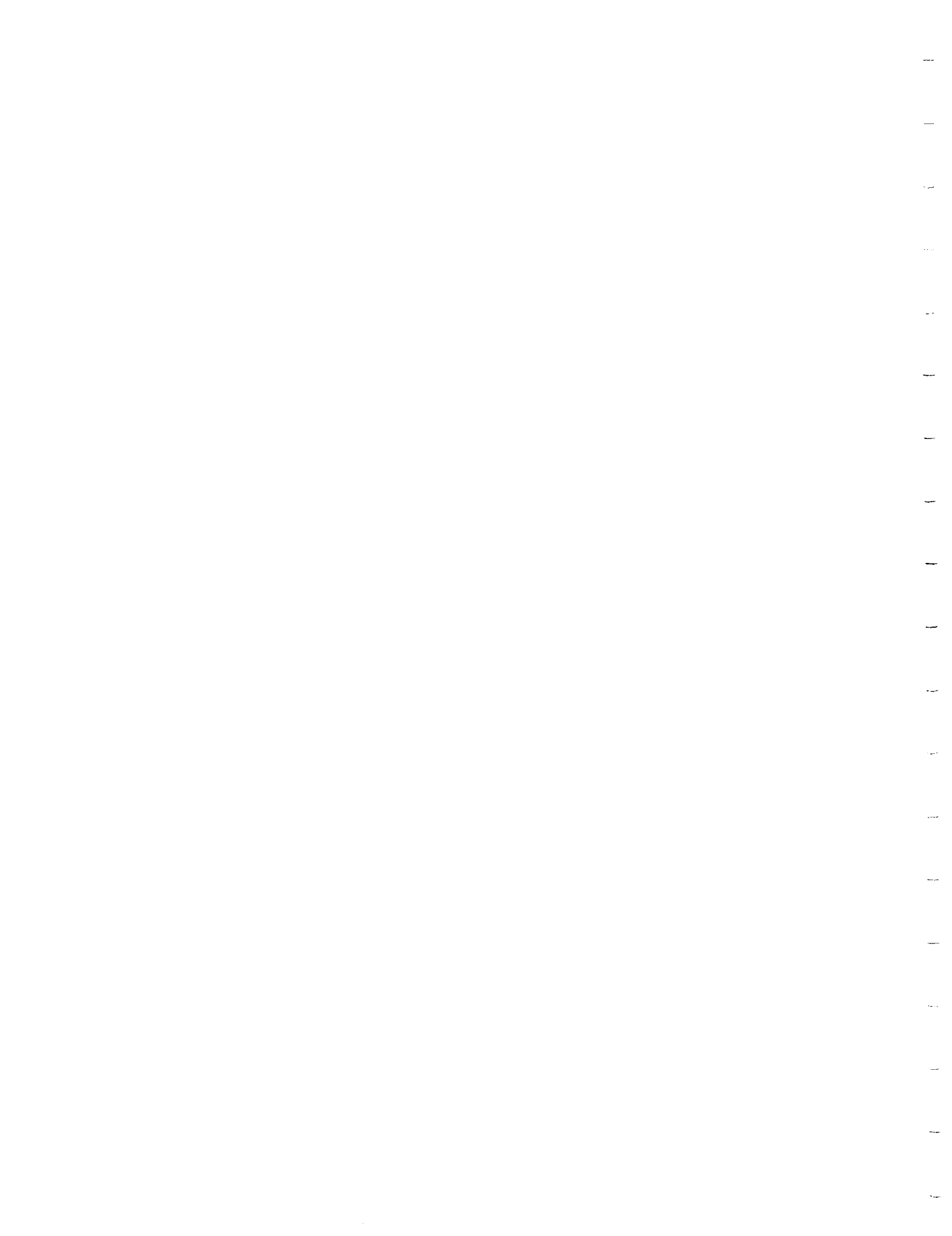
1. **The Dynamic Behavior of Liquids in Moving Containers**, NASA SP-106, 1966. (Reprinted by Southwest Research Institute with corrections, 1981, 1988.)
2. Lomen, D. O., "Digital Analysis of Liquid Propellant Sloshing in Mobile Tanks with Rotational Symmetry," NASA CR-230, 1965. (Computer code available for IBM-PC computers from F. Dodge, SwRI.)
3. Salzman, J. A., and Masica, W. J., "An Experimental Investigation of the Frequency and Viscous Damping of Liquids During Weightlessness," NASA TN D-5058, 1969.
4. Dodge, F. T., and Garza, L. R., "Simulated Low-Gravity Sloshing in Spherical, Ellipsoidal, and Cylindrical Tanks," AIAA Paper 69-1004, AIAA/ASTM/IES 4th Space Simulation Conference, 1969. (See also shortened version in **AIAA J. Spacecraft and Rockets**, 7, Feb. 1970, pp. 204-206.)
5. Peterson, L. D., Crawley, E. F., and Hansman, R. J., "The Nonlinear Coupled Dynamics of Fluids and Spacecraft in Low Gravity," MIT Space Systems Laboratory Report SSL 22-87, 1987.
6. Kaña, D. D., "A Numerical Spherical Pendulum Model for Rotary Liquid Slosh," Final Report, Part 2, SwRI Project 04-9553, 1990.
7. Dodge, F. T., and Garza, L. R. "Experimental and Theoretical Studies of Liquid Sloshing at Simulated Low Gravities, " **Trans. ASME, J. Applied Mechanics**, 90, June 1968, pp. 267-273.
8. Torrey, M. D., Mjolsness, R. C., and Stein, L. R., "NASA-VOF3D: A Three-Dimensional Computer Program for Incompressible Flows with Free Surfaces," LA 11009-MS, 1987.
9. Dominick, S., and Tegart, J., "Fluid Dynamics and Thermodynamics of a Low Gravity Liquid Tank Filling Method," AIAA Paper 90-0509, 1990.
10. Cruse, M. W., Dodge, F. T., Green, S. T., and Unruh, J. F., "Linear Low-G Slosh Model Based on a Finite Element Structural Code," Final Report, SwRI Project 04-9553, 1990.
11. Dodge, F. T., "The Spreading of Liquid Droplets on Solid Surfaces," **J. Colloid and Interface Science**, 121, Jan. 1988, pp. 154-160.



**APPENDIX B**

**COMPUTER CODES**

**PRECEDING PAGE BLANK NOT FILMED**



## B.1 Solution for Equilibrium Surface Shape

The free surface of a fluid in a tank is defined by the following differential equation in the normalized surface coordinates introduced in Section 4.0.

$$\frac{d^2 Z}{ds^2} \frac{dR}{ds} - \frac{d^2 R}{ds^2} \frac{dZ}{ds} - Bo(Z - Z_0) + \frac{1}{R} \frac{dZ}{ds} - \bar{\lambda}_0 = 0 \quad (\text{B.1-1})$$

Five boundary conditions are required to solve this equation. At the centerline of the tank there are four conditions which are specified,

$$R = 0, \quad Z = -Z_0, \quad \frac{dZ}{ds} = 0, \quad \frac{dR}{ds} = 1, \quad \text{at } s = 0 \quad (\text{B.1-2})$$

The fifth condition is defined by the contact angle between the fluid and the tank wall,

$$\frac{dZ}{ds} = \cos \theta_c \quad \text{at } s = s_{wall} \text{ for cylindrical tank} \quad (\text{B.1-3})$$

$$\frac{dZ}{ds} = \cos \left[ \theta_c + \sin^{-1} \left( \frac{Z_0}{R_t} \right) \right] \quad \text{at } s = s_{wall} \text{ for spherical tank}$$

Because Equation (B.1-1) is highly nonlinear, a computational approach to its solution is used. This equation can be reduced to a set of coupled first order equations with the following approach. Consider the relation between the surface coordinates,

$$\left( \frac{dR}{ds} \right)^2 + \left( \frac{dZ}{ds} \right)^2 = 1 \quad (\text{B.1-4})$$

Solving this relation for  $dR/ds$  and differentiating,

$$\frac{dR}{ds} = \left[ 1 - \left( \frac{dZ}{ds} \right)^2 \right]^{\frac{1}{2}} \quad (\text{B.1-5})$$

$$\frac{d^2 R}{ds^2} = - \frac{d^2 Z}{ds^2} \frac{dZ}{ds} \left( \frac{dR}{ds} \right)^{-1} \quad (\text{B.1-6})$$

Substitute this into Eq. (B.1-1) and rearrange to yield,

$$\frac{d^2 Z}{ds^2} = \frac{dR}{ds} \left[ \bar{\lambda}_0 + Bo(Z - Z_0) - \frac{1}{R} \frac{dZ}{ds} \right] \quad (\text{B.1-7})$$

Now solve Eq. (B.1-4) for  $dZ/ds$  and differentiate,

$$\frac{dZ}{ds} = \left[ 1 - \left( \frac{dR}{ds} \right)^2 \right]^{\frac{1}{2}} \quad (\text{B.1-8})$$

$$\frac{d^2Z}{ds^2} = -\frac{d^2R}{ds^2} \frac{dR}{ds} \left( \frac{dZ}{ds} \right)^{-1} \quad (\text{B.1-9})$$

Again, substitute this relation into Eq. (B.1-1),

$$\frac{d^2R}{ds^2} = -[\bar{\lambda}_0 + Bo(Z - Z_0)] \frac{dZ}{ds} + \frac{1}{R} \left( \frac{dZ}{ds} \right)^2 \quad (\text{B.1-10})$$

Four first order differential equations can now be formed,

$$\frac{dZ_1}{ds} = Z_2 \quad (\text{B.1-11})$$

$$\frac{dZ_2}{ds} = \frac{dR_1}{ds} \left[ \bar{\lambda}_0 + Bo(Z_1 - Z_0) - \frac{1}{R_1} \frac{dZ_1}{ds} \right] \quad (\text{B.1-12})$$

$$\frac{dR_1}{ds} = R_2 \quad (\text{B.1-13})$$

$$\frac{dR_2}{ds} = -[\bar{\lambda}_0 + Bo(Z_1 - Z_0)] \frac{dZ_1}{ds} + \frac{1}{R_1} \left( \frac{dZ_1}{ds} \right)^2 \quad (\text{B.1-14})$$

These four equations can be solved with the use of a standard fourth-order Runge-Kutta integration algorithm. The four initial conditions at  $s=0$  are specified to begin the solution. The solution is obtained with various values of  $\bar{\lambda}_0$  until the contact angle condition is satisfied. This method is similar to the "shooting" technique used to solve the Blasius equation for a laminar flat-plate boundary layer profile.

It should be noted that Eqs. (B.1-12) and (B.1-14) contain a singularity at  $R=0$  which must be resolved before the solution can proceed. First, take the limit of Eq. (B.1-12),

$$\lim_{s \rightarrow 0} \left( \frac{dZ_2}{ds} \right) = \bar{\lambda}_0 + \lim_{s \rightarrow 0} \left( \frac{1}{R_1} \frac{dZ_1}{ds} \right) \quad (\text{B.1-15})$$

Using L'Hospital's rule,

$$\lim_{s \rightarrow 0} \left( \frac{dZ_2}{ds} \right) = \bar{\lambda}_0 - \frac{\lim_{s \rightarrow 0} \left( \frac{d^2 Z_1}{ds^2} \right)}{\lim_{s \rightarrow 0} \left( \frac{dR_1}{ds} \right)} = \bar{\lambda}_0 - \lim_{s \rightarrow 0} \left( \frac{dZ_2}{ds} \right) \quad (\text{B.1-16})$$

or,

$$\lim_{s \rightarrow 0} \left( \frac{dZ_2}{ds} \right) = \frac{1}{2} \bar{\lambda}_0 \quad (\text{B.1-17})$$

Similarly, Eq. (B.1-6) can be used,

$$\lim_{s \rightarrow 0} \left( \frac{dR_2}{ds} \right) = \lim_{s \rightarrow 0} \left\{ \frac{d^2 Z_1}{ds} \frac{dZ_1}{ds} \left( \frac{dR_1}{ds} \right)^{-1} \right\} = \left\{ \frac{1}{2} \bar{\lambda}_0 \times 0 \times 1 \right\} \quad (\text{B.1-18})$$

$$\lim_{s \rightarrow 0} \left( \frac{dR_2}{ds} \right) = 0 \quad (\text{B.1-19})$$

A computer program was developed for solving the system of equations, (B.1-11) - (B.1-14). A listing of this routine follows. This routine requires the user to manually iterate on the value of  $\bar{\lambda}_0$  until the desired solution is achieved. This particular version of the code will execute on an IBM-PC when compiled with Microsoft FORTRAN 5.0. Very minor modifications are required to execute the code on other platforms.

An automatically iterating version of this program which uses a Newton-Raphson approach to converge on a value of  $\bar{\lambda}_0$  was also prepared. This approach is highly sensitive to the specific conditions and requires certain program modifications to "tune" the convergence rate for each application. So, it is not presented here.

A sample input file for this program follows the program listing. This file is read with FORTRAN list-directed READ statements; so, the format is rather flexible. A descriptor of each value in the file can be included because of this choice of file reading technique. The values listed here should be contained in a file named GENSURF.INP. These values are appropriate for a spherical tank that is 75% filled for the case of  $Bo=1$ . A value of  $\bar{\lambda}_0 = 2.98068$  (supplied by the user from the keyboard) will provides a contact angle of  $5.0467^\circ$ , which is within 1% of the desired values of  $5^\circ$ .



## B.2 Solution for Slosh Potential and Mechanical Model Parameters

The non-dimensional slosh velocity potential is defined as:

$$\bar{\Phi} = \sum_i b_i \bar{U}_i \quad (\text{B.2-1})$$

where the  $\bar{U}_i$  are the trial solutions from the structural finite element simulation. The  $b_i$  are the modal participation factors, or the eigenvectors, determined from the eigenvalue matrix equation:

$$[A] \{\bar{U}\} = \Omega^2 [B] \{\bar{U}\} \quad (\text{B.2-2})$$

Equation (B.2-2) is derived from numerically integrating the minimum integral, Eq. (4.4-29), with the assumption that  $\partial \bar{U}_i / \partial N = \Omega^2 (1 + Bo) M \bar{U}_i$  on the free surface. The matrix  $A$  is:

$$A_{ij} = \int_0^{s_c} \left\{ M \bar{U}_i \left[ Bo R \left( \frac{dR}{dS} \right) - \frac{\partial}{\partial S} \left( R \frac{\partial}{\partial S} \right) + \frac{1}{R} - R \left( \frac{1}{R_1^2} + \frac{1}{R_2^2} \right) \right] M \bar{U}_j \right\} dS \quad (\text{B.2-3})$$

and the matrix  $B$  is:

$$\int_0^{s_c} M \bar{U}_i \bar{U}_j dS \quad (\text{B.2-4})$$

A QUICKBASIC computer code "LOW-G.BAS" was written to integrate Eqs. (B.2-3) and (B.2-4) numerically. The code computes the required  $S$ -derivatives of  $\bar{U}_j$  of  $[A]$  numerically by fitting a quadratic through the value of the central point and the two adjoining points; the points at the  $S = 0$  and  $S = S_c$  are handled by special formulas.

The code also solves the matrix equation (B.2-2) to determine the eigenvalue  $\Omega^2$  for the fundamental slosh mode and the corresponding  $b_i$  eigenvectors. The slosh wave amplitude  $\bar{H}_c$  at the wall is then computed:

$$\bar{H}_c = \frac{(1 + Bo) M (S = S_c)}{\Omega^2} \sum_i \Omega_i^2 \bar{U}_i \quad (\text{B.2-5})$$

The slosh mass is computed by numerically integrating Eq. (4.4-28):

$$\frac{m_s}{\pi \rho R_o^3} = \left\{ \int_{-D}^{F_c} \bar{\Phi}_w R_w dZ - \frac{[(2K_c R_c - \cos \gamma_c) \cot \gamma_c] H_c}{(1 + Bo) \Omega} \right\}^2 / \int_0^{s_c} \bar{\Phi} \frac{\partial \bar{\Phi}}{\partial N} dS \quad (\text{B.2-6})$$

where the subscript  $w$  indicates that the parameter is evaluated at the tank wall. The normal derivative of  $\bar{\Phi}$  in the denominator of Eq. (B.2-6) is computed from analogy to Eq. (B.2-1) as:

$$\frac{\partial \bar{\Phi}}{\partial N} = M (1 + Bo) \sum_i b_i \Omega_i \bar{U}_i \quad (\text{B.2-7})$$

The other parameters of the mechanical model are computed from Eqs. (4.4-26a) and (4.4-25b). The QUICKBASIC program also computes these parameters.

The code requires the following general input information:

- Bond number
- Filling percent
- Contact angle
- Exponent  $m$  and parameter  $e$  of Eq. (4.4-36)
- Number of nodes on the free surface along the line  $\theta = 0$
- Number of trial modes (1, 2, or 3)

The code also requires the following data for each of the finite element nodal points on the free surface along the line  $\theta = 0$

- Nondimensional nodal coordinates  $R, S$
- Nondimensional derivatives  $dR/dS, d^2R/dS^2, dZ/dS, \text{ and } d^2Z/dS^2$
- Trial potentials  $\bar{U}_i$  for each mode

and the data at each finite element nodal point on the tank wall along the line  $\theta = 0$ :

- Nondimensional nodal coordinates  $R, Z$
- Trial potentials  $\bar{U}_i$  for each mode.

The coordinate data and the various derivatives are available from either the finite element simulation model or from the code described in Section B.1.

A sample set of input data is shown in the following pages for a 50% full tank and Bond number of one. As shown, the data is entered from the terminal. Any of the data for each screen can be corrected when the screen is displayed. The data is saved in two disk files COORD.DAT and MODE.DAT and the case can be run again, and the input data corrected if necessary, by indicating on the first screen that the data is to be read in from the disk files. The computed output is displayed on the screen and, if desired, printed.

A listing of the code is also attached. The code is extensively commented so that the logic flow can be readily followed.

MINIMIZE INTEGRAL TO FIND THE LOW-G SLOSH POTENTIAL  
BY USING THE STRUCTURAL CODE TRIAL FUNCTIONS

Hit RETURN after each entry

Bond No. =  Filling % =  Contact angle at wall (deg) =

Mass function: Exponent =  Constant =

How many trial modes do you want to consider?

How many nodal values are there at the surface and wall?

Eigenvalue of trial modes =

DO YOU WANT TO INPUT NODAL DATA FROM THE (1) TERMINAL OR (2) FILES ?

Input Screen No. 1

DATA FOR **FREE SURFACE** NODES

Enter: Node #, and R, S coordinates of node, starting at R=0.

Use the ENTER or DOWN ARROW key to enter each value from the file.  
Use the UP ARROW key to move back up through the data.

	Node #	R	S		Node #	R	S
1	79	0	0	13	1821	.7745	.93725
2	248	.07792	.07801	14	1900	.81146	1.02973
3	416	.15524	.15594	15	1967	.83453	1.11248
4	582	.23147	.23384	16	2069	.84649	1.18672
5	745	.30611	.31174	17	2069	.84975	1.25334
6	904	.37865	.38971	18	2106	.84636	1.3132
7	1058	.44849	.46773	19	2135	.83806	1.36694
8	1206	.51507	.54585	20	2157	.82629	1.4152
9	1347	.57773	.62408	21	2173	.81224	1.45847
10	1480	.63576	.70239	22	2184	.79681	1.49728
11	1604	.68844	.78076	23	2191	.78074	1.53207
12	1718	.73494	.85907	24	2195	.76457	1.56317
				25	2197	.74871	1.591

Input Screen No. 2

DATA FOR **FREE SURFACE** NODES  
Enter:  $dR/dS$  and  $dZ/dS$  derivatives for each node.

Use the ENTER or DOWN ARROW key to enter each value from the file.  
Use the UP ARROW key to move back up through the data.

	Node #	R' (S)	Z' (S)		Node #	R' (S)	Z' (S)
1	79	1	0	13	1821	.45919	.88832
2	248	.99662	.08198	14	1900	.33774	.94123
3	416	.9865	.16369	15	1967	.21826	.97588
4	582	.96951	.24499	16	2069	.10303	.99465
5	745	.94548	.32566	17	2069	-.00601	.99996
6	904	.91412	.40545	18	2106	-.10773	.99415
7	1058	.87508	.48395	19	2135	-.20132	.97949
8	1206	.828	.5607	20	2157	-.2865	.95804
9	1347	.77246	.63503	21	2173	-.36323	.93166
10	1480	.70807	.70612	22	2184	-.43184	.9019
11	1604	.63449	.77293	23	2191	-.4928	.87012
12	1718	.55154	.83414	24	2195	-.54656	.83738
				25	2197	-.59386	.80457

Input Screen No.3

DATA FOR **FREE SURFACE** NODES  
Enter:  $d^2R/dS^2$  AND  $d^2Z/dS^2$  derivatives of each mode.

Use the ENTER or DOWN ARROW key to enter each value from the file.  
Use the UP ARROW key to move back up through the data.

	Node #	R'' (S)	Z'' (S)		Node #	R'' (S)	Z'' (S)
1	79	0	1.0513	13	1821	-1.2421	.64203
2	248	-.08638	1.0501	14	1900	-1.3836	.49645
3	416	-.17366	1.0465	15	1967	-1.5028	.33608
4	582	-.26284	1.0401	16	2069	-1.5989	.16558
5	745	-.35485	1.0302	17	2069	-1.6722	-.01008
6	904	-.45054	1.0158	18	2106	-1.724	-.18686
7	1058	-.55057	.99553	19	2135	-1.7563	-.36103
8	1206	-.65544	.96788	20	2157	-1.7716	-.52984
9	1347	-.7653	.9309	21	2173	-1.7725	-.69108
10	1480	-.87996	.88238	22	2184	-1.7616	-.84354
11	1604	-.9987	.81982	23	2191	-1.7415	-.98635
12	1718	-1.1201	.7406	24	2195	-1.7143	-1.119
				25	2197	-1.6822	-1.2416

Input Screen No. 4

DATA FOR **FREE SURFACE** NODES  
Enter: Potential values for mode number 1

Use the ENTER or DOWN ARROW key to enter each value from the file.  
Use the UP ARROW key to move back up through the data.

	Node #	Potential		Node #	Potential
1	79	0	13	1821	1.0046
2	248	.08704	14	1900	1.1151
3	416	.17291	15	1967	1.2131
4	582	.25714	16	2069	1.3021
5	745	.34031	17	2069	1.3826
6	904	.42302	18	2106	1.4543
7	1058	.50533	19	2135	1.5171
8	1206	.58777	20	2157	1.571
9	1347	.6702	21	2173	1.6165
10	1480	.75276	22	2184	1.6537
11	1604	.83602	23	2191	1.6834
12	1718	.92011	24	2195	1.7069
			25	2197	1.7266

Input Screen No. 5

DATA FOR **FREE SURFACE** NODES  
Enter: Potential values for mode number 2

Use the ENTER or DOWN ARROW key to enter each value from the file.  
Use the UP ARROW key to move back up through the data.

	Node #	Potential		Node #	Potential
1	79	0	13	1821	-.08276
2	248	.17499	14	1900	-.47634
3	416	.33763	15	1967	-.89097
4	582	.47736	16	2069	-1.3111
5	745	.58819	17	2069	-1.7256
6	904	.6655	18	2106	-2.1232
7	1058	.70452	19	2135	-2.4927
8	1206	.70172	20	2157	-2.8277
9	1347	.65315	21	2173	-3.1221
10	1480	.55491	22	2184	-3.3721
11	1604	.40354	23	2191	-3.5779
12	1718	.19417	24	2195	-3.746
			25	2197	-3.89

Input Screen No. 6

# DATA FOR **FREE SURFACE** NODES

Enter: Potential values for mode number 3

Use the ENTER or DOWN ARROW key to enter each value from the file.  
Use the UP ARROW key to move back up through the data.

	Node #	Potential		Node #	Potential
1	79	0	13	1821	1.2743
2	248	-.42058	14	1900	1.1995
3	416	-.76613	15	1967	.8525
4	582	-.97616	16	2069	.33672
5	745	-1.0243	17	2069	-.28961
6	904	-.90966	18	2106	-.97582
7	1058	-.65127	19	2135	-1.6773
8	1206	-.28438	20	2157	-2.3587
9	1347	.14303	21	2173	-2.9891
10	1480	.57584	22	2184	-3.5445
11	1604	.95534	23	2191	-4.0134
12	1718	1.2164	24	2195	-4.4017
			25	2197	-4.7374

Input Screen No. 7

# DATA FOR **TANK WALL** NODES

Enter: Node #, and R, Z coordinates of node, starting at R=0

Use the ENTER or DOWN ARROW key to enter each value from the file.  
Use the UP ARROW key to move back up through the data.

	Node #	R	Z		Node #	R	Z
1	1	0	-1	13	1743	.9966	-.0821
2	170	.124	-.993	14	1834	.9995	.0322
3	338	.2461	-.9705	15	1912	.9909	.1343
4	504	.3644	-.933	16	1978	.9744	.2247
5	667	.4772	-.8811	17	2033	.9526	.3041
6	826	.5826	-.8154	18	2078	.9276	.3735
7	980	.679	-.7372	19	2114	.9009	.4341
8	1128	.7649	-.6475	20	2142	.8735	.4868
9	1269	.8389	-.5479	21	2163	.8464	.5325
10	1402	.9	-.4398	22	2178	.8201	.5722
11	1526	.947	-.3249	23	2188	.7949	.6068
12	1640	.9794	-.205	24	2194	.771	.6367
				25	2197	.7487	.6629

Input Screen No. 8

DATA FOR **TANK WALL** NODES

Enter: Potential values for mode number 1

Use the ENTER or DOWN ARROW key to enter each value from the file.  
Use the UP ARROW key to move back up through the data.

	Node #	Potential		Node #	Potential
1	1	0	13	1743	.8799
2	170	.05298	14	1834	.9823
3	338	.1089	15	1912	1.085
4	504	.169	16	1978	1.186
5	667	.233	17	2033	1.282
6	826	.3006	18	2078	1.371
7	980	.3716	19	2114	1.451
8	1128	.4462	20	2142	1.522
9	1269	.5243	21	2163	1.582
10	1402	.6063	22	2178	1.632
11	1526	.6926	23	2188	1.672
12	1640	.784	24	2194	1.702
			25	2197	1.727

Input Screen No. 9

DATA FOR **TANK WALL** NODES

Enter: Potential values for mode number 2

Use the ENTER or DOWN ARROW key to enter each value from the file.  
Use the UP ARROW key to move back up through the data.

	Node #	Potential		Node #	Potential
1	1	0	13	1743	.06863
2	170	.06443	14	1834	-.1741
3	338	.1303	15	1912	-.4842
4	504	.1966	16	1978	-.8512
5	667	.2603	17	2033	-1.259
6	826	.3177	18	2078	-1.688
7	980	.3646	19	2114	-2.117
8	1128	.3964	20	2142	-2.527
9	1269	.4074	21	2163	-2.902
10	1402	.3904	22	2178	-3.227
11	1526	.3361	23	2188	-3.497
12	1640	.2328	24	2194	-3.712
			25	2197	-3.89

Input Screen No. 10

DATA FOR **TANK WALL** NODES  
Enter: Potential values for mode number 3

Use the ENTER or DOWN ARROW key to enter each value from the file.  
Use the UP ARROW key to move back up through the data.

	Node #	Potential		Node #	Potential
1	1	0	13	1743	.738
2	170	-.06434	14	1834	.8465
3	338	-.1249	15	1912	.8167
4	504	-.1757	16	1978	.6092
5	667	-.2083	17	2033	.2139
6	826	-.2142	18	2078	-.3489
7	980	-.1858	19	2114	-1.033
8	1128	-.1169	20	2142	-1.78
9	1269	-.00369	21	2163	-2.53
10	1402	.1533	22	2178	-3.226
11	1526	.3457	23	2188	-3.829
12	1640	.5533	24	2194	-4.323
			25	2197	-4.737

Input Screen No. 11

INPUT DATA

Bond Number	Fill Level %	Cont. Ang	Surface Mass Distribution Function
1.0	50.0	5.0	$1.100 - (S/S_{max})^{2.50}$

PARTICIPATION FACTORS OF TRIAL MODES

B(1) = 1.00000	B(2) = 0.01013	B(3) = 0.00026
----------------	----------------	----------------

NON-DIMENSIONAL PARAMETERS OF THE PENDULUM MODEL

$(L_{liq} Vol)/(\pi * Ro^3)$	Slosh M/Liquid M	Pend. L/Ro	Ho/Ro
0.6633	0.2196	1.4881	-0.279
CG Loc./Ro	Spring/ $(\sigma * Ro^2)$	Freq <sup>2</sup> / $((1+B_0)\sigma/(d * Ro^3))$	
0.6856	0.6811	0.6720	

Do you want the above data printed out (Y or N) ?

Output Screen

**LISTING OF  
COMPUTER PROGRAM  
"GENSURF"**



```

c***** P R O G R A M ***** -0001
c***** G E N S U R F ***** -0002
c
c PURPOSE:  Generate the shape of an equilibrium free surface of a
c           liquid at low gravity in sperical and cylindrical
c           containers. -0003
c
c           USAGE:  This program is based heavily on the DYSIM program for
c                   system simulation. This routine employs a fourth-order
c                   Runge-Kutta algorithm to integrate a system of first-order
c                   differential equations. -0004
c
c                   A file which holds the solution parameters and ODE initial
c                   conditions is read. The program requests a value from the
c                   user for RLMB (lambda), the pressure jump parameter. -0005
c                   The program solves the surface equations and determines
c                   the wall contact angle. The user changes the value for
c                   RLMB until the desired value of wall contact angle is
c                   achieved. It should be noted that the solution is highly
c                   sensitive to the value of RLMB. The user should use small
c                   values (RLMB=0.2) initially and iterate from there. -0006
c
c                   A version of this program which employs a Newton-Raphson
c                   technique for converging on a value of RLMB was prepared.
c                   This version is highly problem dependent and is not
c                   available for general use. -0007
c
c MAIN VARIABLES: -0008
c
c   t(1) - Length along the surface of the liquid -0009
c   t(2) - Upper limit for surface length (prevents runaway solution) -0010
c   t(3) - Integration step size along the surface -0011
c   t(4) - Interval at which to record the solution parameters -0012
c   x(1) - Height of the free surface, Z -0013
c   x(2) - First derivative of surface height, dZ/ds -0014
c   x(3) - Radius of the free surface from tank centerline, R -0015
c   x(4) - First derivative of radius, dR/ds -0016
c   n    - Order of system (always set to n=4) -0017
c   m    - Number of outputs (set to m=8) -0018
c
c NOTE:  The values for surface length, height, and radius are -0019
c         normalized with respect to the tank wall radius. -0020
c         This routine uses no set of units. -0021
c
c INPUTS (read from the file called GENSURF.INP): -0022
c
c   tinit - Initial value of surface length -0023
c   fintim - Final value of surface length -0024
c   step - Integration step size along the surface -0025
c   prtstp - Surface length interval for saving solution parameters -0026
c   issflg - Variable step size flag -0027
c   dtllim - Lower limit for step size -0028
c   dtulim - Upper limit for step size -0029
c   errul - Upper limit on error criteria for variable step size -0030
c   errll - Lower limit on error criteria for variable step size -0031
c   iplot - Flag for line printer plot -0032
c   z0 - Initial condition for surface height -0033
c   dzds0 - Initial condition for surface height derivative -0034
c   r0 - Initial condition for surface radius -0035
c   drds0 - Initial condition for surface radius derivative -0036
c   bond - Bond Number -0037
c   thet0 - Contact angle at wall -0038

```

```

c  iclspr - Flag for tank type = 0    for spherical tank      -0064
c                                     .ne. 0 for cylindrical tank -0065
c                                     -0066
c  INPUT from the keyboard: -0067
c                                     -0068
c  rlmb   - Pressure jump parameter -0069
c                                     -0070
c                                     -0071
c  Suggested Values for Inputs -0072
c                                     -0073
c  tinit  - 0.0    Solution should always start at s=0.0      -0074
c  fintim - 5.0    Set to a large value, prevents runaway solution -0075
c  step   - 0.001  Suggested value -0076
c  prtstp - 0.01   Suggested value -0077
c  issflg - 0      Solution should use constant step (issflg = 0) -0078
c                                     Performance is erratic for variable step (issflg=1) -0079
c  dtllim - .001   Dummy variable for issflg=0 -0080
c  dtulim - .05    Dummy variable for issflg=0 -0081
c  errul  - .005   Dummy variable for issflg=0 -0082
c  errll  - .001   Dummy variable for issflg=0 -0083
c  iplot  - 0      0 for no line printer plot -0084
c                                     1 for line printer plot at end of output -0085
c  z0     - -0.06  |----- -0086
c  dzds0  - 0      | -0087
c  r0     - 0      | -0088
c  drds0  - 1      |_____These values are for 75% full spherical tank -0089
c  bond   - 1      | -0090
c  thet0  - 5      | -0091
c  iclspr - 0      | -0092
c  rlmb   - 2.980654 |----- -0093
c                                     -0094
c                                     -0095
c  FILES: -0096
c                                     -0097
c  1  GENSURF.OUT - Holds ASCII output for line printer -0098
c  2  GENSURF.ASC - High precision output table use by other routines -0099
c  3  GENSURF.INP - Parameter input file -0100
c                                     -0101
c                                     -0102
c                                     -0103
c  implicit double precision (a-h,o-z) -0104
c                                     -0105
c  common /sim/ x(20), dx(20), t(4), y(20), n, m , iplot, issflg, -0106
c  1      dtulim,dtllim,tprt -0107
c  common /param/ bond, rlmb, z0, thet0, pi, iqflg, iclspr -0108
c  common/tsave/ tinit -0109
c  common /save/ xsavem(20),xsave(20),tsavem,tsave -0110
c  common /error/ errmax,ierrmx,ierrfl,errll,errul,xtrlim -0111
c                                     -0112
c----- -0113
c  Order of system and number of outputs -0114
c  Set the value of pi for degree-radian conversions -0115
c----- -0116
c                                     -0117
c  n=4 -0118
c  m=8 -0119
c  pi = 4.d0 * atan(1.d0) -0120
c----- -0121
c  Open all files here -0122
c----- -0123
c  open(unit=1, file='GENSURF.out', status='unknown') -0124
c  open(unit=2, file='GENSURF.asc', status='unknown') -0125
c  open(unit=3, file='GENSURF.inp', status='old', mode='read') -0126

```

c-----		-0127
c	Get all of the input parameters	-0128
c-----		-0129
	read(3,*) tinit	-0130
	read(3,*) fintim	-0131
	read(3,*) step	-0132
	read(3,*) prtstp	-0133
	read(3,*) issflg	-0134
	read(3,*) dtllim	-0135
	read(3,*) dtulim	-0136
	read(3,*) errul	-0137
	read(3,*) errll	-0138
	read(3,*) iplot	-0139
	read(3,*) z0	-0140
	read(3,*) dzds0	-0141
	read(3,*) r0	-0142
	read(3,*) drds0	-0143
	read(3,*) bond	-0144
	read(3,*) thet0	-0145
	read(3,*) iclspr	-0146
c-----		-0147
c	Get the jump parameter from the user	-0148
c-----		-0149
	print*, ' Enter the guessed value of pressure jump condition'	-0150
	print*, ' for the desired contact angle=', thet0	-0151
	read(5,*) rlmb	-0152
c-----		-0153
c	Transfer inputs to program variables and other setup stuff	-0154
c-----		-0155
	t(1)=tinit	-0156
	t(2)= fintim	-0157
	t(3) = step	-0158
	t(4) = prtstp	-0159
	x(1) = z0	-0160
	x(2) = dzds0	-0161
	x(3) = r0	-0162
	x(4) = drds0	-0163
	thet0 = thet0 * pi/180.	-0164
	xtrlim = (t(2)-t(1))/t(3) * 10.	-0165
c-----		-0166
c	Record input variables for the user	-0167
c-----		-0168
	write(1,16010)	-0169
	write(1,16020) tinit,fintim,step,prtstp	-0170
	write(1,16030) issflg,errul,errll, dtulim, dtllim, xtrlim	-0171
	write(1,16040) iplot	-0172
	write(1,16050) x(1), x(2), x(3), x(4)	-0173
	write(1,16060) bond, thet0*180./pi, rlmb	-0174
	if (iclspr .eq. 0) then	-0175
	write(1,16070) iclspr	-0176
	else	-0177
	write(1,16080) iclspr	-0178
	endif	-0179
		-0180
		-0181
c-----		-0182
c	Begin the solution	-0183
c-----		-0184
	call dysim	-0185
c-----		-0186
c	Report the results to the user	-0187
c-----		-0188
	if (iclspr .eq. 0) then	-0189

```

        angl = -pi/2.
        ang2 = pi/2.
        if (dx(1) .gt. 0.) angl = atan(-dx(3)/dx(1))
        if (x(1) .lt. 1.) ang2 = asin(x(1))
        angle = ang2 - angl
    else
        angle = pi/2.
        if (abs(dx(1)) .le. 1.) angle = acos(dx(1))
    endif
c
    print*, ' tried for contact angle = ', thet0*180./pi
    print*, ' found contact angle = ', angle * 180./pi
    print*, ' rlmb = ', rlmb
    write(1,16999) rlmb, angle*180./pi
c
    stop
c
16010 format(1h1/' Liquid Free Surface')
16020 format(///5x,'Starting Value of Surf. Length [t(1)] = ',
1      t48,1pe12.5,' sec',/
1      5x,'Final Value of Surf. Length [t(2)] = ',
1      t48,1pe12.5,' sec',/
1      5x,'Step Size [t(3)] = ',
1      t48,1pe12.5,' sec',/
2      5x,'Print/Plot interval [t(4)] = ',
3      t48,1pe12.5,' sec',/)
16030 format(/ 5x,'Step Size Control Flag (issflg) = ',t48,i2,/
1      5x,'Upper Limit on Error Estimate (errul) = ',
1      t48,1pe12.5,/
2      5x,'Lower Limit on Error Estimate (errll) = ',
1      t48,1pe12.5,/
1      5x,'Upper Limit on Step Size (dtulim) = ',
1      t48,1pe12.5,' sec',/
1      5x,'Lower Limit on Step Size (dtllim) = ',
1      t48,1pe12.5,' sec',/
1      5x,'Maximum Number of Steps (xtrlim) = ',
1      t48,1pe12.5,/)
16040 format(/ 5x,'Printer/Plot flag (iplot) = ',t48,i2,/)
16050 format(/ 5x,'Initial Height [x(1)] = ',
1      t48,1pe12.5,' ',/
1      5x,'Initial dZds [x(2)] = ',
1      t48,1pe12.5,' ',/
1      5x,'Initial Radius [x(3)] = ',
1      t48,1pe12.5,' ',/
1      5x,'Initial dRds [x(4)] = ',
1      t48,1pe12.5,' ',/)
16060 format(/ 5x,'Bond Number (bond) = ',
a      t48,1pe12.5,' ',/
1      5x,'Desired Contact Angle (thet) = ',
a      t48,1pe12.5,/
1      5x,'Pressure Jump condition (rlmb) = ',
a      t48,1pe12.5,/)
16070 format(/ 5x,'Tank shape flag (iclspr) = ',
1      t48,i3,' Spherical Tank')
16080 format(/ 5x,'Tank shape flag (iclspr) = ',
1      t48,i3,' Cylindrical Tank')
16999 format(///' For Pressure Jump Parameter (rlmb) = ',1pe12.5/
1      ' Found Contact Angle = ',1pe12.5)
    end

```

```

C***** SUBROUTINE ***** -0249
C***** D E R F U N ***** -0250
      subroutine derfun -0251
C -0252
C Defines the derivative functions to be integrated -0253
C -0254
C These functions are the first order derivatives that define the -0255
C system of model equations to be solved. -0256
C -0257
C -0258
C implicit double precision (a-h,o-z) -0259
C -0260
C common /sim/ x(20), dx(20), t(4), y(20), n, m , iplot, issflg, -0261
1 dtulim,dtllim,tprt -0262
C common /param/ bond, rlmb, z0, thet0, pi, iqflg, iclspr -0263
C common/tsave/ tinit -0264
C common /save/ xsavem(20),xsave(20),tsavem,tsave -0265
C common /error/ errmax,ierrmx,ierrfl,errll,errul,xtrlim -0266
C -0267
C -0268
C ----- -0269
C Derivative functions -0270
C ----- -0271
      dx(3) = x(4) -0272
      dx(1) = x(2) -0273
      if (t(1) .eq. 0.) then -0274
        dx(2) = 0.5 * rlmb -0275
      else -0276
        dx(2) = ( bond*(x(1)-z0) + rlmb)*dx(3) - dx(1)*dx(3)/x(3) -0277
      endif -0278
      if (x(3) .ne. 0.) then -0279
        dx(4) = -(bond*(x(1)-z0)+rlmb)*dx(1) + dx(1)*dx(1)/x(3) -0280
      else -0281
        dx(4) = 0. -0282
      endif -0283
C -0284
C ----- -0285
C Check radius to determine if we are at tank wall -0286
C ----- -0287
      iqflg = 0 -0288
      wllchk = sqrt(x(1)*x(1) + x(3)*x(3)) -0289
      if (iclspr .ne. 0) wllchk = x(3) -0290
      if (wllchk .ge. 1. .or. x(3) .le. 0.) iqflg = 1 -0291
      if (iclspr .ne. 0 .and. dx(3) .le. 0.) iqflg = 1 -0292
C ----- -0293
C Enter outputs to be printed = y(1) through y(m) -0294
C -0295
C Originally: -0296
C -0297
C y(1) = Surface height, Z -0298
C y(2) = Surface height first derivative, dZ/ds -0299
C y(3) = surface height second derivative, d2Z/ds2 -0300
C y(4) = Surface radius, R -0301
C y(5) = Surface radius first derivative, dR/ds -0302
C y(6) = surface radius second derivative, d2R/ds2 -0303
C y(7) = local angle of surface with the 'horizontal' -0304
C y(8) = wall contact angle (valid only at last point in solution) -0305
C ----- -0306
      y(1) = x(1) -0307
      y(2) = x(2) -0308
      y(3) = dx(2) -0309
      y(4) = x(3) -0310
      y(5) = x(4) -0311

```

y(6) = dx(4)	-0312
y(7) = 90.	-0313
if (dx(3) .ne. 0.) then	-0314
y(7) = atan(dx(1)/dx(3)) * 180. /pi	-0315
endif	-0316
if (iclspr .eq. 0) then	-0317
ang1 = -pi/2.	-0318
ang2 = pi/2.	-0319
if (dx(1) .gt. 0.) ang1 = atan(-dx(3)/dx(1))	-0320
if (x(1) .lt. 1.) ang2 = asin(x(1))	-0321
y(8) = (ang2 - ang1) * 180./pi	-0322
else	-0323
y(8) = pi/2.	-0324
if (abs(dx(1)) .le. 1.) y(8) = acos(dx(1))	-0325
c        if (dx(1) .ne. 0.) y(8) = atan(dx(3)/dx(1))	-0326
y(8) = y(8) * 180./pi	-0327
endif	-0328
c	-0329
return	-0330
end	-0331

```

c***** S U B R O U T I N E ***** -0332
c***** D Y S I M ***** -0333
c -0334
c Controls the solution process -0335
c -0336
c----> This routine should not be changed by the user <----- !!!!! -0337
c -0338
c      subroutine dysim -0339
c -0340
c      implicit double precision (a-h,o-z) -0341
c -0342
c      common /sim/ x(20), dx(20), t(4), y(20), n, m , iplot, issflg, -0343
1      dtulim,dtllim,tprt -0344
c      common /param/ bond, rlmb, z0, thet0, pi, iqflg, iclspr -0345
c      common/tsave/ tinit -0346
c      common /save/ xsavem(20),xsave(20),tsavem,tsave -0347
c      common /error/ errmax,ierrmx,ierrfl,errll,errul,xtrlim -0348
c -0349
c      dimension t1(1500), yp(20,1500), ymin(20), ymax(20) -0350
c      integer*2 iy(20),plot(101), blank, star(20) -0351
c -0352
c      data iy, blank /20*'y(',' ' / -0353
c      data star/'1','2','3','4','5','6','7','8','9','A', -0354
1      'B','C','D','E','F','G','H','I','J','K' / -0355
c -0356
c----- -0357
c Setup for solution -- Print initial conditions -0358
c----- -0359
c      call derfun -0360
c -0361
c      tprt = t(1) -0362
c      if ( (t(2)-t(1))/t(4) .le. 1500.) go to 10 -0363
c      write(1,16010) (iy(i),i,i=1,m) -0364
c      iplot=0 -0365
10  lp=1 -0366
c      t1(lp) = t(1) -0367
c      do 20 i=1,m -0368
c          yp(i,lp) = y(i) -0369
20  continue -0370
c      write(1,16001) (iy(i),i,i=1,m) -0371
c      nflin = (m-10)/10 -0372
c      nllin = mod(m,10) -0373
c      m1 = 10 -0374
c      if (m .le. 10) then -0375
c          m1 = m -0376
c          write(1,16020) t(1), (y(i),i=1,m1) -0377
c      else -0378
c          write(1,16020) t(1), (y(i),i=1,m1) -0379
c          if (nflin .eq. 0) then -0380
c              write(1,16030) (y(i),i=11,m) -0381
c          else -0382
c              if (nllin .eq. 0) then -0383
c                  write(1,16040) (y(i),i=11,m) -0384
c              else -0385
c                  write(1,16050) (y(i),i=11,m) -0386
c              endif -0387
c          endif -0388
c      endif -0389
c      do 30 i=1,m -0390
c          ymin(i) = 0.9999*y(i) -0391
c          ymax(i) = 1.0001*y(i) -0392
30  continue -0393
c      k = 0 -0394

```

c-----	-0395
c Write initial conditions to high precision output file	-0396
c-----	-0397
write(2,16060) t(1),(y(i),i=1,7)	-0398
c-----	-0399
c Solution loop	-0400
c-----	-0401
100 continue	-0402
k = k + 1	-0403
if (k .gt. xtrlim) go to 999	-0404
ierrfl = 0	-0405
call rkint	-0406
if (ierrfl .ne. 0) go to 100	-0407
do 110 i=1,m	-0408
if(y(i) .lt. ymin(i)) ymin(i) = y(i)	-0409
if(y(i) .gt. ymax(i)) ymax(i) = y(i)	-0410
110 continue	-0411
if ( t(1) .ge. tprt .or. iqflg .eq. 1) then	-0412
tprt = tprt + t(4)	-0413
nflin = (m-10)/10	-0414
nllin = mod(m,10)	-0415
m1 = 10	-0416
if (m .le. 10) then	-0417
m1 = m	-0418
write(1,16020) t(1), (y(i),i=1,m1)	-0419
else	-0420
write(1,16020) t(1), (y(i),i=1,m1)	-0421
if (nflin .eq. 0) then	-0422
write(1,16030) (y(i),i=11,m)	-0423
else	-0424
if (nllin .eq. 0) then	-0425
write(1,16040) (y(i),i=11,m)	-0426
else	-0427
write(1,16050) (y(i),i=11,m)	-0428
endif	-0429
endif	-0430
endif	-0431
c-----	-0432
c Write to unformatted file	-0433
c-----	-0434
write(2,16060) t(1),(y(i),i=1,7)	-0435
c-----	-0436
c Save stuff for plotting if needed	-0437
c-----	-0438
if (iplot .eq. 1) then	-0439
lp = lp + 1	-0440
t1(lp) = t(1)	-0441
do 120 i=1,m	-0442
yp(i,lp) = y(i)	-0443
120 continue	-0444
endif	-0445
endif	-0446
c-----	-0447
c Test for end	-0448
c-----	-0449
if (iqflg .ne. 1) then	-0450
if (t(1) .lt. t(2)) then	-0451
if ((t(2)-t(1)) .gt. t(3)) go to 100	-0452
t(3) = t(2) - t(1)	-0453
tprt = t(4)	-0454
go to 100	-0455
endif	-0456
endif	-0457

c		-0458
c	Produce the line printer plot	-0459
c		-0460
	if(iplot.eq.0) go to 300	-0461
	write(1,16070) (i,ymin(i),i,ymax(i),i=1,m)	-0462
	write(1,16080)	-0463
	do 230 l=1,lp	-0464
	do 210 j=1,101	-0465
210	plot(j) = blank	-0466
	do 220 i=1,m	-0467
	jp = 1	-0468
	denom = ymax(i) - ymin(i)	-0469
	if (denom .ne. 0.) then	-0470
	jp = (yp(i,l)-ymin(i))/denom * 100 + 1	-0471
	endif	-0472
	plot(jp) = star(i)	-0473
220	continue	-0474
	write(1,16090) t1(1),plot	-0475
230	continue	-0476
c		-0477
	300 continue	-0478
c		-0479
	return	-0480
c		-0481
c	Error conditions	-0482
c		-0483
c		-0484
	999 continue	-0485
	write(1,16999) float(k),xtrlim	-0486
	print 16999, float(k),xtrlim	-0487
	stop	-0488
c		-0489
16001	format('1Tank Free Surface Solution'//	-0490
	1 5x,'T(1)',5x,10(a2,i2,',')',6x)/15x,10(a2,i2,',')',6x))	-0491
16010	format(1x,'***** Error Message from DYSIM *****',//	-0492
	*' The number of data points to be plotted exceeds the dimensioned	-0493
	*number of 1500.'// Decrease final time or increase print interval.	-0494
	*Plot will be suppressed.')	-0495
16020	format(1x,lpd10.3,lp10d11.3)	-0496
16030	format(15x,lp10d11.3 )	-0497
16040	format(10(15x,lp10d11.3/),15x,lp10d11.3 )	-0498
16050	format(10(15x,lp10d11.3/),15x,lp10d11.3 )	-0499
16060	format(lp8d20.10)	-0500
16070	format('1Plot of y(i) versus t(1)'//	-0501
	* (12x,'YMIN(',i2,) = ',lpd10.3,5x,'YMAX(',i2,) =' ,lpd10.3))	-0502
16080	format(/5x,'time',t13,'0.',34x,(y(i)-ymin(i))/(ymax(i)-ymin(i)),'	-0503
	* t114,'1.'/13x,10('!.....'),'!')	-0504
16090	format(1x,lpd11.4,1x,101a1)	-0505
16999	format(lh ,'***** Program Terminated *****/	-0506
	1 ' Iteration count = ',lpd12.4/	-0507
	2 ' Greater than limit of',lpd12.6)	-0508
c		-0509
	end	-0510

```

c***** SUBROUTINE ***** -0511
c***** R K I N T ***** -0512
c -0513
c Performs the integration of the derivatives at each step in the -0514
c solution -0515
c -0516
c----> This routine should not be changed by the user <----- !!!!! -0517
c -0518
c -0519
c      subroutine rkint -0520
c -0521
c      implicit double precision (a-h,o-z) -0522
c -0523
c      common /sim/ x(20), dx(20), t(4), y(20), n, m , iplot, issflg, -0524
1      dtulim,dtllim,tprt -0525
c      common /param/ bond, rlmb, z0, thet0, pi, iqflg, iclspr -0526
c      common /save/ xsavem(20),xsave(20),tsavem,tsave -0527
c      common /error/ errmax,ierrmx,ierrfl,errll,errul,xtrlim -0528
c -0529
c      dimension a(4,20),c(4) -0530
c -0531
c      c(1) = 0.5 -0532
c      c(2) = 0.5 -0533
c      c(3) = 1.0 -0534
c      c(4) = 0.0 -0535
c      do 10 i=1,n -0536
10     xsave(i) = x(i) -0537
        tsave = t(1) -0538
        do 40 k=1,4 -0539
            call derfun -0540
            do 20 i=1,n -0541
20         a(k,i) = dx(i) -0542
            do 30 i=1,n -0543
30         x(i) = xsave(i) + c(k)*a(k,i)*t(3) -0544
            t(1) = tsave + c(k)*t(3) -0545
40     continue -0546
        errmax = 0. -0547
        do 50 i=1,n -0548
            x(i) = xsave(i) + -0549
1            t(3)/6.0*(a(1,i)+2.0*a(2,i)+2.0*a(3,i)+a(4,i)) -0550
            denom = a(2,i)-a(1,i) -0551
            xnum = a(3,i) - a(2,i) -0552
            iiii = 0 -0553
            if (denom .ne. 0.) then -0554
                err = 2.* abs( (a(3,i)-a(2,i))/denom ) -0555
                iiii = i -0556
            elseif (xnum .eq. 0) then -0557
                err = errll*0.998 -0558
            else -0559
                err = errll*1.002 -0560
            endif -0561
            errmax = max(err,errmax) -0562
            if (errmax .eq. err) ierrmx = iiii -0563
50     continue -0564
        t(1) = tsave + t(3) -0565
c----- -0566
c check step size -0567
c----- -0568
        ierrfl = 0 -0569
        if (issflg .ne. 1) go to 506 -0570
        if (errmax .gt. errul) then -0571
            t(3) = t(3) * 0.5 -0572
            if (t(3) .le. dtllim) then -0573

```

	t(3) = dtllim	-0574
	endif	-0575
	t(1) = tsave	-0576
	do 505 i=1,n	-0577
505	x(i) = xsave(i)	-0578
	ierrfl = 1	-0579
	go to 510	-0580
	endif	-0581
	if (errmax .lt. err11) t(3) = t(3) * 1.05	-0582
	if (t(3) .gt. dtulim) t(3) = dtulim	-0583
506	continue	-0584
c		-0585
	call derfun	-0586
c		-0587
510	continue	-0588
c		-0589
	return	-0590
	end	-0591



**LISTING OF  
COMPUTER CODE  
"LOW-G.BAS"**

**PRECEDING PAGE BLANK NOT FILMED**



# LOW-G.BAS

```

' This program uses the trial functions from ADINA to compute the low-g slosh natural
' frequency, the slosh mode shape, the slosh force and torque, and the parameters
' of an equivalent mechanical pendulum model. No more than THREE trial modes are
' allowed. The number of nodal points along the surface line THETA = 0 must be
' >= 13 and <= 25.
' =====
'
' Subroutines defined used in this program.
'
DECLARE SUB AIntegrals (F!(), APartial!(), Coord!(), WH!(), Result!())
DECLARE SUB APart (Coord!(), Kappa2!(), WD2!(), WH!(), Result!())
DECLARE SUB BIntegrals (Coord!(), Func!(), WH!(), Result!())
DECLARE SUB CompDerivs (Coord!(), Value!(), Deriv!())
DECLARE SUB Deriv (Code%, Coord!(), FuncDat!(), FuncDeriv!())
DECLARE SUB InputScreen (FileNo%, Code%, Temp$(), TempNo())
DECLARE SUB LiqVol (Surf!(), Wall!(), Ans1!, Ans2!, DZ!, DeltaElev!,
SurfElev!)
DECLARE FUNCTION PadZero$ (A!, NoDecs!, NoBeforeDec!)
DECLARE SUB ParamModel (MOF!, F2!, SM!, SM2!, PL!, SC!, HO!)
DECLARE SUB PotNorm (SurfP!(), WallP!())
DECLARE SUB PrintOut (F2!, F!(), SM2!, PL!, HO!, CG!, SC!, BI!(), PC%)
DECLARE SUB PrintOut2 (S!(), WH!(), BI!(), F2!, F!())
DECLARE SUB OutputScreen (F2!, SM2!, PL!, HO!, CG!, SC!, BI!(), PCode%)
DECLARE SUB Rad (Coord!(), Temp!())
DECLARE SUB Root (Guess!, DT!, C1!(), C2!(), Answer!)
DECLARE SUB SloshM (S!(), W!(), PS!(), PW!(), TF!(), BI!(), SlsFrq!, Ans1!,
Ans2!)
DECLARE SUB TextIn1 (T$, Max%, NumOnly%, CapsOn%, ExitCode%, Colr%)
DECLARE SUB Vector (F2!, C1!(), C2!(), Result!())
DECLARE SUB WaveHite (Coord!(), NodeDatS!(), TempNo!())

' The following routines are assembly-language routines from the QUICKPAK library.
' Both are used only in the screen input routine "TextIn1". "Peek1%" reads a byte in
' memory; its use here is to determine what kind of monitor is being used, so it can
' be deleted without problem. "QPrint" just prints a text string on the monitor
' screen rapidly, so it can be replaced if needed by a combination of regular LOCATE
' statements and PRINT statements.

DECLARE FUNCTION Peek1% (segment, Address)
DECLARE SUB QPrint (X$, Colr%, Page%)
' =====

DIM ModeS(4, 25), ModeW(4, 25), WavHite(3, 25)
DIM CoordS(7, 25), CoordW(3, 25), RadCurv2(25)
DIM TempStor$(10, 25)
DIM Freq(4)
DIM WavDeriv1(3, 25), WavDeriv2(3, 25)
DIM A1(3, 25), A(3, 3), B(4, 4), Vec(3)

COMMON NoModes%, ModeNo%, NoNodes%, ConstMass, ExpMass, BondNo
COMMON Ang, FillLevel, LiqVolume, LastDZsurf, DeltaElev, SurfElev

CLS      ' clear the screen for the data input routines

' ===== SEGMENT 1      SEGMENT 1      SEGMENT 1 =====
' The code in Segment 1 does the following: (1) puts the name of the program on the
' screen, (2) asks for the number of trial modes and the number of nodal points
' for each mode along the free surface and the wall, and (3) whether the data will
' be entered from the keyboard or read in from disk files named COORD.DAT and

```

```

' MODE.DAT. The code uses some subroutines from QUICKPAK to draw boxes around the
' instruction and input text; the subroutine can be deleted if the QUICKPAK
' library is not available.

```

Start:

```

' Print the program title in a box
CALL Box(1, 5, 6, 75, 2, 12, -1)
COLOR 14: LOCATE 3, 14
PRINT "MINIMIZE INTEGRAL TO FIND THE LOW-G SLOSH POTENTIAL"
LOCATE 4, 17
PRINT "BY USING THE STRUCTURAL CODE TRIAL FUNCTIONS"

' Draw boxes and give instructions for entering the input data:
B$ = SPACE$(75) ' use B$ to clear parts of the screen later
COLOR 7: LOCATE 7, 25: PRINT "Hit RETURN after each entry"
Response$ = "N"

WHILE Response$ = "N" ' repeat instructions until input data is okay
    CALL Box(8, 17, 10, 22, 1, 14, -1)
    LOCATE 9, 6, 1, 5, 7: PRINT "Bond No. = "
    CALL Box(8, 36, 10, 39, 1, 14, -1)
    LOCATE 9, 24: PRINT "Filling % = "
    CALL Box(8, 73, 10, 76, 1, 14, -1)
    LOCATE 9, 43: PRINT "Contact angle at wall (deg) = "
    CALL Box(11, 32, 13, 37, 1, 14, -1)
    LOCATE 12, 6: PRINT "Mass function: Exponent = "
    CALL Box(11, 54, 13, 60, 1, 14, -1)
    LOCATE 12, 42: PRINT "Constant = "

    ' Now get the input:
    LOCATE 9, 18: INPUT "", BondNo ' Bond number
    LOCATE 9, 37: INPUT "", FillLevel ' tank fill level 0 - 100%
    LOCATE 9, 74: INPUT "", Ang ' contact angle at the wall (deg)
    LOCATE 12, 33: INPUT "", ExpMass ' constant in the mass distribution
    LOCATE 12, 55: INPUT "", ConstMass ' exponent in the mass distribution
    ' Is the data okay?
    LOCATE 14, 10
    INPUT "Are all of the input numbers okay (Y,N) ? ", Response$
    Response$ = UCASE$(Response$) ' convert to uppercase
    IF Response$ = "N" THEN
        LOCATE 8, 1 ' clear out the data
        FOR I = 1 TO 6
            PRINT B$
        NEXT I
    END IF
WEND ' end of the "WHILE-WEND" input loop

LOCATE 14, 1: PRINT B$ ' clear out the line of text

' Get the number "NoModes%" of trial modes and the number "NoNodes%" of
' nodal values per mode along THETA=0 from the structural simulation, and
' the trial natural frequencies:
Response$ = "N"
WHILE Response$ = "N" ' do until the data is okay
    CALL Box(14, 52, 16, 54, 1, 14, -1)
    LOCATE 15, 6
    PRINT "How many trial modes do you want to consider? "
    CALL Box(16, 64, 18, 67, 1, 14, -1)
    LOCATE 17, 6
    PRINT "How many nodal values are there at the surface and wall? "
ModeAgain:
    LOCATE 15, 53: INPUT "", NoModes%
    IF NoModes% > 3 THEN CALL Chime(6): GOTO ModeAgain
NodeAgain:
    LOCATE 17, 65: INPUT "", NoNodes%

```

```

IF NoNodes% < 13 OR NoNodes% > 25 THEN CALL Chime(6): GOTO NodeAgain
LOCATE 20, 6: PRINT "Eigenvalue of trial modes = "
FOR NF% = 1 TO NoModes%
    IColumn% = 23 + 11 * NF%
    IColumn2% = IColumn% + 10
    CALL Box(19, IColumn%, 21, IColumn2%, 1, 14, -1)
    LOCATE 20, IColumn% + 1: INPUT "", Freq(NF%)
NEXT NF%
LOCATE 22, 10
INPUT "Are these last input numbers okay (Y,N) ? ", Response$
Response$ = UCASE$(Response$) ' convert to uppercase
IF Response$ = "N" THEN
    LOCATE 14, 1
    FOR I = 1 TO 10 ' clear out the data
        PRINT B$
    NEXT I
END IF
WEND ' end of "WHILE-WEND" loop for modal data
LOCATE 22, 1: PRINT B$
' Find out whether whether the nodal coordinates, trial potential values,
' etc., will be given from the terminal or from data files:
FileAgain:
CALL Box(22, 76, 24, 78, 1, 14, -1)
LOCATE 23, 6
PRINT "DO YOU WANT TO INPUT NODAL DATA FROM THE (1) TERMINAL OR (2) FILES ? "
LOCATE 23, 77: INPUT "", Response$
Answer = VAL(Response$) ' If Response$=1 the data will be typed in
IF Answer = 1 OR Answer = 2 THEN
    GOTO Cont
ELSE
    CALL Chime(6) ' input a number <> 1 or 2 or other bad answers
    GOTO FileAgain
END IF
' ===== END OF SEGMENT 1 END OF SEGMENT 1 =====
' ===== SEGMENT 2 SEGMENT 2 SEGMENT 2 =====
' This segment of code gets (1) coordinates of the equilibrium free surface,
' (2) the required derivative values of the equilibrium free surface, (3)
' the coordinates of the finite element nodes along THETA=0, and (4) the
' values of the trial potentials at these nodes.
Cont:
SELECT CASE Answer
CASE 1 ' Type INPUT at the terminal
    ' ===== Option to type in the data input =====
    The following segment gets the typed in data using subroutines. The
    ' subroutines use the QUICKPAK routine TEXTIN!.BAS to allow data
    ' correction anywhere on the screen, without including a lot of code.
    ' The subroutine can be deleted if QUICKPAK is not available but the
    ' input requests will have to be redone to allow a mistake made in
    ' typing in the input to be corrected. The input is saved in files
    ' COORD.DAT (for the R,S coordinates and R',Z',R",Z" of each nodal
    ' point) and MODE.DAT (for the potential values at each node).
    ' Get data for surface nodes and store in array "CoordS()." Row 1
    ' of CoordS stores the node number, row 2 stores the R coord, row 3
    ' stores the S coord. The derivative R' is stored in row 4, Z' is
    ' stored in row 5, R" is stored in row 6, and Z" is stored in row 7.
    ' The first screen gets the node number and R and Z. The second screen
    ' gets R' and Z'. The third screen gets R" and Z".

```

```

CALL InputScreen(0, 1, TempStor$(), CoordS())           ' get R and S
CALL InputScreen(0, 2, TempStor$(), CoordS())           ' R' and Z'
CALL InputScreen(0, 3, TempStor$(), CoordS())           ' R" and Z"

' Get the potential values at each surface node and store in array
' ModeS(). Row 1 is the node # from CoordS(), row 2 the potential
' values for the first mode, row 3 the values for the second mode,
' and so on -- Row I+1 is the Mode I data.
FOR K = 1 TO NoModes%
    ModeNo% = K
    CALL InputScreen(0, 4, TempStor$(), ModeS())
NEXT K

' Get the data for the R,Z coordinates of the wall nodes and store in
' array CoordW(). Row 1 is the node # data, Row 2 is R, and Row 3 is Z.
' First, though, empty out the unneeded surface data in TempStor$.
FOR I = 1 TO 10
    FOR J = 1 TO 25
        TempStor$(I, J) = ""
    NEXT J
NEXT I
CALL InputScreen(0, 5, TempStor$(), CoordW())           ' R and Z

' Get potential values for each wall node point and store in ModeW().
' Row 1 is the node #, Row 2 is the first mode, and so on.
FOR K = 1 TO NoModes%
    ModeNo% = K
    CALL InputScreen(0, 6, TempStor$(), ModeW())
NEXT K
' ===== End of option to type in the input data =====
' ===== Start of option to enter data from disk files =====
CASE 2

' Read the surface and wall coordinate data from COORD.DAT file into
' the array TempStor$(). Rows 1 - 7 of TempStor$() will contain the
' surface node #'s and coord. data, and rows 8 - 10 will contain the
' wall node #'s and coord. data.
OPEN "COORD.DAT" FOR INPUT AS #1
FOR I = 1 TO 10
    FOR J = 1 TO NoNodes%
        INPUT #1, TempStor$(I, J)
    NEXT J
NEXT I
CLOSE #1

' Send the surface coordinate data forward for display on the screen
' and ask the user if the data is okay. Note that COORD.DAT is
' erased and then rewritten after verification.
CALL InputScreen(1, 1, TempStor$(), CoordS())
CALL InputScreen(1, 2, TempStor$(), CoordS())
CALL InputScreen(1, 3, TempStor$(), CoordS())

' Read the surface and wall modal values form MODE.DAT. The surface
' values are stored in TempStor$(), without deleting the surface
' node numbers. The wall values are stored temporarily in the array
' ModeW() and will later be read into TempStor$().
OPEN "MODE.DAT" FOR INPUT AS #1
FOR J = 1 TO 2 * NoModes%
    FOR I = 1 TO NoNodes%
        IF J = 1 THEN TempStor$ = STR$(CoordS(1, I))           ' node #
        IF J <= NoModes% THEN INPUT #1, TempStor$(J + 1, I)
        IF J > NoModes% THEN

```

```

        JJ = J - NoModes%
        INPUT #1, ModeW(JJ, I)
    END IF
NEXT I
NEXT J
CLOSE #1

' Send the surface mode data forward for display on the screen and
' ask the user if the data is okay. MODE.DAT is erased and then
' rewritten with the verified data.
FOR I = 1 TO NoModes%
    ModeNo% = I
    CALL InputScreen(1, 4, TempStor$(), ModeS())
NEXT I

' Now move the wall coordinate data from the last three rows of
' TempStor$() to the first three rows, so that the data will be
' displayed correctly on the screen. Note that the last three rows
' were not overwritten by the surface data input routines above.
FOR I = 1 TO NoNodes%
    TempStor$(1, I) = TempStor$(8, I)
    TempStor$(2, I) = TempStor$(9, I)
    TempStor$(3, I) = TempStor$(10, I)
NEXT I

' Send the wall coordinate data forward for display on the screen and
' ask the user if the data is okay. COORD.DAT is not erased by this
' operation, but the verified data overwrites the previous wall data.
CALL InputScreen(1, 5, TempStor$(), CoordW())

' Move the wall coord. data from the array CoordW() to the first row
' of TempStor$() and the wall modal data from the array ModeW() to
' rows 2, 3, and 4.
FOR I = 1 TO NoModes%
    FOR J = 1 TO NoNodes%
        IF I = 1 THEN TempStor$(1, J) = STR$(CoordW(1, J))
        TempStor$(I + 1, J) = STR$(ModeW(I, J))
    NEXT J
NEXT I

' Send the wall modal data forward for display on the screen and ask
' the user to verify the data. MODE.DAT is not erased by this
' operation, but the verified data overwrites the previous wall data.
FOR K = 1 TO NoModes%
    ModeNo% = K
    CALL InputScreen(1, 6, TempStor$(), ModeW())
NEXT K

' All the data has been displayed, checked, rewritten to COORD.DAT and
' MODE.DAT, and stored in Coord() and Mode() arrays.

' ===== End of option to enter data from disk files =====

CASE ELSE
    ' Just a safety check
    CLS : CALL Chime(6): GOTO Start
END SELECT
' end of loops to get input data

' ===== END OF SEGMENT 2 END OF SEGMENT 2 =====
' ===== SEGMENT 3 SEGMENT 3 SEGMENT 3 =====

' This segment does the numerical integrations. First, the trial potentials
' are normalized to have a maximum magnitude of one.
CALL PotNorm(ModeS(), ModeW())

' Compute the mean radius squared of the free surface at each node:
CALL Rad(CoordS(), RadCurv2())

```

```

' Compute the partial wave height for the trial functions WH = M*Potential
' where M=the mass distribution = ConstMass - (S/Smax)^ExpMass
CALL WaveHite(CoordS(), ModeS(), WavHite())

' Compute the derivatives: R(WH)' and (R(WH)')'. By numerical experi-
' mentation, it has found that the derivative (R(WH)')' must be formed
' slightly differently than R(WH)'.

' Compute the (WH)' derivative
CALL Deriv(1, CoordS(), WavHite(), WavDeriv1())

' Now multiply by R to get R(WH')
FOR I = 1 TO NoModes%
  FOR J = 1 TO NoNodes%
    WavDeriv1(I, J) = WavDeriv1(I, J) * CoordS(2, J)
  NEXT J
NEXT I

' Compute the (R(WH)')' derivative
CALL Deriv(2, CoordS(), WavDeriv1(), WavDeriv2())

' Compute and store in A1() the j-th part of the A() integrals. This
' is the part that is multiplied by WH-j and then integrated.
CALL APart(CoordS(), RadCurv2(), WavDeriv2(), WavHite(), A1())

' Compute the total Aij integrals
CALL AIntegrals(Freq(), A1(), CoordS(), WavHite(), A())

' Compute the Bij integrals
CALL BIntegrals(CoordS(), ModeS(), WavHite(), B())

' Compute the eigenfrequencies and eigenvectors. We must find the
' eigenfrequencies by trial and error since A() is not
' symmetric, and so most eigenvalue extraction routines will not work.
FirstGuess = 0: Delta = .1
CALL Root(FirstGuess, Delta, A(), B(), Freq2)

' The first Eigenfrequency Freq2 has been computed, so now compute
' the eigenvectors Vec() (or modal participation factors)
CALL Vector(Freq2, A(), B(), Vec())

' ===== END OF SEGMENT 3 END OF SEGMENT 3 =====
' ===== SEGMENT 4 SEGMENT 4 SEGMENT 4 =====
' This segment computes the parameters of the mechanical model.

' First, calculate the volume of liquid (non-dimensional): LiqVolume
CALL LiqVol(CoordS(), CoordW(), LiqVolume, LiquidCG, LastDZsurf, DeltaElev,
SurfElev)

' Calculate the non-dimensional slosh mass (ratio to liquid mass that
' fills the tank completely).
CALL SloshM(CoordS(), CoordW(), ModeS(), ModeW(), Freq(), Vec(), Freq2, SMass,
MFRatio)

' Compute the other mechanical model parameters
CALL ParamModel(MFRatio, Freq2, SMass, SMass2, PendL, Spring, HO)

' ===== END OF SEGMENT 4 END OF SEGMENT 4 =====
' ===== SEGMENT 5 SEGMENT 5 SEGMENT 5 =====
' This segment displays the results on the terminal screen, and also prints
' the results out if the user desires. The printed results can include
' the details of the wave height amplitude along the surface.

CALL OutputScreen(Freq2, SMass2, PendL, HO, LiquidCG, Spring, Vec(),
PrintCode%)

```



```

/ ***** AINTEGRALS *****
/ This routine computes each entry in the Aij matrix by numerical
/ integration, using linear interpolation. F() is the ADINA eigenvalues,
/ APartial() is the j-th part of each integrand APart(), Coord(3,I) is the
/ "S" coordinate of each node point, WH() is the wave height (not including
/ the freq. term), and the answers are stored in Result() to be returned
/ to the calling program.
/
SUB AIntegrals (F(), APartial(), Coord(), WH(), Result())
  SHARED NoNodes%, NoModes%
  FOR I = 1 TO NoModes%
    FOR J = 1 TO NoModes%
      Sum = 0
      AFreq = F(J)
      FOR K = 1 TO NoNodes%
        SELECT CASE K
          ' First determine the right Delta-S
          CASE 1
            ' first delta-S interval
            Delt = (Coord(3, 2) - Coord(3, 1)) / 2
          CASE NoNodes%
            ' last delta-S interval
            Delt = (Coord(3, NoNodes%) - Coord(3, (NoNodes% - 1))) / 2
          CASE ELSE
            ' interior delta-S interval
            Delt = (Coord(3, (K + 1)) - Coord(3, (K - 1))) / 2
        END SELECT
        Sum = Sum + APartial(J, K) * WH(I, K) * Delt
      NEXT K
      Result(I, J) = Sum * AFreq
    NEXT J
  NEXT I
END SUB

```

```

' ***** APART *****
' This subroutine computes the j-th part of the Aij integral at each
' node point, for later numerical integration. Coord(2,I) is the "R"
' coordinate of each node and Coord(4,I) is R', Curvat2() is the square
' of the mean curvature at each node, WD2() is the second derivative
' computed by Deriv(2) at each node, WH() is the wave height (not
' including freq) at each node, and the answer is stored in Result()
' to be sent back to the calling program.
'
SUB APART (Coord(), Curvat2(), WD2(), WH(), Result())
  SHARED NoModes%, NoNodes%, BondNo
  FOR I = 1 TO NoModes%
    FOR J = 1 TO NoNodes%
      R = Coord(2, J): RPrime = Coord(4, J): C2 = Curvat2(J) * Coord(2, J)
      IF J = 1 THEN
        Second = (C2 - BondNo * R * RPrime) * WH(I, J)
      ELSE
        Second = (C2 - 1 / R - BondNo * R * RPrime) * WH(I, J)
      END IF
      First = WD2(I, J)
      Result(I, J) = First + Second
    NEXT J
  NEXT I
END SUB

```

```

' ***** BINTEGRALS *****
' This subroutine computes the elements of the array Bij by numerical
' integration, using linear interpolation. Coord(2,I) is the "R"
' coordinate of each node, Func() is the normalized potentials, WH() is
' the wave height (not including the freq. term), and the answers are
' stored in Result() to be returned to the calling program.
'
SUB BIntegrals (Coord(), Func(), WH(), Result())
  SHARED NoNodes%, NoModes%
  FOR I = 1 TO NoModes%
    FOR J = 1 TO NoModes%
      Sum = 0
      FOR K = 1 TO NoNodes%

        SELECT CASE K
          CASE 1
            Delt = (Coord(3, 2) - Coord(3, 1)) / 2
          CASE NoNodes%
            Delt = (Coord(3, NoNodes%) - Coord(3, (NoNodes% - 1))) / 2
          CASE ELSE
            Delt = (Coord(3, (K + 1)) - Coord(3, (K - 1))) / 2
        END SELECT

        ' Got to skip over the number of the node in Func()
        Sum = Sum + Coord(2, K) * Func(J + 1, K) * WH(I, K) * Delt
      NEXT K
      Result(I, J) = Sum
    NEXT J
  NEXT I
END SUB

```

```

' ***** DERIV *****
' This subroutine computes the derivative of FuncDat() and stores it in
' FuncDeriv(). Coord(3,I) is the "S" coordinate along the surface.
' The derivatives are complicated because the spacing of the "S" points
' is not uniform. A quadratic is fitted through each three points and
' the derivative of the middle point is evaluated. Special formulas
' are used for the first and last points. When Code%=2, the derivative
' is the average of the linear (backwards) derivative and the quadratic derivative
'
SUB Deriv (Code%, Coord(), FuncDat(), FuncDeriv())
  SHARED NoModes%, NoNodes%
  IF Code% = 1 THEN
    AvgFact1 = 0:      AvgFact2 = 1      ' Discard the linear average
  ELSE
    AvgFact1 = .5:      AvgFact2 = .5      ' Weight the linear and quad derivs.
    equally
  END IF
  FOR I = 1 TO NoModes%
    FOR J = 1 TO NoNodes%
      SELECT CASE J      ' First, compute the backward and forward
                        ' differences of S
        CASE 1
          DF = Coord(3, 2) - Coord(3, 1)
          DR = Coord(3, 2)
        CASE NoNodes%
          DF = Coord(3, NoNodes%) - Coord(3, (NoNodes% - 1))
          DR = Coord(3, (NoNodes% - 1)) - Coord(3, (NoNodes% - 2))
        CASE ELSE
          DF = Coord(3, (J + 1)) - Coord(3, J)
          DR = Coord(3, J) - Coord(3, (J - 1))
      END SELECT
      SELECT CASE J      ' Now compute the values of the function at the rear,
                        ' middle, and forward point, and the appropriate
                        ' differences
        CASE 1
          FR = -FuncDat(I, 2)
          FF = FuncDat(I, 2):  FM = FuncDat(I, 1)
          First = (FM - FR) / DR
          Second = FM * (DF - DR) / (DF * DR)
          Third = (FF * DR / DF - FR * DF / DR) / (DF + DR)
          FuncDeriv(I, 1) = First * AvgFact1 + (Second + Third) * AvgFact2
        CASE NoNodes%
          FF = FuncDat(I, NoNodes%)
          FM = FuncDat(I, (NoNodes% - 1))
          FR = FuncDat(I, (NoNodes% - 2))
          First = (FF - FM) / DF
          Second = FM * (DF + DR) / (DF * DR)
          Third = (FF * (2 + DR / DF) + FR * DF / DR) / (DF + DR)
          FuncDeriv(I, NoNodes%) = First / 2 + (Third - Second) / 2
        CASE ELSE
          FF = FuncDat(I, (J + 1))
          FM = FuncDat(I, J)
          FR = FuncDat(I, (J - 1))
          First = (FM - FR) / DR
          Second = FM * (DF - DR) / (DF * DR)
          Third = (FF * DR / DF - FR * DF / DR) / (DF + DR)
          FuncDeriv(I, J) = First * AvgFact1 + (Second + Third) * AvgFact2
      END SELECT
    NEXT J
  NEXT I
END SUB

```

```

/ ***** INPUT SCREEN *****
/ Sets up the terminal screen for input. This uses a QUICKPAK routine
/ TextIn1() that allows the arrows to be used to input data anywhere and
/ to back up through the data to correct any bad entries. If QUICKPAK
/ is not available, the data can be entered (after modifying the code)
/ but it will be more difficult to correct a bad entry without starting
/ over from scratch for each set of input data.

```

```

/   Meaning of the parameters:
/   File%:      0 = data will be typed in from the terminal
/               1 = data will be read in from the data disk files
/   Code%:      1 = input surface node # and R and S
/               2 = input surface R' and Z'
/               3 = input surface R" and Z"
/               4 = input surface potential values for each mode
/               5 = input wall node # and R and Z
/               6 = input wall potential values for each mode
/   Temp$():    used to transfer data to Txt$ for display on the
/               screen, and to store input data temporarily after
/               it has been entered
/   TempNo():   used to accumulate the input data and return the
/               data to the main program for storage in the right
/               array
/   FileCode%:  1 = "open" disk files for data input
/               2 = "append" data to disk files
/

```

```

SUB InputScreen (File%, Code%, Temp$(), TempNo())

```

```

  SHARED NoModes%, ModeNo%, NoNodes%

```

```

  CLS :          COLOR 11, 0:          FileCode% = 0

```

```

/ ===== SECTION 1      SECTION 1      SECTION 1 =====
/ This section puts the right titles and instructions on the screen.

```

```

  SELECT CASE Code%

```

```

    CASE 1 TO 4

```

```

      LOCATE 1, 20:          PRINT "DATA FOR "
      LOCATE 1, 29:          COLOR 15, 0:  PRINT "FREE SURFACE "
      LOCATE 1, 42:          COLOR 11, 0:  PRINT "NODES"

```

```

    CASE 5 TO 6

```

```

      LOCATE 1, 20:          PRINT "DATA FOR "
      LOCATE 1, 29:          COLOR 15, 0:  PRINT "TANK WALL "
      LOCATE 1, 39:          COLOR 11, 0:  PRINT "NODES"

```

```

  END SELECT

```

```

  LOCATE 2, 10

```

```

  SELECT CASE Code%

```

```

    CASE 1

```

```

      PRINT "Enter: Node #, and R, S coordinates of node, starting at R=0."

```

```

    CASE 2

```

```

      PRINT "Enter: dR/dS and dZ/dS derivatives for each node."

```

```

    CASE 3

```

```

      PRINT "Enter: d2R/dS2 AND d2Z/dS2 derivatives of each mode."

```

```

    CASE 4

```

```

      PRINT "Enter: Potential values for mode number "

```

```

      LOCATE 2, 49: COLOR 14, 0: PRINT ModeNo%

```

```

    CASE 5

```

```

      PRINT "Enter: Node #, and R, Z coordinates of node, starting at R=0"

```

```

    CASE 6

```

```

      PRINT "Enter: Potential values for mode number "

```

```

      LOCATE 2, 49: COLOR 14, 0: PRINT ModeNo%

```

```

  END SELECT

```

```

IF File% = 0 THEN          ' instructions for typing input data
    COLOR 15, 0
    LOCATE 4, 8:           PRINT "Use the "
    COLOR 14, 0: LOCATE 4, 16: PRINT "ENTER "
    COLOR 15, 0: LOCATE 4, 22: PRINT "or "
    COLOR 14, 0: LOCATE 4, 25: PRINT "DOWN ARROW "
    COLOR 15, 0: LOCATE 4, 37: PRINT "key after entering each value."
    LOCATE 5, 8:           PRINT "Use the "
    LOCATE 5, 16: COLOR 14, 0: PRINT "UP ARROW "
    COLOR 15, 0: LOCATE 5, 25: PRINT "key to move back through the input
data."
ELSE                        ' instructions for reading input from files
    COLOR 15, 0
    LOCATE 4, 8:           PRINT "Use the "
    COLOR 14, 0: LOCATE 4, 16: PRINT "ENTER "
    COLOR 15, 0: LOCATE 4, 22: PRINT "or "
    COLOR 14, 0: LOCATE 4, 25: PRINT "DOWN ARROW "
    COLOR 15, 0: LOCATE 4, 37: PRINT "key to enter each value from the file."
    LOCATE 5, 8:           PRINT "Use the "
    LOCATE 5, 16: COLOR 14, 0: PRINT "UP ARROW "
    COLOR 15, 0: LOCATE 5, 25: PRINT "key to move back up through the data."
END IF

SELECT CASE Code%
    CASE 1                  ' Print titles over input columns for R,S input data
        LOCATE 7, 5: PRINT "      Node #      R      S      Node #"
R        S"
    CASE 2                  ' Print titles over input columns for R',Z' input data
        LOCATE 7, 5: PRINT "      Node #      R' (S)      Z' (S)      Node #"
R' (S)      Z' (S)"
    CASE 3                  ' Print titles over input columns for R'', Z'' input data
        LOCATE 7, 5: PRINT "      Node #      R'' (S)      Z'' (S)      Node #"
R'' (S)      Z'' (S)"
    CASE 4                  ' Print titles over input columns for nodal values input
        LOCATE 7, 5: PRINT "      Node #      Potential      Node #"
Potential"
    CASE 5
        LOCATE 7, 5: PRINT "      Node #      R      Z      Node #"
R        Z"
    CASE 6                  ' Print titles over input columns for nodal values input
        LOCATE 7, 5: PRINT "      Node #      Potential      Node #"
Potential"
END SELECT

' ===== END OF SECTION 1      END OF SECTION 1 =====
' ===== SECTION 2      SECTION 2      SECTION 2 =====
' This section gets the screen display in shape to continue with data
' input.

' Print out the numbers from 1 to NoNodes% on the screen in two
' columns, 1 to 12 and 13 to NoNodes%, to help organize the input.
FOR N = 1 TO NoNodes%
    IF N <= 12 THEN
        LOCATE 7 + N, 3: PRINT N
    ELSE
        LOCATE 7 + N - 12, 42: PRINT N
    END IF
NEXT N

```

```

' When entering the modal values, the surface or wall node numbers are
' also displayed in the columns, but we have to retrieve them from Temp$
' and store them in TempNo() so they can be displayed. The node numbers
' are already available when entering the coordinate data.
IF Code% = 4 OR Code% = 6 THEN
  FOR M = 1 TO NoNodes%
    TempNo(1, M) = VAL(Temp$(1, M))
  NEXT M
END IF

' Now, for the wall input, change Code% so that the same routines can
' be used as for the surface nodes; also change FileCode% so that data is
' appended to the existing disk files rather than overwriting them.
IF Code% = 5 THEN Code% = 1: FileCode% = 1
IF Code% = 6 THEN Code% = 4: FileCode% = 1

' Now print the node numbers on the screen:
SELECT CASE Code%
  CASE 2 TO 4
    FOR N = 1 TO NoNodes%
      IF N <= 12 THEN
        LOCATE 7 + N, 10: PRINT TempNo(1, N)
      ELSE
        LOCATE 7 + N - 12, 50: PRINT TempNo(1, N)
      END IF
    NEXT N
END SELECT

' ===== END OF SECTION 2 END OF SECTION 2 =====
' ===== SECTION 3 SECTION 3 SECTION 3 =====
' This long segment gets the screen input and checks to see if it is
' okay. Most of the code just allows the cursor to move up and down
' on the screen to correct any bad entry, without having to enter all
' the data over again. The parameter ExC% indicates whether the piece
' of input is okay (ExC%=0) so the cursor can be moved to the next line,
' or that the piece of data is wrong (ExC%<>0) and will be re-entered.
' ExC% is set by how the user ends the entry (RETURN, etc., or UP ARROW,etc)

' First, decide what column to put the cursor into initially.
N = 1: NN = N
  IF Code% = 1 THEN M1 = 10 ' Put cursor in "Node No" col
  IF Code% = 2 OR Code% = 3 THEN M1 = 20 ' Put cursor in 2nd col
  IF Code% = 4 THEN M1 = 30 ' Put cursor in 3rd col

' When typing in the modal values, we need to clear out the coordinate data
' from Temp$() so that it is not displayed on the screen incorrectly.
IF Code% = 4 AND File% = 0 THEN
  FOR I = 1 TO NoNodes%
    Temp$(ModeNo% + 1, I) = ""
  NEXT I
END IF

Insurf: ' we keep coming back here for the next piece of data

COLOR 7, 0
SELECT CASE M1
  ' Txt$ is the data that will be displayed on the screen initially
  CASE 10, 50
    Txt$ = Temp$(1, N) ' node numbers
  CASE 20, 60
    Txt$ = Temp$(2 * Code%, N) ' R, R' or R" (surface) or R (wall)
  CASE 30, 70
    IF Code% <> 4 THEN
      Txt$ = Temp$(1 + 2 * Code%, N) ' S, Z' or Z" (surface) or Z (wall)
    ELSE

```

```

        Txt$ = Temp$(ModeNo% + 1, N)      ' modal potential values at nodes
    END IF
END SELECT

LOCATE 7 + NN, M1
' Now get the piece of data; it is returned in Txt$
CALL TextIn1(Txt$, 8, 0, 0, ExC%, 7)

IF ExC% = 0 THEN
    ' data is okay, so store it, move the cursor, and get the next data piece
    SELECT CASE M1
        CASE 10, 50
            Temp$(1, N) = Txt$
            TempNo(1, N) = VAL(Txt$)      ' change the text input to a number
            M1 = M1 + 10
            GOTO Insurf
        CASE 20, 60
            Temp$(2 * Code%, N) = Txt$
            TempNo(2 * Code%, N) = VAL(Txt$)
            M1 = M1 + 10
            GOTO Insurf
        CASE 30
            IF Code% <> 4 THEN
                Temp$(1 + 2 * Code%, N) = Txt$
                TempNo(1 + 2 * Code%, N) = VAL(Txt$)
            ELSE
                Temp$(ModeNo% + 1, N) = Txt$
                TempNo(ModeNo% + 1, N) = VAL(Txt$)
            END IF
            IF N < 12 THEN
                N = N + 1: NN = N
                M1 = 10
                IF Code% = 2 OR Code% = 3 THEN M1 = 20
                IF Code% = 4 THEN M1 = 30
            ELSE
                N = N + 1: NN = N - 12
                M1 = 50
                IF Code% = 2 OR Code% = 3 THEN M1 = 60
                IF Code% = 4 THEN M1 = 70
            END IF
            GOTO Insurf
        CASE 70
            IF Code% <> 4 THEN
                Temp$(1 + 2 * Code%, N) = Txt$
                TempNo(1 + 2 * Code%, N) = VAL(Txt$)
            ELSE
                Temp$(ModeNo% + 1, N) = Txt$
                TempNo(ModeNo% + 1, N) = VAL(Txt$)
            END IF
            IF N < NoNodes% THEN
                N = N + 1: NN = N - 12
                M1 = 50
                IF Code% = 2 OR Code% = 3 THEN M1 = 60
                IF Code% = 4 THEN M1 = 70
                GOTO Insurf
            ELSE
                LOCATE 23, 10: COLOR 15, 0
                INPUT "Is all your data correct (Y,N)? ", Response$
                Response$ = UCASE$(Response$)
                IF Response$ = "Y" THEN
                    GOTO Finish
                ELSE
                    ' start this screen all over again
                    N = NoNodes%
                    NN = NoNodes% - 12
                END IF
            END IF
        END CASE
    END SELECT

```

```

                M1 = 70
                GOTO Insurf
            END IF
        END IF
    END SELECT
ELSE
    ' piece of data is bad, so don't store it and back up the cursor. This
    ' is complicated because we have to jump to a new column when the cursor
    ' has backed all the way to the top of the previous one, and we also
    ' have to make sure that the cursor does not leave the data input area.
    SELECT CASE M1
        CASE 30, 70
            IF Code% <> 4 THEN
                M1 = M1 - 10
                GOTO Insurf
            ELSE
                IF M1 = 70 THEN
                    IF N = 13 THEN
                        M1 = 30
                        N = N - 1
                        NN = N
                        GOTO Insurf
                    ELSE
                        M1 = 70
                        N = N - 1
                        NN = N - 12
                        GOTO Insurf
                    END IF
                ELSE
                    N = N - 1
                    IF N < 1 THEN
                        CALL Chime(8)
                        N = 1
                        NN = N
                        GOTO Insurf
                    ELSE
                        NN = N
                        GOTO Insurf
                    END IF
                END IF
            END IF
        CASE 20
            IF Code% = 1 THEN
                M1 = M1 - 10
                GOTO Insurf
            ELSE
                N = N - 1
                IF N < 1 THEN
                    CALL Chime(8)
                    N = 1
                    M1 = 20
                    GOTO Insurf
                ELSE
                    M1 = 30
                    NN = N
                    GOTO Insurf
                END IF
            END IF
        CASE 60
            IF Code% = 1 THEN
                M1 = M1 - 10
                GOTO Insurf
            
```

```

ELSE
    IF N = 13 THEN
        M1 = 30
        N = N - 1
        NN = N
        GOTO Insurf
    ELSE
        M1 = 70
        N = N - 1
        NN = N - 12
        GOTO Insurf
    END IF
END IF
CASE 10
    N = N - 1
    IF N < 1 THEN
        CALL Chime(8)
        N = 1
        M1 = 10
        GOTO Insurf
    ELSE
        M1 = 30
        NN = N
        GOTO Insurf
    END IF
CASE 50
    IF N = 13 THEN
        M1 = 30
        N = N - 1
        NN = N
        GOTO Insurf
    ELSE
        M1 = 70
        N = N - 1
        NN = N - 12
        GOTO Insurf
    END IF
END SELECT
END IF
' ===== END OF SECTION 3      END OF SECTION 3      =====
' ===== SECTION 4      SECTION 4      SECTION 4      =====
' This section writes the good data to the disk data files.
Finish:
' Write the surface coordinate data after all three screens of data
' have been entered:
IF Code% = 3 THEN
    OPEN "COORD.DAT" FOR OUTPUT AS #1      ' This wipes out all existing data
    FOR I = 1 TO 7
        FOR J = 1 TO NoNodes%
            WRITE #1, TempNo(I, J)
        NEXT J
    NEXT I
    CLOSE #1
END IF
' Append the wall coordinate data after it has been completely entered:
IF Code% = 1 AND FileCode% = 1 THEN
    OPEN "COORD.DAT" FOR APPEND AS #1
    FOR I = 1 TO 3
        FOR J = 1 TO NoNodes%
            WRITE #1, TempNo(I, J)
        NEXT J
    
```

```

    NEXT I
    CLOSE #1
END IF

' Write the nodal data after all the modes have been entered:
IF Code% = 4 AND ModeNo% = NoModes% THEN
    ' check to see if the data is for the surface nodes:
    IF FileCode% = 0 THEN
        OPEN "MODE.DAT" FOR OUTPUT AS #1      ' This wipes out existing data
        FOR I = 1 TO NoModes%
            FOR J = 1 TO NoNodes%
                WRITE #1, TempNo(I + 1, J)    ' Skip the node #'s
            NEXT J
        NEXT I
        CLOSE #1
    END IF
    ' check to see if the data is for the wall nodes:
    IF FileCode% = 1 THEN
        OPEN "MODE.DAT" FOR APPEND AS #1
        FOR I = 1 TO NoModes%
            FOR J = 1 TO NoNodes%
                WRITE #1, TempNo(I + 1, J)    ' Skip the node #'s
            NEXT J
        NEXT I
        CLOSE #1
    END IF
END IF

END SUB

```

```

' ***** LIQVOL *****
' This subroutine computes the non-dimensional volume occupied by the
' liquid and the non-dimensional location of the center of mass.
' The volume = pi * RT^3 * K, where RT is the non-dimensional
' radius to the tank wall from the origin of the coordinate system.
' RT must be equal to ONE if the input is given correctly. This routine
' computes K, assuming that RT=1. The dimensional volume is the non-
' non-dimensional volume multiplied by the radius RO to the tank wall;
' or Volume = pi * RO^3*K. The center of mass is referenced to the
' bottom of the tank.
'
SUB LiqVol (Surf(), Wall(), Ans1, Ans2, DZ, DeltaElev, SurfElev)
  SHARED NoNodes%
  DIM ZSurf(25)

  ' We first have to compute the Z coordinates of the free surface nodes
  ' since they were not asked for in the input. The Z's are computed
  ' by integrating the values of Z'.

  ZSurf(1) = 0
  FOR I = 2 TO NoNodes%
    AvgSlope = (Surf(5, (I - 1)) + Surf(5, I)) / 2
    DeltaZ = AvgSlope * (Surf(3, I) - Surf(3, (I - 1)))
    ZSurf(I) = ZSurf(I - 1) + DeltaZ
  NEXT I

  DZ = ZSurf(NoNodes%) - ZSurf((NoNodes% - 1))

  ' Estimate the elevation of the free surface center from the tank bottom
  ' First, compute distance tank bottom is below Z = 0:
  DeltaElev = -Wall(3, 1)
  ' Then, the free surface elevation is:
  ZSurf(1) = DeltaElev + (Wall(3, NoNodes%) - ZSurf(25))
  ' Save ZSurf(1)
  SurfElev = ZSurf(1)
  ' Correct the other free surface elevations:
  FOR I = 2 TO NoNodes%
    ZSurf(I) = ZSurf(I) + ZSurf(1)
  NEXT I

  ' Now can do the numerical integration. Differential volume =
  ' (Rad to wall)^2 * DeltaZ of wall -
  ' (Rad to liq surface)^2 * DeltaZ of surface

  Ans1 = 0:           Ans2 = 0
  Ans1Temp = 0:       Ans2Temp = 0
  Ans3Temp = 0:       Ans4Temp = 0
  FOR I = 1 TO NoNodes%
    ' First set up the right DeltaZ's
    SELECT CASE I
      CASE 1
        ' first Delta-Z interval
        DZSurf = (ZSurf(2) - ZSurf(1)) / 2
        DZWall = (Wall(3, 2) - Wall(3, 1)) / 2
      CASE NoNodes%
        ' last Delta-Z interval
        DZSurf = (ZSurf(NoNodes%) - ZSurf(NoNodes% - 1)) / 2
        DZWall = (Wall(3, NoNodes%) - Wall(3, (NoNodes% - 1))) / 2
      CASE ELSE
        ' interior Delta-Z interval
        DZSurf = (ZSurf(I + 1) - ZSurf(I - 1)) / 2
        DZWall = (Wall(3, (I + 1)) - Wall(3, (I - 1))) / 2
    END SELECT
  NEXT I

```

```

DeltaVol1 = (Wall(2, I) ^ 2) * DZWall
DeltaVol2 = (Surf(2, I)) ^ 2 * DZSurf
Ans1Temp = Ans1Temp + DeltaVol1
Ans2Temp = Ans2Temp + DeltaVol2
Ans3Temp = Ans3Temp + (Wall(3, I) + DeltaElev) * DeltaVol1
Ans4Temp = Ans4Temp + ZSurf(I) * DeltaVol2
NEXT I
Ans1 = Ans1Temp - Ans2Temp          ' liquid volume
Ans2 = (Ans3Temp - Ans4Temp) / Ans1  ' liquid c.g.
END SUB

```

```

' ***** OUTPUTSCREEN *****
' This subroutine displays the input data and the computed results on
' the screen. It also asks if the user wants printed copies.
'
SUB OutputScreen (F2, SM2, PL, HO, CG, SC, BI(), PCode%)
  SHARED FillLevel, BondNo, Ang, ConstMass, ExpMass, NoModes%, NoNodes%
  SHARED LiqVolume
  Pi = 4 * ATN(1)
  CLS

  ' ===== Display the input =====
  COLOR 11: LOCATE 1, 35: PRINT "INPUT DATA"
  COLOR 15: LOCATE 2, 5: PRINT "Bond Number Fill Level % Cont. Ang"
  LOCATE 2, 44: PRINT "Surface Mass Distribution Function"
  CALL Box(3, 7, 5, 13, 1, 14, -1) ' draw some boxes for the output
  CALL Box(3, 20, 5, 27, 1, 14, -1)
  CALL Box(3, 33, 5, 40, 1, 14, -1)
  CALL Box(3, 48, 5, 74, 1, 14, -1)
  LOCATE 4, 8: PRINT USING "##.##"; BondNo ' format and print output
  LOCATE 4, 22: PRINT USING "##.##"; FillLevel
  LOCATE 4, 35: PRINT USING "##.##"; Ang
  LOCATE 4, 50: PRINT USING "##.###"; ConstMass
  LOCATE 4, 56: PRINT USING " - (S/Smax)^#.##"; ExpMass

  ' ===== end of input display =====
  ' ===== display the computed results =====
  COLOR 11: LOCATE 6, 22: PRINT "PARTICIPATION FACTORS OF TRIAL MODES"
  FOR I = 1 TO 3
    Edge1% = 10 + 25 * (I - 1)
    Edge2% = Edge1% + 10
    CALL Box(7, (Edge1%), 9, (Edge2%), 1, 14, -1)
  NEXT I
  COLOR 15: LOCATE 8, 4
  PRINT "B(1) =": LOCATE 8, 12: PRINT "1.00000"
  LOCATE 8, 29
  PRINT "B(2) =": LOCATE 8, 37: PRINT USING "###.###"; BI(2)
  LOCATE 8, 54
  PRINT "B(3) =": LOCATE 8, 62: PRINT USING "###.###"; BI(3)

  COLOR 11
  LOCATE 10, 15: PRINT "NON-DIMENSIONAL PARAMETERS OF THE PENDULUM MODEL"
  COLOR 15
  LOCATE 11, 2: PRINT "(Liq Vol)/(("; CHR$(227); " * Ro^3)"
  LOCATE 11, 27: PRINT "Slosh M/Liquid M"
  LOCATE 11, 49: PRINT "Pend. L/Ro"
  LOCATE 11, 68: PRINT "Ho/Ro"

  CALL Box(12, 5, 14, 15, 1, 14, -1)
  LOCATE 13, 7: PRINT USING "###.###"; LiqVolume
  CALL Box(12, 29, 14, 39, 1, 14, -1)
  LOCATE 13, 31: PRINT USING "###.###"; SM2
  CALL Box(12, 48, 14, 59, 1, 14, -1)
  LOCATE 13, 50: PRINT USING "###.###"; PL
  CALL Box(12, 66, 14, 75, 1, 14, -1)
  LOCATE 13, 67: PRINT USING "###.###"; HO

  LOCATE 15, 5: PRINT "CG Loc./Ro"
  LOCATE 15, 28: PRINT "Spring/(("; CHR$(229); " * Ro^2)"
  LOCATE 15, 50: PRINT "Freq^2/(("; " (1+Bo)"; CHR$(229); " / (d * Ro^3))"
  CALL Box(16, 5, 18, 16, 1, 14, -1)
  CALL Box(16, 26, 18, 45, 1, 14, -1)
  CALL Box(16, 58, 18, 71, 1, 14, -1)

```

```

LOCATE 17, 7:      PRINT USING "###.####"; CG
LOCATE 17, 32:     PRINT USING "###.####"; SC
LOCATE 17, 62:     PRINT USING "###.####"; F2
'  ===== end of results display =====

LOCATE 21, 5
PRINT "Do you want the above data printed out (Y or N) ?"
LOCATE 21, 55, 1, 5, 7: INPUT "", Response$
Response$ = UCASE$(Response$)
IF Response$ = "N" THEN
    PCode% = 0:      EXIT SUB
ELSE
    PCode% = 1
END IF

LOCATE 23, 5
PRINT "Do you also want the surface wave data printed (Y or N) ?"
LOCATE 23, 63: INPUT "", Response$
Response$ = UCASE$(Response$)
IF Response$ = "N" THEN PCode% = 1 ELSE PCode% = 2
END SUB

```

```

' ***** PADZERO *****
' This subroutine turns a number into a text string for printing. The string
' can be specified to have a given number of decimal places "NoDecs" and
' a given number of digits before the decimal "NoBeforeDec" If the
' number is a floating point number with a negative exponent and the
' value of the exponent is greater than the NoDecs, then the string
' is set equal to zero; otherwise the number is turned into a string that
' looks like a decimal number. At this time, nothing is done to
' floating point numbers with positive exponents; the string is just the
' number.
'
FUNCTION PadZero$ (A, NoDecs, NoBeforeDec)
A$ = STR$(A)
A$ = LTRIM$(RTRIM$(A$)) ' Get rid of all blank spaces
C$ = MID$(A$, 1, 1)
' In case the number is negative, keep the same number of digits before
' the decimal point.
IF C$ = "-" THEN NoBeforeDec = NoBeforeDec + 1
' find if it is a floating point number
FOR I = 2 TO LEN(A$) ' skip any possible "-" signs for negative #'s
    B$ = MID$(A$, I, 1)
    IF B$ = "-" THEN Flag = 1: NF = I + 1 ' negative exponent
    IF B$ = "+" THEN Flag = 2: NF = I + 1 ' positive exponent
NEXT I
SELECT CASE Flag
CASE 1 ' The number has a negative exponent
    Num1 = VAL(MID$(A$, NF, 1)): Num2 = VAL(MID$(A$, (NF + 1), 1))
    IF Num1 > 0 OR Num2 > NoDecs THEN ' the number is too small
        A$ = "0." ' make it equal to 0.000....
        FOR I = 1 TO NoDecs
            A$ = A$ + "0"
        NEXT I
    ELSE ' turn the number into a decimal number
        IF C$ = "-" THEN
            B$ = MID$(A$, 2, 1) ' get the first digit
            FOR I = 4 TO (LEN(A$) - 4) ' skip - sign, 1st digit, and
                B$ = B$ + MID$(A$, I, 1) ' the decimal point, and don't
            NEXT I ' count the "E-XX" at end
            FOR I = 1 TO (Num2 - 1)
                B$ = "0" + B$
            NEXT I
            A$ = C$ + "0." + B$
        ELSE
            B$ = MID$(A$, 1, 1) ' get the first digit
            FOR I = 3 TO (LEN(A$) - 4) ' skip 1st digit and decimal point
                B$ = B$ + MID$(A$, I, 1) ' and don't count the "E-XX"
            NEXT I
            FOR I = 1 TO (Num2 - 1)
                B$ = "0" + B$
            NEXT I
            A$ = "0." + B$
        END IF
    END IF
CASE ELSE ' The number has no exponent or a postive exponent
END SELECT
' if it is a negative number, make it start with "-0."
IF C$ = "-" AND MID$(A$, 2, 1) = "." THEN
    B$ = ""
    FOR I = 3 TO LEN(A$)
        B$ = B$ + MID$(A$, I, 1)
    
```

```

        NEXT I
        A$ = "-0." + B$
    END IF

    ' Find out where the decimal point is
    DecLoc = 0
    FOR I = 1 TO LEN(A$)
        B$ = MID$(A$, I, 1)
        IF B$ = "." THEN DecLoc = I
    NEXT I

    ' if the first character is "." then add a zero before it
    IF DecLoc = 1 THEN A$ = "0" + A$: DecLoc = 2
    IF C$ = "-" AND MID$(A$, 2, 1) = "." THEN
        B$ = ""
        FOR I = 3 TO LEN(A$)
            B$ = B$ + MID$(A$, I, 1)
        NEXT I
        A$ = "-0." + B$
    END IF

    ' if there is no "." then add one at the end
    IF DecLoc = 0 AND NoDecs > 0 THEN A$ = A$ + ".": DecLoc = LEN(A$)

    ' if the number has too many decimal places, then cut the extra ones
    IF ((LEN(A$) - DecLoc) >= NoDecs) THEN
        B$ = ""
        FOR I = 1 TO (DecLoc + NoDecs)
            B$ = B$ + MID$(A$, I, 1)
        NEXT I
        A$ = B$
    END IF

    ' if there are not enough "0" at the end, add enough of them, but
    ' first, find out how many "0" to add
    NoPad = NoDecs - (LEN(A$) - DecLoc)

    ' now add the "0"s
    FOR I = 1 TO NoPad
        A$ = A$ + "0"
    NEXT I

    ' now see if there are enough spaces before the decimal point
    IF NoBeforeDec > (DecLoc - 1) THEN ' if not, add blank spaces
        NoPad = NoBeforeDec - (DecLoc - 1)
        FOR I = 1 TO NoPad
            A$ = " " + A$
        NEXT I
    END IF

    ' All done, so send the string back
    PadZero$ = A$
END FUNCTION

```

```

' ***** PARAMMODEL *****
' This subroutine computes the non-dimensional parameters of the
' pendulum model: SM2 = SlosH Mass / Liquid Mass in tank;
' PL = Pendulum Length / RO
' SC = Spring Constant / (surface tension * RO^3)
' HO = HingePointLocation / RO
' Note: F2 = SlsFreq (i.e, non-dimensional natural frequency ^ 2)
'       SM = SlosHMass / LiquidMass in Full Tank
'       MOF = Moment / Force (non-dimensional)
'
SUB ParamModel (MOF, F2, SM, SM2, PL, SC, HO)
  SHARED LiqVolume, FillLevel, DeltaElev, SurfElev
  SHARED BondNo
  Pi = 4 * ATN(1)
  ' Compute the slosH mass ratio to the actual liquid mass
  SM2 = SM / (FillLevel / 100)
  ' Compute the pendulum length ratio to tank radius
  PL = 1 / F2
  ' Compute the spring constant ratio to (surface tension * RO ^2)
  SC = SM2 * Pi * LiqVolume / F2
  ' Compute the hinge point location ratio to tank radius
  HO = MOF + SC / ((1 + BondNo) * (SM2 * Pi * LiqVolume) * PL * F2)
  HO = HO + SurfElev ' reference to tank bottom
END SUB

```

```

' ***** POTNORM *****
' This subroutines finds the largest value of the trial potentials for
' each mode and uses it to normalize all the nodal values for that mode.
'
SUB PotNorm (SurfP(), WallP())
  SHARED NoModes%, NoNodes%
  FOR I = 2 TO (NoModes% + 1)          ' Skip over the node ID number
    PotMax = ABS(SurfP(I, 1))          ' First guess for maximum value
    FOR J = 2 TO NoNodes%
      IF ABS(SurfP(I, J)) > PotMax THEN PotMax = ABS(SurfP(I, J))
    NEXT J
    FOR J = 1 TO NoNodes%
      SurfP(I, J) = SurfP(I, J) / PotMax   ' This is the normalization
      WallP(I, J) = WallP(I, J) / PotMax
    NEXT J
  NEXT I
END SUB

```

```

' ***** PRINTOUT *****
' This printout routine prints out the input data, the trial results,
' and the mechanical model paramters. It uses the function "PadZero$"
' to make strings with a specified number of decimal places and leading
' digits out of the numerical data for easier control of the printing.
'
SUB PrintOut (F2, F(), SM2, PL, HO, CG, SC, BI(), PC%)
  SHARED FillLevel, BondNo, Ang, ConstMass, ExpMass, NoModes%, NoNodes%
  SHARED LiqVolume
  DIM F$(3)
  CLS

  ' ===== Display the input =====
  LPRINT SPC(27); "===== INPUT DATA ====="
  A$ = "Bond Number  Fill Level(%)  Cont. Ang"
  B$ = "Surface Mass Distribution Function"
  LPRINT SPC(4); A$; SPC(4); B$

  B$ = PadZero$(BondNo, 1, 2)      ' 1 decimal place, two spaces or digits
  F$ = PadZero$(FillLevel, 1, 2)   ' (cont'd) before the decimal place
  A$ = PadZero$(Ang, 1, 2)
  C$ = PadZero$(ConstMass, 3, 2)
  E$ = PadZero$(ExpMass, 1, 2)

  LPRINT SPC(7); B$; SPC(10); F$; SPC(9); A$; SPC(12); C$; " - (S/Smmax)^"; E$
  LPRINT
  LPRINT SPC(20);
  LPRINT "Trial Freq 1"; SPC(4); "Trial Freq 2"; SPC(4); "TrialFreq 3"
  FOR I = 1 TO 3
    F$(I) = PadZero$(F(I)), 5, 2)
  NEXT I
  LPRINT SPC(13);
  FOR I = 1 TO 3
    LPRINT SPC(8); F$(I);
  NEXT I

  ' ===== end of input display =====
  ' ===== display the results =====
  LPRINT : LPRINT SPC(27); "===== RESULTS ====="
  LPRINT SPC(15); "***** PARTICIPATION FACTORS OF TRIAL MODES *****"
  FOR I = 1 TO 3
    F$(I) = PadZero$(BI(I)), 5, 2)
  NEXT I

  LPRINT SPC(10);
  FOR I = 1 TO 3
    I$ = LTRIM$(RTRIM$(STR$(I)))
    LPRINT SPC(4); "B("; I$; ") = "; F$(I);
  NEXT I

  LPRINT : LPRINT
  LPRINT SPC(10);
  LPRINT "***** NON-DIMENSIONAL PARAMETERS OF THE PENDULUM MODEL *****"
  L$ = PadZero$(LiqVolume, 4, 2)
  S$ = PadZero$(SM2, 4, 1)
  P$ = PadZero$(PL, 4, 2)
  H$ = PadZero$(HO, 3, 3)
  LPRINT SPC(10);
  LPRINT "Liq Vol/"; CHR$(227); "Ro^3"; SPC(3);
  LPRINT "Slosh Mass/Liq Mass"; SPC(3);
  LPRINT "Pend. L/Ro"; SPC(7);
  LPRINT "Ho/Ro"

  LPRINT SPC(12); L$; SPC(13); S$; SPC(11); P$; SPC(6); H$

```

```

C$ = PadZero$(CG, 4, 2)
S$ = PadZero$(SC, 4, 2)
F$ = PadZero$(F2, 4, 2)
LPRINT : LPRINT SPC(10);
LPRINT "Liq. CG/Ro"; SPC(8);
LPRINT "Spring/"; CHR$(229); "Ro^2"; SPC(8);
LPRINT "Freq^2/["; "(1+Bo)"; CHR$(229); "/(dRo^3)]"
LPRINT SPC(11); C$, SPC(2); S$; SPC(20); F$
' ===== end of results display =====
IF PC% = 1 THEN LPRINT CHR$(12) ELSE LPRINT : LPRINT
END SUB

```

```

' ***** PRINTOUT2 *****
' This subroutine prints out the wave height data
'
SUB PrintOut2 (S(), WH(), BI(), F2, F())
  SHARED NoNodes%, NoModes%, BondNo
  DIM W(4), W$(4)
  LPRINT SPC(22); "|***** WAVE HEIGHTS ON SURFACE *****|"
  LPRINT SPC(23); "ADINA"; SPC(7); "ADINA"; SPC(7); "ADINA";
  LPRINT SPC(7); "Slosh"
  LPRINT SPC(10); "S Coord."; SPC(4); "Trial 1"; SPC(5); "Trial 2";
  LPRINT SPC(5); "Trial 3"; SPC(6); "Mode 1"
  LPRINT SPC(9); "-----"; SPC(5); "-----"; SPC(5); "-----";
  LPRINT SPC(5); "-----"; SPC(5); "-----"
  FOR I = 1 TO NoNodes%
    LPRINT SPC(11);
    S$ = PadZero$(S(3, I), 4, 1)
    W(1) = WH(1, I)
    W(2) = 0
    W(3) = 0
    SELECT CASE NoModes%
      CASE 2
        W(2) = WH(2, I)
      CASE 3
        W(2) = WH(2, I)
        W(3) = WH(3, I)
      CASE ELSE
    END SELECT
    W(4) = 0
    FOR J = 1 TO 3
      W(4) = W(4) + BI(J) * F(J) * W(J)
      W(J) = W(J) * SQR(F(J)) * (1 + BondNo)
    NEXT J
    W(4) = W(4) * (1 + BondNo) / SQR(F2)
    FOR J = 1 TO 4
      W$(J) = PadZero$(W(J), 4, 2)
    NEXT J
    W = 5
    X = 5
    Y = 5
    Z = 5
    B$ = LTRIM$(W$(1)): IF MID$(B$, 1, 1) = "-" THEN X = 4
    B$ = LTRIM$(W$(2)): IF MID$(B$, 1, 1) = "-" THEN Y = 4
    B$ = LTRIM$(W$(3)): IF MID$(B$, 1, 1) = "-" THEN Z = 4
    B$ = LTRIM$(W$(4)): IF MID$(B$, 1, 1) = "-" THEN W = 4
    LPRINT S$; SPC(X); W$(1); SPC(Y); W$(2); SPC(Z); W$(3); SPC(W); W$(4)
  NEXT I
  LPRINT CHR$(12) ' feed paper out
END SUB

```

```

' ***** RAD *****
' This subroutine computes the expression  $(1/R1^2 + 1/R2^2)$  where R1
' and R2 are the mean radii of curvature of the free surface. R1 =
'  $Z(S)"R(S)' - Z(S)'R(S)"$  and  $R2 = Z(S)'/R$ .
'
SUB Rad (Coord(), Temp())
  SHARED NoNodes%
  FOR I = 1 TO NoNodes%
    R11 = Coord(7, I) * Coord(4, I)
    R12 = Coord(5, I) * Coord(6, I)
    ' When computing R2 must allow for fact that R=0 at the first node
    IF I = 1 THEN R2 = Coord(7, I) ELSE R2 = Coord(5, I) / Coord(2, I)
    Temp(I) = (R11 - R12) ^ 2 + R2 ^ 2
  NEXT I
END SUB

```

```

' ***** ROOT *****
' This subroutine finds the (non-dimensional freq.)^2 for of the first mode.
SUB Root (Guess, DT, C1(), C2(), Answer)
  SHARED NoModes%
  DIM CS(3, 3)
  SELECT CASE NoModes%
    CASE 1 ' Only one term; solve it directly
      Answer = C1(1, 1) / C2(1, 1)
      IF Answer < 0 THEN PRINT "Eigenvalue is negative!": END
    CASE 2 ' Two terms; use quadratic formula
      RQuad = C2(1, 1) * C2(2, 2) - C2(1, 2) * C2(2, 1)
      RMid1 = C1(1, 1) * C2(2, 2) + C1(2, 2) * C2(1, 1)
      RMid2 = C1(1, 2) * C2(2, 1) + C1(2, 1) * C2(1, 2)
      RMid = RMid1 - RMid2
      RConst = C1(1, 1) * C1(2, 2) - C1(1, 2) * C1(2, 1)
      RootTerm = RMid ^ 2 - 4 * RQuad * RConst
      IF RootTerm < 0 THEN PRINT "Eigenvalue is complex!": END
      Answer1 = (-RMid + SQR(RootTerm)) / (2 * RQuad)
      Answer2 = (-RMid - SQR(RootTerm)) / (2 * RQuad)
      IF Answer1 < 0 AND Answer2 < 0 THEN PRINT "Eigenvalue is < 0": END
      IF Answer1 < 0 THEN Answer = Answer2
      IF Answer2 < 0 THEN Answer = Answer1
      IF Answer1 > 0 AND Answer2 > 0 THEN
        IF Answer1 < Answer2 THEN Answer = Answer1 ELSE Answer = Answer2
      END IF
    CASE 3 ' Three terms; expand the determinant and iterate
      WHILE DT > .000001
        FOR I = 1 TO 3 ' Calculate determinant for "Guess"
          FOR J = 1 TO 3
            CS(I, J) = C1(I, J) + Guess * C2(I, J)
          NEXT J
        NEXT I
        Term1 = CS(1, 1) * (CS(2, 2) * CS(3, 3) - CS(3, 2) * CS(2, 3))
        Term2 = CS(1, 2) * (CS(2, 1) * CS(3, 3) - CS(3, 1) * CS(2, 3))
        Term3 = CS(1, 3) * (CS(2, 1) * CS(3, 2) - CS(3, 1) * CS(2, 2))
        StartVal = Term1 - Term2 + Term3 ' Determinant value
        TestVal = StartVal
        Test = StartVal * TestVal: K = 1
        WHILE Test > 0 ' When Test < 0 we have bracketed the root
          Guess = Guess + DT
          FOR I = 1 TO 3
            FOR J = 1 TO 3
              CS(I, J) = C1(I, J) + Guess * C2(I, J)
            NEXT J
          NEXT I
          Term1 = CS(1, 1) * (CS(2, 2) * CS(3, 3) - CS(3, 2) * CS(2, 3))
          Term2 = CS(1, 2) * (CS(2, 1) * CS(3, 3) - CS(3, 1) * CS(2, 3))
          Term3 = CS(1, 3) * (CS(2, 1) * CS(3, 2) - CS(3, 1) * CS(2, 2))
          TestVal = Term1 - Term2 + Term3
          Test = StartVal * TestVal: K = K + 1
          IF K > 100 THEN PRINT "No Convergence": END
        WEND
        Guess = Guess - DT ' back up one value to get new StartValue
        DT = DT / 10 ' decrease the iteration jump
      WEND
  Answer = Guess
END SELECT
END SUB

```

```

' ***** SLOSHM *****
' This subroutine computes the non-dimensional slosh mass of the
' pendulum model and makes it non-dimensional by dividing by the liquid mass
' that will completely fill the tank = pi * RO^3*LiqVolume/(FillLevel/100).
' The subroutine also computes the ratio of the moment to the force.
' The mass is returned as Ans1, the ratio is returned as Ans2.
'
SUB SloshM (S(), W(), PS(), PW(), TF(), BI(), SlsFrq, Ans1, Ans2)
  SHARED NoNodes%, NoModes%, FillLevel, BondNo, LiqVolume
  SHARED Ang, ConstMass, ExpMass, LastDZsurf, DeltaElev, SurfElev

' S() = coordinate matrix for free surface
' W() = coordinate matrix for wall
' PS() = potential values at free surface nodes
' PW() = potential values at wall nodes
' TF() = matrix of trial (eignevalues)^2
' BI() = matrix of "b" modal participation factors

' First, compute the nondimensional force and moment amplitudes
' The first component is the surface tension effect at the tank walls
' Sine of the wall angle X at the contact line:
NN% = NoNodes%:      NN1% = NN% - 1
DeltaZ = W(3, NN%) - W(3, NN1%)
DeltaR = W(2, NN%) - W(2, NN1%)
SineX = DeltaZ / SQR(DeltaZ ^ 2 + DeltaR ^ 2)

' Curvature of free surface at the contact line:
WallCurv1 = S(7, NN%) * S(4, NN%) - S(5, NN%) * S(6, NN%)
WallCurv2 = S(5, NN%) / S(2, NN%)
WallCurv = WallCurv1 + WallCurv2

' Value of the normal derivative of the potential at the contact line:
WallMass = ConstMass - 1:      ' this is parameter "e"
PotDeriv = 0
FOR I = 1 TO NoModes%
  PotDeriv = PotDeriv + PS((I + 1), NN%) * TF(I) * BI(I)
NEXT I
PotDeriv = PotDeriv * WallMass * (1 + BondNo)

' Value of wave amplitude at the contact line:
WaveAmp = PotDeriv / SQR(SlsFrq)

' Average the finite element contact angle and the input contact angle:
RS = S(2, NN%):      RS1 = S(2, (NN% - 1))
Rw = W(2, NN%):      RW1 = W(2, (NN% - 1))
ZW = W(3, NN%):      ZW1 = W(3, (NN% - 1))
Term1 = (RS - RS1) * (Rw - RW1) + (LastDZsurf) * (ZW - ZW1)
Term2 = SQR((RS - RS1) ^ 2 + (LastDZsurf) ^ 2)
Term3 = SQR((Rw - RW1) ^ 2 + (ZW - ZW1) ^ 2)
Cosine = Term1 / (Term2 * Term3)
Sine = SQR(1 - Cosine ^ 2)
Ang1 = ATN(Sine / Cosine)
AngleTrue = (Ang1 + Ang * 3.14159 / 180) / 2
Cosine = COS(AngleTrue)
Sine = SIN(AngleTrue)

' The surface tension force:
Rc = S(2, NN%):      ScriptRc = 1 / WallCurv
SurfForce = (Cosine - (Rc / ScriptRc) * SineX) * Cosine / Sine
SurfForce = SurfForce * WaveAmp
IF SurfForce > 0 THEN SurfForce = 0

```

```

' The surface tension moment:
Fc = (W(3, NoNodes%) - W(3, 1)) - SurfElev
FirstPart = Cosine - ((Rc / ScriptRc) + (Rc / Fc) * Sine) * SineX
FirstPart = FirstPart * Cosine / Sine
SurfMoment = FirstPart * Fc * WaveAmp

' Pressure component of force and moment:
PresForce = 0: PresMoment = 0
FOR I = 1 TO NoNodes%
  SELECT CASE I
    CASE 1
      DZ = (W(3, 2) - W(3, 1)) / 2
    CASE NoNodes%
      DZ = (W(3, NN%) - W(3, (NN% - 1))) / 2
    CASE ELSE
      DZ = (W(3, (I + 1)) - W(3, (I - 1))) / 2
  END SELECT
  FOR J = 1 TO NoNodes%
    Rw = W(2, I)
    Z = DeltaElev + W(3, I) - SurfElev ' referred to free surface
    TrialPotential = PW((J + 1), I) * BI(J)
    PresForce = PresForce + TrialPotential * Rw * DZ
    PresMoment = PresMoment + TrialPotential * Rw * Z * DZ
  NEXT J
NEXT I

Force = PresForce + (SurfForce) / ((1 + BondNo) * SQR(SlsFrq))
Moment = PresMoment + (SurfMoment) / ((1 + BondNo) * SQR(SlsFrq))
IF Force < 0 THEN CLS : PRINT "The Slosh Force is Negative!": END
Ans2 = Moment / Force

' The non-dimensional kinetic energy of the liquid:
KinEnergy = 0
SMax = S(3, NN%)
FOR I = 1 TO NoNodes%
  SELECT CASE I
    CASE 1
      DS = (S(3, 2) - S(3, 1)) / 2
    CASE NoNodes%
      DS = (S(3, NN%) - S(3, (NN% - 1))) / 2
    CASE ELSE
      DS = (S(3, (I + 1)) - S(3, (I - 1))) / 2
  END SELECT
  RS = S(2, I): SS = S(3, I)
  SurfMass = (ConstMass - (SS / SMax) ^ ExpMass) * (1 + BondNo)
  PotDeriv = 0
  Pot = 0
  FOR J = 1 TO NoNodes%
    PotDeriv = PotDeriv + BI(J) * TF(J) * SurfMass * PS((J + 1), I)
  NEXT J
  FOR J = 1 TO NoNodes%
    Pot = Pot + PS((J + 1), I) * BI(J)
  NEXT J
  KinEnergy = KinEnergy + PotDeriv * Pot * RS * DS
NEXT I

' Now compute the slosh mass. The mass is ratioed to the liquid mass that
' fills the tank.
Ans1 = (Force) ^ 2 * (FillLevel / 100) / (KinEnergy * LiqVolume)
END SUB

```

```

/ ***** TEXTIN *****
/ This subroutine is taken from the QUICKPAK set of functions. It is a
/ data entry routine that allows the cursor to be moved all over the
/ screen and permits the entered data to be corrected at any time.
/
/                               Entry Parameters
/ T$ = string to be input or edited (use the name of your choice)
/ Max = maximum number of characters allowed
/ Colr is the combined foreground and background colors that will be used
/ CapsOn = force automatic conversion to upper case if 1
/       Note: CapsOn is not used here
/ NumOnly = allow only numeric input if 1
/
/                               Exit Parameters
/
/ T$ = final edited string (the name passed as input to the function)
/ ExitCode indicates how editing was terminated -
/   0 = Enter, Tab, Down-Arrow, Right-Arrow past end, or field filled
/   1 = Shift-Tab, Up-Arrow, or Left-Arrow past beginning
/   2 = Esc key pressed
/
/                               Local Variables
/
/ X$ is a copy of the string while being input or edited
/ Insert holds status of insert mode
/ Curpo holds current cursor position relative to the beginning of the line
/ Length keeps track of the current length of the string
/ Clr = 1 if the monitor is a color monitor, for setting cursor size
/ A and A$ are temporary scratch variables
SUB TextIn1 (T$, Max, NumOnly, CapsOn, ExitCode, Colr) STATIC
DEFINT A-Z
TInitialize:
    Clr = 0                                'determine monitor type
    IF Peek1%(0, &H463) <> &HB4 THEN Clr = 1
    X$ = T$                                'X$ is a working copy of
                                          ' the input string
TC:
    ExitCode = 0: Insert = 0: Curpo = 1    'initialize flags
    Length = LEN(X$)
    IF Length > Max THEN EXIT SUB          'already to big to edit
    X$ = X$ + SPACE$(Max - Length)        'pad with trailing spaces
    QPrint X$, Colr, -1
    LOCATE , , 1                          'turn on the cursor
    GOSUB TInsertOff                      'set cursor size according to display
TGetKey:
    'disallow insert if cursor past end
    IF Curpo > Length AND Insert <> 0 THEN GOSUB TInsertOff
    IF Curpo > Max GOTO TEnter              'field is filled, handle as Enter key
    A$ = INKEY$
    IF A$ = "" GOTO TGetKey
    IF LEN(A$) = 1 GOTO TRegularKey
    A$ = RIGHT$(A$, 1)                    'it was an extended key, get the code

```

```

ON INSTR(CHR$(15) + ".GHKMOPRSstu" + CHR$(19), A$) GOTO TShiftTab, TClear,
THome, TUp, TLeft, TRight, TEndKey, TDown, TIns, TDel, TCtrlLeft, TCtrlRight,
TCtrlEnd, TRestore

```

```

GOTO TGetKey 'none of the above, get again

```

```

TShiftTab:

```

```

ExitCode = 1 'user wants to go back a field
GOTO TEnter 'handle as if it were the Enter key

```

```

TClear:

```

```

X$ = "" 'Alt-C, erase the current string
GOSUB TInsertOff 'clear insert mode and restore cursor
LOCATE , POS(0) - (Curpo - 1)
GOTO TC 'and start all over again

```

```

THome:

```

```

LOCATE , POS(0) - (Curpo - 1) 'put cursor at beginning of line
Curpo = 1 'show cursor as being on 1st character
GOTO TGetKey

```

```

TUp:

```

```

ExitCode = 1 'user wants to go back a field
GOTO TEnter 'handle as if it were the Enter key

```

```

TLeft:

```

```

IF Curpo = 1 GOTO TShiftTab 'cursor is on the first character,
'handle as if it were a Shift-Tab
Curpo = Curpo - 1 'update Curpo
LOCATE , POS(0) - 1 'back up the cursor
GOTO TGetKey

```

```

TRight:

```

```

Curpo = Curpo + 1 'update Curpo
LOCATE , POS(0) + 1 'advance the cursor on the screen
GOTO TGetKey

```

```

TEndKey:

```

```

LOCATE , POS(0) + (Length - Curpo) + 1 'put cursor at the end of the line
Curpo = Length + 1 'update Curpo
GOTO TGetKey

```

```

TDown:

```

```

GOTO TEnter

```

```

TIns:

```

```

IF Insert THEN 'insert is already on, turn it off
GOSUB TInsertOff
GOTO TGetKey
END IF
IF Curpo > Length GOTO TGetKey 'ignore Ins if cursor is past the end
IF Length = Max GOTO TGetKey 'also ignore if field is full
Insert = 1 'set the insert flag
IF C!r THEN 'set cursor size according to display
LOCATE , , , 0, 7
ELSE
LOCATE , , , 0, 13
END IF
GOTO TGetKey

```

```

TDel:

```

```

IF Curpo > Length GOTO TGetKey 'ignore Del if cursor is past end

```

[illegible]

```

LOCATE , POS(0) - (Curpo - 1)      'locate cursor at beginning of line,
GOTO TInitialize                    ' and start all over again

TRegularKey:
  IF A$ < " " THEN                  'a control key
    ON INSTR(CHR$(8) + CHR$(9) + CHR$(13) + CHR$(27), A$) GOTO TBackspace,
    TTabKey, TEnter, TEscape
    GOTO TGetKey                    'none of the above
  END IF
  IF CapsOn THEN                    'convert to upper case if requested
    IF A$ >= "a" AND A$ <= "z" THEN A$ = CHR$(ASC(A$) AND 95)
  END IF
  IF NumOnly THEN                   'disallow non-numeric if requested
    IF A$ < "0" OR A$ > "9" THEN
      PLAY "L1603EC"
      GOTO TGetKey
    END IF
  END IF
  QPrint A$, Colr, -1               'print character
  LOCATE , POS(0) + 1
  Curpo = Curpo + 1                 'show cursor being ahead
  IF Insert GOTO THandleInsert
  MID$(X$, Curpo - 1, 1) = A$       'assign the character
  'cursor is past end, increase length
  IF Curpo > Length + 1 THEN Length = Curpo - 1
  'field complete, handle as Enter key
  IF Length = Max AND Curpo > Length GOTO TEnter
  GOTO TGetKey

THandleInsert:
  Length = Length + 1               'show string being 1 character longer
  MID$(X$, Curpo) = MID$(X$, Curpo - 1) 'move characters one position ahead
  MID$(X$, Curpo - 1, 1) = A$       'assign the current character
  QPrint MID$(X$, Curpo, Length - Curpo + 1), Colr, -1 're-print X$
  IF Length = Max GOTO TEnter        'field complete, handle as Enter key
  GOTO TGetKey

TBackspace:
  IF Curpo = 1 GOTO TGetKey          'can't back up any more, ignore
  Curpo = Curpo - 1                 'show cursor being 1 character before
  LOCATE , POS(0) - 1               'back up the cursor
  GOTO TDel                          'handle as if it were the Delete key

TTabKey:                             'reserved for your Tab routine if you
                                      ' want to handle it differently

TEnter:
  GOSUB TInsertOff                  'clear insert, restore cursor size
  X$ = LEFT$(X$, Length)            'retain only the current length
  T$ = X$                           'assign the string
  LOCATE , , 0                      'turn off the cursor
  EXIT SUB

TEscape:
  ExitCode = 2                      'show that the user pressed Escape
  GOTO TEnter                       'handle as if it were the Enter Key

TInsertOff:

```

'clear Insert mode and restore cursor, depending on monitor type

Insert = 0

IF C1r THEN

LOCATE , , , 6, 7

ELSE

LOCATE , , , 12, 13

END IF

RETURN

END SUB

```

/ ***** VECTOR *****
/ This subroutine computes the eigenvectors or modal participation factors
,
SUB Vector (F2, C1(), C2(), Result())
DEFSNG A-Z
SHARED NoModes%
DIM CR(3, 3)
SELECT CASE NoModes%
CASE 1
    Result(1) = 1
CASE 2
    Result(1) = 1
    Result(2) = -(C1(1, 1) + F2 * C2(1, 1)) / (C1(1, 2) + F2 * C2(1, 2))
CASE 3
    Result(1) = 1
    FOR I = 1 TO 3
        FOR J = 1 TO 3
            CR(I, J) = C1(I, J) + F2 * C2(I, J)
        NEXT J
    NEXT I
    TermTop = CR(2, 2) * CR(1, 1) - CR(2, 1) * CR(1, 2)
    TermBot = CR(1, 2) * CR(2, 3) - CR(1, 3) * CR(2, 2)
    Result(3) = TermTop / TermBot
    Result(2) = (-CR(1, 3) * Result(3) - CR(1, 1)) / CR(1, 2)
END SELECT
END SUB

```

```

' ***** WAVE HITE *****
' This subroutine computes the wave height of the trial functions.
' However, the frequency multiplication term is not included.
'
SUB WaveHite (Coord(), ModeS(), TempNo())
  SHARED NoModes%, NoNodes%, ConstMass, ExpMass
  SMax = Coord(3, NoNodes%) ' Value of S coord at contact point
  FOR I = 1 TO NoNodes%
    DistMass = ConstMass - (Coord(3, I) / SMax) ^ ExpMass
    FOR J = 1 TO NoModes%
      TempNo(J, I) = DistMass * ModeS((J + 1), I)
    NEXT J
  NEXT I
END SUB

```